МОСКОВСКИЙ ГОСУДАРСТВЕННЫЙ УНИВЕРСИТЕТ
ИМЕНИ М.В.ЛОМОНОСОВА
БИОЛОГИЧЕСКИЙ ФАКУЛЬТЕТ

На правах рукописи

Хао Цзинжао

Исследование молекулярных механизмов действия пестицидов на фотосинтетический аппарат высших растений

Специальность 1.5.2. Биофизика (биологические науки)

ДИССЕРТАЦИЯ
на соискание ученой степени
кандидата биологических наук

Научный руководитель:

доктор биологических наук, профессор,
Максимов Георгий Владимирович

доктор биологических наук,
профессор, академик РАН,
Рубин Андрей Борисович

Москва – 2025

LOMONOSOV MOSCOW STATE UNIVERSITY
BIOLOGICAL FACULTY

As a manuscript

HAO JINGRAO

Investigation of Molecular Mechanisms of Pesticide Action on Photosynthetic Apparatus of Higher Plants

Specialty 1.5.2 - Biophysics

DISSERTATION (THESIS)
for the Degree Candidate of Biological Sciences

Scientific supervisor:
Prof. PhD, Dr.Sc.
George V. Maksimov
Prof. PhD, Dr.Sc.
Academician of the Russian Academy of Sciences,
Andrey Borisovich Rubin

Moscow – 2025

CONTENT

LIST OF ABBREVIATIONS

RS – Raman scattering

TMX - Thiamethoxam

CL - Clothianidin

DF – Delayed fluorescence

MR kinetics - Kinetics of modulated reflection signal at 820 nm

φ_{Eo} - The quantum yield for electron transport

ψ_{Eo} - Probability that an electron moves further than Q_A^-

ABS/RC - Absorption flux per reaction center (RC)

F_V/F_M - The maximal quantum yield of PSII photochemistry

PI_{ABS} - An indicator of plant PSII performance per the absorbed energy.

OEC- Oxygen-evolving complex

Q_A- The primary quinone electron acceptor in PSII

RC - Reaction center

δ_{R0} - Electron acceptor on the PSI acceptor side

φ_{Ro} - The quantum yield of terminal PSI electron acceptor reduction

$P680^+$ - Oxidized primary donor

$P700^+$ - Reoxidation of the plastoquinone pool due to the outflow of electrons to PSI

MV - Methylviologen

DCBQ - Dichlorobenzoquinone

$DCPIPH_2$ – Donating electrons to plastocyanin

Chl - Chlorophyll

PS - Photosystem

PQ - Plastoquinone

Q_B - The secondary quinone electron acceptor in PSII

P700 - Reaction center pigment of PSI

Cyt b/f - Cytochrome b6/f complex

DCMU - 3-(3,4-Dichlorophenyl)-1,1-dimethylurea

O, J, I, P - Particular steps in light-induced Chl fluorescence curve

ETC - Electron transport chain

OLCs – Oxygen-releasing complexes

EPR - Electron paramagnetic resonance

1. Introduction

Neonicotinoids are widely used in the global market to protect crops from insects. Although, neonicotinoids have high insecticidal activity and low toxicity to mammals. There is still damage found to humans and the environment (Hladik et al., 2018). The mode of action of neonicotinoid insecticides is based on interactions with nicotinic acetylcholine receptors (nAChRs) in the insect central nervous system, resulting in insect death. (Ihara & Matsuda, 2018).

In addition to the insecticidal mode of action, neonicotinoid insecticides can also interact with various plant processes such as plant growth, photosynthesis, biosynthetic reactions, and molecular composition to increase or decrease crop yield (Jan et al., 2020; D. A. Todorenko et al., 2021). However, the mechanisms of how neonicotinoids affect pigment are still unknown.

The availability of photosynthesis is crucial for yield: because photosynthesis is an important part of plant metabolism and is sensitive to different ecological factors(S. I. Allakhverdiev, 2020).

Carotenoids are essential pigments for photosynthesis. They are able to absorb the blue-green region of the solar spectrum and transfer the absorbed energy to (bacterial) chlorophyll, thereby expanding the wavelength range of light capable of driving photosynthesis (Hashimoto et al., 2016).

Spectrum methods are powerful tools for studying molecular mechanisms (Aliyeva et al., 2020; X. X. Han et al., 2022). In order to study the molecular mechanism of the action of pesticides on pigments. In this paper, the photosynthetic reaction and conformational changes of the molecules were analyzed by spectrum and other physical methods.

2. Literature Review

2.1 Chloroplast

Chloroplasts are found in green algae and higher plants. It is a plastid that plays an important role in photosynthesis (Finkeldey & Gailing, 2013a). They are organelles in plant cells that contain chlorophyll; since photosynthesis takes place in chloroplasts, they play a vital role in life on Earth. Chloroplasts develop from proplastids, as do chromoplasts, leucoplasts, and other plastids (Finkeldey & Gailing, 2013b). The presence of functional DNA in chloroplasts (chloroplast DNA (cpDNA)) and other plastids is one of the major findings supporting their origin as prokaryotic (cyanobacterial) symbionts during the early evolution of life. Different types of plastids in higher plants contain the same DNA (Stocking & Gifford, 1959).

In addition to biosynthetic pathways such as the synthesis of pigments (chlorophyll and carotenoids), conversion of carbon dioxide to carbohydrates, reduction of sulfur and nitrogen, and other biosynthetic pathways directly related to photosynthesis, several other metabolic pathways exist in chloroplasts. These organelles produce or participate in the production of a range of essential compounds required by other cellular compartments. For example, they are the primary site of biosynthesis of fatty acids, tetrapyrroles, isoprenoids, and amino acids, as well as purines, pyrimidines, and pentoses needed to build nucleic acids. Therefore, in addition to photosynthesis, chloroplasts also play other important roles in the maintenance of the metabolism of the plant as a whole as well as of the cell. The complex and diverse nature of the chloroplast's activities may derive from the fact that the chloroplast was originally a living organism. (Rascio, 2013).

The uniqueness of chloroplasts is based on their ability to use solar radiation to generate metabolic energy equivalents while directing these equivalents with high productivity into a series of anabolic reactions in the chloroplast stroma or exporting them into the cytoplasm and other regions (e.g., sugar passing through the plant Phloem output in). They achieve this by integrating and fine-tuning biophysical and biochemical reactions to create an efficient and self-contained metabolic factory (Fig. 1) (Kirchhoff, 2019).

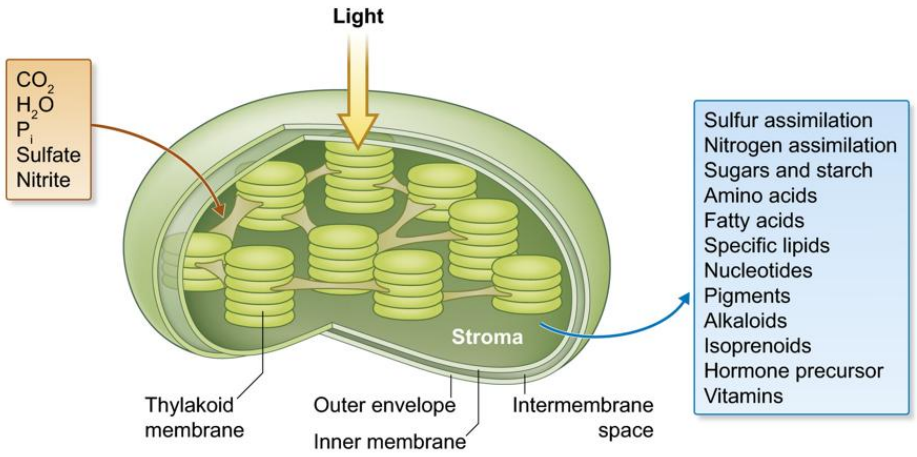

Fig. 1. Overall structure of higher plant chloroplasts and overview about its metabolic competence. The chloroplast takes low-energy components (orange box) and converts them into high-energy metabolites (blue box) by using sunlight energy (Kirchhoff, 2019).

Not only high plants consist of chlorophyll, Chlorophyll and carotenoids of 22 species of dinoflagellates were analyzed by thin-layer chromatography, and chlorophyll c1 and c2 were analyzed using two-dimensional sucrose plates and one-dimensional polyethylene plates. In 19 of these species, polymethine was the dominant carotenoid, while in 3 species fucoxanthin was the dominant carotenoid. In polymethine-containing species, 5 carotenoids are always present, accounting for more than 95% of the total carotenoids. These are dinoflavins (± neodinogens), comprising an average of 64% of the total carotenoids, diazoflavin, diazoflavin, beta-carotene, and a polar, unidentified pink Lutein. The other six carotenoid components are present in small or trace amounts in this species but have not been identified. Two of these are widespread; the other 4 are restricted to one or two species (Jeffrey et al., 1975).

Rigorously reducing the complexity of excitation transport in PSII in the presence of weak quenching, the process consists of thousands of rate constants down to a single parameter: the excitation diffusion length (LD) in the antenna. In response to fluctuating light intensities, qE acts as a "tap" that adjusts the excitation flux through the excitation diffusion length to open the

RC were found. Interactions between qE and open RCs leading to sterically heterogeneous competition were found. Mechanisms linking excitation transport and quenching in proteins to Chl fluorescence and PSII light harvesting will become particularly valuable (Bennett et al., 2018).

2.2 Photosynthetic pigments

Photosynthetic pigments are colored substance that absorbs visible radiation. There are many kinds of photosynthetic pigments: carotene, Xanthophyll, Phaeophytin a, Phaeophytin b, chlorophyll a and chlorophyll b (Sharp, 2015The main role of chlorophyll a and b is to convert the energy of sunlight into chemical energy (Rys et al., 2014).

Carotenoids are a ubiquitous group of natural pigments. Carotenoids have shown potent antioxidant properties which have abundant conjugated double bonds. (Krinsky, 1989; Terao, 1989) Not only fruits and vegetables are rich in carotenoids, but also in animals. Plasma carotenoids and adipose carotenoids have been considered to reduce or monitor the risk of cardiovascular disease (Street et al., 1994; Wang et al., n.d.). More than 750 carotenoids have been reported and are widely synthesized in photosynthetic organisms, some non-photosynthetic prokaryotes, and a few animals (Takaichi, 2011).

Carotenoids are usually divided into two groups: 1) xanthophylls an oxygen-containing carotenoid derivative containing oxygen atoms, including lutein, violaxanthin etc (Fig. 2) (Britton et al., 2004).; and 2) carotenes a type of non-oxygen-containing hydrocarbons that include α-carotene, lycopene, and β-carotene.(Giorio et al., 2007). Many carotenoids have vitamin A activity, with beta-carotene having the highest vitamin A activity. Carotenoids that do not have vitamin A activity, are known as non-vitamin A carotenoids, such as lutein. (Toti et al., 2018).

Carotenoids, like chlorophyll, are essential pigments for photosynthesis and play a role in the photosynthetic system by combining with peptides to form pigment-protein complexes in vesicle-like membranes. In the non-photosynthetic organs of photosynthetic organisms, carotenoids act as photoprotectants, antioxidants and precursors of synthetic plant hormones to maintain their normal life activities. Carotenoids are precursors for the production of vitamin A in

animals and are of great research value in the biomedical field and the food industry due to their antioxidant properties (Armstrong, 1997).

Carotenoids have long chains of conjugated double bonds, with a central double bond that has almost bilateral symmetry. Common carotenoids include lycopene (containing a C40 ($C_{40}H_{56}$) tetraterpene structure consisting of eight isopentenyl pyrophosphate (IPP) units) and its derivatives α- and β-carotene, and lutein cetin, zeaxanthin and astaxanthin. The covalent polyene structure in the carbon skeleton of carotenoids is not very stable, and photochemically-guided oxidative cleavage will occur under certain conditions, resulting in a large number of cleavage products. This property also allows the introduction of oxygen to the terminal groups and cyclization, which gives the different carotenoids their antioxidant properties and distinctive colors. (Armstrong, 1997; Britton, 1995; Lichtenthaler, 1999).

The conjugated double-bond structure of carotenoids exhibits strong reducing properties by facilitating electron transfer in redox reactions. This enables carotenoids to scavenge reactive oxygen and nitrogen produced during the metabolism of organisms, making them excellent antioxidants. β-carotene and lycopene can increase vascular NO bioavailability, significantly reduce nitric oxide inactivation and inhibit ROS production and nitrotyrosine (ONOO-) formation. This has a positive effect on maintaining vascular oxidative imbalance and inflammation associated with cardiovascular disease (CVD). Lycopene also reduces oxidative damage to DNA, making it a promising cancer therapy (di Tomo et al., 2012; Khachik et al., 2002; Obermüller-Jevic et al., 1999; Omenn et al., 1996).

Zeaxanthin and lutein have been identified as the xanthophylls that constitute the macular pigment of the human retina. The relative concentration of lutein to zeaxanthin in the macula is distinctive (Tanumihardjo, 2013). Zeaxanthin is a natural lutein-carotenoid found in plants, algae and microorganisms that plays an important role in the prevention of age-related eye diseases such as macular degeneration and cataracts, and is also used in the food, pharmaceutical and nutraceutical industries for its powerful antioxidant and anti-cancer properties. (Zhang, Liu, et al., 2018).

Isopentenyl pyrophosphate (IPP) and dimethylallyl diphosphate (DMAPP) are biological precursors of carotenoids. They are produced via two biosynthetic pathways: methyl pentaerythritol-4-phosphate (MEP) which occurs in plant organelles and fungi and mevalonate

(MVA) which occurs mainly in plant cytoplasm and bacteria. Because carotenoid synthesis and accumulation occur mainly in the plastids, carotenoids in higher plants are synthesized via the MEP pathway (Rodríguez-Concepción, 2010). (C. Li et al., 2020; T. Sun et al., 2022; Z. Sun et al., 1998).

It was demonstrated that Arabidopsis CYP97A3 encodes a fourth carotenoid hydroxylase whose in vivo activity is directed primarily against the β-loop of α-carotene and secondarily against the β-loop of β-carotene. The Cyp97 allele, lut5-1, resulted in the accumulation of α-carotene to levels comparable to those of wild-type β-carotene and its stable adulteration of the photosynthesis system, while conversely the β-carotene-derived lutein was reduced by 35%. LUT5-1 still produced 80% of wild-type lutein levels, suggesting that at least one other carotene hydroxylase could partially compensate for the loss of CYP97A3 activity. A model proposed by (J. Kim & DellaPenna, 2006)for the preferred pathway of lutein synthesis in plants: β-ring hydroxylation of α-carotene by CYP97A3 to produce zeaxanthin, followed by ε-ring hydroxylation of zeaxanthin by CYP97C1 to produce lutein (Fig. 3).

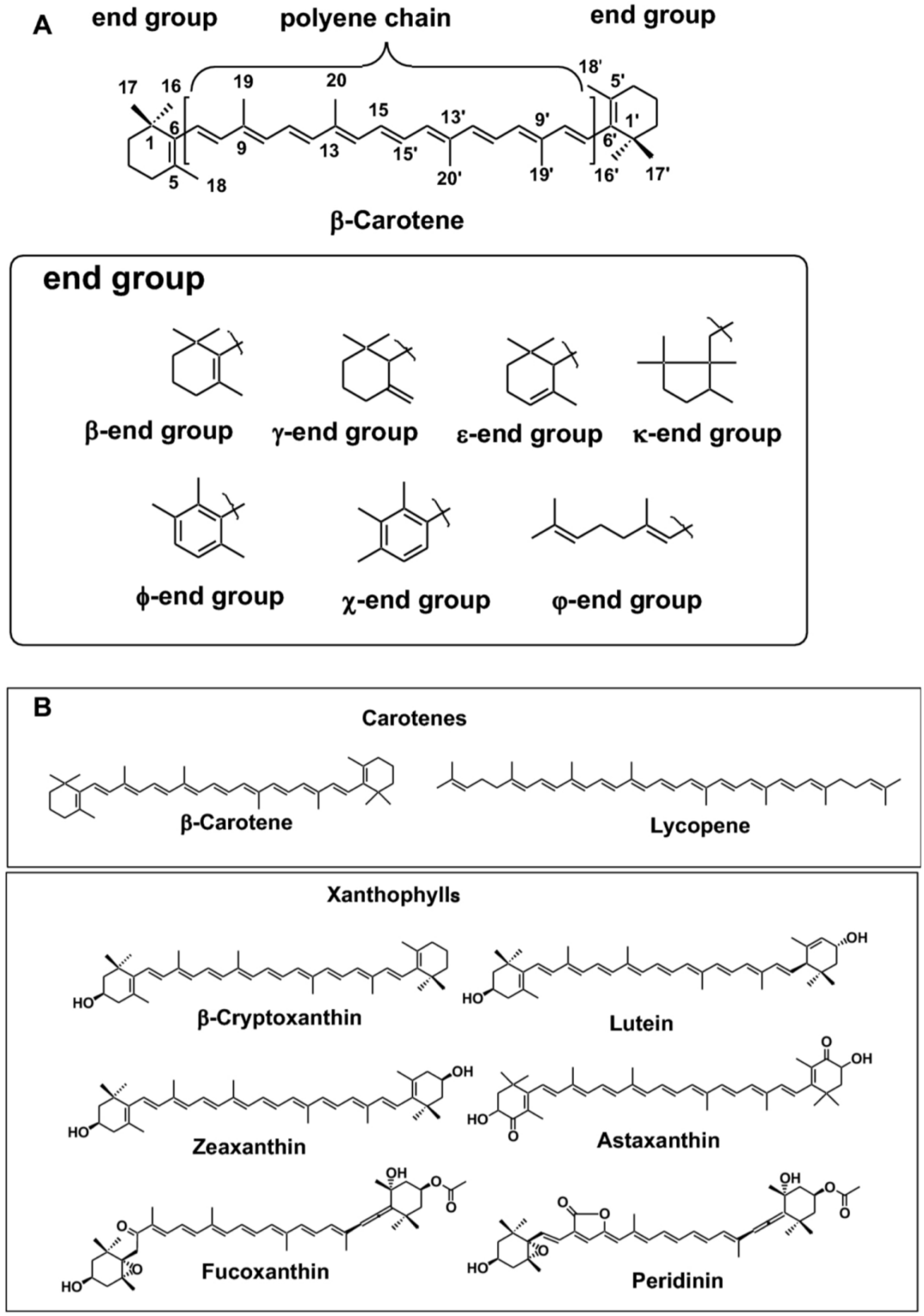

Fig. 2. A) Structures of carotenoids and end groups. B) Structures of typical carotenes and xanthophylls(Maoka, 2020)

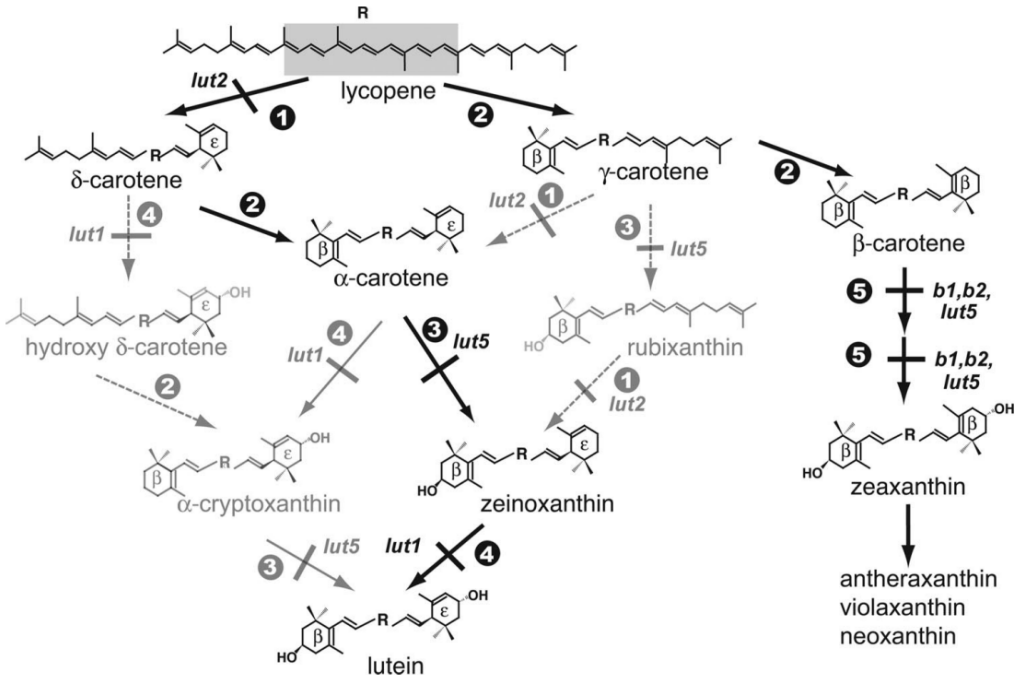

Fig. 3. Pathway showing all possible routes to xanthophyll synthesis in Arabidopsis.(J. Kim & DellaPenna, 2006)

The core pathway of carotenoid synthesis is described as the following three major steps: (i) synthesis of phenyl pyrophosphate and formation of dimethylallyl pyrophosphate, (ii) synthesis of geranyl pyrophosphate, and (iii) carotenoids themselves. This pathway responds to differences in several carotenoid organisms and provides an evolutionary perspective (Alcaíno et al., 2016).

The intake of carotenoids with vitamin A activity is particularly important for organisms that cannot synthesize carotenoids directly from scratch. It is widely available in vegetables and fruits. Retinol is synthesized as a precursor to vitamin A-active carotenoids and plays a crucial role in cellular differentiation and visual development. (Olson, 1996).

Epidemiologic and biological studies have long been conducted to investigate and understand the role of carotenoids in the prevention and treatment of chronic human diseases. Some bone-related diseases are also related to oxidative stress, such as osteoporosis. Carotenoids include beta carotene, and lycopene may counteract the associated effects of oxidative stress through its antioxidant properties. Studies have shown that people with osteoporosis have relatively low levels of antioxidant vitamins and enzymes, while carotenoids have shown

promising value in minimizing disease risk of bone and preventing osteoporosis (L. Kim et al., 2003; Melhus et al., 1999; PARK et al., 1997; Rao et al., 2003).

In addition, β-carotene has been shown to have a direct effect on ovarian function, and the concentration of β-carotene in the ovary of dairy cows is directly related to its fertility. Supplementing dairy cows with beta-carotene has been proven to have a positive impact on the commercial value of livestock production (Kaewlamun et al., 2011; Marcek et al., 1985).

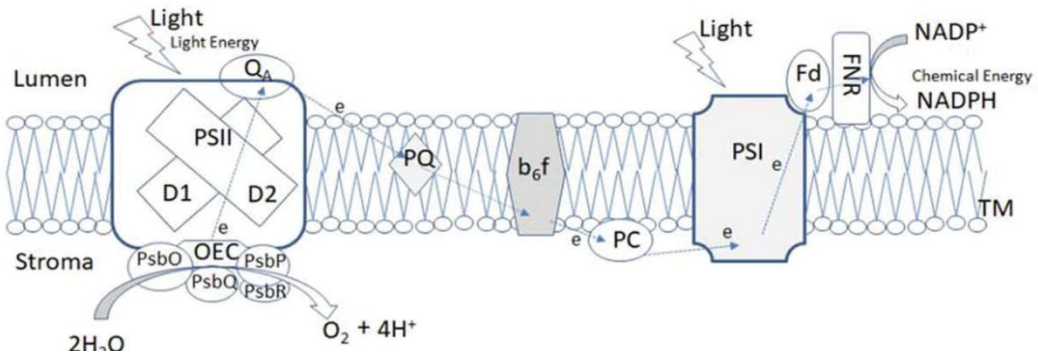

Fig. 4. Distribution of different proteins of the photosynthetic apparatus embedded in thylakoid membranes. Systematic scheme for conversion of light energy into chemical energy via photosynthetic electron transport chain between PSII and PSI (Gupta, 2020).

OJIP curve is widely used to study PS. In the dark-adapted state, all photosynthetic reaction centers are in a relaxed state, which means that the ground state is filled with electrons. Simultaneously, the electron transport chain between PSII and PSI is also in a relaxed state. This means that the free plastoquinone (PQ) pool behind the plastoquinone A (Q_A), plastoquinone B (Q_B) and PSII reaction centers is completely oxidized. In this so-called "open" (O) state (=F_0), the fluorescence quantum yield of the system is small, with "O" standing for "origin" (minimum fluorescence) and "P" for "peak" (maximum fluorescence), J and I represent the inflection points between O and P levels. Furthermore, Fo is the fluorescence intensity at the “O” level, while Fm is the intensity at the P level, and Fv (Fv =Fm−Fo) is the variable fluorescence. Because an incident photon has the greatest chance of inducing charge separation at one of the reaction centers. When the photosystem begins to receive light, charge separation will occur and electrons will be transferred to the PQ cell via Q_A and Q_B. This will increase the fluorescence quantum yield, since further incident photons are no longer readily accepted by the partially saturated

electron transport chain. The "J" state of fluorescence kinetics has been reached when the majority of electrons in the leaf's individual reaction centers have reduced the Q_A molecules at these reaction centers. The next level "I" of fluorescence quantum yield is reached when Q_B is also reduced. When the PQ pool reaches its reduction peak, the fluorescence quantum yield also reaches its peak, the "P" level (Khan et al., 2021; Schansker et al., 2014).

2.3 Neonicotinoid pesticides

In recent decades, there has been more and more use of pesticides. Intensive use of pesticides can lead to affect non-target host plants in many ways. Neonicotinoid insecticides are a class of insecticides that act through specific actions on neuronal nicotinic acetylcholine receptors (nAChRs) (Ford & Casida, 2006). Neonicotinoid insecticides have high insecticidal activity and low mammalian toxicity, but neonicotinoid insecticides have limited insecticidal activity and high mammalian toxicity. In the mid-1980s, Bayer of Germany successfully developed the first neonicotinoid pesticide, imidacloprid, which has a novel mode of action, strong toxicity, high efficiency, broad-spectrum, and good environmental compatibility, and attracted people's attention immediately after its introduction. Some large foreign pesticide companies have entered the research field of synthesizing nicotine analogs, making neonicotinoid pesticides a hotspot for research and development (Hermsen et al., 1998; Yamamoto et al.,1995, 1998)

The success of these insecticides is attributed to this mechanism of action, as they act as potent agonists of insect nAChRs with low affinity for vertebrate nAChRs, thereby reducing the potential risk of toxicity and improving safety in non-target species. However, although neonicotinoids are considered safe, their presence in the environment may increase the risk of exposure and toxicity.

In general, juvenile exposure to neonicotinoid insecticides alters proper neuronal development, leading to reduced neurogenesis and altered migration, and induces neuroinflammation. In adulthood, neonicotinoids cause neurobehavioral toxicity, and these effects are associated with their modulation of nAChRs, resulting in neurochemical changes. These changes included reduced expression of nAChRs, altered acetylcholinesterase activity,

and marked changes in the function of the nigrostriatal dopaminergic system. All of these effects lead to the activation of a series of intracellular signaling pathways that generate oxidative stress, neuroinflammation and ultimately neuronal death. Changes in nAChR function induced by neonicotinoids may be responsible for most of the effects observed in different studies. Costas-Ferreira & Faro, 2021)

The selectivity of neonicotinoid insecticides is due to the differential binding of these molecules to their target sites (nicotinic acetylcholine receptors), which is stronger in insects than in vertebrates (Casida & Durkin, 2013; Tomizawa & Casida, 2003). The nicotinic acetylcholine receptors of the neuroexcitatory cholinergic system are targets of nicotine and neonicotinoid insecticides in insects and mammals. Nicotinic acetylcholine receptors regulate the flow of Na^+ and K^+ through neuronal postsynaptic membrane channels (Hogg et al., 2003). Acetylcholine opens and closes channels to maintain a dynamic ratio of intracellular to extracellular Na^+ and K^+ concentrations, which is required to initiate electrical signalling in postsynaptic neurons. Both nicotine and neonicotinoid insecticides act as agonists of the nicotinic acetylcholine receptor - the Na^+/K^+ ionophore (Seifert, 2014a). Structural differences between insect and mammalian receptors determine selectivity for neonicotinoid insecticide toxicity in insects and nicotine toxicity in vertebrates (Matsuda et al., 2005). The proposed concept of the neonicotinoid electronegative pharmacophore model takes into account the presence of a positively charged site unique to insect receptors that specifically interact with the negatively charged tip of the neonicotinoid spacer, And the protonation of nicotinic nitrogen at physiological pH is the determinant of their strong binding to vertebrate receptors. It also negatively affects their penetration into the insect's central nervous system compared to non-ionized and more hydrophobic neonicotinoid insecticides (Seifert, 2014b).

Stress induced by pesticides on nontarget organisms can lead to elevated levels of reactive oxygen species (ROS) that can have detrimental effects on biochemical activities, cellular metabolism, and other physiological activities (Kouzmanova & Allakhverdiev, 2014; Shakir et al., 2018).

Neonicotinoids target the cholinergic system within the central nervous system (CNS) of insects. However, in mammals the cholinergic system exists in both the peripheral nervous system (PNS) and the CNS (I. Yamamoto & J.E. Casida, 1999).

(C. K. Jones et al., 2011)

The persistence, metabolism, and uptake of all seven neonicotinoid insecticides varied in spinach seedlings, suggesting that neonicotinoid insecticides have different chemical properties. When spinach seedlings were hydroponically treated with each of the seven neonicotinoids, metabolites identified in leaves indicated nitro reduction, cyan hydrolysis, sulfoxidation, demethylation, imidazolidine, and thiazolidine Hydroxylation followed by olefin formation, oxadiazinane hydroxylation and ring opening, and chloropyridyl dichlorination(Ford & Casida, 2008)

Based on our findings on the effect of acetylcholine on wheat protoplast expansion and leaf section unfolding in primary wheat, it is proposed that ACh affects protoplast expansion and leaf unfolding through mAChR and nAChR. like animal cells.(Levey, 1996; Takahashi, 2019). The mAChRs might be associated with a phosphatidyl-inositol-dependent pathway(Antonsson, 1997; Hokin, 2003). This leads to the opening of Ca^{2+}- channels, and nAChR is independent of phosphatidylinositol. The similarity between the roles of ACh via mAChR and R via phytochrome in protoplast expansion and leaf unfolding suggests that they share a common signaling pathway (Tretyni et al., 1992).

The maximum concentrations of clothianidin and its chemical analogue thiamethoxam in surface waters were found to be 3 and 22μg/L, respectively(T. A. Anderson et al., 2013; Morrissey et al., 2015). Although 55.7 μg/L of CL and 63.4 μg/L of TMX were found in puddles formed on the surface of corn fields(Samson-Robert et al., 2014). There are research shows that different maize has different uptake of pesticides (Mörtl et al., 2020). Pesticide also has influence on gene expression (House et al., 2021).

2.4 Using Raman spectroscopy to investigate pigment structure and activity

Raman spectroscopy is in honor of Indian physicists Sir C.V. Raman and K.S. Krishnan (Louden, 1989). With the advancement of CCDs the performance of detectors improved for Raman spectroscopy (RS). (Neuville et al., 2014).

Raman scattering is the inelastic scattering of light radiation on molecules of matter that is accompanied by a significant change in radiation frequency (Jayasooriya & Jenkins, 2002; R. R. Jones et al., 2019). Molecules of matter polarize and scatter light under the combined influence of ultraviolet, visible, or near-infrared light. In the case of Raman scattered light, in contrast to Rayleigh scattering, spectral lines not found in the spectrum of the excitation light appear in the spectrum of the scattered light, and these spectral lines differ by an amount from the frequency of the initial radiation source (Hanson et al., 2016; Yu et al., 2019). The molecular structure of the material determines the number and position of the lines that arise, allowing you to accurately identify the sample. Since the bands of RS characterize the vibrations of chemical bonds and the geometry of scattering molecules, RS is widely used to estimate conformational changes in molecules of interest (Schneider, 2004).

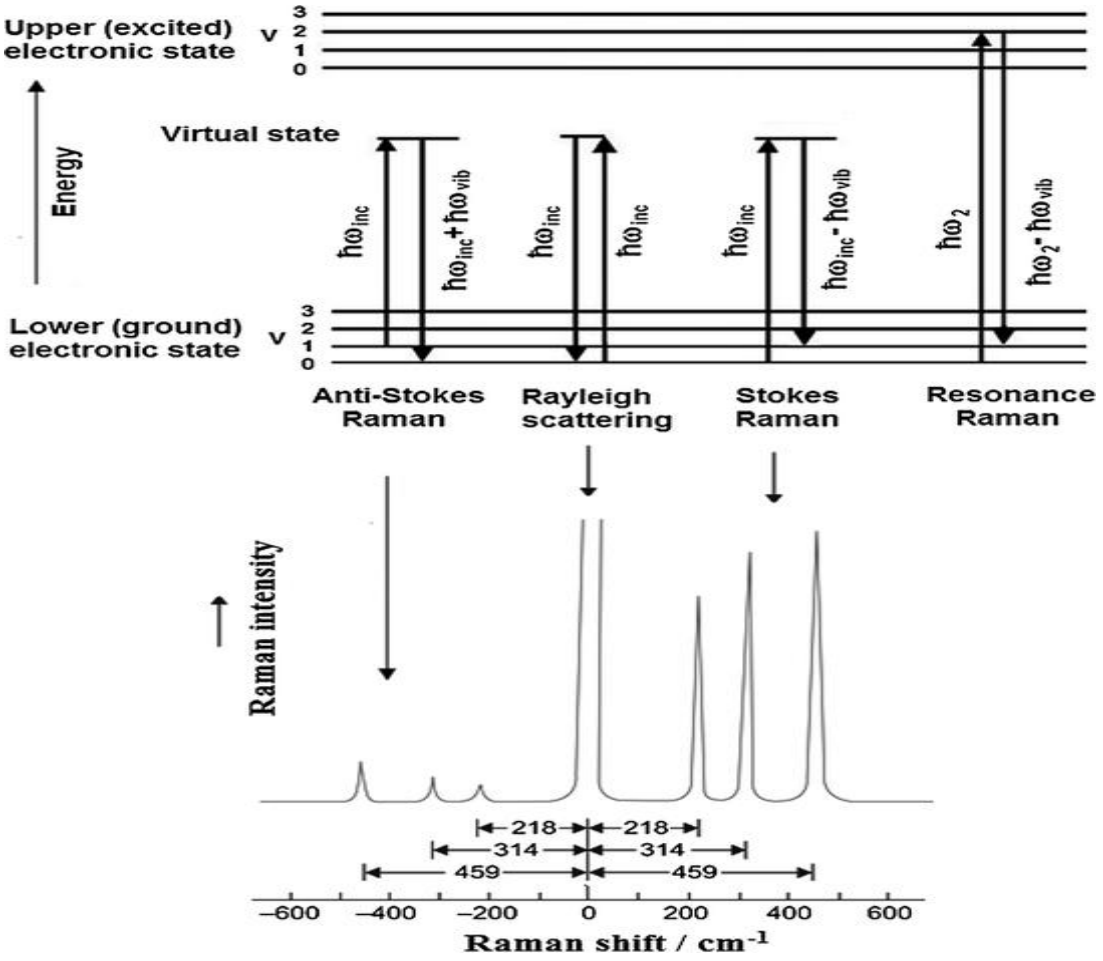

Fig. 5. Simplified Jablonski diagram illustrating the Rayleigh, NRS and RRS processes and corresponding Raman spectrum of CCl_4, v–the vibrational quantum numbers (Prochazka, 2016).

Raman scattering of light is based on further changes in the wavelength of light emitted from a sample and the interaction of monochromatic laser irradiation with matter (Y.-S. Li & Church, 2014; Prochazka, 2016). RS takes place due to the movement of electrons in the molecule and the vibration of the atom's nucleus (Zhang, Sun, et al., 2018). The field in which the electron cloud resides depends on the relative positions of the nuclei. At this point, the structure of the nucleus depends on the ability of the electron cloud to deform under electromagnetic waves and electric fields, while the structure of the nucleus changes with frequency when vibrated within the molecule (Fr et al., 1987). Molecular nuclei can oscillate as electron clouds deform (Kalukula et al., 2022). RS changes the wavelength of incident light due to the excitation of molecules, and the molecules jump from an initial energy level n to a virtual energy level m. RS differs from Rayleigh scattering in that Rayleigh scattering returns the molecule to the initial energy level when the molecule switches, whereas Raman scattering enters another vibrational state I with a different energy (Erasmus & Comins, 2019).

There are the following types of Raman scattering:

In the Raman spectrum of carotenoids, the following bands have the highest intensity i.e. characteristic bands:

1. Peak at 1527 cm^{-1} indicates the telescoping vibration of the conjugated double bond C = C near the center of the hydrocarbon chain. It shifts to higher frequencies when the configuration of the trans-cis position of the molecule changes. The larger the spectral shift the closer the cis position of the bond is to the center of the molecule (Finkelshtein & Shamsiev, n.d.);

2. Peak at 1156 cm^{-1} represents the υ(C-C) and υ(C-C) homo-phase stretching vibrations of the polyene chain(Qin et al., 2011);

3. Peak at 1190 cm^{-1} characterization of carotenoid 15-cis conformational changes;

4. Peak at 1009 cm^{-1} characterization of C-CH_3 stretching vibrations coupled to C-C stretching modes or with C-H in-plane bending (Grudzinski et al., 2016);

5. Peak at 960 cm^{-1} characterizes out-of-plane C–H modes (Prinsloo et al., 2004);

Since Raman spectroscopy is a non-destructive in vivo research method, it can be used to analyze living cells, spores, bacteria, tissues, viruses and single biomolecules. In the early 1990s, RS was used for the first time to study the interaction of an antibiotic (doxorubicin) with DNA and to analyze living cells as well as the introduction of colloidal nanoparticles into cells via

endocytosis. At present, the introduction of nanoparticles into cells is still the most widely used approach (Gorelik et al., 2014).

Raman spectroscopy is a promising method for rapid diagnostic and non-destructive analysis of samples with different properties because of its high sensitivity. Most remote sensing studies have an applied character, which indicates that their results have great application potential in analytical practice. High-priority areas for RS research include biological systems at different tissue levels (cells and organelles, erythrocytes, bacteria, viruses, human cells of all types, including diseased cells, especially malignant tumors), pharmaceuticals, food and environmental objects. (Olivo & Dinish, 2015).

Raman spectroscopy combined with advanced statistical analysis forms a single universal method that is reliable, cost-effective, non-invasive, and allows early diagnosis of all forms of cancer (Ralbovsky & Lednev, 2020). As a rapid, label-free, non-destructive analytical measurement requiring little sample preparation, RS shows great promise in liquid biopsy cancer detection and diagnosis by fusing each patient's plasma and saliva Raman spectra Together, the follow-up analysis model provided impressive sensitivity, specificity, and accuracy of 96.3%, 85.7%, and 91.7%, respectively. The results further confirmed that the metabolites differing by Raman spectroscopy were the same as those modeled by mass spectrometry, harmonizing the Raman spectroscopy and mass spectrometry models and validating the potential ability of RS to assess metabolite composition. This research enhances the relevance of Raman spectroscopy to provide added value by probing the unique chemical composition of biological fluid sources (Koster et al., 2022).

Uncontrolled cell proliferation during malignant transformation of cells and tissues increases the production of DNA, RNA and proteins and disrupts lipid metabolism. These changes, at the biochemical level, occur much earlier than the onset of clinical symptoms. Therefore, Raman-based methods can be used to detect alterations in molecular features, and Raman spectroscopy can be used as a biomarker map for early disease classification and tumour grading. In addition, since RS does not require extensive sample preparation or labelling, this information can be obtained without destroying the material and can be subjected to additional processing and analysis after acquisition, which in the case of cancer diagnosis is essential to create a complete picture of a single tumour (Hanna et al., 2021).

Surface-enhanced Raman scattering (SERS) is a suitable tool for new technologies because of its high sensitivity and low loss. SERS materials modified with DNA aptamers provide specificity for SERS biosensors. Existing SERS-based nanosensors for rapid virus detection are either not suitable for quantitative assays, or have complex structures and are expensive to implement. Herein, a colloidal solution-based SERS nanosensor is presented that combines the rapidity and specificity of the quantitative assay of the SARS-CoV-2 virus, distinguishing it from other respiratory viruses (Zavyalova et al., 2021). In our work, we will propose a method for recording the SERS of carotenoids using nanosensors made of silver colloids.

2.5 Maize studied by spectroscopy methods

One of the tasks of our research will be to identify the molecular characteristics of pigments in genetically modified plants, which is important for diagnostics and selection. The period from 1954 to the present has been characterized by great success in maize breeding and the production of high-quality hybrid seeds, resulting in more than 1,500 cereal and silage hybrids (Fehr, 2015). Process prerequisites and modern technologies for the efficient production of hybrid maize seeds, breeding work and mass production of commercial and silage hybrid seeds (Bulut et al., 2019).

In the context of said developments, many scientific disciplines (physiology, biochemistry, biophysics, biotechnology, breeding, spectroscopy) have been linked to the objective of modernizing and effectively implementing contemporary maize breeding and seed production programs. The interdependence between research production and practical use and food science has been linked to the objective of modernizing and effectively implementing contemporary maize breeding and seed production programs. (Radenovic et al., 2016, 2021, 2023). Alongside the outstanding results achieved in the selection and breeding of standard cereals and maize silage hybrids, there is an urgent need to improve the chemical composition of cereals to produce new inbred lines and better quality maize hybrids, especially in terms of essential bioactive compounds. In addition, a great deal of work has been done to improve and develop methods for the conservation of maize hybrid plants in new whole plant and grain silage forms. Silage is plant-derived feed that has undergone biological fermentation or chemical preservation. Silage corn growing methods differ somewhat from commercial corn growing methods. It is important

to produce the maximum amount of silage of high quality per unit area. Today, silage is the basis for cost-effective modern animal husbandry. (Bulut et al., 2019).

Using near-infrared to classify haploid and diploid seeds and distinguish haploid, double haploid, and diploid plants from different genotypes used as donors. Diploid, haploid, and diploid plants from 34 source populations were evaluated and differentiated. Spectral data were collected from all seed and leaf samples using a portable Micro-NIR device. The data were then preprocessed by principal component analysis and partial least squares discriminant analysis (PLS-DA). The method enables the classification of haploid and diploid seeds as well as haploid, diploid and diploid plants with 100% accuracy, constituting a fast, simple, Non-destructive and reliable method for haploid identification in maize, and more efficient than visual analysis (Rodrigues Ribeiro et al., 2023). Near-infrared spectroscopy data are useful tools for predicting maize kernel yield and have shown promising results in evaluating genetically independent breeding populations (Lane et al., 2020).

Near-infrared and visible hyperspectral imaging has been extensively studied for detecting various internal and external qualities of corn. Near-infrared hyperspectral imaging can be effectively used to accurately detect kernel firmness (>62%), seed variety classification (83-94%), and fungal infestation (91-95%) of corn kernels (Rathna Priya & Manickavasagan, 2021).

Raman technology is a robust, non-invasive, biochemically selective phenotyping technique that can distinguish not only the level of drought tolerance of genetically diverse genotypes but also the near-isogenic level of drought tolerance. The robustness of this technique is that it can be performed on two-week-old seedlings and requires as little as a week without water. Climate change increases the likelihood of short-term drought stress occurring under natural field conditions in most parts of the world. Therefore, the use of this technique could speed up the breeding process in many areas that do not otherwise offer reliable drought stress conditions. Furthermore, this in vivo phenotyping technique provides a fast and accurate method to select drought-tolerant genotypes (Altangerel et al., 2021). The first and key step in planting is the determination of seed variety and quality, which affects the yield and quality of grain. Therefore, the identification of seed varieties is of great significance. Raman spectroscopy has a significant effect on identifying the variety of seeds (Liu et al., 2022).

2.6 Investigation using Multi-Function Plant Efficiency Analyzer

As methods that allow us to study changes in the molecular structure and function of pigments in whole tissues (leaf, seed) directly for diagnosing plants in the field, we used not only the new Raman method, but also proven fluorescent methods. Multi-Function Plant Efficiency Analyser is an advanced lab-based system for investigation of plant photosynthetic efficiency which combines high quality fast fluorescence kinetic and P700+ absorbance studies with ground-breaking Delayed Fluorescence (DF) measurements providing one of the most comprehensive systems for the investigation of plant photosynthetic efficiency available. The M-PEA is a laboratory-based measurement system consisting of a control unit and a precise, robust sensor unit housing all optical emitters and detectors for all measuring elements. The M-PEA-1 sensor unit includes a high-intensity red actinic light source, a far-red light source, an instant fluorescence detector, and a modulated emitter/detector pair for P700+ absorbance measurements. The M-PEA-2 also includes a high-sensitivity delayed fluorescence detector and a detector for measuring leaf absorbance.

It is possible to analyze the physiological state of the photosynthetic machinery in vivo by detecting the parameters of JIP based on rapid recordings of chlorophyll fluorescence. Decreased photochemical efficiency, increased non-photochemical dissipation and reduced number of active photosystem II (PSII) reaction centers were observed in most of the nutrient-deficient samples. By using M-Pea, nutrient deficiencies in corn and tomato plants can be identified. (Kalaji, Oukarroum, et al., 2014)

Nine short-term independent studies of two M-PEA units were performed on several plant species with different functional traits and exposure to different kinds of abiotic stresses. The study examined the consistency of plant responses with three sets of simultaneously measured signals: delayed fluorescence, delayed fluorescence, and modulated reflectance of 820 nm light. A decrease in F_V/F_M and an increase in F_0, V were the most common responses associated with PF parameters. Principal component analysis (PCA) revealed that the combination of PF and MR parameters is a powerful tool for plant stress phenotypes, while MR parameters are associated with different functional group-related physiological strategies to cope with stress factors (Salvatori et al., 2014).

2.7 Infrared spectroscopy

Infrared (IR) spectra is a new type of technology that can detect the chemical structure of the material that wild use in chemical experiments. Lately, it's also been used on biological structure detection. IR technology is highly energy efficient consumes less water and is environmentally friendly compared to conventional heating. In addition, it is also reduced heating time, uniform heating, reduced quality losses, versatile, simple, and compact equipment, and significant energy saving (Aboud et al., 2019; Rastogi, 2012a).Infrared technology is more energy-efficient, less water-consuming and environmentally friendly than traditional heating methods. In addition, infrared technology is characterised by high heat transfer rate, short heating time, uniform heating, low energy consumption, good product quality and food safety. (Aboud et al., 2019).

The current challenge for feeding a growing population that would almost reach 10 billion over next 30 years is creating the need to improve existing crops and develop new crops with even higher yielding, more nutritious, and with climate change resilient characteristics (Hickey et al., 2019a).

The composition of corn in terms of primary metabolites with major nutritional importance (proteins, carbohydrates, fat) along with the mineral composition has been shown to be comparable or even better than common cereal crops such as rice and wheat. (Ranilla, 2020)

Ensuring the quality and safety of the use of botanicals and supplements requires effective and accurate analytical methods. Infrared spectroscopy has been applied to the quantitative analysis of compounds in complex matrices such as phytopharmaceuticals and chemometrics-supported supplements. Impact of spectral pre-processing and variable selection on the quantitative analysis of phytochemicals and adulterants in plant-based drugs and supplements using infrared spectroscopy. Selected quantitative analytical studies of plant-based drugs and supplements using spectral pre-processing techniques and variable selection for processing data analysis(Junaedi et al., 2021).

In the near infrared spectrum, light can penetrate biological tissues and be absorbed by chromophores such as oxyhaemoglobin and deoxyhaemoglobin. Oligochannel fNIRS is sufficient to estimate overall brain function, and it has become an important tool for assessing

cerebral oxygenation and autoregulatory function in stroke and traumatic brain injury patients in the intensive care setting. Multi-channel near-infrared spectroscopy has improved the spatial resolution of fNIRS for mapping the brain in certain task modalities such as language mapping. Advances in signal processing technology have shifted fNIRS towards individual clinical applications for the detection of certain types of seizures, assessment of autonomic function, and cortical spreading inhibition(Chen et al., 2020).

2.8 Density functional theory (DFT) calculations

During the first few decades of applying quantum mechanics (QM) calculations in vibrational spectroscopy, they were limited by the level of Har Three-Fock calculations, leading to considerable deviations in calculated and experimental frequencies. The emergence and rapid development of density functional theory (DFT) approximation methods have increased the practical application of QM calculations in vibrational spectroscopy of polyatomic molecules.(Baiz et al., 2020; Yagi et al., 2019). Relatively simple tools such as Hartree-Fock levels or standard DFT type calculations have had good success at comparative levels. The advent of new methods for density flooding has increased the number of vibrational spectra that can be calculated with appropriate accuracy (Baseden & Tye, 2014). Most commonly used density functions require the use of special so-called scaling factors (correction coefficients) in order to maintain good agreement between theoretical and experimental frequencies (Sim et al., 2022). At the same time, the development of different density functional models has produced suitable approximations, resulting in theoretical frequencies that can be used without any corrections (Su & Xu, 2017).

The article presents a method for simulating Raman spectra of defective materials based on a combination of empirical potentials and first-principles calculations. Empirical potentials are used to estimate the vibrational modes of the flawed system, which are then combined with Raman tensors estimated from first-principles calculations. This approach not only enables reliable simulation of Raman spectroscopy, but also provides insight into the physics of vibrational modes in defect systems and how they can be probed with Raman spectroscopy (Kou et al., 2020). Combine DFT calculation and Raman spectroscopy is good to understand the

structure of different objects (Giese & McNaughton, 2001a, 2001b). DFT is also used to study IR spectroscopy and other technics (Choudhary et al., 2020; Raczyńska et al., 2005).

2.9 General aim

The aim of the work was to study the molecule mechanisms of neonicotinoids insecticide on photosynthetic pigments of chloroplast and different genotypes maize. In this study, it is planned to use efficient optical methods (Raman spectroscopy, IR spectroscopy, AFM, EPR and fluorimetry) to determine the molecule mechanisms of specific pesticides on pigments molecular structure and function.

We assume that the data obtained can be used to form a technology for testing the pollution of plants and distinguishing responses of plants of different genotypes to pollution.

The aim of the work was to study the molecular mechanisms of the effect of neonicotinoid insecticides (TMX, and its derivative, CL) on the molecular structure and functions of photosynthetic pigments of various corn genotypes (inbred corn line zppl 225 and hybrid line zp 341).

To achieve the goal of the work, the following tasks were set:

1). To investigate the content and functional properties of plant leaf pigments using Raman spectroscopy, IR spectroscopy, AFM, EPR and variable chlorophyll fluorescence ("JIP test").

2) To investigate the molecular properties of leaf pigments exposed to pesticides on the whole plant (spraying the leaves and applying the pesticide to the soil);

3) To investigate the effect of the TMX derivative, CL on the molecular structure of pigments (chlorophyll, carotenoids) in chloroplasts, as well as on the morphology of the chloroplast, the viscosity of the membrane and the generation of ROS.

4) To investigate the role of the molecular structure of pigments in the formation of resistance to the action of pesticides in various genotypes of corn.

5) To develop additional experimental and theoretical approaches to study the conformation of pigment molecules of various corn genotypes (inbred corn line zppl 225 and hybrid line zp 341) using IR and Raman spectra (SERS).

3. Materials and Methods

3.1 Plant growth of maize

For germination, 60 maize seeds (*Zea mays L.*, Institut za kukuruz "Zemun Polje", Belgrade, Serbia) were selected for planting. Followed by treatment with 3% hydrogen peroxide solution for 30 min, the seeds were rinsed with running water and fixed on gauze without touching each other and water was placed under the gauze to keep the seeds moist and without touching each other (at room temperature of 25°C) until the seeds took root and then they were planted in the soil (1:1 mixture of vermiculite and black soil) under a constant temperature of 25°C in the presence of 24 hours of sunlight. Each seed was then sown into the soil (1:1 mixture of vermiculite and black soil) under 24 hours of sun at a constant temperature of 25°C.The scheme of the experiments shows as Fig. 6. TMX [5-methyl-3-(2-chlorothiazol-5-ylmethyl)-1,3,5-oxadiazinane-4-ylidene-N-nitroamine] were performed on different period of plant growth. TMX(a) and TMX (d) were performed on maize seed irrigation (day 4); TMX(c) and TMX(d) were performed on 3rd leaf appearance (day 8).

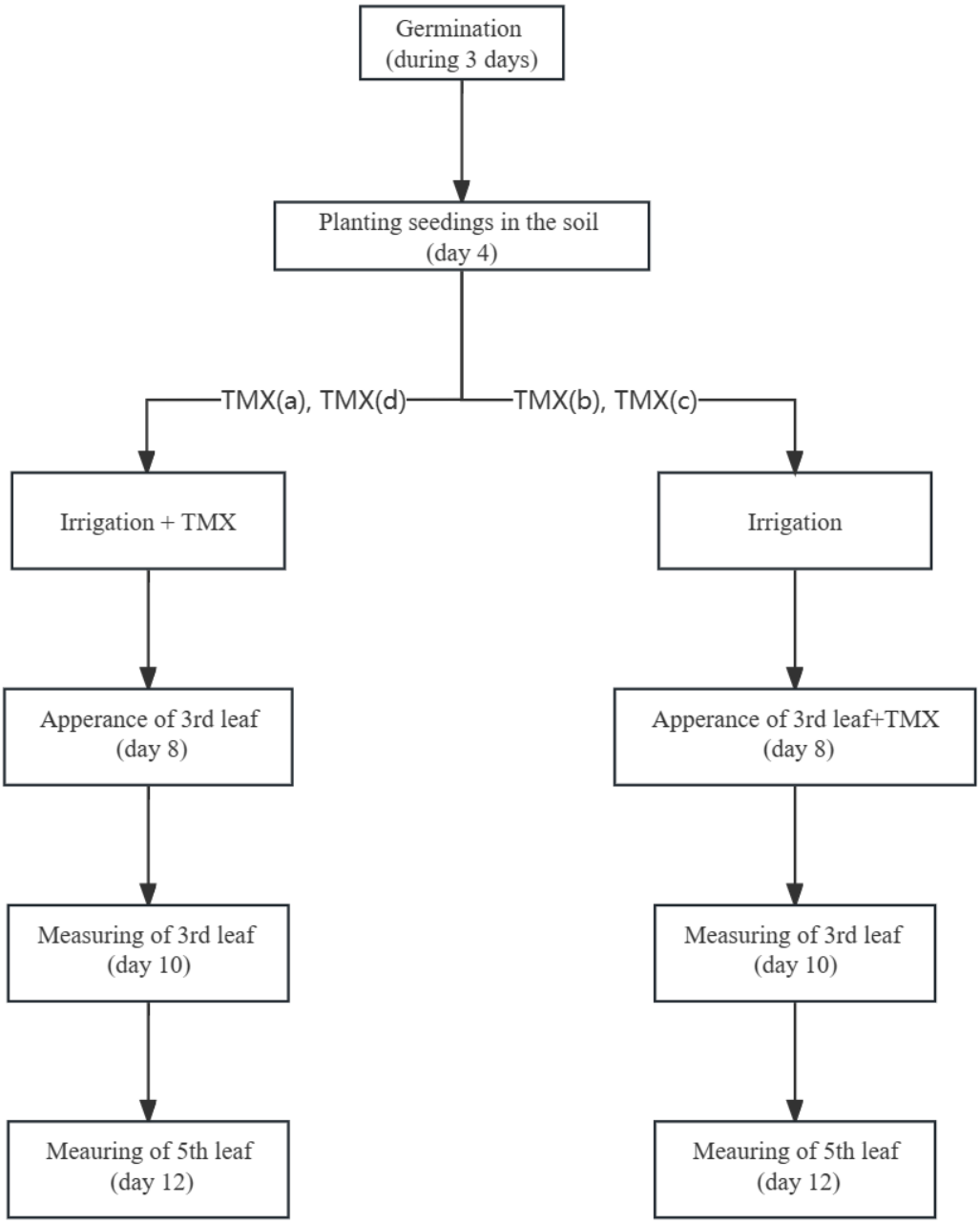

Fig. 6. Scheme of the experiments

3.2 Cultivation method of pea (*Pisum sativum L.*).

For germination, seeds of pea (*Pisum sativum L.*, cv. Nemchinovsky 46) were treated for 3 days in moist gauze and transferred to standard Knoop medium (1/5) for hydroponics (Reski & Abel, 1985). The seedlings were grown for 10 days under a light intensity of 100 μmol photons m^{-2} $with^{-1}$ in a 14 h light/10 h dark regime of temperature of 24^{o} C. The top of the plants was cut

off to prevent growth and transferred to new Knop 1/5 medium, cultured for 7days. Medium were replaced every day (Todorenko et al., 2020).

3.3 Preparation of chloroplast from maize leaf

Pre-weighed maize leaves (*Zea mays L.*, Zheng 958) were separated from the veins and the leaves were cut up and cooled in plastic bags in preparation for the subsequent milling operation (approx. 10 g). The pulverised leaves were ground three times (10 seconds each) in pre-cooled buffer which contain 0.04 M sucrose, 20 mM Tris-HCl (pH 7.8), 35 mM NaCl, 1 mM EDTA (grinding must be carried out at a temperature of 0-4 °C). After filtration of the homogenate through four nylon layers. After centrifugation of the filtered fluid (1500 rpm, 5 min, 4 °C). Transfer the supernatant to a pre-cooled tube and centrifuge again (4000 rpm, 4 °C, 10 min) to obtain a precipitate. The precipitate is dissolved in buffer which contain 15 mM NaCl, 400 mM sucrose, 50 mM Mes-NaOH (pH 6.5). and stored frozen for further experiments (add 30% glycerol and store at -73 °C).

3.4 Chloroplast separation of pea

Two clothianidin product YIMAO (Sigma-Aldrich, CN) and FUWEI (Boken Agriculture, CN) was used. The upper leaves of the peas were homogenized three times (10 s each time) with a blender in buffer A which contain 50 mM tricin (pH 7.8), 400 mM sucrose, 10 mM $NaCl_2$, 5 mM $MgCl_2$. The resulting homogenate was filtered through 4 layers of nylon, followed by centrifugation (300 g, 1min, 0-4° C). The supernatant was poured into a centrifuge tube and centrifuged (5000 g, 5 min). The precipitate containing chloroplasts was homogenized in a small amount of buffer B which contain 50 mM tricin (pH 7.6), 400 mM sucrose, 10 mM $NaCl_2$. The chloroplasts were frozen in liquid nitrogen and stored at -80 C^o.

3.5 Separation of BBY particles by PSII

BBY particles (in honor of Berthold, Babcock and Yocum) capable (PSII+Mn) and incapable (PSII-Mn) of photoinduced O $release_2$ were performed according to the previously described technique(Lovyagina et al., 2022a). BBY-particles of PSII-Mn do not contain external

proteins of the oxygen-releasing complex (ORC), manganese cations, and calcium cations. Extraction of manganese cations from PBMCs was performed by treat with 0.8 M Tris-HCl buffer (pH 8.5) for 15 min at 0.5 mg/mL chlorophyll, temperature 22^{o} C in room light. The obtained PSII preparations were placed in a buffer C which contain 400 mM sucrose, 15 mM NaCl, 50 mM MES/NaOH, pH 6.5, frozen in nitrogen solution and stored at -80 ℃.

3.6 Treatment of chloroplasts with clothianidin and determination of pigment content

Clothianidin was purchased from the company Sigma-Aldrich (PESTANAL, analytical standard, 99.9% purity). CL were resuspended in buffer B or C to 20-25 μg/mL CL. Clothianidin (CL) was added at a final concentration of 22 or 110 μg/L and incubated for 10 min at 4° C in the dark condition. Same volume of distilled water was added to the control. The required volume of chloroplasts was then placed to buffer (temperature about 27^{o} C), incubated for 2 min at room temperature and measured. Chlorophyll content has been measured spectrophotometrically in 95% ethanol (Lichtenthaler, 1987).

3.7 Measure the relation among different chemical bonds by Raman spectroscopy

Raman spectroscopy used in changes in the conformation of TMX effect of maize leaves is a DFS 24 Raman spectrometer (LOMO, RF) with a 473 nm laser (laser power 3 mW) (Ciel, Eurolase), and a SIDS 1/3648 (Troitsk, RF) recording system -matrix TCD1304DG (Toshiba, Japan) with filter LPO2-473RS-50 (Shemrock, USA) (Karger et al., 2016; Александровна & Александрович, и д.) When recording the spectra on computer, software from SIDS (Troitsk, Russia) was used. The facility for research was developed at the Department of Biophysics, Biological Faculty, Moscow State University. Lomonosov.

Spectra of CL, Triple-Chlorophyll (which contain Chlorophyll complex, Soybean oil, Gelatin, Glycerin, Titanium dioxide, Chlorophyllin (GNC, USA)), Beta-carotene (which contain Soybean oil, Gelatin, Glycerin, Corn oil (GNC, USA)) and chloroplasts were recorded by

resonance Raman scattering spectroscopy using a Renishaw inVia Laser Confocal Microscopic Raman Spectrometer equipped with lasers operating at 488 nm (50mW) and 532 nm (500mW). The glass slide with a coverslip to compact the solution was fixed on top of the stage and the signal recorded with a laser power intensity of 5% (x5 objective, numerical aperture 0.12) during the course of the experiment. The research facilities were developed at the Department of Biophysics, Biological Faculty, at the MSU-BIT University

Raman spectroscopy contains a laser, (1) optics to focus the laser beam onto the sample, a sample plate, (2) collection optics for scattered radiation, a dispersion system to filter out the scattering that is not needed, and a detection system (Fig. 7).

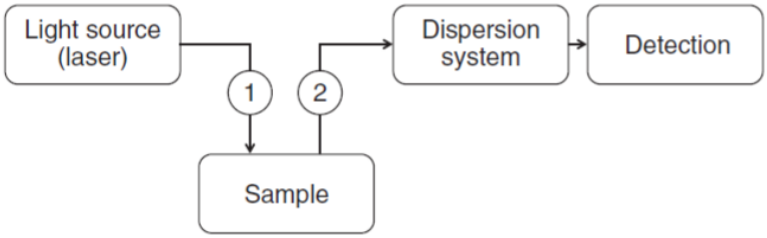

Fig. 7. General diagram of a Raman spectrometer. (1) optics to focus the laser beam on the sample; (2) collection optics for the scattered radiation.

3.8 Fluorescence measurement

In the experiment of maize leaf, multifunctional plant analyzer (M-PEA-2) was used to record light-induced kinetics of fast fluorescence (PF), delayed fluorescence (DF) and modulated reflection / absorption of light at a wavelength of 820 nm (MR) (Hansatech Instruments Ltd., King's Lynn, Norfolk, England). The intensity of the active light is 3000 μmol quanta m^{-2} s^{-1} and the duration of illumination is 60 s. The measurements were performed on the adaxial side of the intact leaves, placed in a measuring unit in a special clip-clothespin. Plants were adapted to darkness for 15 min before measurements in order to the reaction centre (RC) of the photosystems to become “open” with oxidized Q_A. Registration of three signals was carried out with the alternation of light and dark intervals, the duration and collection of data of which are described in detail in (Strasser et al., 2010a).

Standard JIP-test were used to analyzed OJIP-curves which describes the energy fluxes through different parts of the electron-transport chain of photosynthesis (Strasser et al., 2004a) with the following fluorescence signals: intensity at 20 μs (F_O), 2 ms (F_J), 30 ms (F_I), F_M (maximum level of fluorescence). These characteristics were used to calculate the probability of electron transport beyond the limits of Q_A– (ψ0), maximum quantum yield of photochemistry of PSII (F_V/F_M), energy flux absorbed by one active reaction center (ABS / RC), and the functional activity index PSII related to the absorbed energy (PI_{ABS})(Strasser et al., 2004a).

In the experiment of chloroplast, fluorescence light induction kinetics (OJIP curves) were recorded by a Plant Efficiency Analyzer (PEA) (Hansatech, UK). Chlorophyll fluorescence was stimulated by red light (λ =650 nm) with an intensity of 1500 μU m^{-2} s^{-1}. The following JIP-test parameters were used to analyse the OJIP curves (Strasser et al., 2004b): fluorescence intensity at 50 μs (Fo), 300 μs (F_{300} μs), 2 ms (F_J), relative O-J phase amplitude (Vj=(Fj-Fo)/Fv), maximum fluorescence yield (Fm), initial O-J fluorescence growth phase slope (Mo = 4×(F300mx-Fo)/Fv), electron transport efficiency (Pet = (Fm-$F_{2мс}$)/($F_{2мс}$ -Fo)), photochemical efficiency of PSII (Fv/Fo = (Fm-Fo)/Fo), maximum photochemical energy conversion efficiency of PSII (Fv/Fm= (Fm-Fo)/Fo).

The algae Chl fluorescence measurement**.** OJIP transients and delayed fluorescence (DF) induction *were recorded* using the high sensitivity fluorimeter FKMS-2 designed at the Faculty of Biology of Lomonosov Moscow State University (Lovyagina et al., 2022b)**.** The excitation source for chlorophyll fluorescence was blue light with a maximum at 445 nm and a PPFD of 7500 μmol (photon) m^{-2} s^{-1}**.** Measurement of delayed fluorescence in the interval from 10 μs to 1 ms was carried out according to a protocol similar to MPEA-2 (Multifunctional Plant Efficiency Analyzer, Hansatech, King's Lynn, Norfolk, UK) (Strasser et al., 2010). The samples were kept in the dark for 15 min before measurements. Chlorophyll content**.** Algal cells were harvested by centrifugation at 2000 x g for 3 min. Chlorophyll (Chl) was extracted from cells with 95% ethanol, and determined spectrophotometrically (Lichtenthaler, 1987).

The algae OJIP transients were carried out with a Plant Efficiency Analyzer (Hansatech, King's Lynn, Norfolk, UK) according to the standard procedure. Red light (maximum emission at 650 nm, PPFD 2500 μmol (photon) m^{-2} s^{-1}) was used as an excitation light. Before the measurement, cells were dark adapted for 15 min and then collected on glass fiber filter.

The algae Microscopic imaging**.** The measurements were carried out on the microscope Axioplan 2 imaging MOT (Zeiss, Germany) using the software Axio Vision 4.2 (Zeiss). The cells were identified using transmitted light, while the living cells were detected in fluorescent light on a counting chamber. The fluorescence was excited in the blue region (excitation maximum at 450 nm). The fluorescence emission was separated from the excitation light using a broadband filter (λ>515 nm).

Table 1 List of the selected JIP-test photosynthetic parameters derived from the light-induced Chl fluorescence kinetics (OJIP-transients).

Parameter	Description
$V_J = (F_J - F_O)/(F_M - F_O)$	Variable fluorescence at time 2 ms
$V_I = (F_I - F_O)/(F_M - F_O)$	Variable fluorescence at time 30 ms
$\varphi_{Po} = (F_M - F_O)/F_M = F_V/F_M$	Probability of excitation energy trapping in PSII (maximum quantum yield of PSII photochemistry)
$\psi_{Eo} = (F_M - F_J)/F_V$	Probability of electron transfer from Q_A to the PQ pool
$\varphi_{Eo} = (F_M - F_J)/F_M$	Quantum yield for reduction of PQ pool (at t = 0)
$\delta_{Ro} = (F_M - F_I)/(F_M - F_J)$	Probability of electron transfer from PQ pool to terminal electron acceptors of PSI
$\varphi_{Ro} = (F_M - F_I)/F_M$	Quantum yield for reduction of electron acceptors in PSI

$PI_{ABS} = RC/ABS \times F_V/F_M \times \times (1 - F_V/F_M)^{-1} \times \psi_{Eo} \times (1 - \psi_{Eo})^{-1}$	Performance index on absorption base
$PI_{total} = PI_{ABS} \times (1 - \delta_{Ro})^{-1}$	Total performance index

Dark decay kinetics of chlorophyll fluorescence (Q_A -reoxidation) and delayed fluorescence (DF) were recorded by FKMS-2 device (Lomonosov Moscow State University, Russia) (Volgusheva et al., 2022). Chlorophyll fluorescence was excited by blue light (λ =445 nm) with an intensity of 5000 μU m^{-2} s^{-1}. The attenuation of fluorescence was recorded 56 μs after a saturation flash of 250 μs (10 s). M-PEA-2 was use to measured delayed fluorescence in the submillisecond interval (10 μs to 1 ms) (Hansatech, King's Lynn, Norfolk, UK) (Strasser et al., 2010c).

3.9 Detection pigment concentration by absorption spectroscopy

The content of photosynthetic pigments (chlorophyll A, B and carotenoids) was determined spectrophotometrically in 100% acetone extract (Hitachi-557, Japan) and calculated by Holm-Vettstein's formulas.

3.10 Detection of chemical composition and molecular structure using IR spectroscopy

IR spectroscopy with Fourier transform (FT-IR spectroscopy) was used to registered IR spectra of maize seeds (*Zea mays L.*, Institut za kukuruz "Zemun Polje", Belgrade, Serbia) zp 633, zp 677, zp 684, zp735 in the range of 400-4000 cm^{-1} with a measurement step of 4 cm^{-1} (Shimadzu Corp., Japan). The leaves were homogenized in an agate mortar buffer (50 mM tricine, 400 mM sucrose, 10 mM NaCl, 5 mM MgCl2 pH = 7.8) and rolled into a tablet with potassium bromide (KBr) in a ratio of 1: 100.

Traditionally IR spectroscopy study the spectrum of radiation that passed through sample. The method for studying infrared radiation reflected from sample surface based on Attenuated Total Internal Refraction (ATIR), specular reflection, and other types of reflections.

Attenuated Total Refraction (ATR) is the most popular infrared spectroscopy method due to it si possible to study sample that are opaque to inforared radiation and it can diredtly analysis in the field. ATR is based on beam reflection at the interface between two phases: sample phase with a lower refractive index and ATR crystal phased with a relatively high refractive index. Amolst complete refelction of the beam from the surface of the sample is observed if the radiation beam is incident onthe pline of the sample at an angle of incidence greater thant hte critical one. Light emission penetrates a small depth into the sample phsed where it is partially absorbed (Fig. 8). With the same stimulation, this process repeat, then the absoption spectrum will be obtained.

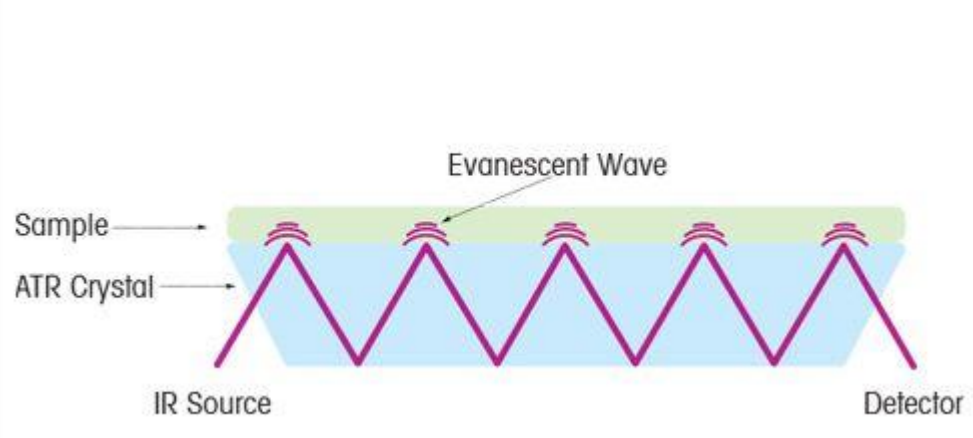

Fig. 8. Optical path of IR radiation in an ATR crystal

3.11 Studies of the O_2 release rate of and chloroplasts chlorophyll fluorescence inductions kinetics (OJIP transient)

The rate of O_2 release and uptake was determined by Clark electrode (Oxygraph Plus unit, Hansatech, UK) at a light intensity of 1500 μmol photons m-2 s -1, temperature 23°C, and 10 μg/mL Chl. PSII was assayed for its oxygen delivery activity in the presence of 0.125 mM 2,6-dichlorobenzoquinone (DCBQ). The rate of electron transport from H2O or reduced

dichlorophenol-indophenol (DCPIP-H2) to methylviologen (MV) was determined by the rate2 of uptake of O_2 (Curtis et al., 1975). The O_2 release $rate_2$ of BBY particles was measured in the presence of the artificial electron acceptor DCBQ (200 μM).

The photoinduced electron transport rate in BBY particles of PSII was recorded on a SPECORD UV-VIS spectrophotometer (Carl Zeiss Jena, Germany) as described in (Lovyagina et al., 2022a). The excitation light is XBDROY LED (Cree Inc., USA, λ 450 nm, light intensity 1500 μmol photons m^{-2} s^{-1}). 40 μM 2,6-dichlorophenolindo-phenol ($DCPIPH_2$) was used as an electron acceptor; photoinduced changes of optical density were recorded at a wavelength of 600 nm; hydrogen peroxide (100 μM final concentration) was used as an electron donor for PSII preparations without PBMCs. The mechanism of this effect is as follows: the Mn(II) cation binds to the high-affinity Mn-binding site in PSII (-Mn), is oxidized by a radical of the redox-active tyrosine-161 residue of protein D1 (YZ-), after which the Mn(III) cation is reduced by hydrogen peroxide (Inoué & Wada, 1987).

3.12 Preparation of nanostructured substrates for enhance the Raman scattering

In this part of the work, we developed a method for SERS of carotenoids, which we propose to use to diagnose the state of this pigment in the whole plant. Substrate with a nanostructured coating based on carotene samples applied (2 - 0.02 pmol/mL or 37 nmol/L - 3.7 nmol/L) silver. Nanostructured substrates were obtained in accordance with the technique described in (He et al., 2018a). An aqueous solution of sodium hydroxide (0.1 M NaOH, high purity water, Milli-Q, Millipore) was added dropwise to a freshly prepared solution of 0.01 M aqueous silver nitrate until the blackish-brown silver (I) completely oxidized. The oxide thus prepared was thoroughly washed with deionized water and dissolved in twice the molar excess of a 10 % aqueous solution of ammonia to give 0.01 M solution of a complex of silver (I). Millex-LCR syringe filter units (Millipore, pores 0.45 μm) were used to filter the resulting complex transparent silver solution. The initial ammoniacal silver (I) oxide solution was nebulized into a mist. 1–5 micron droplets were run on 'warm' glass, alumina or microporous silica substrates (270 °C) for 40–60 min (possible 250 °C, deposition thickness 45 nm) (Semenova et al., 2014).

3.13 Atomic force microscopy for investigate chloroplast topography

The structural integrity of chloroplasts was maintained by fixation in 0.5% glutaraldehyde (Ted Pella) for 1 h, then washed 4 times with distilled water and air-dried. Cell images were obtained using a NTEGRA SPECTRA AFM complex (NT-MDT Co., Russia) and a Nova registration program (NT-MDT Co., Russia). Measurements were carried out in a semi-contact mode using NSG 10-A cantilevers; the average coefficient of elasticity was 11.8 N/m, and the radius of the tip curvature was 10 nm. The size of a scanned image was 20x20 μm or 5x5 μm (256 × 256 points); the scanning rate was 0.5–1 Hz.

3.14 Electron paramagnetic resonance spectroscopy

The membrane fluidity of chloroplasts was estimated using electron paramagnetic resonance spectroscopy. To probe this, we employed 16-doxylstearic acid, an analogue of spin-labeled stearic acid (Sigma, St. Louis, MO, USA), which is located as close as 2.2 nm from the surface of the membrane(Schreier-Muccillo et al., 1976). Control and CL treated chloroplast suspension was concentrated to 2.8 mg Chl/mL followed by the addition of 0.1 mM 16-doxylstearic acid. PR spectra were recorded at 23-24 oC on a RE 1308 EPR (Russia) spectrometer with a constant magnetic field intensity, microwave power and a time constant of 3338 Gs, 22mW, and 0.1 s, respectively, were used. The rotational correlation time (τ), as a measure of membrane fluidity, was calculated as previously described (Rodnenkov et al., 2005).

3.15 Statistical analysis

Significant differences were determined by using one-way ANOVA, and means were analyzed using the Tukey test. The differences at $p< 0.05$ were considered statistically significant.

3.16 Quantum mechanical calculations

In this part of the work, we have developed a method for theoretically assessing the molecular structure of carotenoids, which we propose to use to form a system of neural networks when diagnosing the state of this pigment in the whole plant. To identify the type of carotenoids existed in the investigated samples, series of quantum mechanical calculations have been carried out for all cis- isomers and trans- of carotene, beta-cryptoxanthin, lycopene, lutein, and zeaxanthin at the different levels of density functional theory (DFT) with different basis sets. A few functionals (B3LYP, BVP86, PBE1PBE) have been used in calculations with different basis sets (6-31+G**, DGDZVP, TZVP), Optimized geometry parameters for the equilibrium conformation have been obtained and confirmed by frequency calculations. DFT calculations have been performed without any restrictions on the symmetry of structure using the program GAUSSIAN 09 package (Revision D.01) (Rastogi, 2012). A comparison of the results obtained at different tested levels of theory shows that the quality of the optimized geometry parameters at all levels is very close, and the BVP86/TZVP frequencies are in better agreement with the experimental ones and can be used to interpret the spectra of organic molecules. virtually no scaling procedure (Hickey et al., 2019). The results of calculations at the BVP86/TZVP level have been used for the detailed interpretation of vibrational spectra. Other calculation levels used predict frequencies that are higher than the experimental ones. However, when using the BVP86/TZVP results, it is important to note that some predicted frequencies may be slightly redshifted (to the low frequency region) compared to the experimental frequencies.

4. Results and Discussion

4.1 Study of the effect of thiamethoxam spray on two maize genotypes leaves.

In this series of experiments, thiamethoxam was spray on the leaves when 3rd leaf appearance (day 4. see chapter Methods). Fluorescence parameters and Raman spectra were

recorded in order to study the effect of thiamethoxam on leaf pigments. It was found, there is no significant difference between zp 341 hybrid maize line and zppl 225 inbred maize line in leaf pigment composition, but there were significant changes in the different genotypes following thiamethoxam application. It was found, there no change of thiamethoxam -treated hybrid line zp 341 in the pigment composition. In contrast, thiamethoxam decreased the content of chlorophyll in leaves of inbred line zppl 225 to 0.61 mg/g (17% reduction in chlorophyll a and 24% reduction in chlorophyll b; $p < 0.05$).

Using the OJIP transients of both hybrid zp 341 and inbred zppl 225 maize leaves had typical characteristic phases patterns. This pattern reflects the sequential reduction of carriers in the photosynthetic electron transport chain between the two photosystems (Fig. 9, A, D) (Strasser et al., 2004c;Stirbet & Govindjee, 2012a).

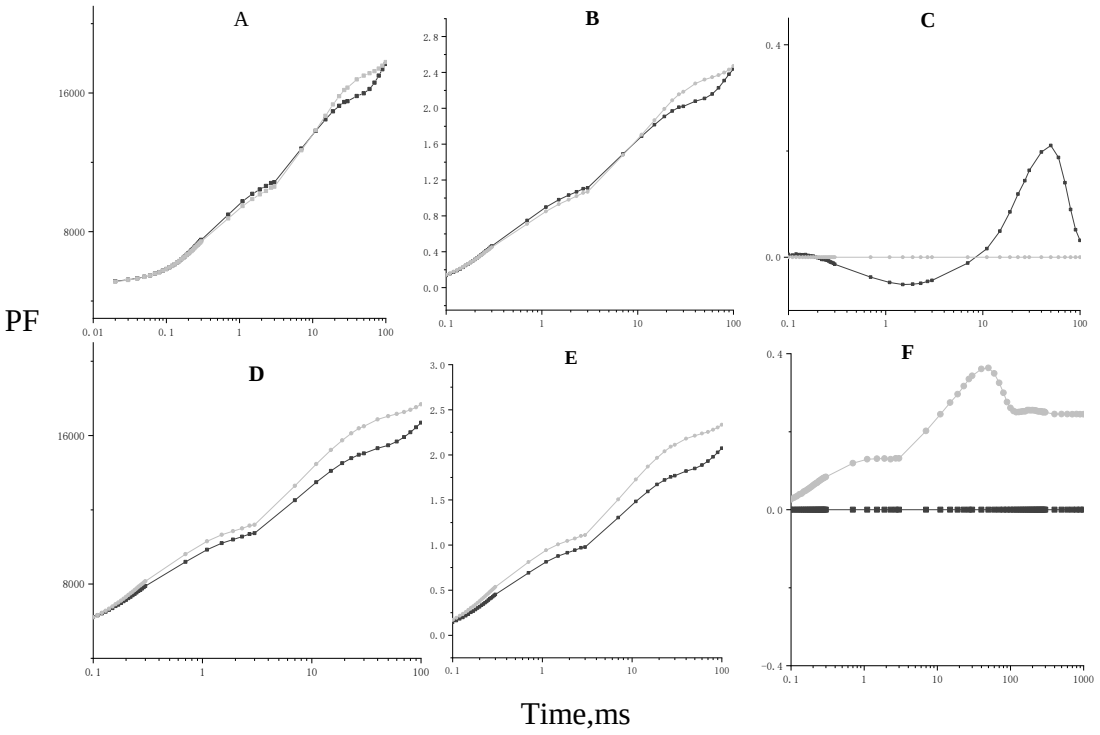

Fig. 9. OJIP curves of maize leaves (A, D), the derived curves of relative variable fluorescence Vt=(Ft-F0)/(FM-F0) after normalization to O levels (B, E) and the difference in the values of the functions ΔVt = Vt(TMX)- Vt(control) (C,E) for the inbred line zppl 225 (A,B,C)

and the hybrid zp 341 (D,E,F) in control(1) and upon thiamethoxam treatment(2). O, J, I and P are 20 μ s, 2ms, 30ms, and 300ms peaks of the induction curve

Thiamethoxam treated sample caused changes in the OJIP of both maize type (Fig. 9, A, D). Normalization of the induction curves derive the relative fluorescence variable (V_t) function. The increase in ΔV_t of zp 341 and zppl 225 in O-J phase indicated the accumulation of reduced Q_A. The reduced Q_A due to the increased proportion of Q_B non-reducing centres of PSII, unable to conduct electron transport along the electron transport chain.(Lazár, 2006). The increase in ΔVt of thiamethoxam-treated zppl 225 at the O-J and J-I stages indicated the accumulation of reduced Q_A and plastoquinone molecules, which were unable to carry out the electron transfer of the dark photosynthetic reaction (Kalaji, Jajoo, et al., 2014).

Table 2. JIP-test parameters derived from analysis of OJIP induction curves for leaves of zp 341 and zppl 225 upon thiamethoxam treatment (M±SEM). *Difference from control are statistically significant (P< 0.05). Values are calculated on the based n=5

Fluorescence parameter	Zppl 225	Zppl225+TMX	Zp 341	Zp 341+TMX
F_V/F_M	0.749±0.004(100 %)	0.740±0.004 (99%)	0.740±0.010(100 %)	0.710±0.010(97%)
ψEo	0.69±0.01(100%)	0.65±0.01(95%)*	0.67±0.01(100%)	0.76±0.02(100%)
ABS/RC	2.62±0.09(100%)	2.93±(112%)	2.57±0.12(100%)	2.95±0.18(115%)
PI_{ABS}	2.50±0.01(100%)	1.77±0.15(71%)*	2.24±0.23(100%)	1.70±0.09(76%)*

The JIP-test was used in an attempt to reveal the action of thiamethoxam on important photosynthetic parameters derived from the OJIP transients (Table 2). The F_V/F_M correlates with the thermal quantum yield of primary photochemical reactions of PSII and is used as an indicator of the efficiency of photosynthesis. There was no statistically significant difference between control and thiamethoxam-treated leaves of both maize type leaf in F_V/F_M.

The correlation between PI_{ABS} and plant viability reflects the function of PSA under current stresses (Živčák et al., 2014). It shows significant change under thiamethoxam treatment, PI_{ABS} decreased by 29% and 24% in thiamethoxam treated zppl 225 and zp 341 leaves, respectively.

The reduction of PI_{ABS} in thiamethoxam treated zppl 225 leaves was due to a significant reduction in electron transfer (ψ_{Eo}) on the PSII receptor side. In contrast, the reduction of zp 341 leaves PI_{ABS} might be related to a minor decrease in PSII photochemistry (F_V/F_M) and increased ABS/RC.

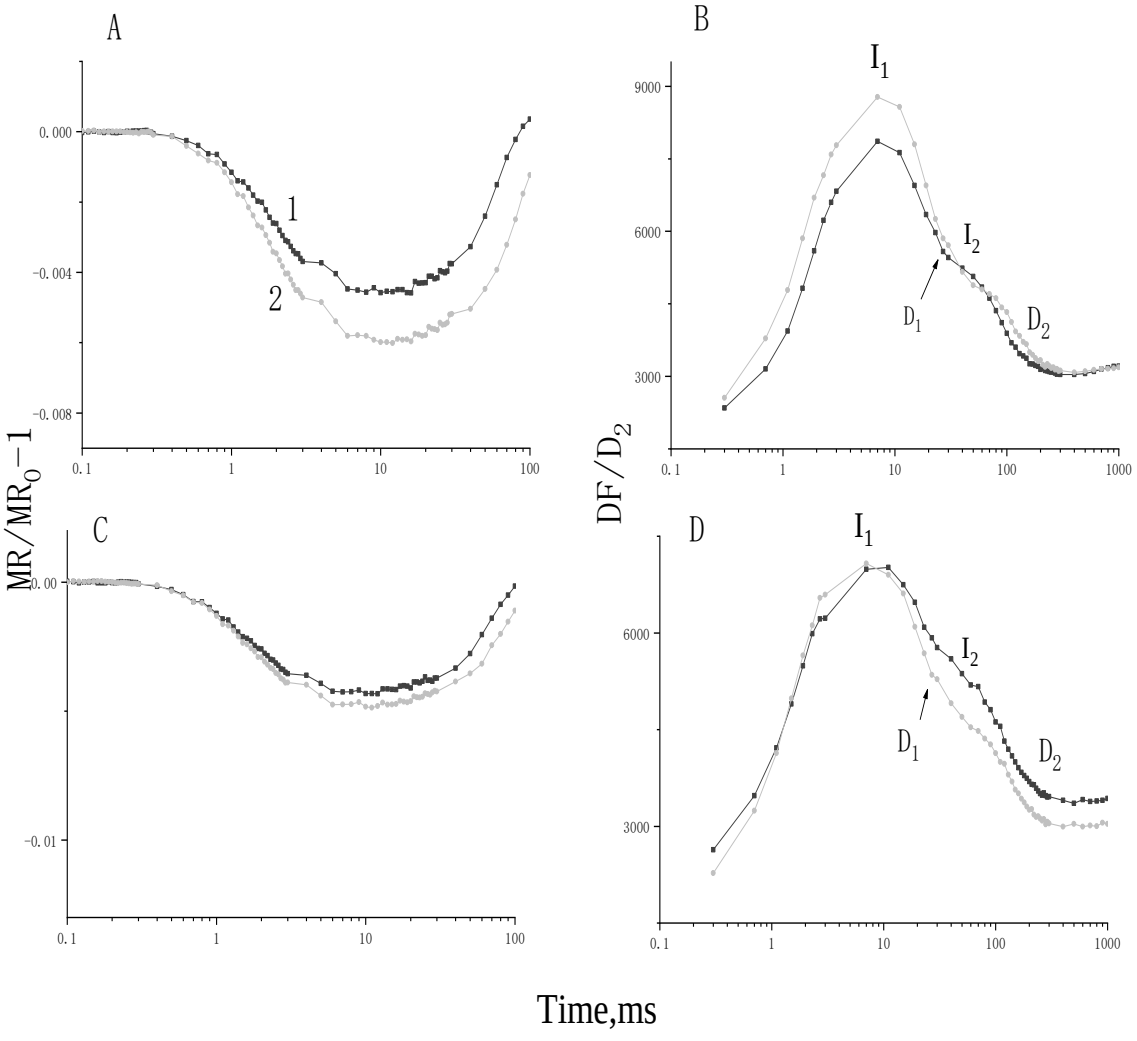

Fig. 10. Light-induced kinetics of modulated reflection at λ =820nm (MR) (A,C) and delayed fluorescence (DF) normalized to the minimum signal level D2 at 200ms (B,D) in leaves of maize inbred line zppl 225 (A,B) and hybrid zp 341(C,D) in control (1) and upon thiamethoxam treatment (2). MR kinetics are normalized and expressed as MR/MR0-1, where

MR0 is the signal intensity at 0.7 ms. I_1, I_2, D_1, D_2 are maximums and minimums on the DF induction curve.

Redox transformation of the molecular reaction center of PSI (P700) after TMX treatment was evaluated by MR kinetics (Fig. 10, A, C) (Schansker et al., 2003). The MR kinetic signal drop during the first 15-20 ms reflects P700 oxidation (fast phase) and reaches a minimum at 20 ms (MR_{min}). MR_{min} is a transient steady state in which the rates of P700 oxidation and reductions are equal. Subsequently, the MR signal (slow phase) increases to a maximum at 200 ms (MR_{max}) due to the electron-donating reduction rate of PSII being superior to the oxidation rate(Strasser et al., 2010c).

Leaf redox P700 transformations of both maize types were altered by thiamethoxam (Fig. 9, A, C). zppl 225 leaves showed chlorophyll changes in both the fast and slow phases of MR and were associated with a decrease of MR amplitude at 20 ms (Fig. 10, A). Analysis of MR kinetics showed an increase in reduced PSI receptors and a decrease in oxidized PSI receptors in zppl 225 leaves at the influence of thiamethoxam. This might be due to a reduced receptor pool on the receptor side of PSI. In contrast, there is no change in MR kinetics for zp 341(Fig. 10, B).

The rate of the recombination reaction in PSII is depended one membrane energization, so DF is proportional to the rate of the recombination reaction in PSII. The fast phase of DF associated with membrane potential formation(Goltsev et al., 2009a). Fig. 10 B, D shows the induction curves of DF normalized to the minimum fluorescence D_2. The decrease of the I_1 peak during the microsecond time scale may be due to a decrease in the Z+ reduction rate of oxygen-4MnCa and/or a decrease in the QA reoxidation rate of oxygen-4MnCa (disturbed electron transfer on the PSII receptor side of the oxidizing complex (OEC)), which is induced by the oxidizing complex (OEC) of oxygen-4MnCa (Goltsev et al., 2009a). During thiamethoxam action, I_1 amplitudes were reduced by 23% and 21% in zppl 225 and zp 341 leaves compared to controls, respectively.

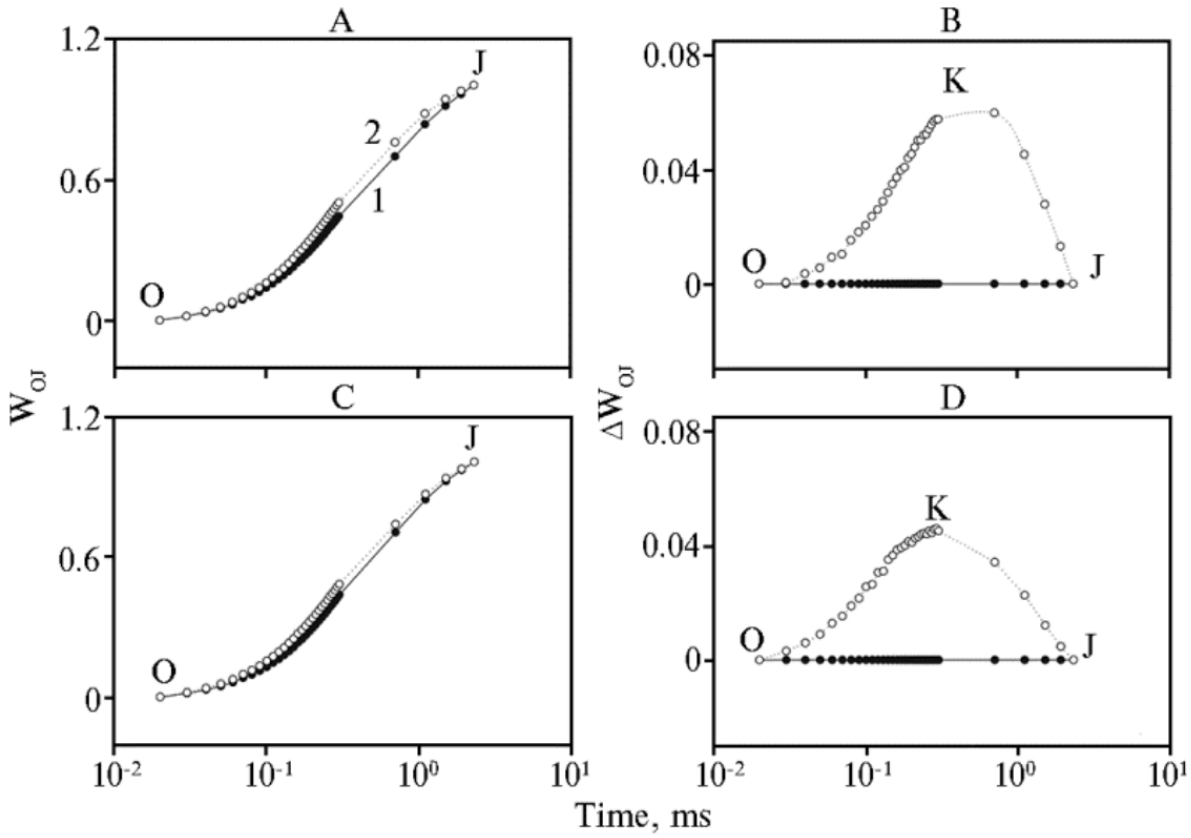

Fig. 11. The relative variable fluorescence W_{OJ} between the O and J levels (A, C) and the difference in the function values ΔW_{OJ} (B, D) in leaves of maize inbred line zppl 225 (A, B) and hybrid line zp 341 (C, D) in control (1) and upon TMX treatment (2). O, K, J are the peaks on the induction curve at 20 μ s, 300 μ s, and 2 ms.

The state of the OEC and its ability to supply electrons to P680+ via Z+ can be monitored by the appearance of additional peaks on the PF induction curve. For compare the OEC state, the relative fluorescence W_{OJ} $((F_t-F_o)/(F_J-F_O))$ (Fig. 11, A, C) and the difference in functional values ΔW_{OJ} $(W_{OJ(TMX)} - W_{OJ(control))}$ (Fig. 11, B, D) were calculated. In thiamethoxam treated leaves of both maize species, (at 300 μs, peak K appeared between O and J) due to OEC limitation which is characteristic for changes during high temperature stress (Fig. 11, B, D) (Strasser et al., 2004e).

Characteristic peaks of carotenoids due to electron valence vibrations in the polyene chains of the molecule were identified in Raman spectra of maize leaves (Fig. 12). Peak at 1520 cm^{-1} reflects carbon double -C=C- bonds. Peak at 1160 cm^{-1} widely assigned to a combination of C-C

stretching and C-H in-plane bending vibrations. Peak at 1006 cm^{-1} reflects CH_3 in-plane rocking vibrations.

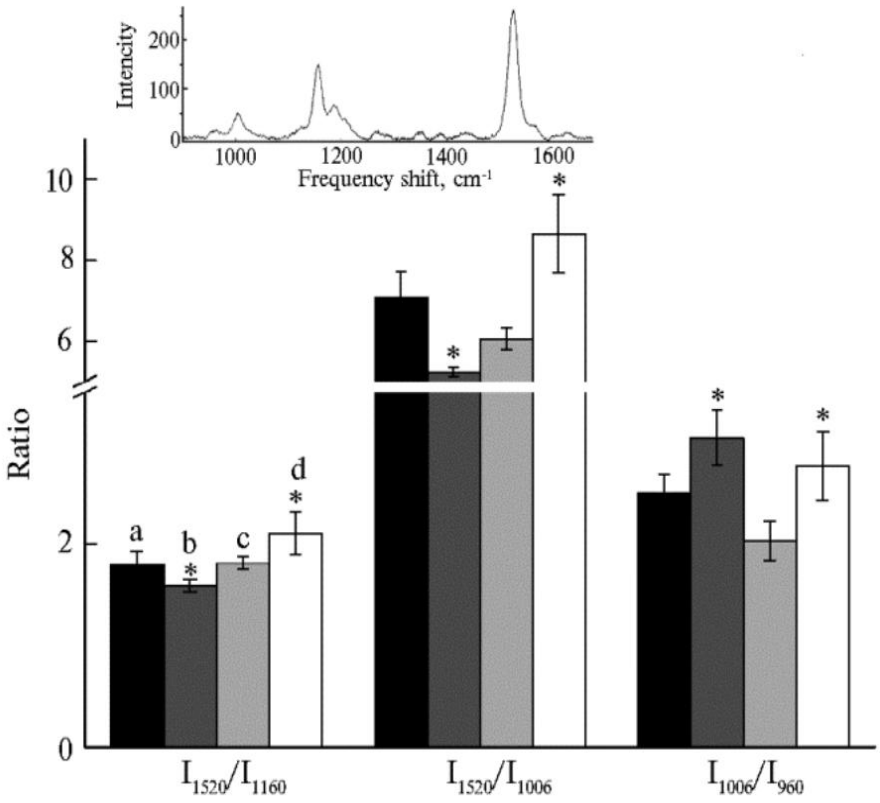

Fig. 12. Changes in the Raman spectra of carotenoids in maize leaves of two genotypes after treatment with thiamethoxam. a- zppl 225, b- zppl 225 +TMX, c – zp 341, d – zp 341 + TMX. Asterisks denote a statistically significant difference ($P < 0.05$). The inset shows the Raman spectrum of leaf carotenoids for the inbred line zppl 225.

It was found, the ratio of I_{1006}/I_{960} bands in maize leaves increased after thiamethoxam application (Fig. 12). At the of thiamethoxam action, the I_{1520}/I_{1006} ratio of zppl 225 decreased by 26%. In the leaves of the zp 341 hybrid, thiamethoxam caused a 43% and 16% increase in the ratios of I_{1520}/I_{1006} and I_{1520}/I_{1160}, respectively, suggesting a conformational change in the carotenoids.

Summary of this chapter. Interestingly, the zppl 225 inbred line was found to have lower chlorophyll, which could indicate that synthesis of these pigments was decreased under TMX, as

well as the ratio of carotenoids to chlorophyll (a + b), which is usually associated with increased carotenoid content under conditions of stress. However, there was no change in pigment composition in the leaves of the zp 341 hybrid.

Kinetic curves of PF describe the energy fluxes in different parts of the photosynthetic electron transport chain, and analysis by JIP test showed that the effect of thiamethoxam on the PSII photochemistry (FV/FM) of leaves of both studied genotypes was not significant ($p > 0.05$). Changes on the side of the PSII receptor were detected in leaves of the zppl 225 inbred strain, where a decrease in electron transport probability (ψ_{Eo}) on the side of the PSII receptor resulted in a decrease in the function of PSII (PI_{ABS}).

So, spraying maize plants with the insecticide thiamethoxam resulted in reduced chlorophyll content in leaves of the zppl 225 inbred line. In zppl 225 and zp 341, thiamethoxam was determined to affect the functional activity of PSII, to decrease PI_{ABS} parameters, and to reduce the pigment-like membrane potential. Interesting, the thiamethoxam action caused opposite changes in the conformation of carotenoid molecules, but not in their content.

4.2 Study of the effect of thiamethoxam inject to the soil of two maize genotypes.

It is obvious that when fields are treated with pesticides, part of the substance ends up in the soil. In this series of experiments, the effect of the pesticide on *Nastenia* leaves was examined if it entered the soil. In this series of experiments, thiamethoxam solution was inject into soil at 4^{th} day when seedling in the soil (TMX(a)) and inject into soil at 8^{th} day (TMX(b)). The fluorescence parameters and Raman spectra were recorded in order to study the effect of pesticide of pigments in leaves.

It was found, plant height and leaf length/width were measured for two maize genotypes without the supplement (control) and with thiamethoxam added 20 days after the seedlings were buried in the soil. The leaf length of control plants of both maize genotypes was approximately 12-13 cm. With the addition of thiamethoxam on day 4 (TMX (a)), zppl 225 and zp 341 increased leaf length/width by 13% and 1%, respectively. However, there was no increase in leaf length for both maize genotypes when thiamethoxam was added on day 8 (TMX (b)). Control

plants of both maize genotypes were approximately 16-18 cm in height after thiamethoxam treatment in both applied variants slightly increased plant height in maize genotypes compared to controls. Thus, in zppl225, plant height increased by 6% and 2% under TMX (a) and (b), respectively, while in zp 341, plant height increased under TMX (a) and (b), respectively 4% and 6%.

In this experiment, the pigment content of two maize genotypes during the thiamethoxam treatment was measured (Table 3). After 12 days, the pigment composition of different maize genotypes was slightly different. The total amount of chlorophyll is 0.52 mg/g in zppl 225 and 0.64 mg/g in zp 341. It was found, in the presence of thiamethoxam, the chlorophyll content in zp 341 decreased from 0.64 mg/g to 0.31 mg/g (b). The initial carotenoid contents in zppl 225 and zp 341 were 0.14 and 0.13 mg/g, respectively.

It was found, thiamethoxam treatment decreased the carotenoids contents in leaf maize genotypes. In zppl 225 leaf, carotenoids decreased from 0.14 mg/g to 0.11 mg/g under TMX (a) treatment and from 0.09 mg/g to TMX (b) treatment, whereas in zp 341, carotenoids decreased from 0.13 mg/g to 0.11 mg/g to 0.07 under TMX (a) treatment and 0.07 under TMX (b) treatment.

Table 3. The pigment content in the leaves of the zp 341 and zppl 225 at thiamethoxam action on the 4th (TMX (a)) and the 8th days (TMX (b)) by root irrigation (day 12). Statistically significant results are indicated: *, P< 0.05. Parameters in parenthesis are expressed as a percentage of control value. Values are calculated on the based n=5

Pigment content	zppl 225	zppl 225 + TMX (a)	zppl 225 + TMX (b)	zp 341	zp 341 + TMX (a)	zp 341 + TMX (b)
Chl a (mg/g)	0.39 ± 0.01 (100%)	0.44 ± 0.01 (114%)	0.41 ± 0.01 (105%)	0.47 ± 0.01 (100%)	0.56 ± 0.01 (119%)	0.24 ± 0.01 (53%)*
Chl b (mg/g)	0.13 ± 0.01 (100%)	0.15 ± 0.01 (112%)	0.13 ± 0.01 (102%)	0.17 ± 0.01 (100%)	0.19 ± 0.02 (112%)	0.08 ± 0.01 (53%)*
Chl a + Chl b (mg/g)	0.52 ± 0.03 (100%)	0.59 ± 0.01 (113%)	0.54 ± 0.02 (104%)	0.64 ± 0.04 (100%)	0.75 ± 0.03 (117%)	0.31 ± 0.02 (53%)*
Carotenoids (mg/g)	0.14 ± 0.01 (100%)	0.01 ± 0.02 (75%)	0.09 ± 0.01 (66%)*	0.13 ± 0.01 (100%)	0.11 ± 0.02 (98%)	0.07 ± 0.005 (64%)*

In this study, the OJIP transients were recorded for maize hybrid (zp341) and inbred line (zppl 225) under thiamethoxam treatment, which was added 4th day when seedling seeds (a) and

8^{th} day when 3^{rd} leaf of plant appear (b) (Fig. 11). It was found, the kinetics have a typical pattern for plants grown during the standard conditions with the J, I, and P steps at 2, 30, and ~200 ms for control group of zp 341 and zpple 225, respectively. It was found, thiamethoxam treated plant showed modifications of the OJIP transients on the 10^{th} and 12^{th} days of growing. In zppl 225, the shape of the OJIP transient remained unchanged during thiamethoxam treatment (a), whereas pesticide-treated zp 341 showed increased levels of Chl fluorescence at the O-J-I-P step at day 10 compared to the control (Fig. 13 a, b). It was found, that thiamethoxam increased its effect in zppl 225 plants, as evidenced by a decrease in the JIP phase under TMX (a) at day 12 (Fig. 13 c) and an increase in the I-P step under thiamethoxam (b) compared to the control. In the case of thiamethoxam, the effect on zp 341 OJIP transients was the same as in 10- and 12-day-old leaves (Fig. 13 d).

In addition, the JIP was employed to reveal the role of thiamethoxam action on important photosynthetic parameters controlled from the OJIP transient (Fig. 14). One of the most physiological and widely used photosynthetic parameters is the F_V/F_M (or φ_{Po}) ratio, which characterizes the maximum quantum yield of PSII photochemistry (Papageorgiou & Govindjee, 2004). In control plants, the F_V/F_M value was approximately 0.76. This parameter did not change after 10 and 12 days in both variants of thiamethoxam treatment experiments. The hybrid line (zp 341) treated with TMX (a) has showed difference in the relative variable fluorescence at J step (OJ-phase) (V_J) and I step (OI-phase) (V_I) ($P < 0.05$). On the 10^{th} day, the V_J and V_I values at zp 341 under TMX(a) treatment increased by 9% compared with the control and slight increases in V_J and V_I during thiamethoxam indicate disturbed electron transport in PSII.

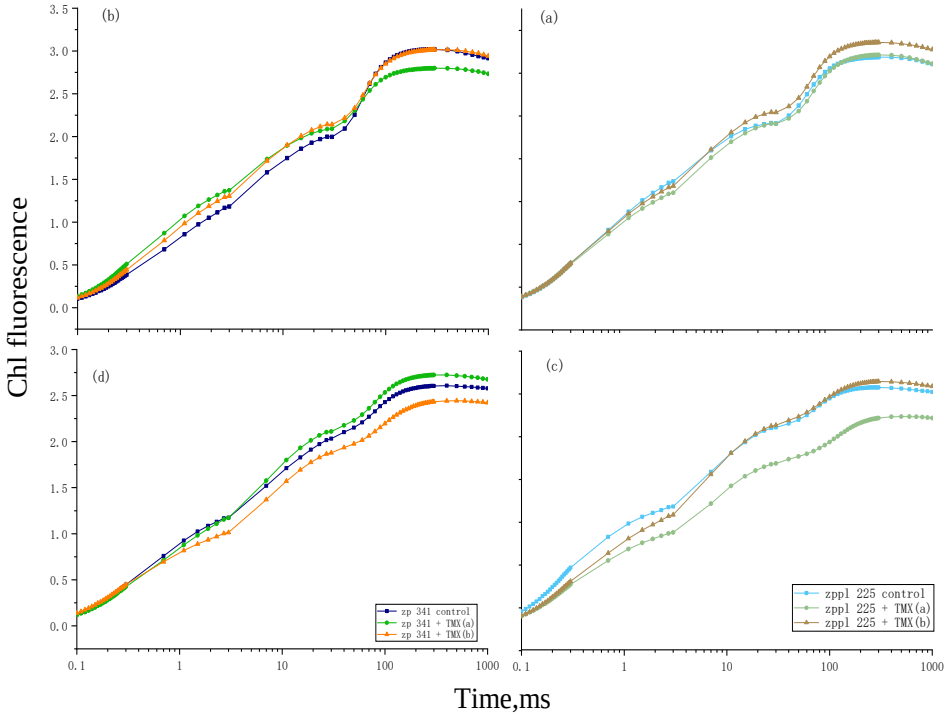

Fig. 13. OJIP transients recorded in maize leaves of the zppl 225 (a, c) and zp 341 (b, d) under TMX treatment. (a, b) 3rd leaf (day 10); (c, d) 5th leaf (day 12) of maize zppl 225 (a, c) zp 341 during thiamethoxam which added on the 4th (TMX (a)) and the 8th days (TMX (b)) by root irrigation; n = 5 for each sample.

It was found, the probability of electron transfer from Q_A to the PQ pool (ψ_{Eo}), depends on the functional state of the donor and/or acceptor side of PSII. At thiamethoxam treatment, ψ_{Eo} decreased ($P < 0.05$) in zp 341 but remained unchanged in zppl 225. ψ_{Eo} was increased in leaves of zppl 225 under TMX (b) treatment ($P < 0.05$).

The quantum yield (φ_{Eo}) of electron transport is proportional to F_V/F_M and ψ_{Eo}. At thiamethoxam treatment, the φ_{Eo} value of zp 341 leaves decreased due to the significant decrease of ψ_{Eo} value, while the F_V/F_M remained unchanged at the 10th day. During thiamethoxam treatment, the probability of electron transfers from the intersystem electron carrier to the reducing end electron acceptor on the PSI acceptor side (δ_{R0}) in zp 341 decreased ($P < 0.05$). The quantum yield of terminal PSI electron acceptor reduction (φ_{Ro}) was about 0.26 in zp 341 leaves and decreased in TMX-treated plants. In contrast, the δ_{R0}, φ_{Eo}, and φ_{Ro} values of zppl 225 remained unchanged after 10 days. However, the δ_{R0} and φ_{Ro} values of zppl 225 increased ($P >$

0.05) under TMX (a) and remained unchanged or slightly decreased ($P > 0.05$) after 12 days under TMX (b).

It was found, the parameters PI_{ABS} and PI_{total} differed in response to the two thiamethoxam treatment variants in leaves of maize genotypes. PI_{ABS} describes the photosynthetic index relative to absorption, combining three PSII characteristic parameters: the maximum quantum yield of PSII photochemistry (Fv/Fm), the density of active PSII reaction centre per antenna (RC/ABS), and the electron probability from Q_A transfer to PQ pool (ψEo). In this experiment, the PI_{ABS} of zppl 225 under thiamethoxam was slightly increased compared to the control on day 10 ($P > 0.05$). In contrast, zp 341 under thiamethoxam, especially PI_{ABS} decreased during TMX(a) treatment ($P < 0.05$). In most cases, the PI_{ABS} values of leaves of both genotypes increased after 12 days, indicating amplification of plant performance at thiamethoxam treatment. The total index (PI_{total}) of zp 341 attributable to PSII, PSI functional activity and electron transport between them decreased on thiamethoxam ($P < 0.05$), while the value of this parameter did not change significantly in zppl 225 leaves after 10 days. On day 12, an increase in PI_{total} was observed in inbred line (zppl 225) leaves during thiamethoxam treatment. However, in zp 341, PI_{total} increased under TMX (a), while the value of this parameter did not change significantly ($P > 0.05$) under TMX (b).

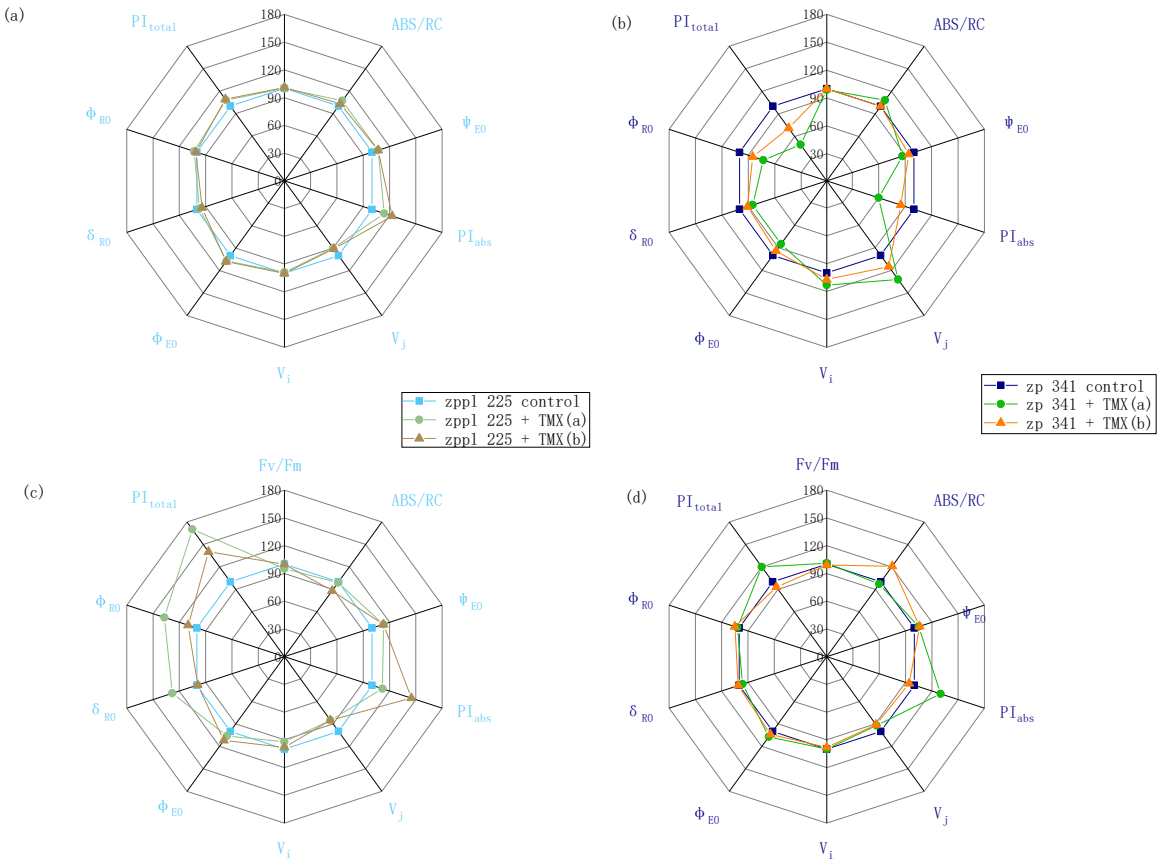

Fig. 14. Radar plot of JIP-test parameters maize of the zppl 225 (a, c) and zp 341 (b, d) under TMX treatment. (a, b) 3rd leaf (day 10); (c, d) 5th leaf (day 12) of maize of the inbred line (zppl 225) (a, c) and hybrid (zp 341) under TMX which added on the 4th (TMX (a))and the 8th days (TMX (b)) by root irrigation. Parameter values are expressed as percentage of control value (control = 100%). n=5 for each sample.

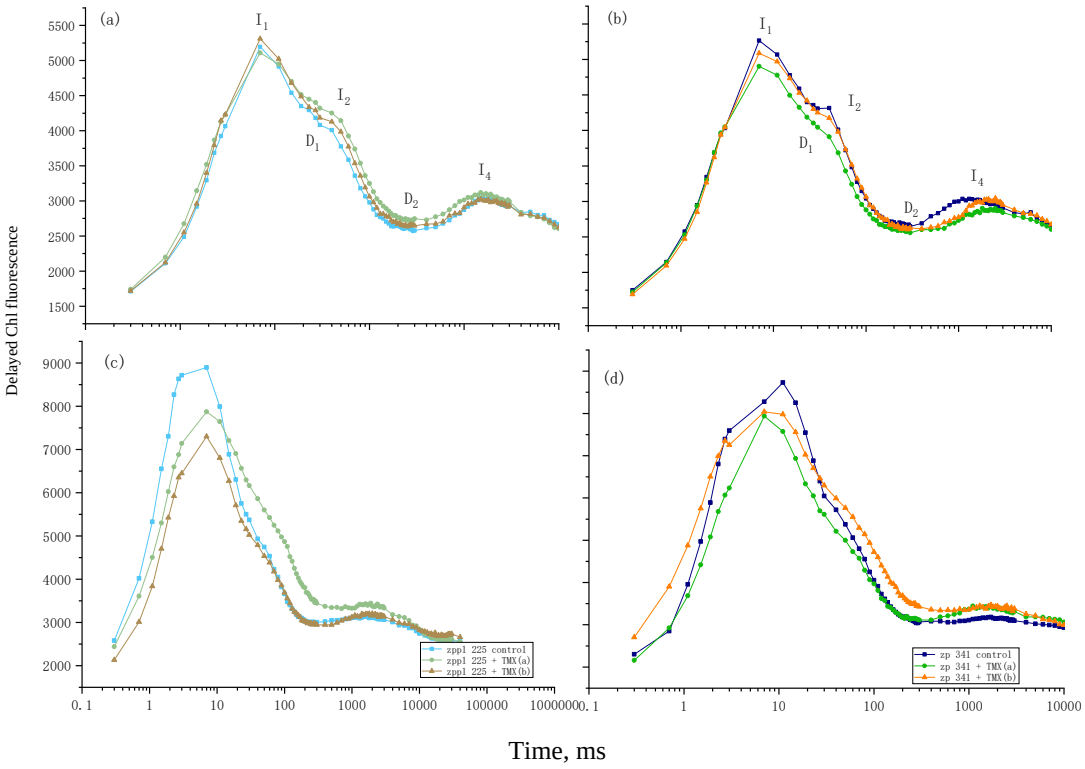

Fig. 15. Light-induced delayed Chl fluorescence (DF) kinetics recorded in maize leaves of the zppl 225 (a, c) and zp 341 (b, d) under thiamethoxam which added on the 4th (TMX (a)) and the 8th days (TMX (b)) by root irrigation. I_1, D_1, I_2, D_2, I_4 are the extremum and inflection points of the kinetics. (a, b) 3rd leaf (day 10); (c, d) 5th leaf (day 12) of maize of zppl 225 (a, c) and zp 341; n = 5 for each sample.

Delayed fluorescence (DF) is one of the methods to monitor changes in thylakoid membrane electrical conduction. DF is closely connected with the photochemical reaction of PSII reaction centre (RC). The kinetics of DF decay are related to the charge recombination process between the reduced main acceptor Q_A^- and the oxidized main donor P680+ in PSII over a time interval of microseconds to milliseconds. The DF induction curve has several maxima, called peaks (I_n), and several minima (D_n). The observed maximum in the millisecond range (I_1) DF curve at 3-7 ms coincides with peak J in the rapid fluorescence induction curve (OJIP curve). The formation of I1 is due to the accumulation of PSII RCs in the $S_3P680^+Q_A^-$, $Z^+P680Q_AQ_B^-$ and $S_3P680Q_A^-$states, which are responsible for charge recombination and emission of DF quanta, as well as enhancement of the potential across the DF membrane due to the generated

electricity. The second maximum (I_2) coincides with I-P of the OJIP curve and is associated with reoxidation of the plastoquinone pool due to electron efflux to PSI ($P700^+$). The presence of a peak I_4 in the millisecond range is associated with the formation of a transmembrane proton gradient (ΔpH), which increases the rate constant of the radiative transitions in the PSII RC. The timing of the I_4 peak coincides with the slowness of the kinetics of light-induced fluorescence observed after the P peak.

The DF induction curves recorded in control zppl 225 and zp 341 and under thiamethoxam treatment are show in Fig. 15. In controls, the kinetic curve exhibited a rapid phase with a peak (I_1) and shoulder (I_2) at 7 ms and 40 ms, respectively, and an intermediate inflection point D_1 at approximately 30 ms. The ensuing slow phase has a peak I_4 at about 1.5 seconds. A dip D_2 with a minimum value of 300 ms separates the fast and slow phases.

It was found, during thiamethoxam slightly affected the DF induction curve at day 10 in the leaves of both maize genotypes. In contrast, we observed a significant change in the thiamethoxam induction profile at day 12. Thus, the kinetic patterns measured in zp341 and zppl 225 showed a decrease in the magnitude of I_1, while I_2 and I_4 remained unchanged. Peak I_1 was shifted from 7 ms to about 10 ms in control and thiamethoxam treated zp 341 plants (Fig. 15 d). In zp 341 and zpp l225, a decrease in the energy of thylakoid membranes under thiamethoxam resulted in a decrease in I_1 after 12 days.

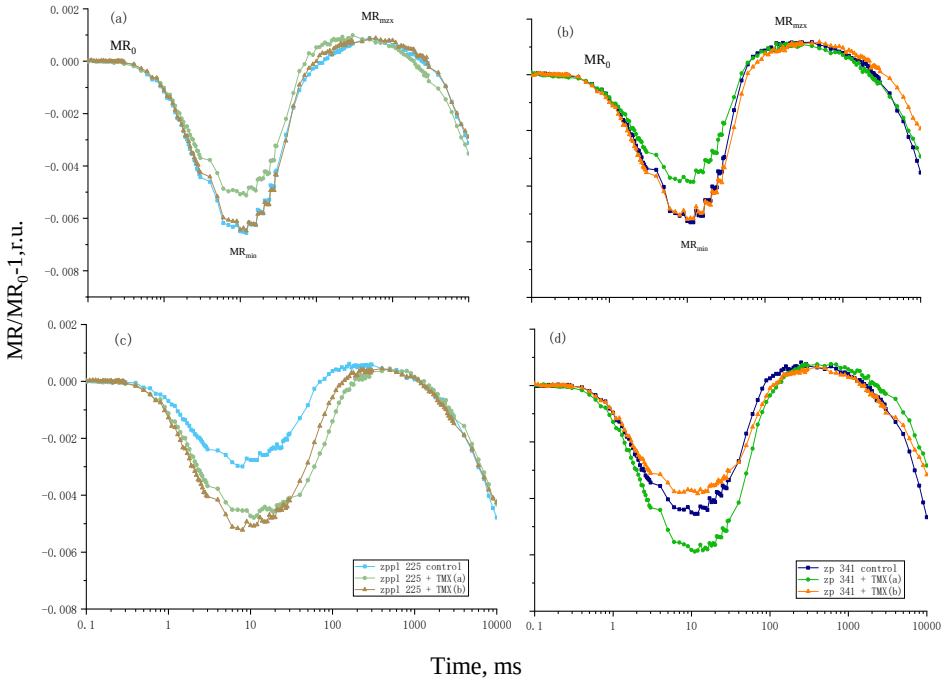

Fig. 16. Modulated 820 nm reflection (MR) kinetics recorded in maize leaves of the zppl 225 (a, c) and zp 341 (b, d) under thiamethoxam which added on the 4th (TMX (a)) and the 8th days (TMX (b)) by root irrigation. Kinetic curves are normalized to the initial value at 0.7ms (MR0). (a, b) 3rd leaf (day 10); (c, d) 5th leaf (day 12) of maize of the zppl 225 (a, c) and zp 341; n = 5 for each sample.

Modulated reflectance signal at 820 nm (MR) kinetics reflecting the dynamics of the redox transition of P700 pigments and plastocyanin (Stirbet & Govindjee, 2012b)(Fig. 16). It was found, for maize leaves treated with thiamethoxam, an effect on the kinetic pattern was shown. The magnitudes of the fast phase $\Delta MR_{fast}/MR_0 = (MR_0 - MR_{min})/MR_0$ and the slow phase $\Delta MR_{slow}/MR_0 = (MR_{max} - MR_{min})/MR_0$ are calculated from the MR transient (Strasser et al., 2010d). Under TMX (a), the amplitudes of the fast and slow phases in leaves of both genotypes were significantly decreased ($P < 0.05$), while in the case of TMX (b) treatment, the MR amplitude was significantly lower after 10 days compared with the control remained unchanged (Fig. 16 a, b). After 12 days, the MR amplitude of zp 341 decreased under TMX (b) (Fig. 16 d). However, the MR amplitude of zppl 225 was increased under TMX (b) treatment (Fig. 16 c).

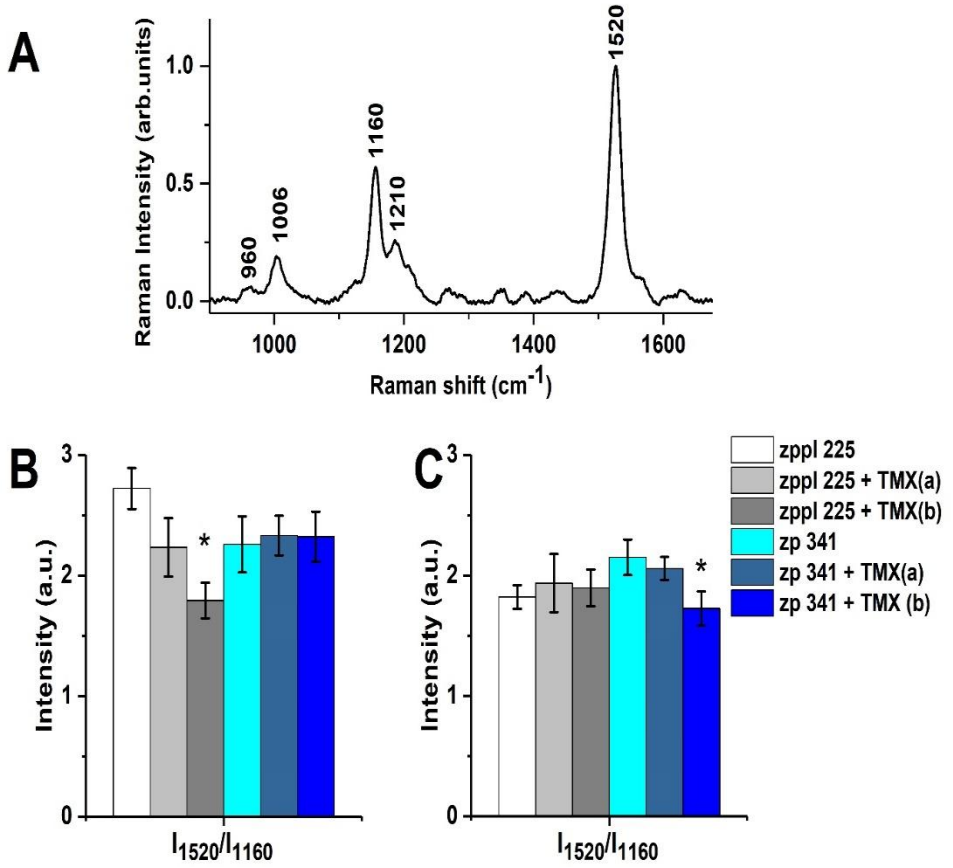

Fig. 17. Raman spectrum of leaf's carotenoids (A). I_{1520}/I_{1160} ratio of the Raman spectrum of zppl 225 and zp 341 on 10th day (B), and 12th day (C) measurement, which added on the 4th day (TMX(a)) and 8th day (TMX(b)) during root irrigation. Statistically results are indicated: *, $P < 0.05$; $n = 5$ for each sample.

In this series of experiments, we investigated changes in RS parameters of carotenoids in control and after thiamethoxam treated plants leaves (Fig. 6). As noted earlier, the energy bands characterize the stretching vibrations of the π-electrons in the molecule (Fig. 17A). In Raman spectrum, 1160 and 1520 cm^{-1}bands correspond to the –C–C– and –C=C– vibrations of the carotenoid molecule bond, and the change in the intensity ratio I_{1520}/I_{1160} reflects changes in the contribution of –C=C– bonds vs. –C–C- bonds of the polyene chain (Vlasov et al., 2020).

It was found, in the presence of thiamethoxam, the absolute value of the intensity and the position of the bands in the Raman spectrum are the same as in the control. The Raman spectra and I_{1520}/I_{1160} ratio of carotenoids of zppl 225 and zp 341 grown under thiamethoxam treatment for 10 (B) and 12 (C) days are shown in Fig. 17. It was found, the conformation of carotenoids

did not differ between the control samples of the two genotypes. However, a decrease in I_{1520}/I_{116} was observed in the leaves of zppl 225 under TMX treatment, indicating a double -C=C - the contribution of the bond is reduced. On the other hand, in zp 341, a decrease in I_{1520}/I_{1160} was found after 12 days of thiamethoxam treatment. Possibly, the decrease in the -C=C- bond contribution is consistent with the decrease in carotenoid content.

Summary of this chapter. In this study, thiamethoxam was added to the soil in two ways by root irrigation after 4 days after planting (TMX (a)) and after 8 days of growth (TMX (b)), we applied the fluorescence method and RS was used to analyse the changes in photosynthesis of two genotypes of maize plants treated with thiamethoxam. It was found that the F_V/F_M ratio of plants under the two thiamethoxam treatments did not change throughout the growth period, suggesting that the main photochemical reactions were not affected. These results are consistent with our previous study showing that thiamethoxam had no significant effect on PSII photochemistry in leaves of the two genotypes studied by foliar spraying. PI_{ABS} and PI_{total}, which evaluate plant performance, exhibited ambiguous patterns compared to F_V/F_M. In the leaves of the inbred line zppl 225, the values of these parameters increased, indicating improved photosynthetic efficiency during thiamethoxam. In fact, thiamethoxam can improve physiological and metabolic activity (Macedo et al., 2013b). It was found, whereas in the hybrid zp 341, the values of PI_{ABS} and PI_{total} decreased, indicating a worsened photosynthetic effect due to electron migration from the Q_A to the PQ pool (ψ_{Eo}) and a reduced probability of electron transport from the PQ pool to the PSI terminal electron acceptor (δ_{R0}). PSI centres showed relative tolerance to the TMX(b) treatment in the leaves of the two maize genotypes. In contrast, under TMX(a) treatment, significant changes in the amplitudes of the fast and slow phases of MR kinetics were observed in leaves of both genotypes, indicating a reduction in oxidation of PC and $P700^+$ ($\Delta MR_{fast}/MR_0$), and a subsequent reduction in ($\Delta MR_{slow}/MR_0$). In both maize genotypes, the obtained parameter $\Delta MR_{fast}/MR_0$ decreased after 10 days of TMX, demonstrating a decrease in the amount of oxidizable P700 and PC. In zp 341, the decrease in $\Delta MR_{slow}/MR_0$ coincided with an increase in PF V_I amplitude and a decrease in φ_{R0} and δ_{R0} parameters, indicating a decrease in electron flux from the PQ pool to PSI. Therefore, the rate of $P700^+$ reduction decreases due to the limitation of electrons from PSII. After 12 days, a change in MR

amplitude under TMX (b) treatment (decrease in $\Delta MR_{fast}/MR_0$ and $\Delta MR_{slow}/MR_0$) was observed only in zp 341 leaves, consistent with a decrease in chlorophyll and a change in carotenoid conformation (decrease of -C = C- peak). DF remained practically unaltered in leaves of both maize genotypes under thiamethoxam treatment after 10 days. However, decrease in fast phase (I_1 peak) in leaves of these maize genotypes was noticed after 12 days indicating decrease the electric component of electrochemical potential. Possible, these results may be related to the accumulation or metabolism of thiamethoxam during growth period. According to RS, the changes of carotenoids conformation (decrease in contribution of –C=C– bonds) was found in zppl 225 after 10 days whereas in zp 341 after 12 days under thiamethoxam treatment.

4.3 The effect of different concentrations thiamethoxam.

In this series of experiments, thiamethoxam was spray on the leaves when 3rd leaf appearance (day 8) (TMX(c)) and spray on the soil when seedling into the soil (day 4) (TMX(d)). In order to study the effect of the pesticide on the pigment status of the leaves, fluorescence parameters and Raman spectra were recorded twice: on day 10 and on day 12.

4.3.1 Two concentrations of TMX spray on leaves (day 8) (TMX(c))

In this series of experiment, we studied the changes of Raman spectra parameters of carotenoids in the control and in the plants after TMX(c) treatment (Fig. 18, Fig. 19). In Raman spectrum bands attributed to carotenoids (1520 and 1160 cm^{-1}) were revealed. The mentioned band characterise stretching vibration of π-electrons in the molecule. In the presence of thiamethoxam, the absolute values of the intensities and the position of the bands in the Raman spectrum are same as in the control. The presence of peaks at 1160 cm^{-1} in the Raman spectra indicates the state of carotenoids characteristic of the 15-cis conformation and does not change under thiamethoxam treatment.

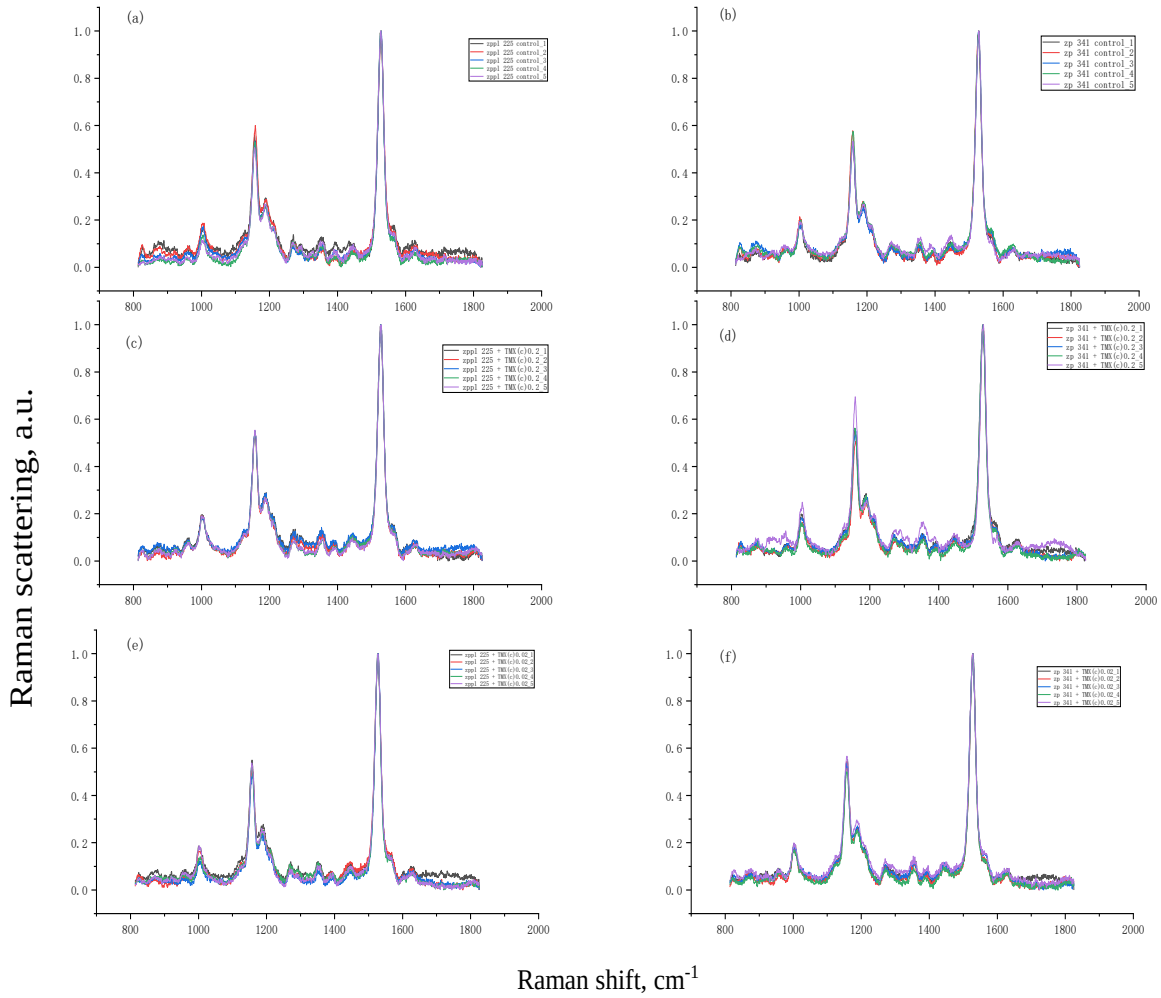

Fig. 18. Raman spectra recorded in maize leaf of the zppl 225 (a, c, e) and zp 341 (b, d, f) under (TMX(c)) treatment with 0.2 mg/mL (c, d); (e, f) 0.02 mg/mL of (TMX(c)); measurements were made at day 10. n = 5 for each sample.

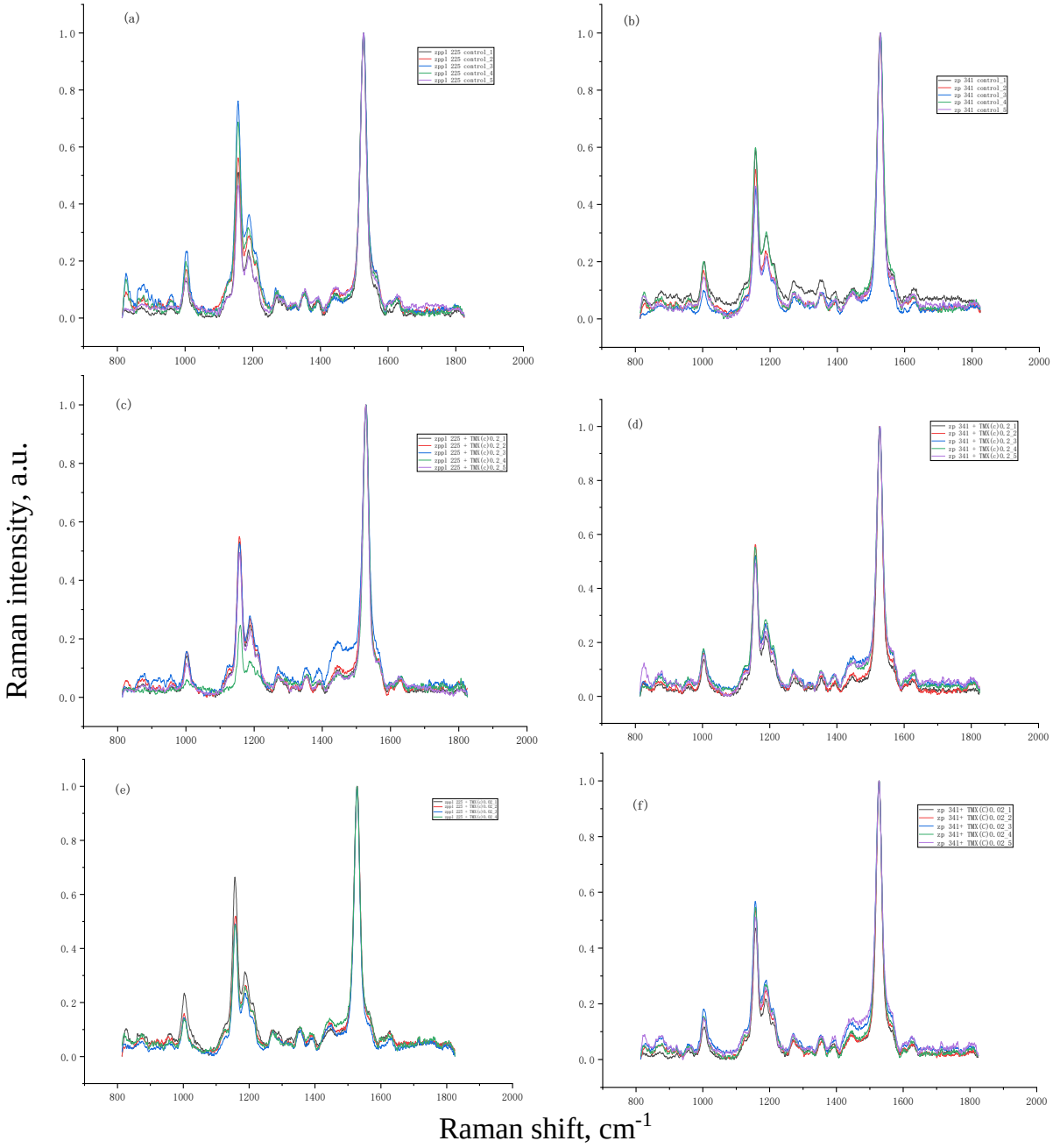

Fig. 19. Raman spectra recorded in maize leaf of the zppl 225 (a, c, e) and zp 341 (b, d, f) under (TMX(c)) treatment with 0.2 mg/mL (c, d); (e, f) 0.02 mg/mL of (TMX(c)); measurements were made at day 12. n = 5 for each sample.

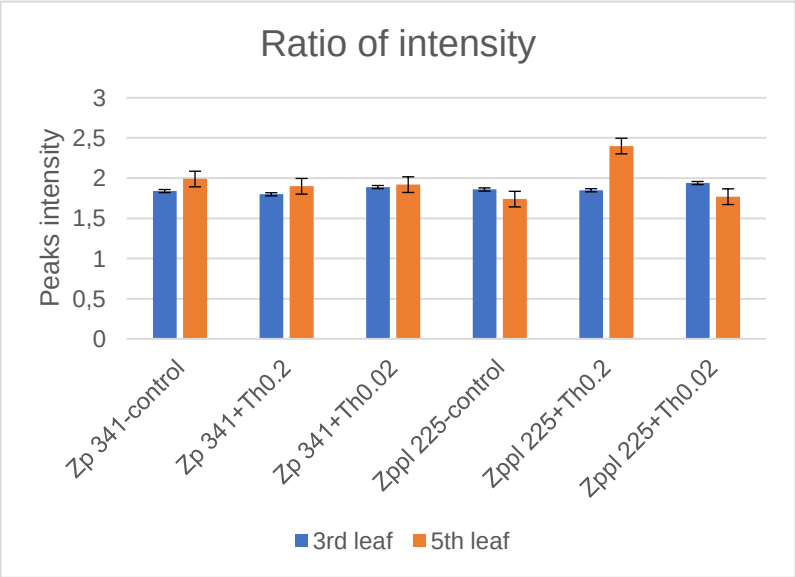

Fig. 20. I_{1520}/I_{1160} ratio of the Raman spectrum of zppl 225 and zp 341 at TMX(c) concentration of 0.2 mg/mL and 0.02 mg/mL. The measurement performed at 3rd leaf (day 10) and 5th leaf (day 12). n=5 for each sample.

In this study, the comparison effects of TMX(c) at 0.2 mg/mL and 0.02 mg/mL concentrations spray TMX(c) on the surface of 3rd leaf (measurement on day 10) treatment, was found (Fig. 20): the thiamethoxam at 0.02mg/mL stimulated a significant and opposite changes in the molecular conformation of carotenoids. It was found, during 12 days, the leaves of hybrid (zp 341) show a similar intensity ratio (I_{1520}/I_{1160}). 0.2 mg/mL TMX(c) significantly different from Zppl 225 (Fig. 20). The 0.2 mg/mL TMX causes RS intensity increase in both Zp 341 and Zppl 225, compare of the result obtain on day 10 and day 12. This result may suggest that thiamethoxam at 0.02 mg/mL does not result in a significant change in the conformation of the carotenoid molecule

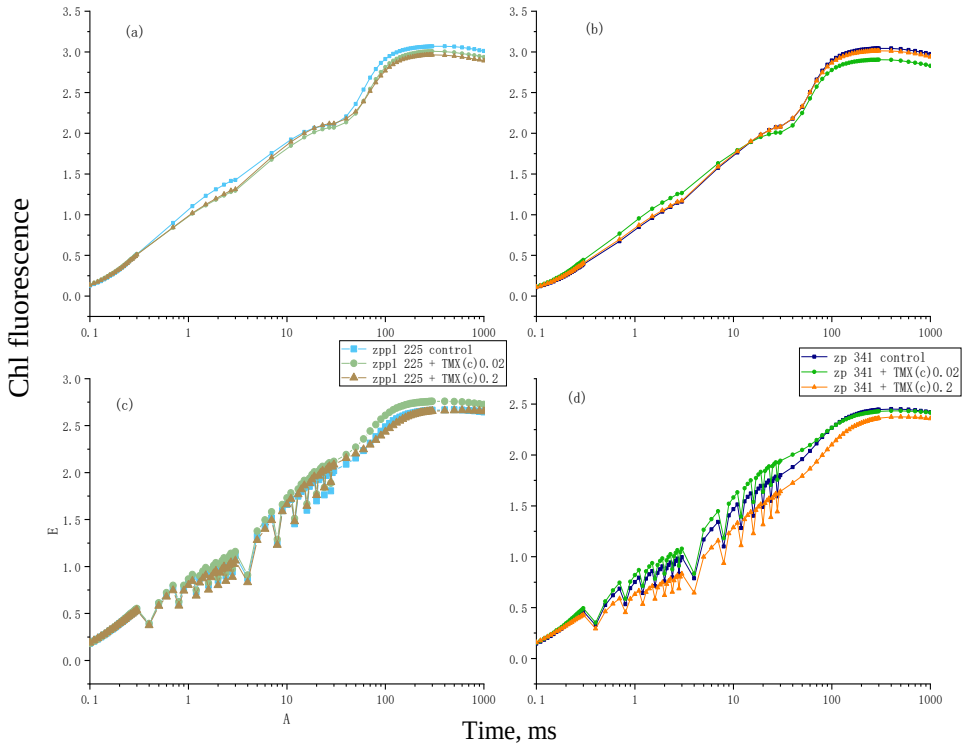

Fig. 21. OJIP transients recorded in maize leaves of the zppl 225 (a, c) and zp 341 (b, d) during TMX treatment. (a, b) 3rd leaf (day 10); (c, d) 5th leaf (day 12) of zppl 225 (a, c) and zp 341; n = 5 for each sample.

Table 4. JIP-test parameters derived from analysis of OJIP induction curves for leaves of zp 341 and zppl 225 during TMX treatment added on the 3rd leaf (day 8). Measurements performed on 10th day. Values are calculated on the base n=5

Fluorescence parameter	zppl 225	zppl 225+TMX 0.2	zppl 225+TMX 0.02	zp 341	zp 341+TMX 0.2	zp 341+TMX 0.02
F_V/F_M	0.77±0.005 (100%)	0.76±0.005 (99%)	0.76±0.004 (99%)	0.76±0.005 (100%)	0.76±0.008 (97%)	0.75±0.005 (98%)
ABS/RC	2.10±0.044 (100%)	2.30±0.065 (110%)	2.36±0.080 (112%) *	2.07±0.052 (100%)	2.13±0.048 (103%)	2.13±0.069 (103%)
ψEo	0.62±0.043 (100%)	0.65±0.022 (105%)	0.65±0.022 (105%)	0.71±0.015 (100%)	0.70±0.023 (99%)	0.66±0.016 (93%)
PI_{ABS}	2.65±0.561 (100%)	2.51±0.237 (95%)	2.60±0.198 (98%)	3.73±0.355 (100%)	3.54±0.642 (95%)	2.77±0.194 (74%) *

Table 5. JIP-test parameters derived from analysis of OJIP induction curves for leaves of zp 341 and zppl 225 upon thiamethoxam treatment on the 3rd leaf (day 8). Measurements performed on 12th day. Values are calculated on the base n=5

Fluorescence parameter	zppl 225	zppl 225+TMX 0.2	zppl 225+TMX 0.02	zp 341	zp 341+TMX 0.2	zp 341+TMX 0.02
F_V/F_M	0.74±0.003 (100%)	0.75±0.008 (99%)	0.74±0.010 (100%)	0.72±0.026 (100%)	0.72±0.008 (100%)	0.71±0.016 (99%)
ABS/RC	3.05±0.044 (100%)	2.99±0.130 (98%)	3.21±0.063 (105%)	3.00±0.262 (100%)	2.09±0.158 (97%)	3.46±0. 156 (115%) *
ψEo	0.67±0.034 (100%)	0.66±0.065 (99%)	0.69±0.020 (103%)	0.67±0.123 (100%)	0.65±0.027 (97%)	0.73±0.026 (109%)
PI_{ABS}	1.91±0.385 (100%)	2.03±0.597 (106%)	1.95±0.260 (102%)	2.08±1.067 (100%)	1.63±0.117 (78%) *	1.93±0.226 (93%)

OJIP transients were recorded in inbred line leaves (zppl 225) and hybrid ling (zp 341) of maize during action of 0.2 mg/mL and 0.02 mg/mL thiamethoxam, which were added after 3rd leaf appearance (Fig. 21). In control maize plants of zppl 225 and zp 341, the kinetics displayed a pattern typical of plants grown at standard conditions, with J, I, and P steps of 2, 30, and ~200 ms, respectively. It was found, the transient changes in OJIP at 10 and 12 days of growth (Table 4,Table 5). The most adequate parameter of the JIP-test is the F_V/F_M ratio which correlates with the maximal quantum yield of the PSII primary photochemical reaction and is used as an indicator of photosynthesis efficiency. There are no statistically significant differences between control and maize after TMX treatment.

The correlation between PI_{ABS} and plant viability reflects the current functioning of PSA under stress. Compare with the control and TMX treated group on 10th day measurement, zp 341 treated by 0.2 mg/mL thiamethoxam and 0.02 mg/mL decreased by 5% and 26%; zppl 225 treated by 0.2 mg/mL and 0.02 mg/m thiamethoxam are not significant (Table 4). Compare with the control and thiamethoxam treated group on 12th day measurement, zp 341 treated by 0.2 mg/mL TMX and 0.02 mg/mL decreased by 22% and 7%; for zppl 225 difference is not

significant (Table 5). The significant decrease of zp 341 due to the decrease of electron transport at acceptor side of PSII.

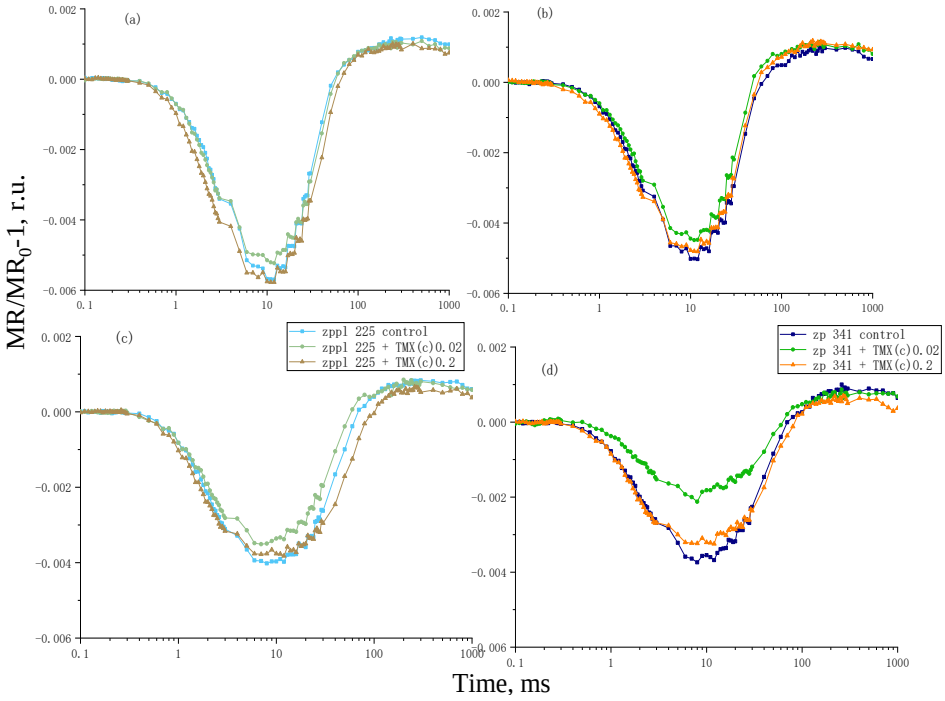

Fig. 22. Modulated 820 nm reflection (MR) kinetics recorded in maize leaves of the zppl 225 (a, c) andzp 341 (b, d) during TMX which added on the 4th (TMX (c)) by Kinetic curves are normalized to the initial value at 0.7ms (MR_0). (a, b) 3rd leaf (day 10); (c, d) 5th leaf (day 12) of maize of the zppl 225 (a, c) and zp 341; n = 5 for each sample.

MR kinetics upon thiamethoxam treatment has been investigated. It is known, MR_{min} is a transient steady state which P700 oxidation and re-reduction rates are equal. Absorption at λ = 820 nm decreases and the MR signal (slow phase) increases to a maximum (MR_{max}) at about 200 ms due to the superior reduction rate of electron donation by PSII to the oxidation rate. (Furutani et al., 2020). Thiamethoxam action led to changes in the redox P700 transformations in leaves of both the hybrid line (zp 341) and inbred line (zppl 225) (Fig. 22). It was found, 0.02 mg/mL thiamethoxam cause significant increase rate in fast phase and slow phased on zp 341. For Zppl 225, difference between two concentrations is not as significant as Zp 341, but 0.02 mg/mL thiamethoxam still cause more decreased than 0.2 mg/mL thiamethoxam and control.

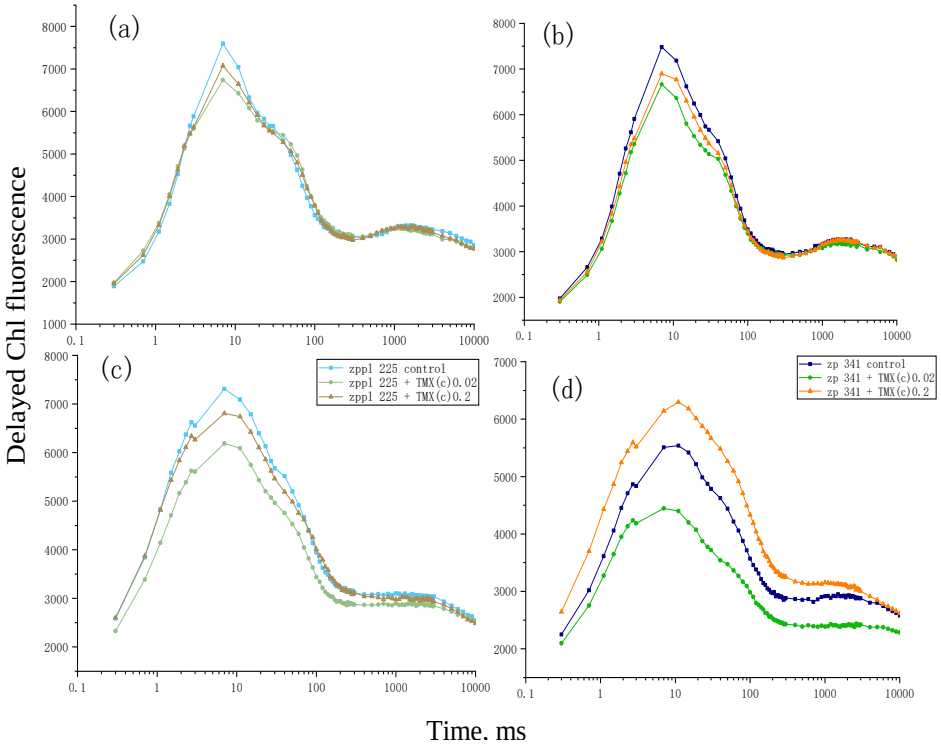

Fig. 23 Light-induced delayed Chl fluorescence (DF) kinetics recorded in maize leaves of the zppl 225 (a, c) and p 341 (b, d) under TMX which added on the 8th day(TMX (c)) spray on the leaves. (a, b) 3rd leaf (day 10); (c, d) 5th leaf (day 12) of maize of the zppl 225 (a, c) and zp 341; n = 5 for each sample.

Delayed fluorescence is proportional to the rate of recombination reactions in PSII, which is influenced by thylakoid membrane energisation. (Goltsev et al., 2009b) The fast phase of DF has two peaks I_1 (~ 7 ms) and I_2 (~ 100 ms) before dropping to a minimum of D_2 (~ 200 ms). Fig. 23 shows that the induction curves of zp 341 and zppl 225 DF which treated by thiamethoxam. It was found, I_1 amplitude decreased in zppl 225 which might due to the decrease in the Q_A re-oxidation rate (disturbance of electron transport on the acceptor side of PSII) and/or a decrease in the Z^+ reduction from 4MnCa of oxygen-evolving complex (OEC). It was found, low concentration of TMX caused more effect on zppl 225. For zp 341, measurement performed on 10^{th} day, I_1 amplitude also decreased for both concentrations. But the measurement performed on 12^{th} day, high concentration increased I_1 amplitude and low concentration decreased I_1 amplitude.

4.3.2 The Raman spectra parameters of carotenoids in the plants under two concentrations of TMX spray action on soil (day 4) (TMX(d))

In this series of experiment, we studied the RS of carotenoids in the control and in the plants during TMX(d) treatment (Fig. 24,Fig. 25). In Raman spectrum bands attributed to carotenoids (1520 and 1160 cm^{-1}) were revealed. The mentioned band characterise stretching vibration of π-electrons in the molecule. In the presence of thiamethoxam, the absolute values of the intensities and the position of the bands in the Raman spectrum are same as in the control. The presence of peaks at 1160 cm^{-1} in the Raman spectra indicates the state of carotenoids characteristic of the 15-cis conformation and does not change during thiamethoxam treatment.

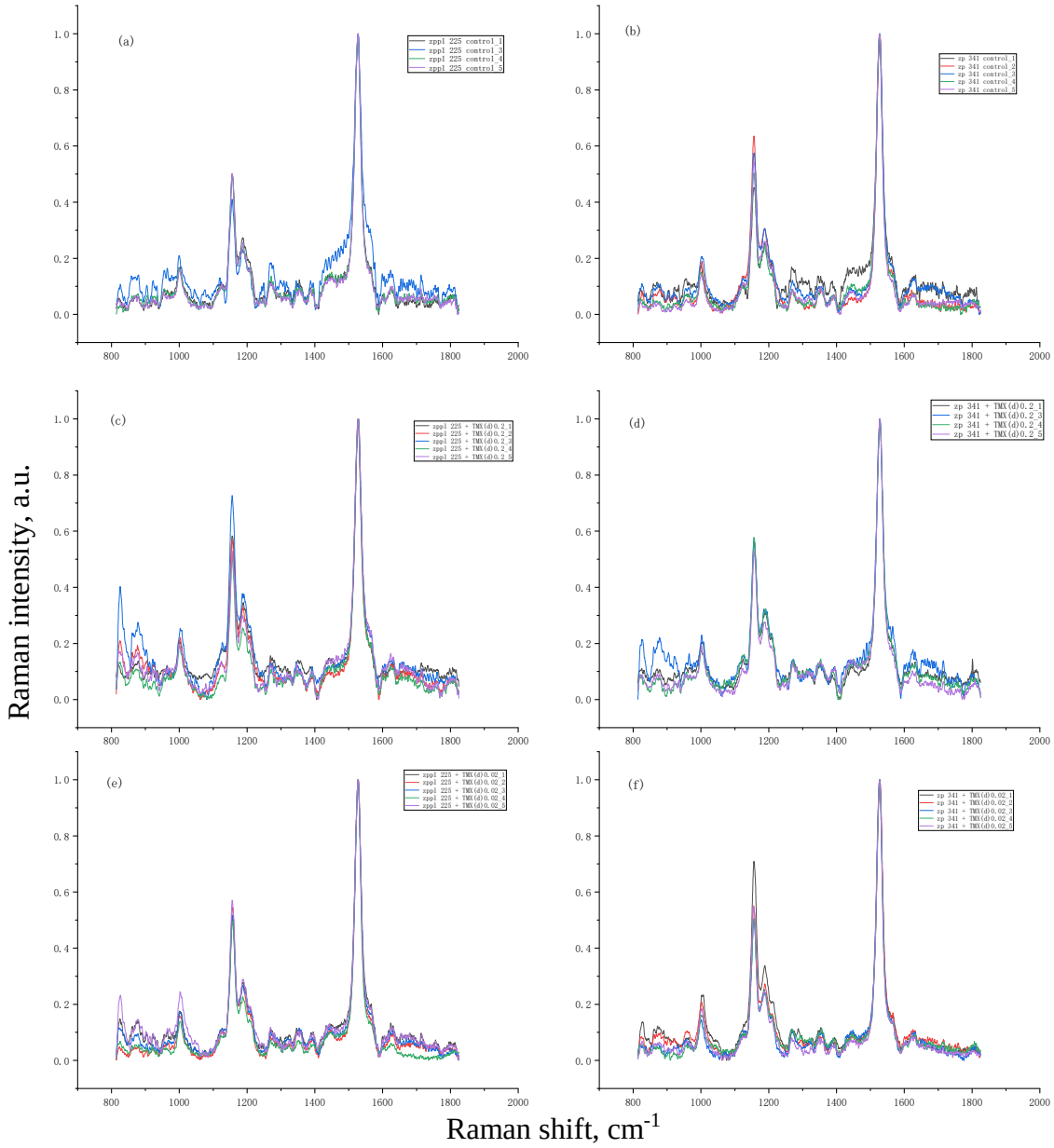

Fig. 24. Raman spectra recorded in maize leaf of the zppl 225 (a, c, e) and zp 341 (b, d, f) during (TMX(d)) treatment with 0.2 mg/mL (c, d); (e, f) 0.02 mg/mL of (TMX(d)); measurements were made at day 10. n = 5 for each sample.

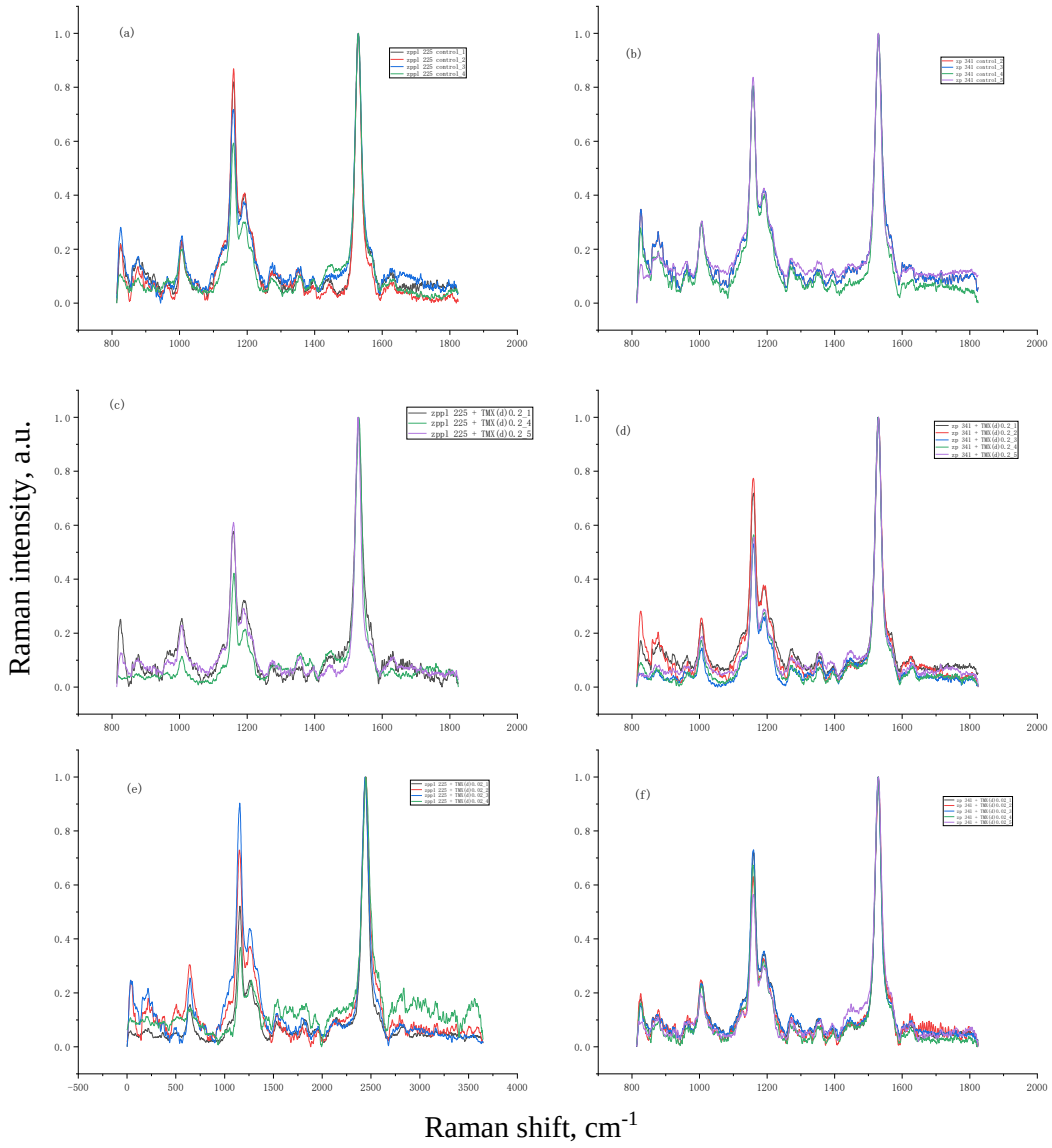

Fig. 25. Raman spectra recorded in maize leaf of the zppl 225 (a, c, e) and zp 341 (b, d, f) during (TMX(d)) treatment with 0.2 mg/mL (c, d); (e, f) 0.02 mg/mL of (TMX(d)); measurements were made at day 12. n = 5 for each sample.

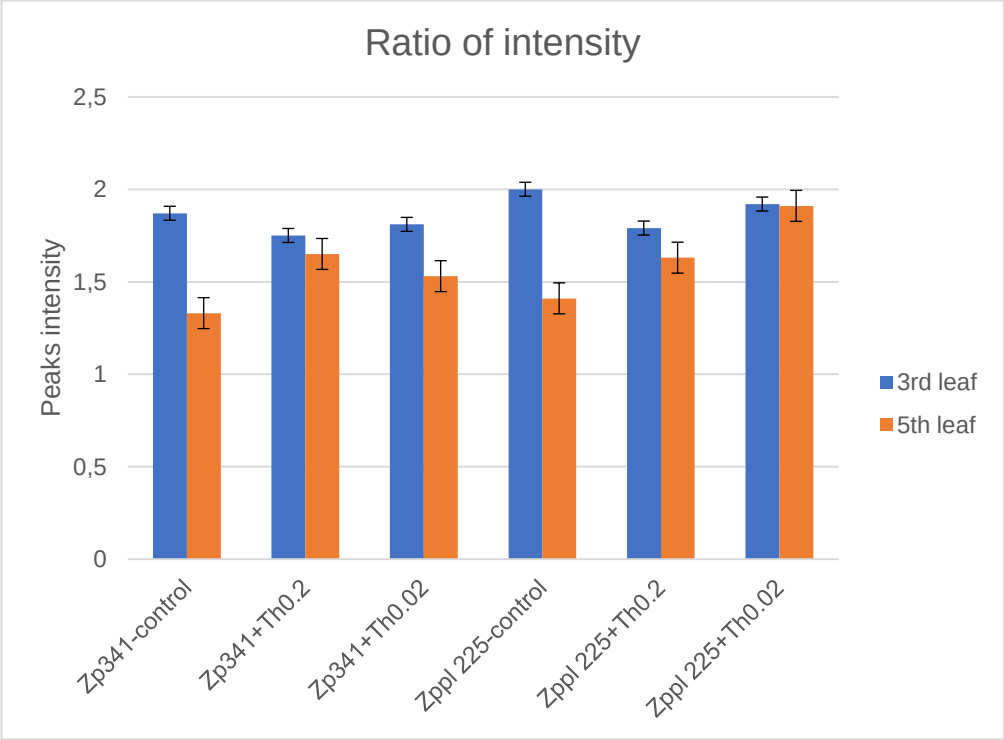

Fig. 26. I_{1520}/I_{1160} ratio of the Raman spectrum of zppl 225 and zp 341 during TMX(d) concentration of 0.2 mg/mL and 0.02 mg/mL. measurement performed at 3rd leaf (day 10) and 5th leaf (day 12). n=5 for each sample.

Comparison of TMX(d) at 0.2 mg/mL and 0.02 mg/mL concentrations treatment, concentration has significant impact on spray TMX(d) on the surface of 3rd leaf (measurement on day 10) (Fig. 24). TMX(d) at 0.2mg/mL has been determined to cause significant and opposite changes in the molecular conformation of carotenoids. Results on day 12, TMX(d) show difference between zppl 225 and zp 341 (Fig. 25). For further analyse, I_{1520}/I_{1160} ratio of the Raman spectrum has been calculated (Fig. 26). During 0.2 mg/mL TMX effects more on zp341 then 0.02 mg/mL thiamethoxam, but, on the other hand, 0.02 mg/mL TMX shows more effect then 0.2 mg/mL TMX on zppl 225.

Comparing with effect of TMX(c) and TMX(d), spray thiamethoxam on soil drives more influence than spray on the leaf when 3rd leaf appearance. The experimental results showed that carotenoid molecules conformational changed dramatically when zppl 225 maize was exposed to low concentrations of thiamethoxam. It was found, the application of thiamethoxam caused conformational changes in carotenoid molecules in leaves.

4.3.2.1.2 M-pea-2 investigation of the effect of a pesticide on the state of pigments molecules in leaves.

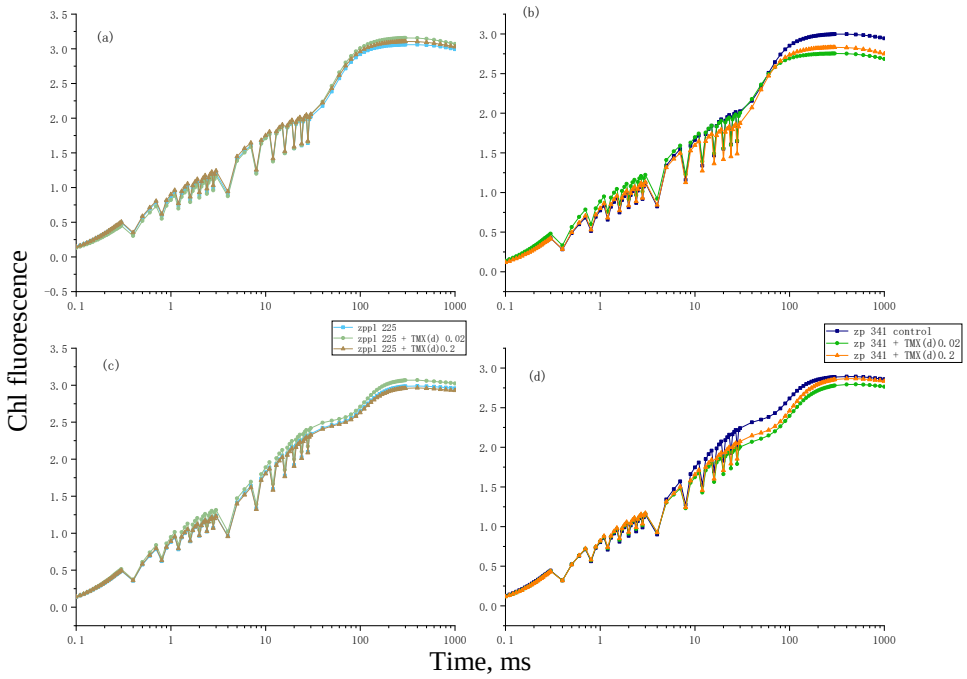

Fig. 27. OJIP transients recorded in maize leaves of zppl 225 (a, c) and zp 341 (b, d) under TMX(d) treatment. (a, b) 3rd leaf (day 10); (c, d) 5th leaf (day 12) of maize zppl 225 (a, c) and zp 341; n = 5 for each sample.

Table 6. JIP-test parameters derived from analysis of OJIP induction curves for leaves of two maize genotypes during TMX treatment added on the planting seeding in the soil (day 4). Measurements performed on 10th day. Values are calculated on the base n=5

Fluorescence parameter	zppl 225	zppl 225+TMX 0.2	zppl 225+TMX 0.02	zp 341	zp 341+TMX 0.2	zp 341+TMX 0.02
F_V/F_M	0.76±0.040 (100%)	0.77±0.002 (101%)	0.77±0.002 (101%)	0.76±0.013 (100%)	0.75±0.009 (99%)	0.75±0.005 (99%)
ABS/RC	2.56±0.042 (100%)	2.38±0.179 (93%)	2.39±0.077 (93%)	2.42±0.089 (100%)	2.46±0.225 (102%)	2.38±0. 098 (98%)
ψEo	0.70±0.021 (100%)	0.70±0.026 (100%)	0.71±0.037 (101%)	0.72±0.024 (100%)	0.66±0.057 (92%)	0.70±0.024 (97%)
PI_{ABS}	2.96±0.240 (100%)	3.30±0.673 (111%)	3.36±0.599 (114%) *	3.37±0.587 (100%)	2.39±0.747 (71%) *	2.88±0.431 (85%) *

Table 7. JIP-test parameters derived from analysis of OJIP induction curves for leaves of two maize genotypes upon TMX treatment added on the planting seeding in the soil (day 4). Measurements performed on 12th day. Values are calculated on the base n=5

Fluorescence parameter	zppl 225	zppl 225+TMX 0.2	zppl 225+TMX 0.02	zp 341	zp 341+TMX 0.2	zp 341+TMX 0.02
F_V/F_M	0.76±0.011 (100%)	0.77±0.007 (101%)	0.76±0.011 (100%)	0.76±0.010 (100%)	0.75±0.007 (99%)	0.75±0.011 (99%)
ABS/RC	2.38±0.191 (100%)	2.29±0.114 (96%)	2.40±0.225 (88%) *	2.36±0.114 (100%)	2.28±0.166 (97%)	2.21±0. 159 (94%)
ψEo	0.67±0.055 (100%)	0.65±0.049 (97%)	0.66±0.027 (99%)	0.69±0.078 (100%)	0.67±0.066 (97%)	0.67±0.025 (97%)
PI_{ABS}	2.72±0.517 (100%)	2.72±0.470 (100%)	2.61±0.330 (96%)	3.03±1.013 (100%)	2.66±0.623 (89%) *	1.75±0.284 (58%) *

The JIP-test was employed in order to the thiamethoxam action on the important photosynthetic parameters derived from the OJIP transient (Table 6,Table 7). There are no statistically significant differences between control and maize after thiamethoxam treatment.

The correlation between PI_{ABS} and plant viability reflects the current functioning of PSA under plants stress. It was found, TMX treated group on 10th day measurement, zp 341 treated by 0.2 mg/mL TMX and 0.02 mg/mL, PI_{ABS} decreased by 29% and 15%; zppl 225 treated by 0.2 mg/mL and 0.02 mg/m TMX increased by 11% and 14% (Table 6). Compare with the control and TMX treated group on 12th day measurement, zp 341 treated by 0.2 mg/mL TMX and 0.02 mg/mL PI_{ABS} decreased by 11% and 42%; for zppl 225 difference is not significant (Table 7). The significant decrease of zp 341 due to the decrease of electron transport at acceptor side of PSII (ψ_{E0}).

So, compare experiments TMX(c) and TMX(d), spray thiamethoxam fction on the soil, when seedling the seeds cause more influence than spray on leaves when 3rd leaf appearance. It was found, thiamethoxam cause decrease of electron transport at acceptor side of PSII. hybrid line (zp 341) is more sensitive to thiamethoxam effect than inbred line (zppl 225).

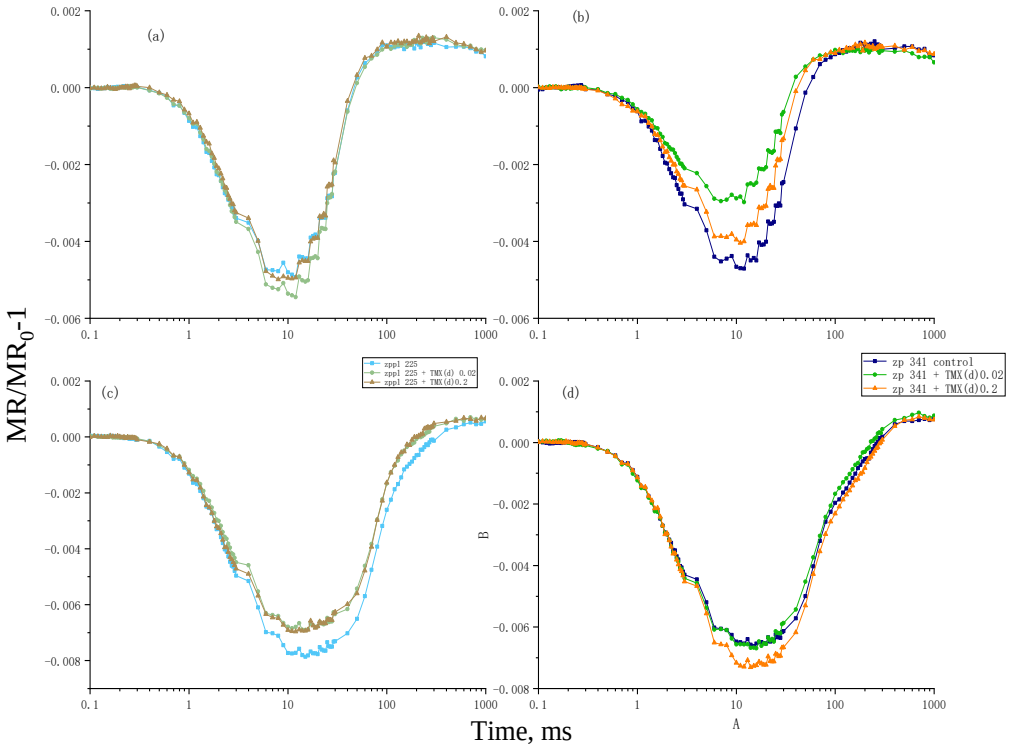

Fig. 28. Modulated 820 nm reflection (MR) kinetics recorded in maize leaves of the zppl 225 (a, c) and zp 341 (b, d) under TMX(d) which added on the 4th (TMX (c)) by Kinetic curves are normalized to the initial value at 0.7ms (MR_0). (a, b) 3rd leaf (day 10); (c, d) 5th leaf (day 12) of maize of zppl 225 (a, c) and zp 341; n = 5 for each sample.

In MR kinetics measurements on 10th day (Fig. 28. a,b), two concentrations of thiamethoxam cause zp 341 both decreased rate in fast phased and slow phase. Possible, it due to a decrease in the acceptor pool. It was found, in 12th day measurements (Fig. 28. c,d), high concentration of thiamethoxam cause rate increase of zp 341 MR kinetics, but for zppl 225, different concentration didn't cause much difference.

Compare results with TMX(c) and TMX(d), treatment of thiamethoxam time cause different influence by the concentration. Hybrid line (zp 341) is more sensitive than inbred line (Zppl 225).

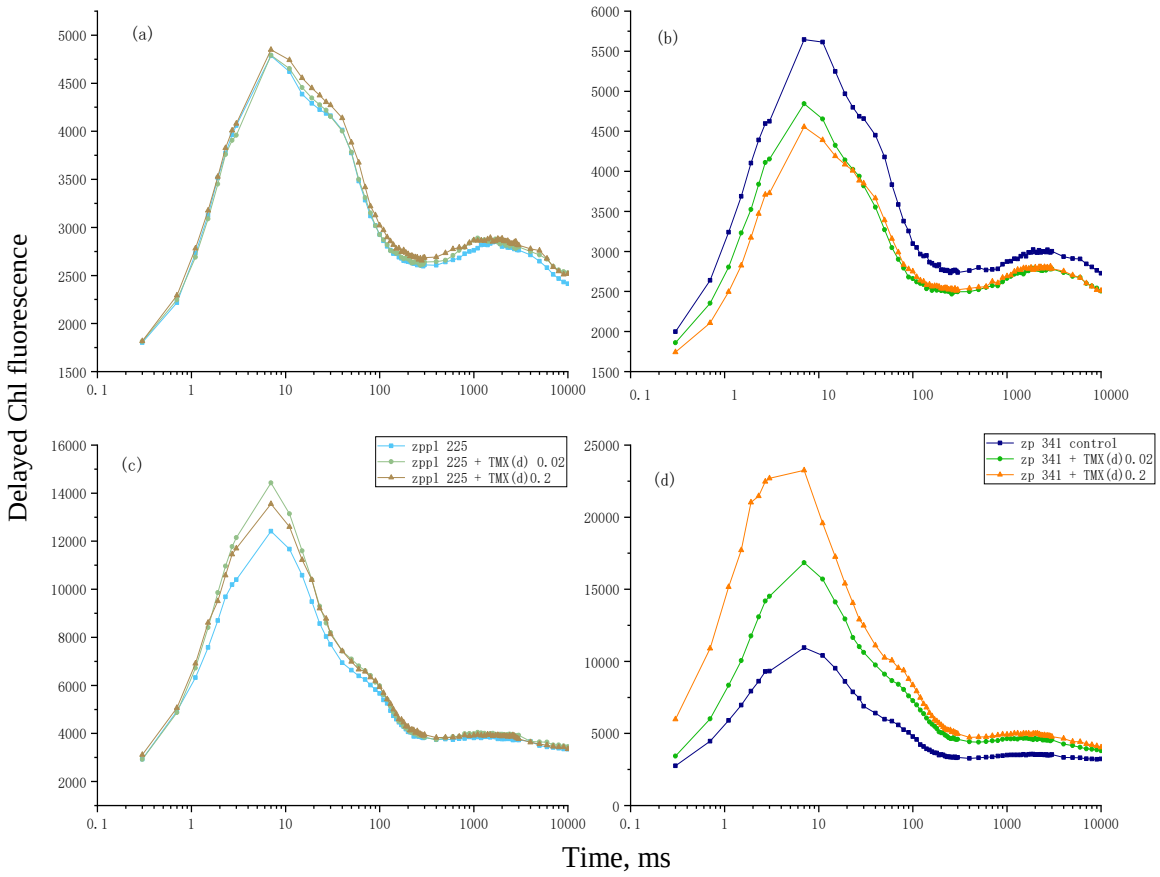

Fig. 29. Light-induced delayed Chl fluorescence (DF) kinetics recorded in maize leaves of the inbred line (zppl 225) (a, c) and hybrid (zp 341) (b, d) under TMX which added on the 4th day (TMX (d)) spray on the leaves. (a, b) 3rd leaf (day 10); (c, d) 5th leaf (day 12) of maize of the inbred line (Zppl 225) (a, c) and hybrid (zp 341); n = 5 for each sample.

Fig. 29 shows that the DF induction curves of zp 341 and inbred zppl 225 which treated by thiamethoxam. It was found, I_1 amplitude DF increased in zppl 225 which might due to the increase in the Q_A re-oxidation rate (disturbance of electron transport on the acceptor side of PSII) and/ or increase in the Z^+ reduction from 4MnCa of oxygen-evolving complex (OEC). Using low concentration of thiamethoxam caused more effect on zppl 225. It was found, for zp 341, measurement performed on 10^{th} day, I_1 amplitude also decreased for both concentrations. But the measurement performed on 12^{th} day, both concentrations cause increased I_1 DF amplitude.

So, compare results with TMX(c) and TMX(d), zp 341 is more sensitive to the thiamethoxam treatment. Spray TMX on the soil when seeding the seeds cause more effect than spray on the leaves when 3^{rd} leaf appearance.

4.4 IR spectroscopy investigation of the chemical composition and molecular structure of the different hybrids of maize seeds.

As we have already noted, one of the goals of our work was to identify molecular changes in various genotypes, which will make it possible in the future to formulate a technology for diagnosing and breeding plants in the field. For this type of research, the best method is not the Raman spectroscopy method, but the infrared spectroscopy method, which is what was done in this series of experiments. IR spectroscopy was used to investigate changes in the chemical composition and molecular structure of the seeds of the maize samples. The IR spectra of seeds of maize lines and hybrids revealed 22-24 bands in the range 4000 - 400 cm^{-1}. The main changes in the amplitude of the IR spectra were found in the range 1200 - 900 cm^{-1} and for the band at 3360 cm^{-1}.

Infrared spectra of maize seeds contain plant-specific 1651-1530 cm^{-1} bands (stretching vibrations of C = O in primary, secondary and tertiary amides, bending vibrations of NH and CN in secondary amides of protein molecules, peptides and free amino groups) acid, which also characterizes the OH groups of the cellulose crystallization water), 1050 cm^{-1} - aromatic C–H in-plane deformation vibrations. (Radenovic et al., 2016; 2021;2023) The high-amplitude and broadband infrared spectra found in all seed samples in the 3500-3000 cm^{-1} range may indicate the presence of stretching vibrations of free and bound OH groups, intramolecular and intermolecular hydrogen bonds. Dimers and polymers, as well as stretching vibrations, NH-bonds (primary amides 3540-3480 cm^{-1}, 3420-3380 cm^{-1} , secondary amides 3460-3420 cm^{-1}) and free OH-groups (water, carbohydrate compounds, amino acids), NH-groups (amino acids and their derivatives, proteins).

During the maize seeds study, IR spectra were obtained, which we divided the spectrum into three spectral regions:

Region 1 (called 4000-2800 cm^{-1}): mainly comes from the absorption of methyl, hydroxyl, amino and methylene.

Region 2 (1750-1200 cm^{-1}): mainly the mixed absorption zone of protein, fatty acid and polysaccharide.

Region 3 (1200-800 cm^{-1}): Mainly due to the absorption of starch and polysaccharides.

IR spectra of corn seeds contain plant-specific bands

1. 1651 - 1530 cm^{-1} (stretching vibrations of C = O in primary, secondary and tertiary amides, bending vibrations of N-H and C-N in secondary amides of protein molecules, peptides and free amino acids, also characterize the OH groups of crystalline water of cellulose),

2. 1050 cm^{-1} - aromatic C-H in-plane deformation vibrations.

3. high-amplitude and wide band of the IR spectrum in the range of 3500-3000 cm^{-1} may indicate the presence of stretching vibrations of the free and bound OH-group, intra- and intermolecular H-bonds in dimers and polymers, as well as stretching vibrations, NH-bonds (primary amides 3540-3480 cm^{-1}, 3420-3380 cm^{-1}, secondary amides 3460-3420 cm^{-1}) and free OH-groups (water, carbohydrates, amino acids), NH-groups (amino acids and their derivatives, proteins).

4. IR spectra of seeds are 2919 and 2855 cm^{-1}, which probably indicates the contribution of deformation vibrations of C-H bonds; the amplitude of the 995 cm^{-1} band of the IR spectrum was lower, which indicates a change in the contribution of C - H - bending vibrations of alkenes.

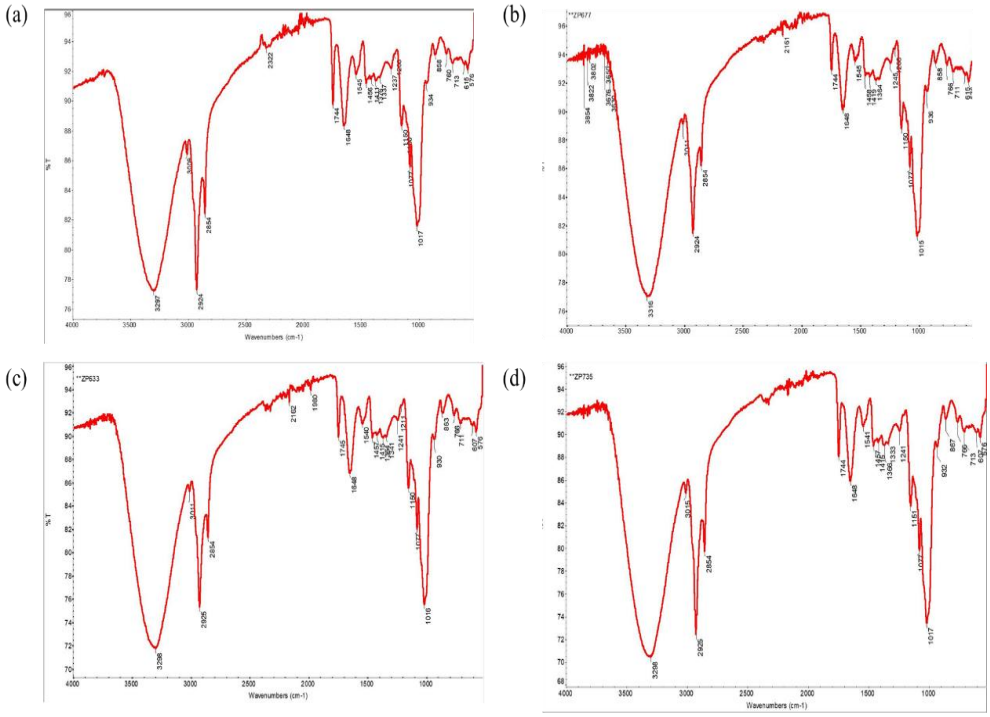

Fig. 30. Infrared spectrum of four maize hybrids. (a) zp 684; (b) zp 677; (c) zp 633, (d) zp 735.

Table 8. Three characteristic peaks of 4 maize hybrids

	wavenumber, cm^{-1}	T%
ZP 684	1017	88.52
	1648	93.82
	1744	94.7
ZP 677	1016	86.56
	1648	95.38
	1744	97.15
ZP 633	1016	82.36
	1648	92.53
	1745	95.1
ZP 735	1017	81.6
	1648	92.99
	1744	93.41

It is known, the peak at 2925 cm^{-1} and peak at 1744 cm^{-1} are the lipid, the peak 1744 cm^{-1} represents the lipid hydroxyl vibration. The peak at 1648 cm^{-1} is the amide I protein. The 1017 cm^{-1} peak can be considered as a representative of carbohydrates. ZP 735 has the highest carbohydrate and lipid content. ZP 684 and ZP 735 are rich in protein (Table 8).

The IR and relative intensities of the main absorption peaks of the four maize types are shown in Fig. 30, respectively. The spectral shapes of the four samples were basically the same, but there were some differences in the positions and relative intensities of the absorption peaks, which indicated that there was no change in the main components, but only a slight difference in the content of each component.

First experiment's results represented the total IR spectra of seed of various corn hybrids. In the following, the contribution of various components in various hybrids seeds will be analysis.

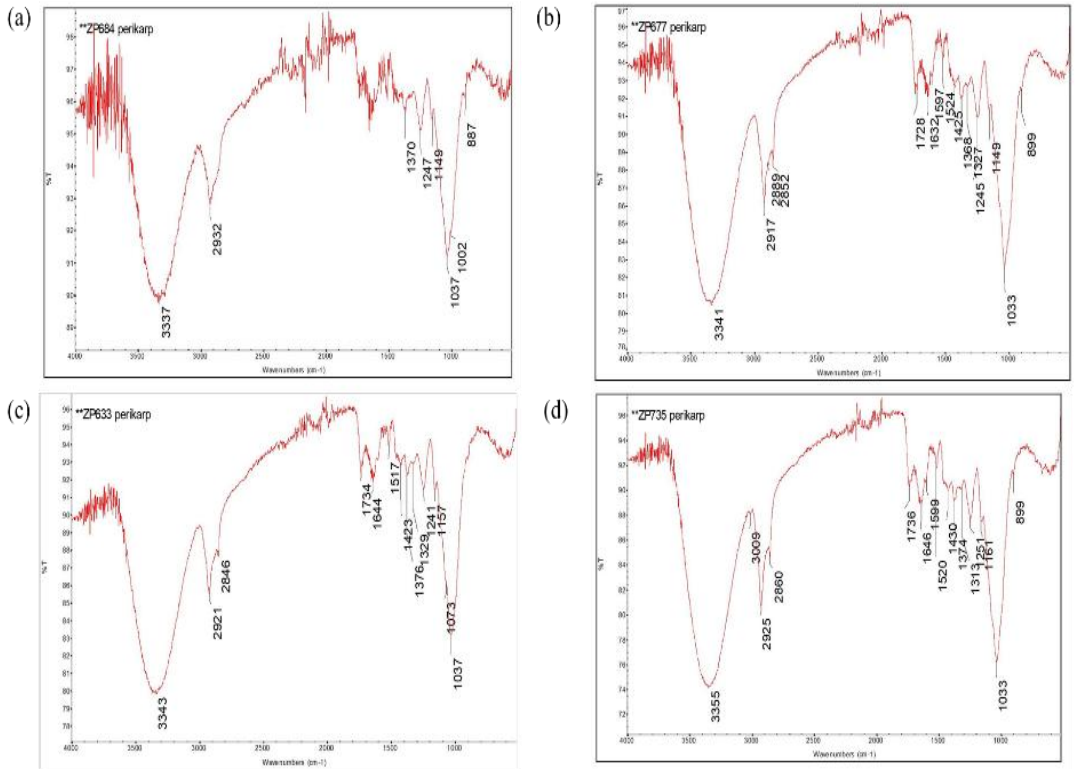

Fig. 31. Infrared spectra of four maize hybrids pericarp. (a) zp 684; (b) zp 677; (c) zp 633, (d) zp 735.

Table 9. Three characteristic peaks of the pericarp of 4 maize hybrids

	wavenumber, cm^{-1}	T%

ZP 684	1037	94.41
	1666	97.48
	1740	98.67
ZP 677	1033	88.8
	1632	96.04
	1728	96.16
ZP 633	1037	88.97
	1644	96.11
	1734	96.41
ZP 735	1033	84.36
	1648	93.94
	1736	94.58

In Fig. 31 it is noted that the intensity of the 1037 cm^{-1} peak is the biggest which means that the main component of the pericarp is starch and polysaccharides. Compared to the pericarp of the four hybrids, ZP 735 contains the richest carbohydrates, proteins and lipids. The differences in protein and lipid are not so significant (Table 9). The positions of the peaks are also displaced, especially the 1017 cm^{-1} peak, which can be taken into account when changing starch components.

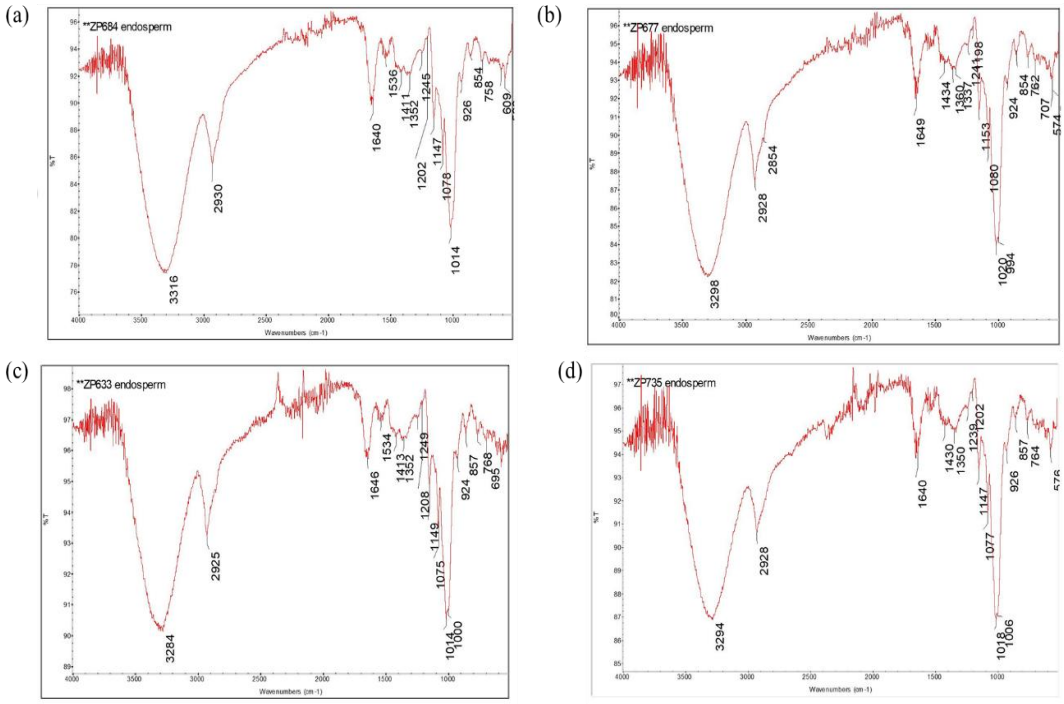

Fig. 32. Infrared spectra of four maize hybrids endosperms. (a) zp 684; (b) zp 677; (c) zp 633, (d) zp 735.

Table 10. Three characteristic peaks of four maize hybrids endosperms

	wavenumber,cm^{-1}	T%
ZP 684	1014	85.5
	1640	94.55
	1735	99.7
ZP 677	1012	87.78
	1649	95.88
	1748	99.3
ZP 633	1009	93.47
	1646	98.03
	1894	99.8
ZP 735	1016	89.91
	1640	97.17
	1868	99.8

Infrared spectra of four maize hybrids endosperm are show in Fig. 32. It was found, that the peak 1014 cm^{-1} has the highest intensity and the 1735 cm^{-1} peak is very weak. It was found, the various hybrids, (Table 10), ZP 684 is rich in carbohydrates and proteins, but the differences in proteins between ZP 684 and ZP 677 are negligible.

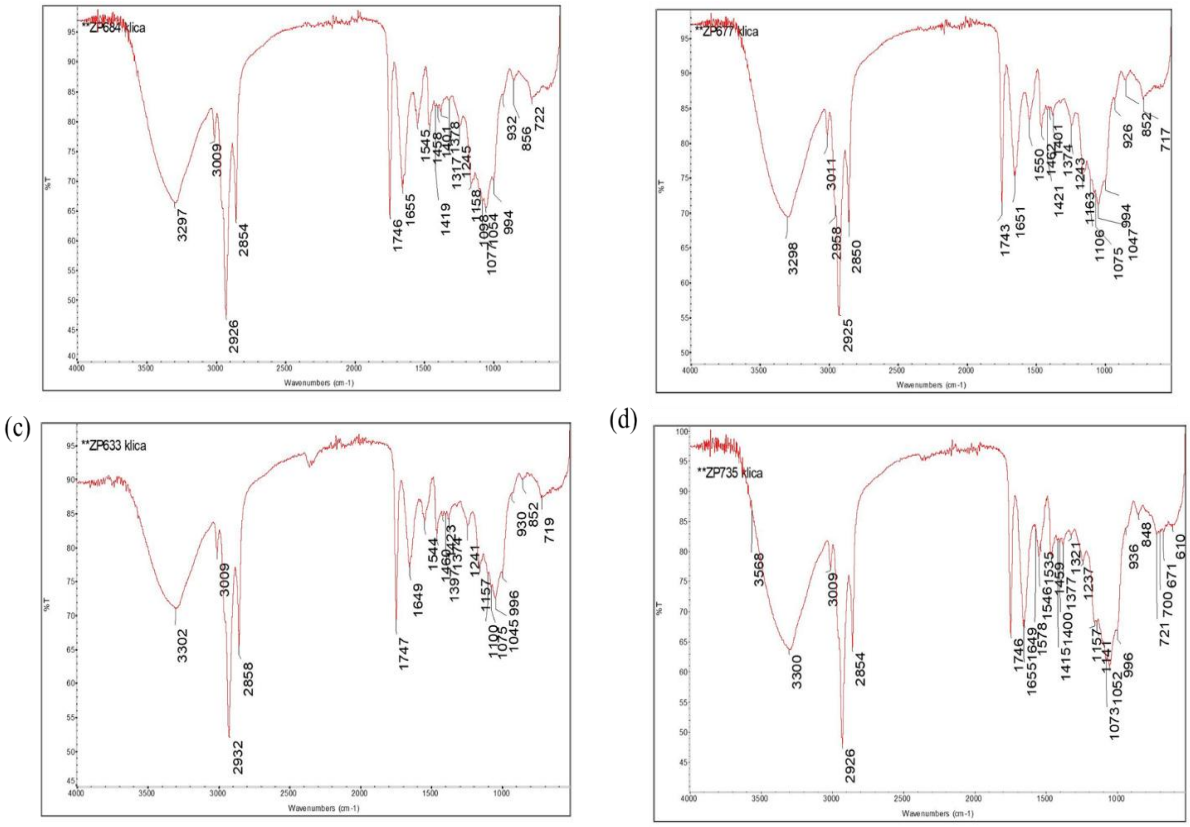

Fig. 33. Infrared spectra of four maize hybrids germs. (a) zp 684; (b) zp 677; (c) zp 633, (d) zp 735.

Table 11. Three characteristic peaks of 4 maize hybrids germs.

	wavenumber, cm^{-1}	T%
ZP 684	1054	79.99
	1655	74.89
	1746	68.49
ZP 677	1047	84.77
	1651	86.72
	1743	78.39
ZP 633	1045	85.57
	1649	89.44
	1747	77.15
ZP 735	1052	76.63
	1655	80.34
	1748	74.05

In Fig. 33, it is presented that the peak of protein and lipids is very strong, among the four hybrids ZP 684 has the highest intensity (Table 11).

In conclusion, it was found, ZP 735 is rich in starch and polysaccharides, but mainly in the pericarp. Of the ZP 684 has the highest protein and lipid intensity, indicating that ZP 684 is the highest oil and quality corn.

In the range of wave numbers from 400 to 4000 cm^{-1} in Surface internal reflection (SIR) spectra of whole grain, endosperm, germs and pericarp of maize revealed bands obtained by IR spectroscopy. By detecting the SIR bands with characteristic band of intensity, it is possible to monitor changes in the content of a number of organic compounds (proteins, lipids, sugars, esters, amides, ketones, aldehydes, carboxylic acids, esters, phenols, alcohols, aromatic hydrocarbons, acyclic compounds, alkenes, alkanes and alkenes) in the seed. By this method, it is possible compare the difference in chemical distribution of different hybrids. It will also increase the profitability of cultivation and the efficiency of breeding not only of maize, but also other agricultural plants.

4.5 Using SERS for studying pigments in plant leaves and seeds.

In our study of plant leaves, we monitored Raman signals from carotenoid molecules. However, the sensitivity can be significantly increased by using silver nanostructures (SERS). In order to investigate the (intensity) dependence of the Raman spectra with silver nanoparticles of different carotene concentration. The vibrational Raman spectrum assignments were outlined in (Kochikov et al., 1985). Raman peaks at 1522, 1106, and 1004 cm^{-1} show in Fig. 34 represent the characteristic peak of carotene molecules. (Deng & Juang, 2014; Huang et al., 2010) Peak at 1522 cm^{-1} assigned to collective C=C stretching mode whose frequency is a function of the effective conjugation length along the backbone of the β-carotene molecule (Legesse et al., 2018). Since the wavelength of the 514 nm laser is very close to the absorption maximum in the UV-vis electron spectrum of carotene, even though they are minor components in blood, the resonance effect selectively enhances the Raman signal of β-carotene (He et al., 2018b).

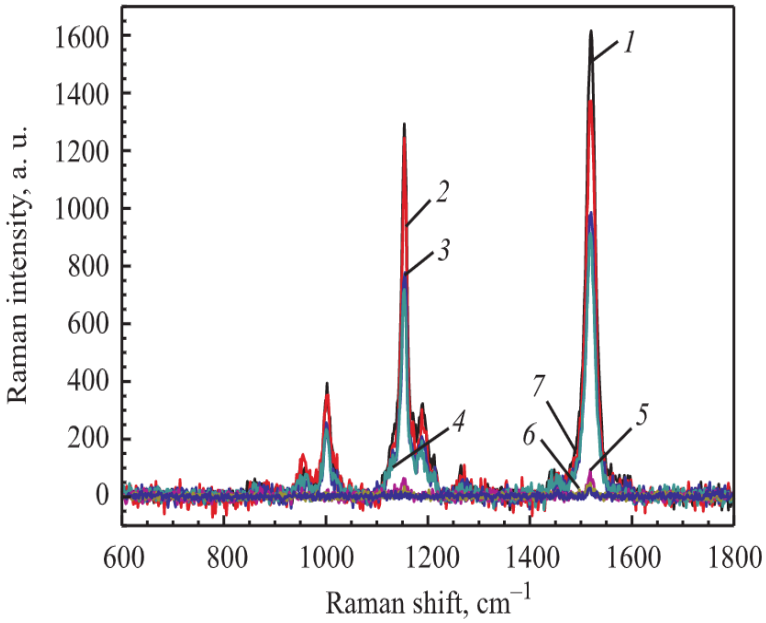

Fig. 34. Raman spectra obtained from β-carotene sample with different concentration. 1 – 20 mg/mL β-carotene (37.2 mM); 2 – 4 mg/mL β-carotene (7.4 mM); 3- 2 mg/mL β-carotene (3.72 mM); 4 – 0.4 mg/mL β-carotene (740 mM); 5 – 0.3 mg/mL β-carotene (372 μM); 6 – 0.04 mg/mL (74 μM); 7 – 0.02 mg/mL β-carotene (37.2 μM).

It was found, that the intensity of Raman spectrum increased with the increase of carotene concentration (0.02-20mg/mL or 37μM-37mM range), and the region with the largest change was (0.25-5mg/mL (466 μM — 931 μM)) (Fig. 35). Therefore, Raman spectroscopy has a sensitivity of 0.02 mg/mL (37 μM) for recording carotene concentrations in solution.

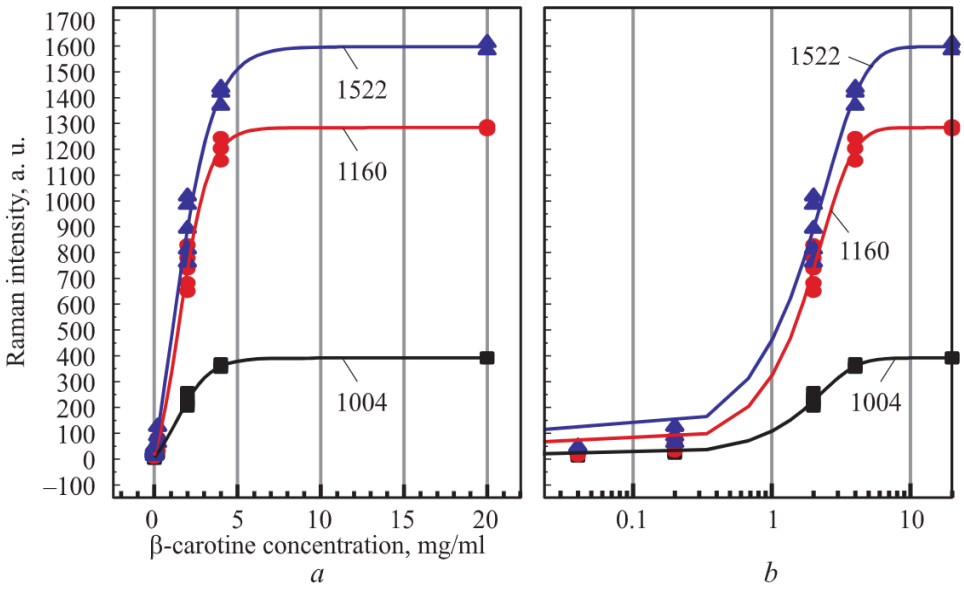

Fig. 35. Calibration graph of different concentration of β – carotene: a – direct relationship; b – decimal logarithm

The next set of experiments focused on the ability to enhance the Raman signal of carotene with nanostructure substrates. It was found that the use of the substrate enhanced the Raman signal when the sample was diluted 10^5-10^6 times Fig. 36 and the substance concentration was 10^{-9} M (Table 12). As a result, the use of nanostructured silver substrates can enhance the Raman scattering of individual carotenoid molecules, which is of importance for biomedical research and diagnostics.

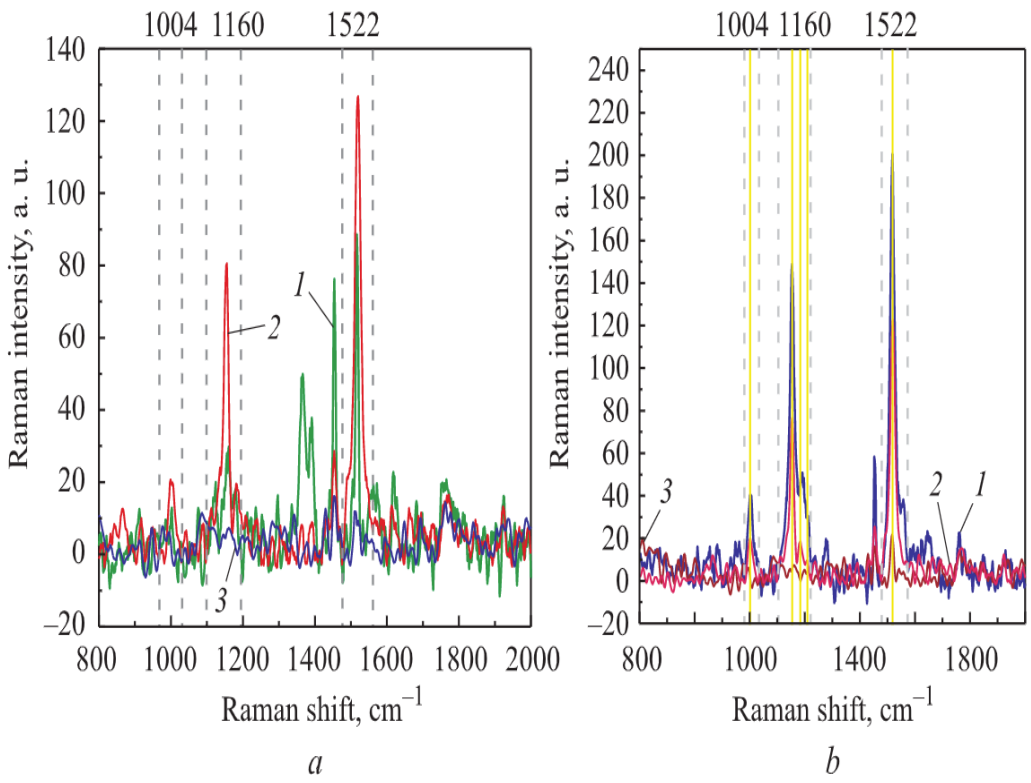

Fig. 36. Raman spectra obtained of diluted to10^6 and 10^5 times sample. 1- sample on a sliver substrate; 2 – sample diluted to 100 times on a sliver; 3 – sample without using substrate (coating).

Depending on the morphology of the nanostructured substrate, the character of the interactions and hence the optimum conditions for enhanced Raman scattering are altered. For this reason, the Raman signal dependence (ratio of characteristic bonds of Raman spectra: I_{1522}/I_{1160}) was investigated to assess the contribution of the stretching vibrations of the double bonds of polyene chains to the Raman spectra. Raman spectra of carotenoid concentrations in solution (I_{1160}/I_{1004}, I_{1522}/I_{1004}) and normalization of the signalling substrates according to the "intramolecular reference"(Fig. 37).

Table 12. Gain factor from Raman spectra (SERS) obtained of diluted to10^6 and 10^5 times sample.

Peak position, cm^{-1}	1004	1160	1522

β - carotene diluted to a concentration of 100,000 fold, with a final concentration of 0.0002 mg/mL			
EF	7702	6444	10617
	6935	4678	8655
	12849	12819	14527
	9954	9550	13454
	11869	10912	15822
	15103	11496	15877
	10735	9316	13159
β - carotene diluted to a concentration of 1,000,000 fold,final concentration of 0.00002 mg/mL			
EF	-	38716	47056
	-	46879	47801
	-	1160	59324
	-	44380	-
	-	21624	71116
	-	33210	-
	-	39430	-
	-	53297	85642
	-	54041	71878
	-	30006	54382
	-	30437	62457
	-	38202	
$EF = (I_{SERS}/I_{cr}) \times (C_{cr}/C_{SERS})$			

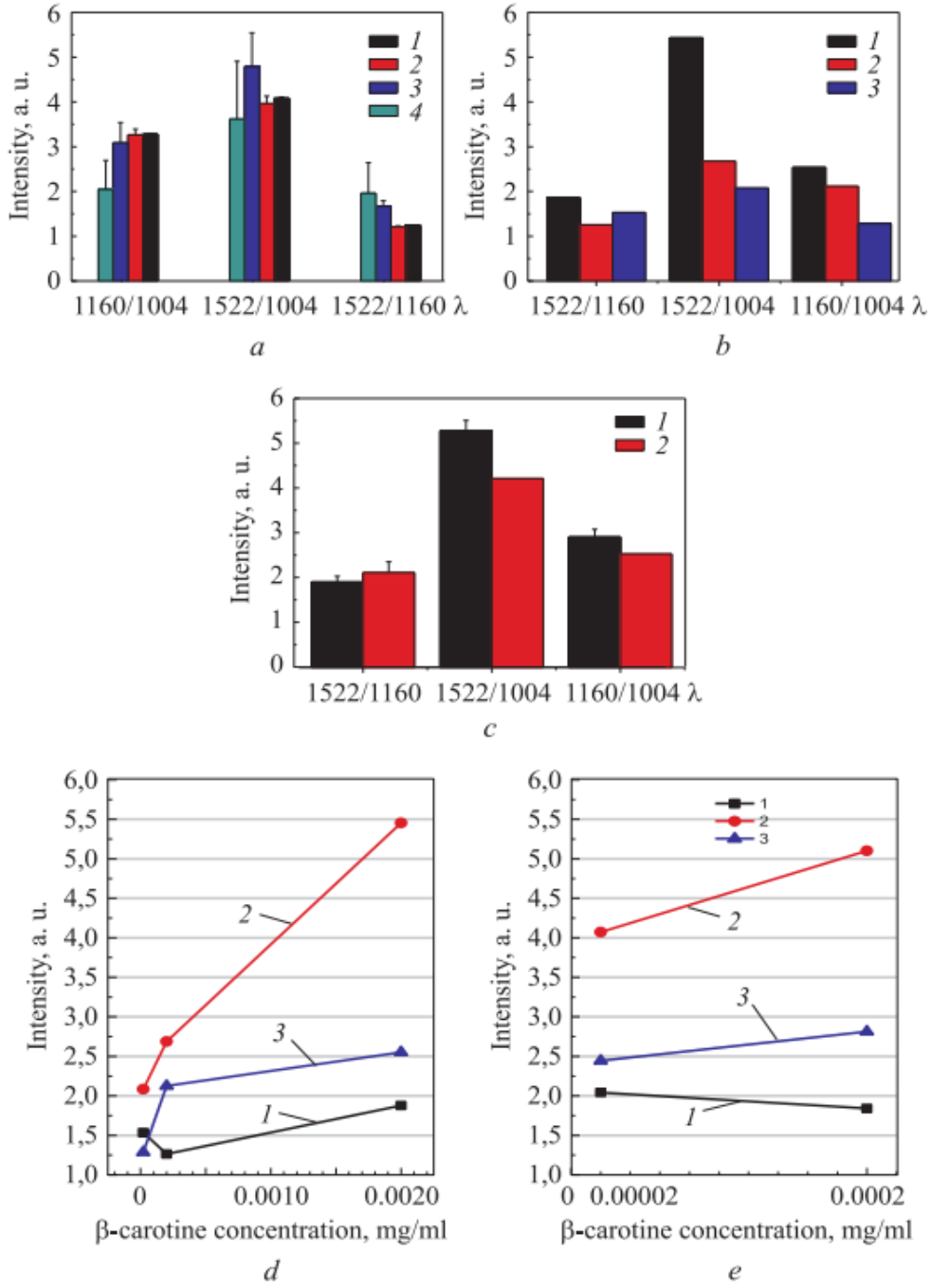

Fig. 37. Peak ratios of β – carotene. a) sample in aqueous solution (1- 20 mg/mL; 2 -2 mg/mL; 3 – 0.2 mg/mL; 4 – 0.02 mg/mL); b) dried sample on silver substrate (1- 0.002 mg/mL; 2 – 0.0002 mg/mL; 3 – 0.00002 mg/mL); c) aqueous solution on a silver substrate (1 – 0.0002 mg/mL; 2 – 0.00002 mg/mL; d) peak ratio of dried sample on silver substrate 1 - I_{1522}/I_{1160}; 2 – I_{1522}/I_{1004}; 3 – I_{1160}/I_{1004}; e) peak ratio of aqueous solution on a silver substrate 1 - I_{1522}/I_{1160}; 2 – I_{1522}/I_{1004}; 3 – I_{1160}/I_{1004}

In order to obtain clearer and more detailed SERS spectra of β-carotene, a series of experiments were performed. Carotene from plasma was diluted 10 to 100 times and

immobilized on nanostructured substrates to detect the Raman signal (Fig. 38). It was found that the main parameters of blood plasma carotene Raman spectrum (band intensity, band position, main band ratio) could be identified and recorded by diluting plasma 100 times. Thus, with the help of Raman it is possible to observe changes in the concentration and conformation of carotenoid molecules. Immobilization of carotenoid molecules on nanostructured matrices significantly increases the sensitivity (amplification factor up to 10^4), which is important for clinical diagnosis. This study shows that Raman spectroscopy with an excitation wavelength of 534 nm can be used as a specific probe for beta-carotene in blood. Analysis of Raman and SERS spectra recorded at 534 nm showed that one of the carotenoids can be detected selectively depending on the preparation of the blood sample using the same excitation line and Raman equipment.

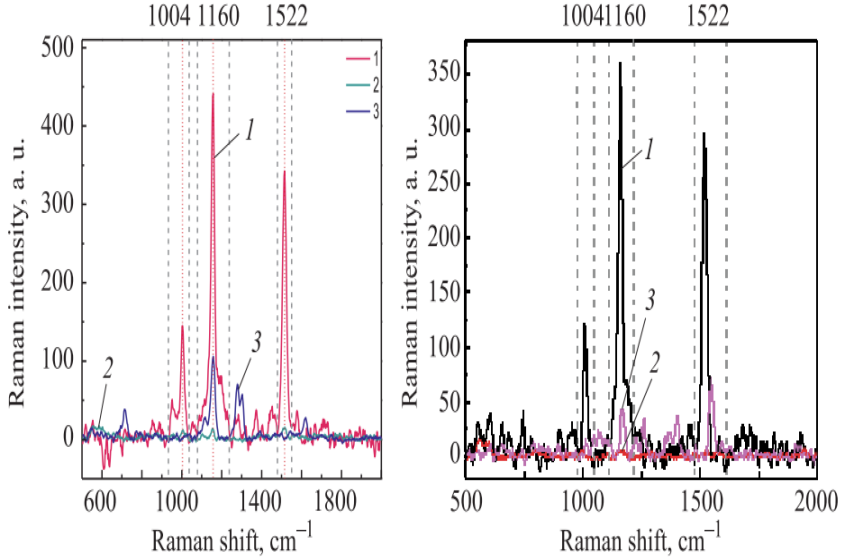

Fig. 38. Raman spectra obtained from blood plasma when diluted: a) 10 times (in solution); b) 100 times (dried) (1 –blood plasma β – carotene sample; 2 – diluted blood plasma β – carotene sample; 3 - diluted blood plasma β – carotene sample on silver substrate)

Using SERS (i.e., mixing colloidal silver with a blood sample), edge labelling occurs, while at normal Raman conditions, resonance enhancement allows direct observation of the β -carotene signature. This highlights the versatility of Raman technology and its promise for biology and agricultural selection (Fig. 39).

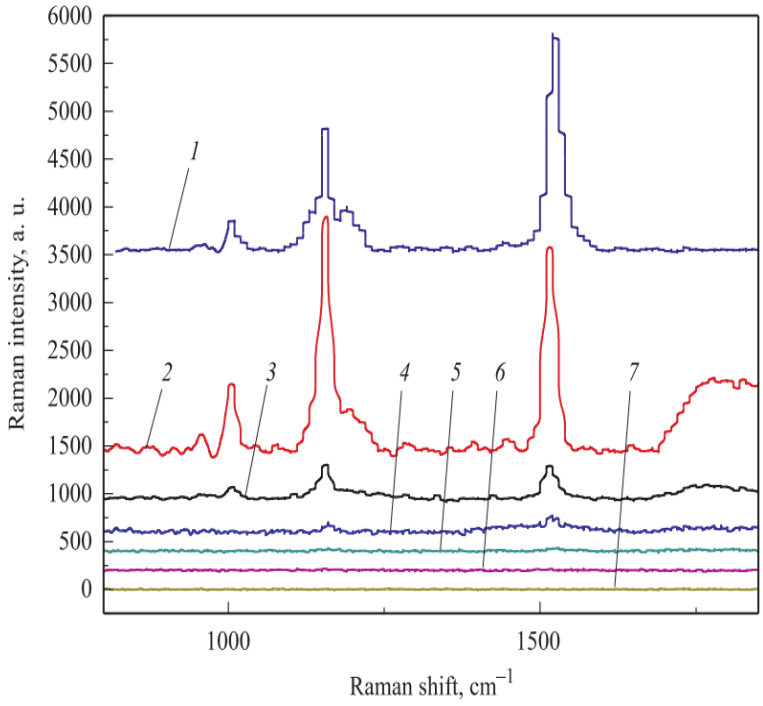

Fig. 39. Raman spectra of carotenoids obtained from different objects: 1 - apple (λ = 473 nm); 2 - undiluted plasma dried on a glass slide; 3 - plasma; 4 - plasma diluted with Alena's buffer 2 times; 5 - plasma diluted with Alena's buffer 10 times; 6 - 100 times;

7 - 1000 times (λ = 532 nm).

In summary, Raman spectroscopy is an advanced method used to study cell physiology, which could help bridge the gaps in our comprehension of these mechanisms. The advantages and other basic details of the method applied to plants (most importantly microalgae) and other species/objects can be seen in the current technology used in the article. Using the substrate, it was found that the Raman signal was enhanced when the sample was diluted 10^5 to 10^6 times and the concentration of substance was 10^{-9} mol/L. Using SERS conditions, coiled-coil labelling occurs, whereas under normal conditions, resonance enhancement allows for direct observation of the carotene signature. This underscores the versatility of Raman technology and the promise it holds for biology and clinical chemistry.

The results of this study show that Raman spectra with an excitation wavelength of 534 nm can be used as a specific probe for carotenoids not only in leaves, bat in the blood and are

implicated in human functioning after using foods with modified carotenoids after treated pesticides plants. Analysis of Raman and SERS spectra recorded at λ = 534 nm revealed that carotenoids can be detected selectively depending on the preparation of blood samples using the same excitation line and Raman equipment.

4.6 Study of changes in the photosynthetic apparatus and morphology of chloroplasts under the action of a pesticide clothianidin

4.6.1 Effect of clothianidin on pigment complexes in chloroplasts using Raman spectroscopy

It is known that when spraying the leaves of higher plants with a pesticide, within 20 minutes the TMX molecule is metabolized to CL (Nauen et al., 2003). In this regard, to study the effect of the in vitro rearrangement of the photosynthetic apparatus CL was used. We used the laser excitation wavelengths were 488 nm and 532 nm to obtain Raman spectra of clothianidin (CL), respectively. (Fig. 40 and Fig. 41). (*These results were jointly obtained with He Yanlin*). Raman spectrum obtained with 532 nm laser excitation have more detail of the structure (Fig. 41) compare to Raman spectrum obtained by 488nm laser (Fig. 40). The intensity of Raman spectrum of CL is very low compare with the intensity of carotenoids. Therefore, the effect of CL itself on the spectrum is not considered.

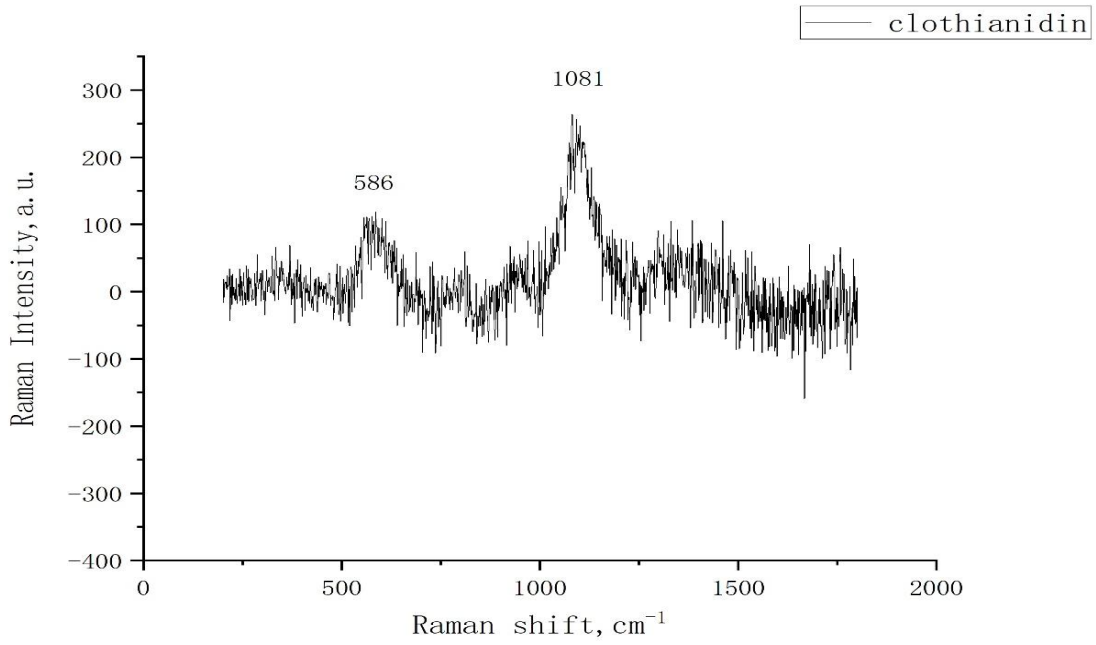

Fig. 40 Raman Spectrum obtained from clothianidin, detected in RS region between 200 and 1800 cm^{-1} (with excitation wavelength of 488nm)

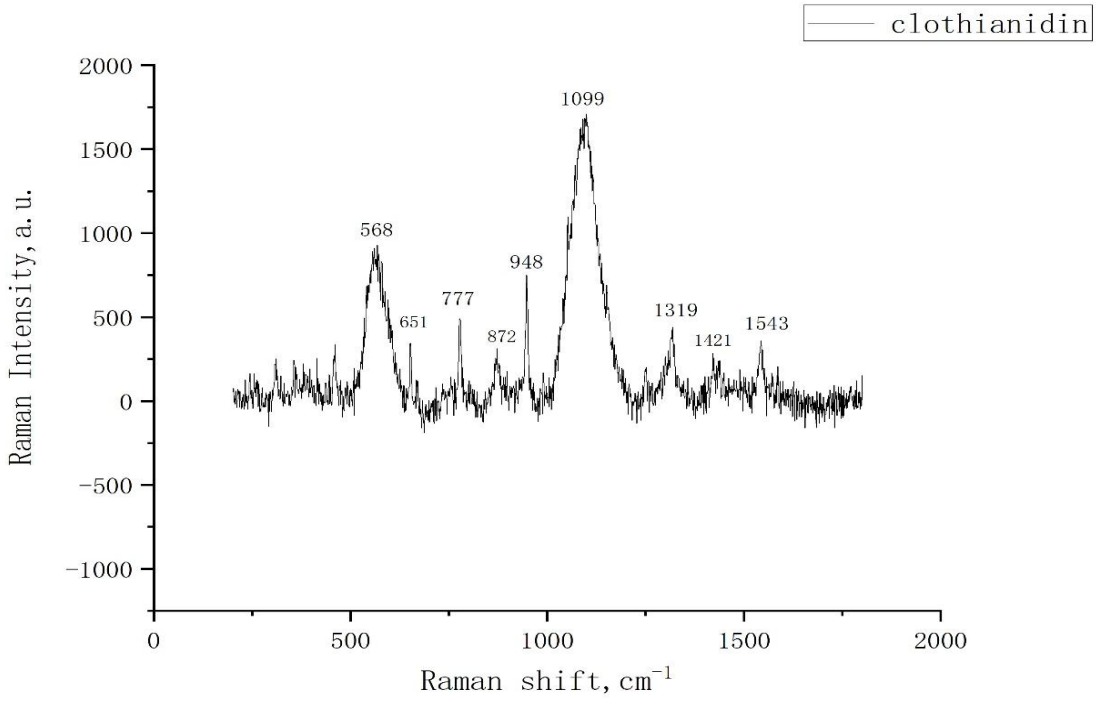

Fig. 41. Raman Spectrum obtained from clothianidin, detected in RS region between 200 and 1800 cm-1 (with excitation wavelength of 532nm)

Raman spectra of β-carotene samples (soybean oil, gelatin, glycerin, corn oil) were obtained, n = 3. Raman spectra of beta-carotene show mainly three peaks with Raman shift around: 1006, 1157, and 1525 cm^{-1} (Fig. 42 and Fig. 43). The Raman spectrum of β-carotene shows three main Raman shift peaks: 1006, 1157 and 1525 cm^{-1} (Fig. 42, Fig. 43). This Raman spectral structure is characteristic of carotenoid molecules. the peak at 1006 cm^{-1} corresponds to the methyl (-C-CH_3) vibration; the peak at 1157 cm^{-1} corresponds to the single-carbon bond vibration; and the peak at 1525 cm^{-1} corresponds to the double-carbon bond vibration. By analysing these characteristic peaks, the structural changes of pigment complexes including β-carotene in chloroplasts can be studied.

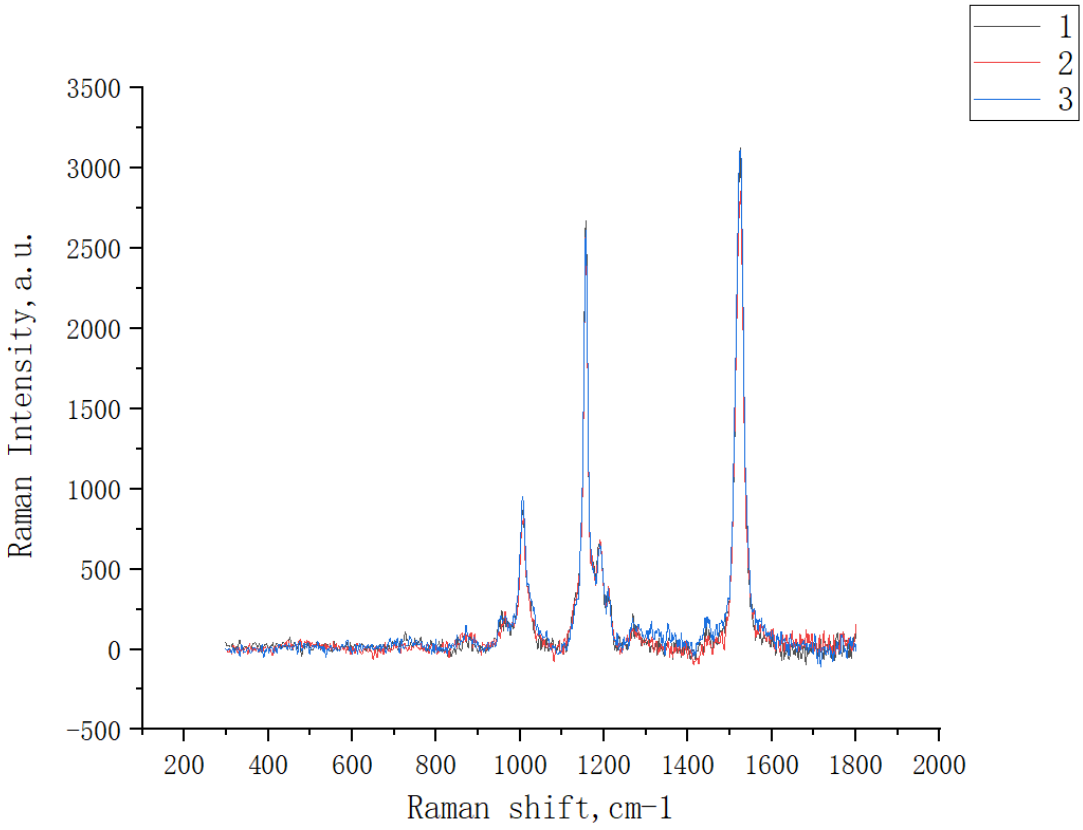

Fig. 42. Raman Spectrum obtained from beta-carotene at 488nm after 20 minutes

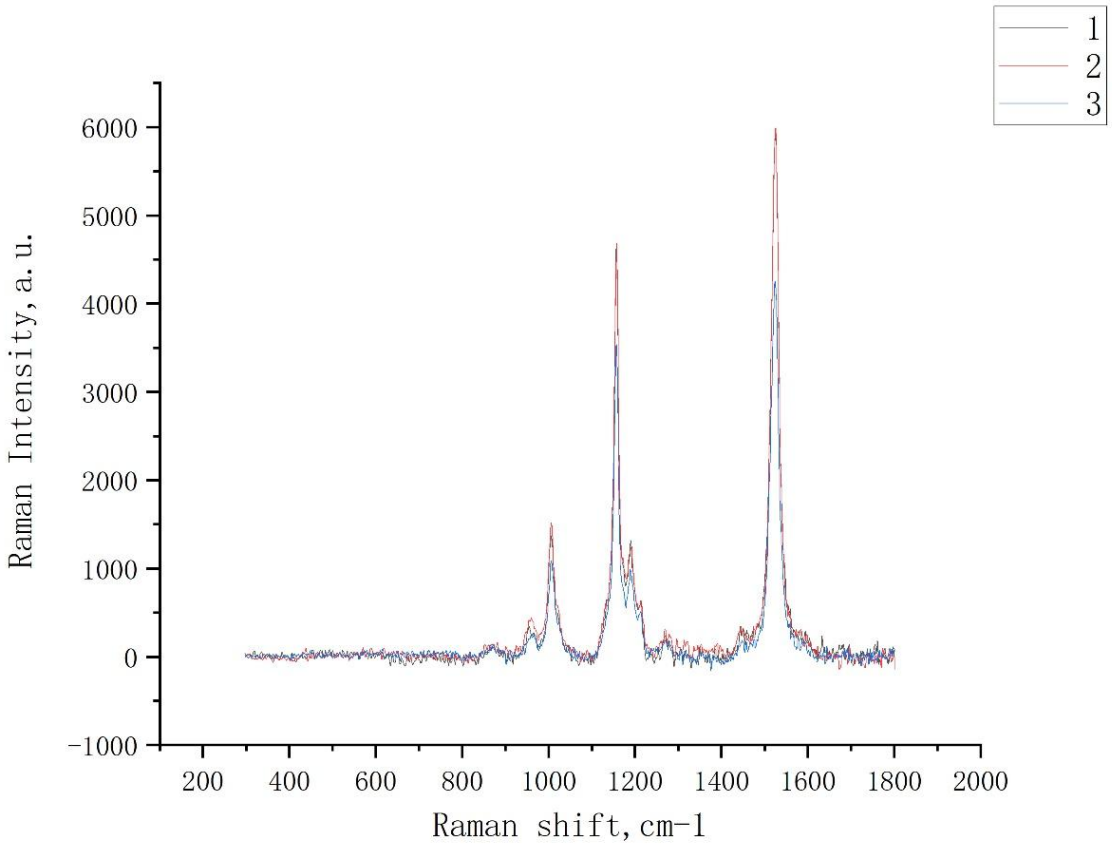

Fig. 43. Raman Spectrum obtained from beta-carotene at 488nm mixed with clothianidin(C1:0.002 mg/mL) after 20 minutes

In order to visually display the changes of the characteristic peaks, the characteristic peaks of each group (control, C1: 0.002 mg/mL, C2: 0.01 mg/mL, C3: 0.02 mg/mL, C4: 0.1 mg/mL, C5: 0.2 mg/mL) at different storage times (t1: 20 minutes, t2: 1 hour, t3: 24 hours) as follows:

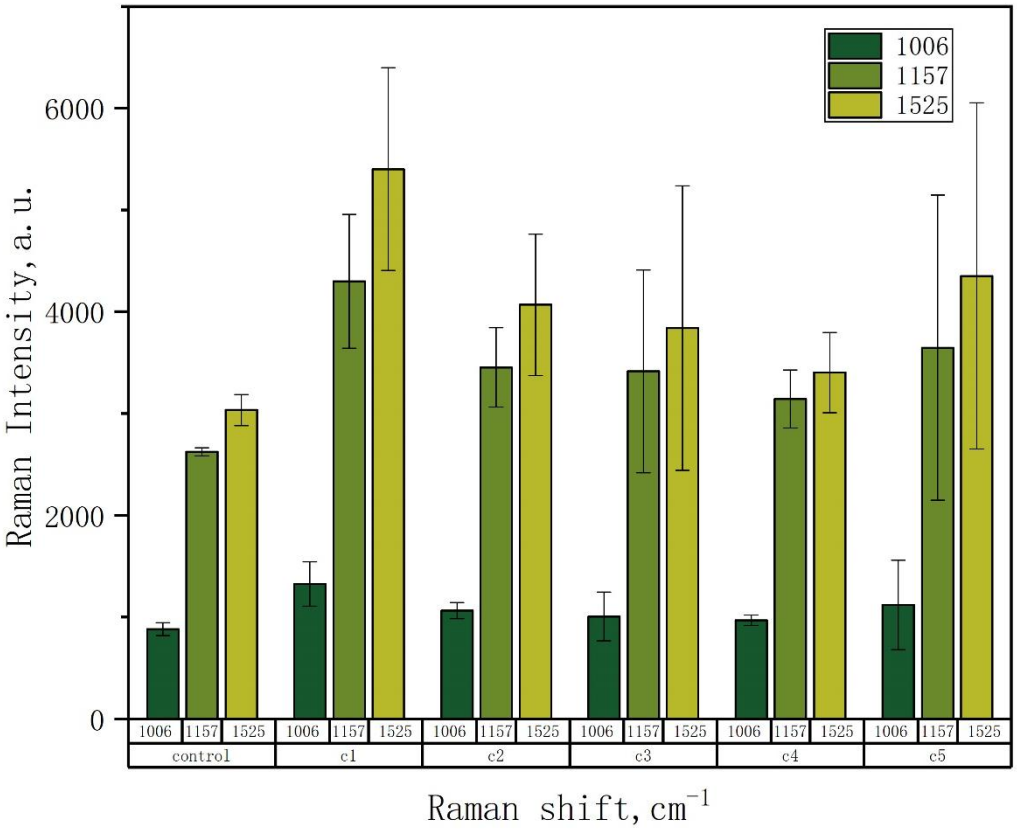

Fig. 44. Dependence of the characteristic peaks of the Raman spectrum of beta-carotene on the concentrations of clothianidin (spectra obtained with excitation at 488 nm for 20 minutes).

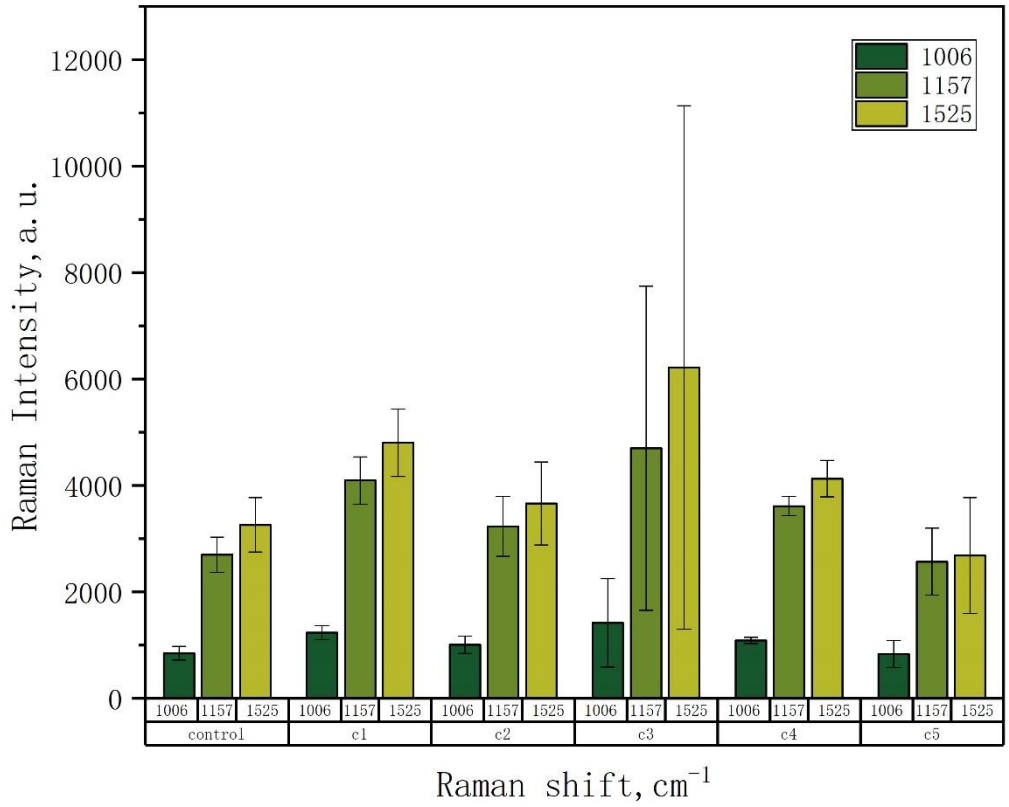

Fig. 45. Dependence of the characteristic peaks of the Raman spectrum of beta-carotene on the concentrations of clothianidin (spectra obtained with excitation at 488 nm for 1 hour).

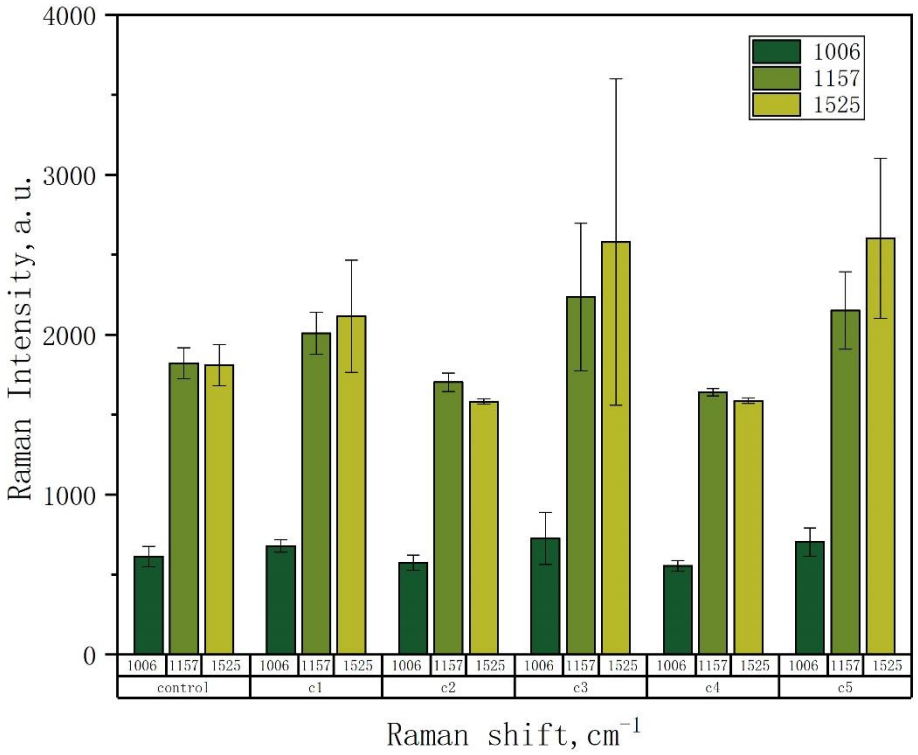

Fig. 46. Dependence of the characteristic peaks of the Raman spectrum of beta-carotene on the concentrations of clothianidin (spectra obtained with excitation at 488 nm for 24 hour).

Raman spectra of six sets of β-carotene samples were obtained at different placement times (t1:20 min, t2:1 h, t3:24 h). Resalts of Fig. 44, Fig. 45, and Fig. 46 shows that, when react for a short period of time, there is a relatively significant decrease in peak 1525 cm^{-1} as the concentration of chlorthalidone increases. After 24 h of reaction, the RS intensities of all three characteristic peaks were significantly decreased and differed, and the relative effects of sample concentration on peak 1157 cm^{-1} and peak 1525 cm^{-1} signals were greatly reduced. Some of the more pronounced deviations might due to the high viscosity effect of the β-carotene supplement mixed with thiamethoxam, as shown in Fig. 46.

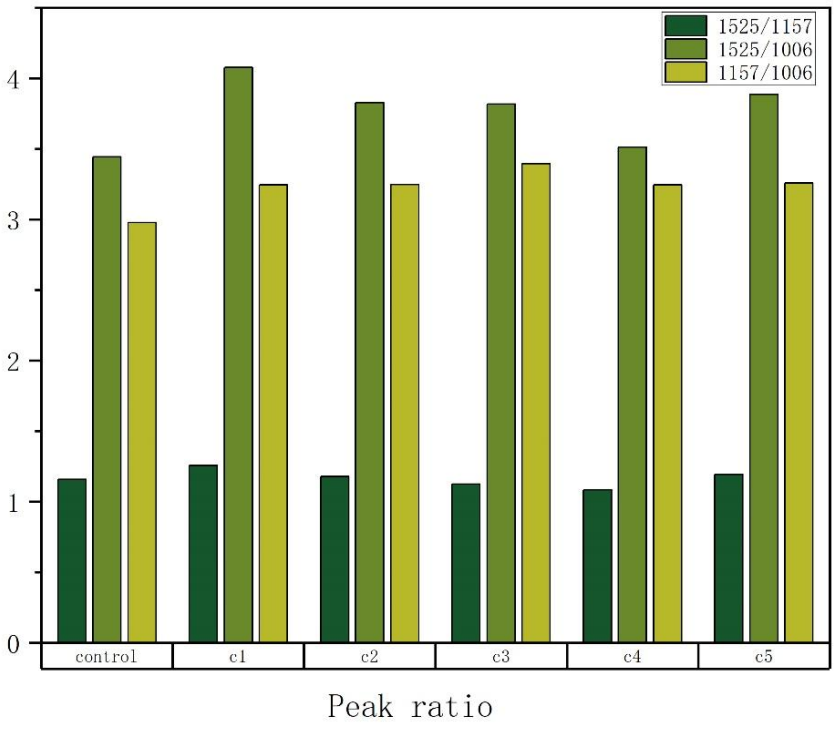

Fig. 47. Dependence of the peak ratio of the Raman spectrum of beta-carotene on the concentration of clothianidin (the spectra were recorded under the action of a 488 nm laser for 20 minutes).

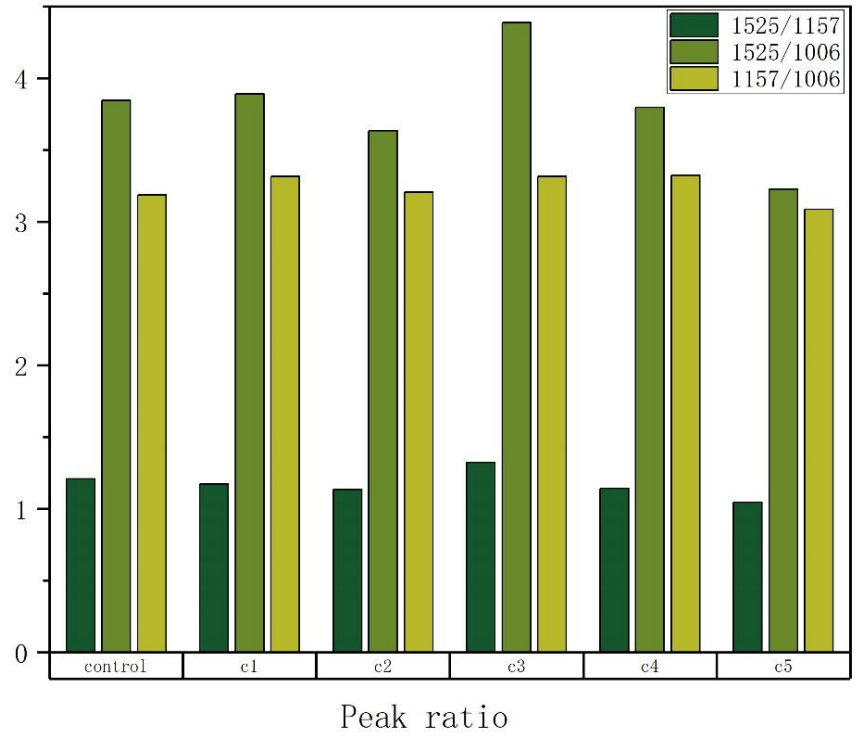

Fig. 48. Dependence of the peak ratio of the Raman spectrum of beta-carotene on the concentration of clothianidin (the spectra were recorded under the action of a 488 nm laser for 1 hour).

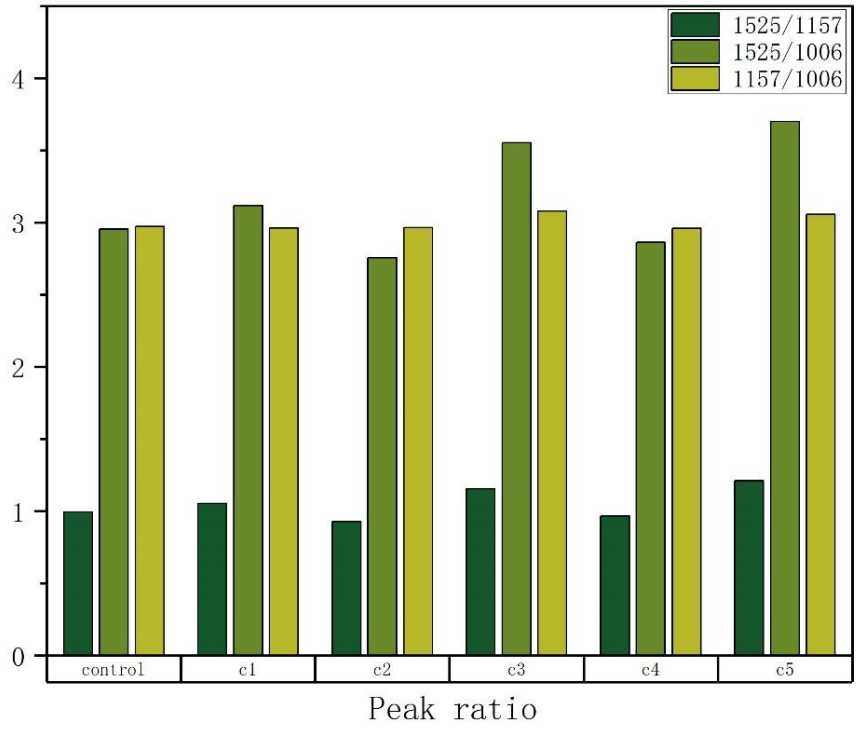

Fig. 49. Dependence of the peak ratio of the Raman spectrum of beta-carotene on the concentration of clothianidin (the spectra were recorded under the action of a 488 nm laser for 24 hour)

Using the results from graphs (Fig. 47,Fig. 48) can be calculated by the ratio between the three characteristic peaks of β-carotene. Graphical analysis showed that the addition of thiamethoxam had a significant effect on both ratios (I_{1525}/I_{1006}, I_{1157}/I_{1006}) after 20 minutes of reaction compared to the control (Fig. 47). This indicates that the reduction of peak at 1006 cm^{-1} is less pronounced than that of the other two peaks during this reaction time. After one hour of reaction (Fig. 48), There was a decrease in the overall rate in the higher concentration group, with a particularly pronounced decrease in I_{1525}/ I_{1006}. In contrast, the differences in the characteristic peak ratios between the low-concentration and control groups were relatively small. After one day (24h), β-carotene samples had the largest difference in I_{1525}/I_{1006} ratios and the smallest difference in I_{1157}/I_{1006} ratios across the concentration gradient. (Fig. 49).

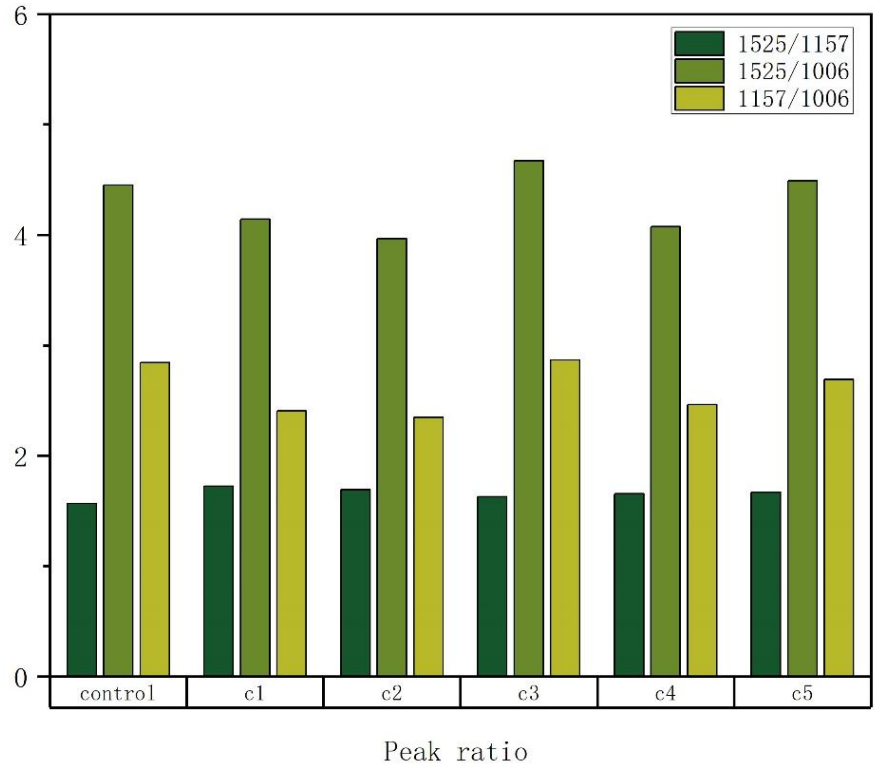

Fig. 50. Dependence of the change in the characteristic ratio of the peaks of the Raman spectrum of chloroplast on the concentration of clothianidin (the spectra were recorded using a laser with 488 nm, for 20 minutes).

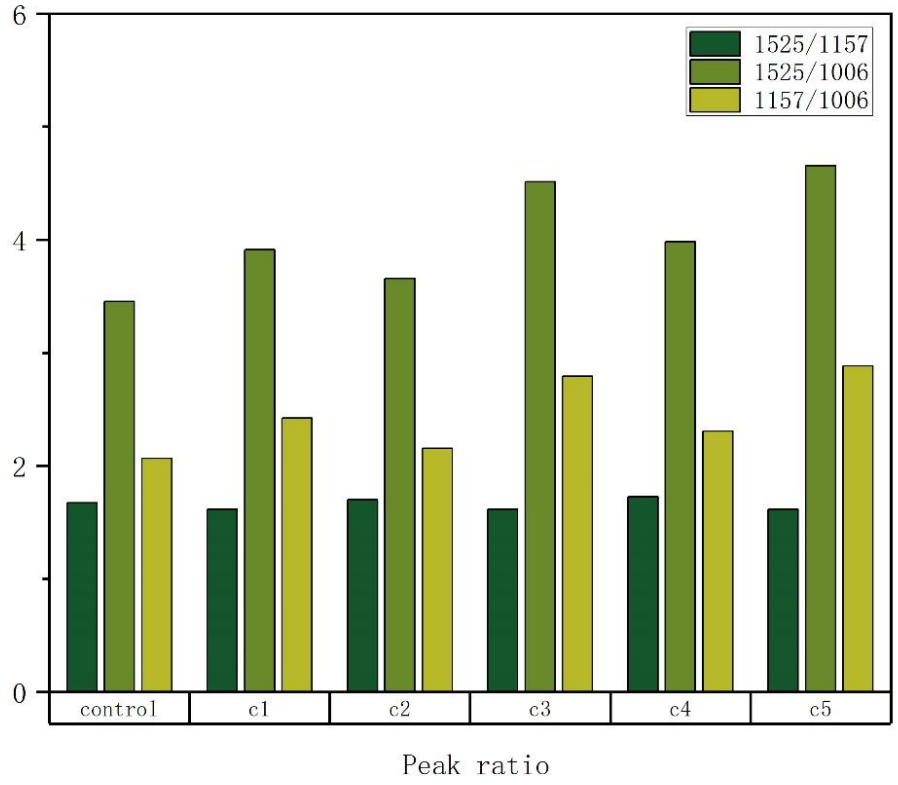

Fig. 51. Dependence of the change in the characteristic ratio of the peaks of the Raman spectrum of chloroplast on the concentration of clothianidin (the spectra were recorded using a laser with 488 nm, for 1 hour).

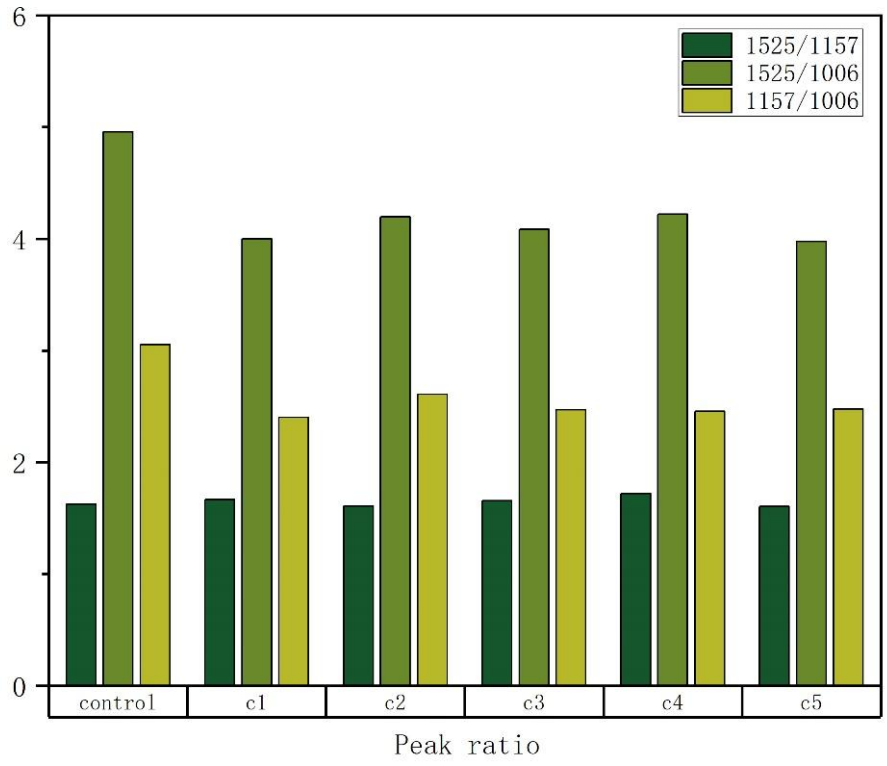

Fig. 52. Dependence of the change in the characteristic ratio of the peaks of the Raman spectrum of chloroplast on the concentration of clothianidin (the spectra were recorded using a laser with 488 nm, for 24 hour).

In the next series of experiments, Raman spectra of chloroplast samples were studied under the same detection parameters. The ratio of the characteristic peaks of the Raman spectra of the chloroplast samples was calculated (Fig. 50 - Fig. 52).

In contrast, CL treatments of chloroplasts were not affected by the different time periods of reaction. Based on the comparison of the dependence of the peak ratios on the introduction of CL, the chloroplast samples similarly reflect more pronounced differences in the other two ratios (I_{1525}/I_{1006}, I_{1157}/I_{1006}). On this basis, the other two ratios (I_{1525}/I_{1006}, I_{1157}/I_{1006}) were analysed. The effect of CL on carbon single and carbon double bonds in chloroplasts was more pronounced than that on -C-CH_3 in methyl groups, which is consistent with previous β-carotene results. It was found, after 1 hour of reaction, the proportion of characteristic peaks obtained in the high

concentration chloroplast mixture group was more significantly different from that of the β-carotene group. This indicates that the effect of CL on the hydrocarbon bond reduction process increases significantly during time. After 24 hours of reaction, all concentrations of mixed chloroplast samples showed relatively large differences compared to the control without thiamethoxam application. The same result was observed in the results for the β-carotene samples, but the effect was more pronounced for the chloroplast samples as well. This suggests that conformations in chloroplasts were more significantly affected by the significant effects of CL. The pesticide dose had less effect on chloroplasts compared to β-carotene dietary supplements. In addition, possible in chloroplasts, the sensitivity of active pigment complexes other than β-carotene to clothianidin also increases significantly with exposure time.

4.6.2 The effect of CL on the speed of electronic transport.

PSII activity was monitored in control and clothianidin-treated chloroplasts by measuring the O_2 release rate in the presence of the electron acceptor DCBQ2 (Table 13). (*These results were jointly obtained with A. Volgushuva and He Yanlin*) In the control sample, the O_2 release rate was 224 μmol/mL clothianidin O_2 h^{-1}, and there was little change in the activity of PSII in the presence of 22 μg/L clothianidin. Increasing the clothianidin concentration to 110 μg/L resulted in a 24% decrease in the O_2 release rate. The efficiency of the entire electron transport chain of photosynthesis is measured by the O_2 uptake rate in the presence of methylviologen (MV), which efficiently transfers electrons from PSI to molecular O_2. When 22 and 110 μg/L CL were used, the O_2 absorption decreased by 15% and 28%, respectively, compared with the control. PSI activity (defined as the O_2 uptake rate from $DCPIPH_2$ (donating electrons to plastocyanin) to MVs) was approximated in control and clothianidin treated chloroplasts.

Table 13. Changes in the rate of O_2 release and absorption in chloroplasts in the presence of CL

processing	O_2 evolution (DCBQ)	O_2 consumption ($H_2O \rightarrow$ MV)	O_2 consumption ($DCPIPH_2 \rightarrow$ MV)
control	224 ± 17	206 ± 19	668 ± 27
22 μg/L CL	217 ± 21	175 ± 23	669 ± 20
110 μg/L CL	170 ± 20*	149 ± 19*	655 ± 15

The rate of release and absorption of O_2 are represented in μmol O_2 (mg Chl)$^{-1}h^{-1}$. *Statistically significant result, $p < 0.05$.

In was found, that low concentrations of pesticides did not alter the activity of PSII but disrupted the ETC between Q_A, quinone pool and cytochrome b6f complex. As the concentration of clothianidin increased, electron transport between photosystems was significantly reduced and PSII function was impaired.

To examine the effect of clothianidin on the function of the local, donor side of PSII, we used functionally active PSII particles (BBY type), i.e., formulations capable of light-induced O_2 formation, and PSII particles without oxygen-releasing complexes (OLCs). From the results in Table 14, it can be seen that the addition of 110 μg/L clothianidin resulted in a 20% reduction in the O_2 release rate, which is consistent with the data obtained from chloroplasts (Table 14). The light-dependent reduction rate of the electron acceptor $DCPIPH_2$ was similarly reduced in active membrane preparations (PSII) and PBMC-free preparations (PSII -Mn, H_2O_2) when treated with clothianidin. The obtained results most likely indicate that pesticides do not directly affect the function of PSII PBMCs. The molecular mechanisms of pesticide interactions are known to be involved in various sites of the photosynthetic ETC, reducing the activity of PSII and impairing electron transport. However, these perturbations are often associated with PBMC damage, decreased maximal efficiency of energy conversion to PSII (Fv/Fm), and changes in D_1 protein stability (Sharma et al., 2019).

Table 14. Investigation of the effect of 110 μg/L CL on the rate of O_2 release and the rate of DCPIP reduction in PSII+Mn and PSII-Mn membranes

Treatment	O_2 evolution, % (DCBQ)	DPC to DCPIP reduction rate, %
PSII+Mn	100±4.9	100±3.4
(PSII+Mn) + 110μg/L CL	80±5.2*	76±4.7*
PSII-Mn	–	100±7.6
(PSII-Mn) +110μg/L CL	–	78±5.3*

The rate of O_2 release in PSII+Mn membranes was 450±22 μmol O_2 (mg Chl)$^{-1}$ h^{-1}. The rate of DCPIP recovery in PSII+Mn and PSII-Mn membranes was 145 ± 5 and 105 ± 8 μmol DCPIP (mg Chl)$^{-1}$ h^{-1} respectively. * $p < 0.05$.

4.6.3 Kinetics of light induction of fluorescence under the action of CL

To analyse in detail the effect of clothianidin on the function of the photosynthetic electron transport chain in chloroplasts, the kinetics of light-induced fluorescence (OJIP) in chloroplasts were tested in the presence of 22 and 110 μg/L clothianidin was studied (Fig. 53). In the control, the OJIP curve of the chloroplast (Fig. 53 control) clearly shows 3 stages (OJ, JI, IP). The OJ stage is due to the light-induced reduction of Q_A, while the JIP stage mainly reduces its reoxidation by reducing Q_B and quinone pools, thereby further accumulating reduced Q_A^-. profound O and P levels in the kinetic curves correspond to the values of Fo and Fm (Stirbet & Govindjee, 2012c). Dark incubation with clothianidin in the presence of 22 μg/L CL for 10 mins did not result in changes in Fo and Fm levels but significantly increased the amplitude of the OJ phase due to the appearance of PSII centres. Possibly, in this condition transfer electrons to the plastoquinone pool and further to the photosynthetic ETC decreased (García et al., 2014). It was found that treatment of chloroplasts with 110 μg/L clothianidin did not actually alter Fo and Fm, and resulted in a larger increase in OJ phase amplitude.

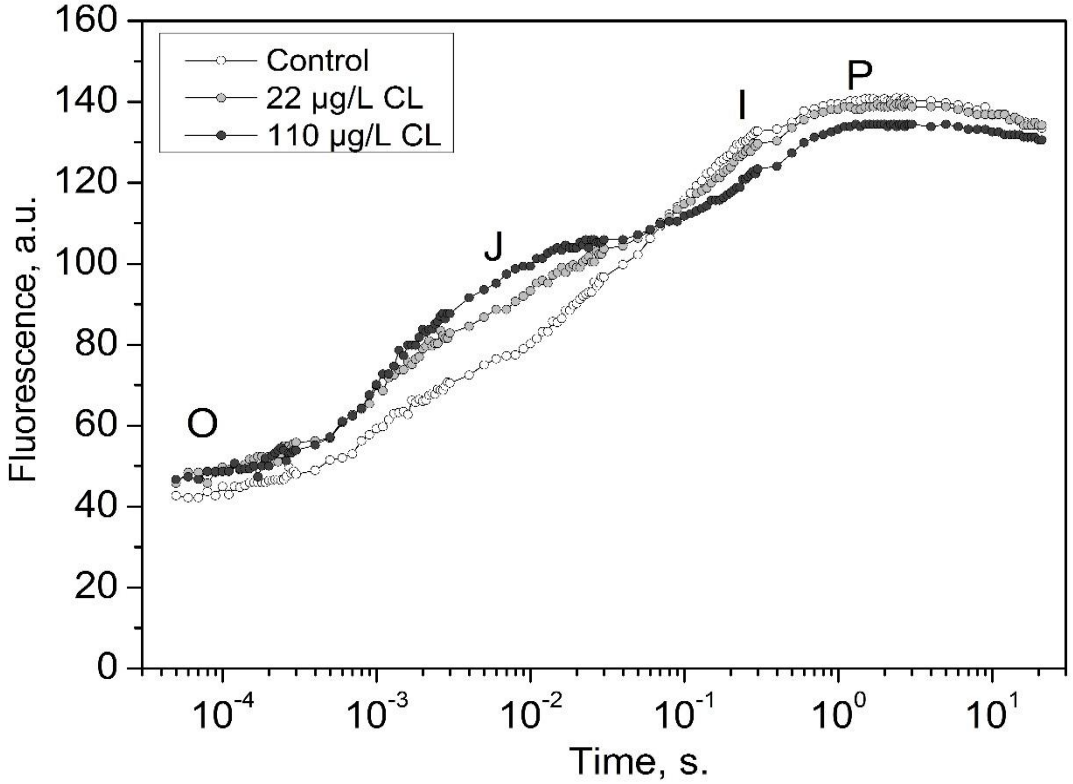

Fig. 53. Dependences of fluorescence induction of pea chloroplasts in the presence of CL (22 and 110 µg/L).

The results of the JIP test (Table 15) used to quantify changes in the OJIP curve (Strasser et al., 2004b) indicate that the OJ phase magnitude (parameter V_J) increased by 39% and 67% when treated with 22 and by 110 µg/L clothianidin. The parameter M_0, which characterizes the reduction rate of Q_A, increased more than 5 times at both clothianidin concentrations. The electron transport efficiency (parameter P_{ET}), i.e. the reoxidation capacity of the secondary quinone Q_B and the quinone pool to Q_A^-, decreased by 37% and 53% in this experiment when treated with 22 and 110 µg/L clothianidin, respectively. Meanwhile, the maximum energy conversion efficiency (Fv/Fm, Fig. 53 inset) of PSII and the ratio of photochemically active to inactive PSII centres (Fv/Fo) were almost unchanged in all samples. The action of clothianidin on chloroplasts likely leads to the accumulation of Q_B-non-reducing PSII centres characterized by high Fv/Fm values and incapable of electron transfer between Q_A and the quinone pool (Henrysson & Sundby, 1990a).

Table 15. The parameters of the JIP test are calculated using the OJIP curves (Fig. 53).

Paramete	control	22 μg/L CL	110 μg/L CL
V_J	0.246±0.02	0.342±0.03*	0.410±0.01*
M_0	0.062±0.03	0.343±0.02*	0.358±0.08*
Pet	3.06±0.15	1.93±0.23*	1.44±0.06*
Fv/Fo	1.48±0.13	1.50±0.18	1.40±0.04
F_V/F_M	0.69±0.02	0.67±0.03	0.65±0.04

* Statistically significant result, $p < 0.05$

4.6.4 Kinetics of dark attenuation of fluorescence under the action of CL

To investigate the oxidation process of reduced Q_A, the kinetic curves of the dark relaxation of chlorophyll fluorescence were measured (Fig. 54). Kinetic curves are known to contain three exponential components. The fast component reflects the electron transfer reaction between Q_A^- and Q_B^-. This medium is characterized by the reoxidation of Q_A^- in PSII centres that do not contain Q_B upon illumination, where Q_B must first bind to the Q_B^- binding site of PSII. The slow component results from recombination between the S2 state (S2 state) of the Q_A^- and oxygen-releasing PSII complex (Vass et al., 1999).

The kinetics of pigment fluorescence decay in chloroplasts was dominated by a fast electron transfer process from Q_A^- to Q_B with a characteristic time of 0.647 ms (τ_1), which indicated efficient electron transport from the acceptor side of PSII (Table 16, control). In 23% of centres (A_2), Q_B must bind to the binding site of PSII for the Q_A^-reoxidation reaction, which takes place within 19.5 ms (τ_2). 13% of the PSII centres (A_3) were unable to undergo direct electron transfer, and the oxidation of Q_A^- occurred via recombination with the PSII donor side in approximately 1709 ms (τ_3).

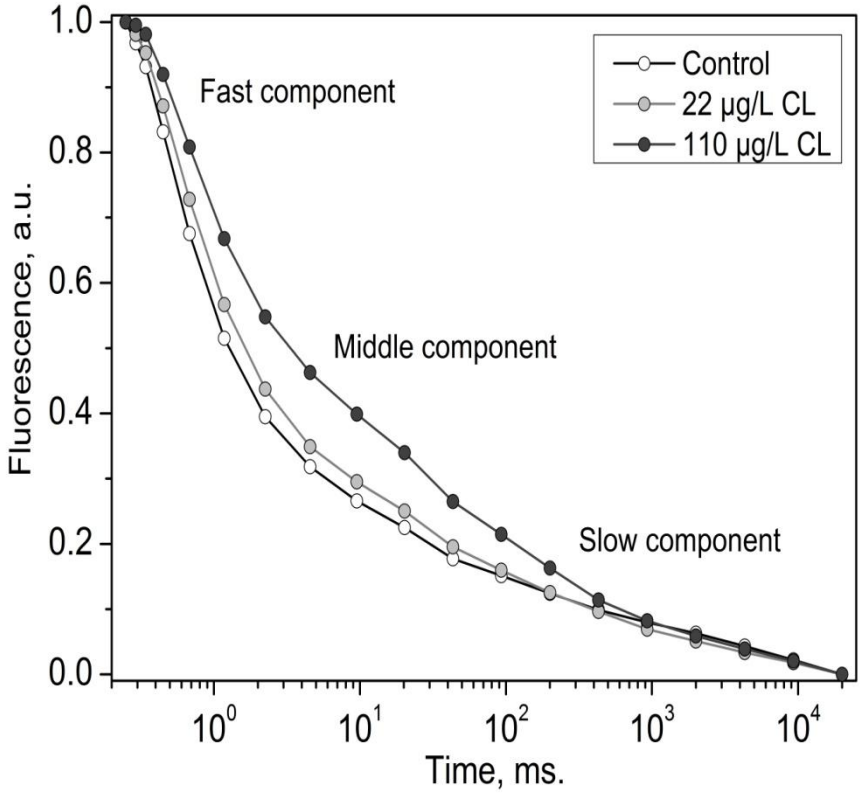

Fig. 54. Investigation of the effect of CL (22 µg/L and 110 µg/L) on the kinetics of variable fluorescence attenuation in pea chloroplasts.

Table 16. Changes in the time constant and amplitude of the kinetics of attenuation of variable fluorescence in the control and chloroplasts treated with 22 or 110 µg/L CL

Parameters	Fast component		Middle component		Slow component	
	A_1 (%)	$\tau_{½,1}$ (ms)	A_2 (%)	$\tau_{½,2}$ (ms)	A_3 (%)	$\tau_{½,3}$ (ms)
control	64±2	0.647±0.05	23±2	19.5±4.5	13±1	1709±586
22µg/L CL	62±3	0.785±0.06	23±2	22.6±5.1	14±1	973±284
110µg/L CL	52±2	0.978±0.09	29±2	31.9±7.0	18±2	1051±303

It was found, incubation of chloroplasts in the presence of 22 and 110 µg/L clothianidin decreased chlorophyll fluorescence decay kinetics (Fig. 54), while 22 µg/L clothianidin concentration caused chlorophyll fluorescence decay. The magnitudes of all three components

(Table 16, A1, A2, A3) were unchanged compared to controls. It was found, at the action of clothianidin, the lifetime constants of the fast component ($\tau_{½}$, 1) and the middle component ($\tau_{½}$, 2) increased by 21% and 16%, respectively, while the slow component ($\tau_{½}$, 3) On the contrary, it decreased. 43%, indicating an increased recombination pathway with the PSII donor side. It was shown that increasing the pesticide concentration to 110 μg/L reduced the proportion of PSII centres capable of directly transferring electrons from Q_A to Q_B by 20% (A_1), while the lifetime constant of the fast component was than reduction of 51% ($\tau_{½}$, 1). Under these conditions, there was a 26% increase in the number of Q_B^- free PSII centres in the binding site (A_2), and a 64% increase in the lifetime of the intermediate component, likely reflecting a decrease in the binding rate of plastoquinone to the site Q_B. PSII. The number of centres capable of recombination reactions with the PSII donor side was increased by 39% and the time of this reaction was accelerated by 38% compared to the control.

It is known, the DCBQ that directly accepts electrons from the Q_A (Graan & Ort, 1986; Satoh et al., 1995) reduced the amplitude of the fast component by 31% and nearly doubled its lifetime compared to untreated DCBQ samples (Table 16). It was found, the magnitude of the intermediate component did not change, while the time constant increased by 26%. Note that the largest changes occur in the Q_A^- recombination reaction and S2 states of DCBQ: the number of centres capable of this reaction more than doubles, while the time constant value drops by 54%. In CL-treated samples, DCBQ resulted in 26% and 23% decrease in A_1 for 22 and 110 μg/L clothianidin, respectively, compared to non-DCBQ-treated samples (Table 16, Fig. 54). However, the lifetime ($\tau_{½,1}$) was only reduced by 64% and 52% for 22 μg/L CL and 110 μg/L clothianidin. In the presence of the acceptor, the amplitude (A_2) and lifetime (($\tau_{½,2}$) of the media composition do not change for both clothianidin concentrations. The magnitude of the slow component (A_2) increased by 200% and 72% for 22 and 110 μg/L clothianidin, respectively. Note that the value of the reaction lifetime constant does not actually change in either case.

4.6.5 Study of changes delayed chlorophyll fluorescence in chloroplasts under the action of clothianidin.

It is well known that the kinetics of fast fluorescence (OJIP and Q_A^- reoxidation) mainly reflect the functional state of PSII, while the kinetics of delayed fluorescence (DF) depend on the activity of PSII centres and the thylakoid membrane energy process (fast phase), and can also characterize the ability to form a proton gradient ΔpH across the membrane (slow phase) (Evans & Crofts, 1973; Goltsev et al., 2009c).

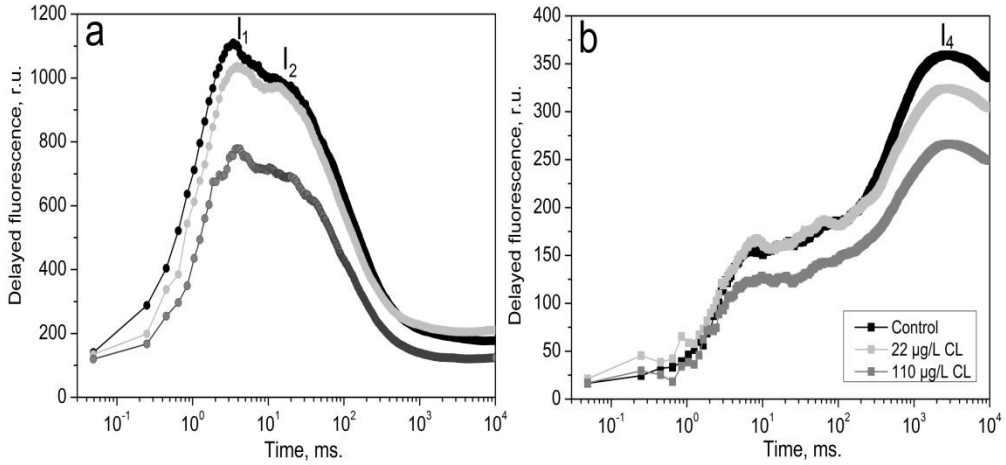

Fig. 55. Effect of 22 and 110 μg/L CL on light-induced delayed Chl fluorescence (DF) kinetics in control and treated chloroplast with (A) or without (B) 0.125 мМ DCBQ.

Fig. 55 shows typical DF curves obtained from control and clothianidin treated chloroplasts. In all samples, two maxima, I_1 and I_2, occur at 3.6 ms and 13.6 ms after the onset of illumination, respectively. There was no difference in fast-phase amplitude between control chloroplasts and chloroplasts treated with 22 μg/L clothianidin (Fig. 55 A), However, treatment of chloroplasts with 110 μg/L clothianidin resulted in a 30% decrease in the amplitude of this phase compared with the control.

In order to determine the surface structure effect by CL of chloroplast, AFM were performed. Fig. 56 shows that clothianidin treated chloroplast surface structure was damaged. The higher the clothianidin concentration, the higher the degree of chloroplast damage. The

damage of surface structure might cause the functional change of PSII. (*These results were jointly obtained with E. Parshina and He Yanlin).*

Changes in the morphology of chloroplasts in the presence of CL are accompanied by changes in the viscosity of membranes. Using EPR spectroscopy, it was found that the value of spin-labeled 16-DS in the chloroplast membrane decreases by 12%, which indicates a decrease in the viscosity of the membrane (arrangement of the "tails" of fatty acids of phospholipids) (Table 17).

Table 17. Investigation of the effect of CL on the parameters of the EPR spectra of spin marks 16-DS(τ) and the content of MDA

Treatment	$\tau \times 10^9$ (c)	MDA (pmol g^{-1}DW)
Control	1.78±0.03	1.3±0.02
110 μg/L CL	1.57±0.01*	1.9±0.06*

*Statistically significant result, $p < 0.05$.

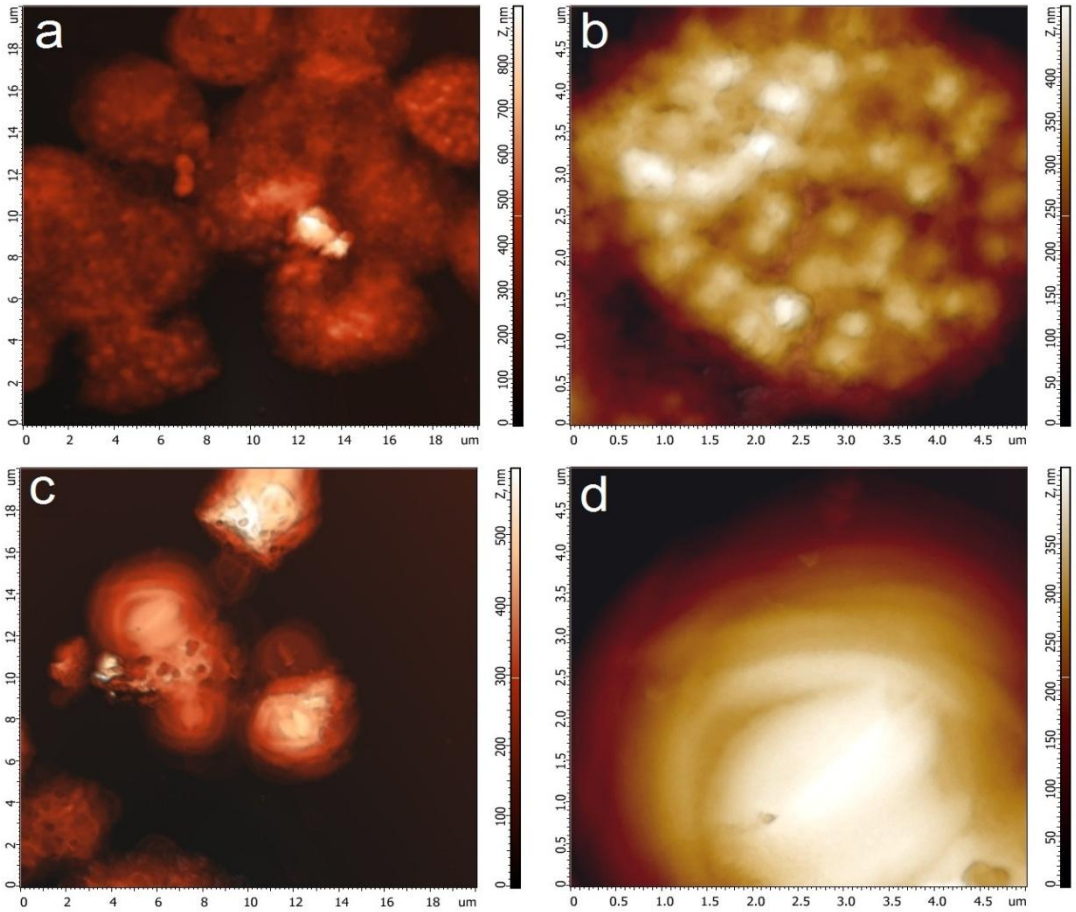

Fig. 56. AFM images of chloroplast control (a, b) and chloroplast treated with 110 μg/L CL (c, d)

According to literature data, the onset of the slow DF phase usually occurs after 1 s after the start of the measurement, but this phase was not induced under our conditions. It is well known that the shape of DF dynamics depends on the excitation light intensity; at high intensities (over 4000 μU m^{-2} s^{-1}), processes leading to slow phase development are rapidly saturated, leading to a rapid decrease in DF intensity to lower levels (Goltsev et al., 2009c). In our experiments, the DF curves were initiated by light with an intensity of 5000 μE m^{-2} s^{-1}. It was found that the fast phase of DF did not occur in the presence of DCBQ (Fig. 57 B), but a slow ΔpH-dependent component of DF was detected in control and poison-treated samples. Note that the amplitude of the DF slow phase was practically unchanged when 22 μg/L clothianidin was added (within 10%) compared to the control, whereas when 110 μg/L clothianidin was added, the WP slow phase The phase amplitude was reduced by 26%.

4.7 Study of the effect of a pesticide on the state of pigments in algae.

Neonicotinoids (NCs) are frequently used insecticides to protect crops from pests. Widespread use leads to its release into soil and water, where it is absorbed by various organisms, leading to adverse effects on the environment and human health (W. Han et al., 2018). Phytoplankton, also called microalgae, are of vital importance to aquatic ecosystems, as they form the basis of the food chain. Microalgae are known to be sensitive indicators of environmental conditions due to their susceptibility to various anthropogenic pollutants (Gosset et al., 2019). NCs have a negative effect on the growth, chlorophyll biosynthesis, photosynthetic electron transport and carbohydrate content of planktonic algae(Jena et al., 2012; B. R. Mohapatra & Bapuji, 1997; P. K. Mohapatra & Mohanty, 1992; Mostafa & Helling, 2002). NCs alter cell morphology and ultrastructure, leading to an increase in biovolume, the size and number of starch granules, as well as the accumulation of lipids and electrodense bodies, which serve as toxin accumulation sites(Asselborn et al., 2015).

The impact of insecticides on algae is dependent on their type and concentration, as well as the species of algae. In the case of *C. vulgaris*, quinalphos and chlorfenvinphos affected the donor sides of PSII, while dimethoate and phorate inhibited the acceptor side (Jena et al., 2012). In *Synechocystis*, dimethoate may have caused alterations in membrane fluidity, leading to the detachment of phycobilisomes from the reaction centres of PS II(P. K. Mohapatra et al., 1997). The respiration rate decreased significantly after dimethoate treatment in green algae, *Tetraselmis* and *Dunaliella* (Mavrogenis et al., 2023), while it increased in the cyanobacteria, *Nostoc* and *Synechocystis* (P. K. Mohapatra et al., 1997) There is a paucity of knowledge regarding the impact of clothianidin (CL) on toxic sensitivity and metabolism in algae. It is therefore imperative to obtain further toxicity data specific to CL.

Microalgae are capable of efficiently removing and degrading pesticide through abiotic removal, bio-adsorption, bioaccumulation, and biodegradation (Nie et al., 2020)**.** Recent studies have shown that *Scenedesmus* sp. exhibits high resistance to thiamethoxam and imidacloprid, and is able to efficiently degrade them mainly through biodegradation. CL is a second-generation neonicotinoid that became available on the market after 2000. Although CL is the breakdown

product of thiamethoxam (J. C. Anderson et al., 2015), suggesting that algae may have the ability to biodegrade CL.

This study investigates the ability of green algae *C. reinhardtii* to remove CL from the medium, the effect of cell concentration on insecticidal toxicity, algal survival at high doses, and the culture's ability to recover after CL removal. Additionally, we studied the development of cellular resistance, the functioning of the photosynthetic electron transport chain and the levels of primary pigments, chlorophyll and carotenoids, under CL treatment. *(These results were jointly obtained with A. Volgushuva and He Yanlin).*

The first part of the experiment was carried out for three weeks using cultures of C. reinhardtii. Fig. 57 shows that the control group without clothianidin had a rapid increase in cell density during the first ten days, followed by a growth arrest phase at high cell concentrations. Both groups of clothianidin with two concentrations (0.11 and 0.22 mg L^{-1} of CL) showed a gradual decrease in cell density in the first two days, followed by a slight increase in the third and second days. A small increase after ten days. This suggests that even in the environment of high clothianidin addition, a small fraction of cells did not lose their activity and completed growth and division over the extended experimental period.

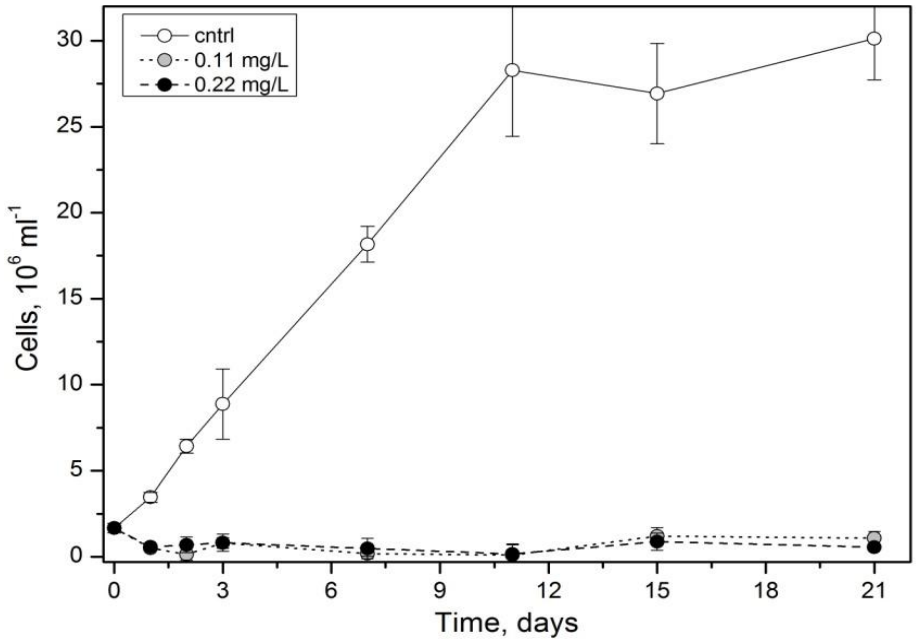

Fig. 57. Cell density in *C. reinhardtii* cultures during incubation with 0 (control), 0.11 mg L^{-1} of CL and 0.22 mg L^{-1} of CL

An additional set of DCMUs is introduced in Fig. 58 to complete the control. DCMU is a highly specific photosynthesis inhibitor that inhibits the flow of electrons from photosystem II to plastoquinone (PQ) by blocking the plastoquinone binding site of photosystem II. It reduces the formation of ATP and NADH, which ultimately inhibits photosynthesis. Fig. 58 shows that the three groups of cells added with three concentrations (4×10^{-4}, 8×10^{-4}, 16×10^{-4} mg/mL) of clothianidin showed different degrees of decrease in cell concentration after two hours. At this time, the medium concentration and high concentration groups were reduced to between 60% and 70%. The results showed that the concentration interval higher than 8×10^{-4} was suitable for introducing clothianidin as the experimental group. The DCMU group blocked the electron transfer from photosynthetic system II to photosynthetic system I, and the cell density dropped to 30% after one day and to about 16% after two days.

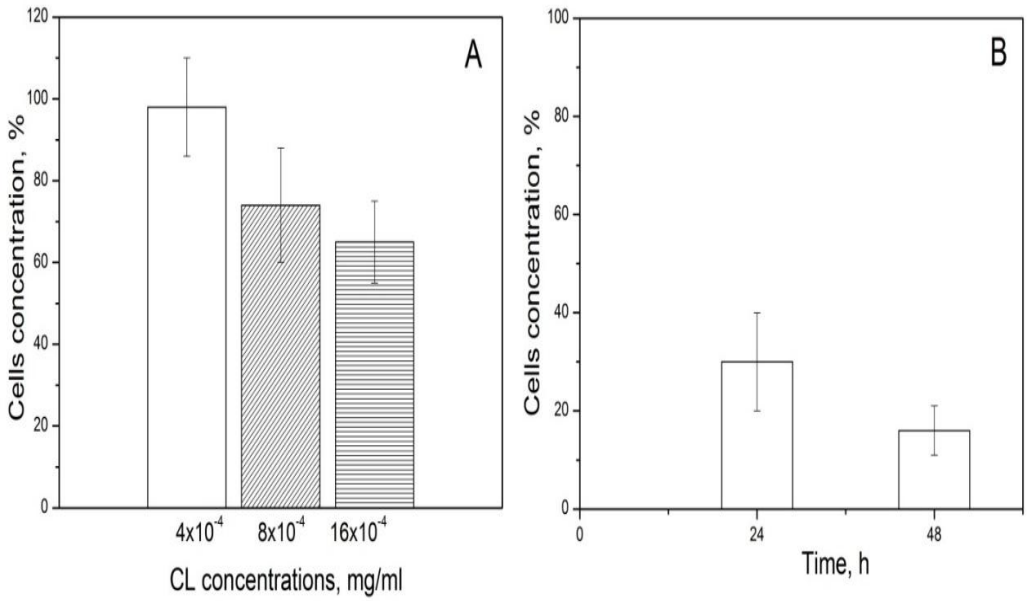

Fig. 58. Cell density in *C. reinhardtii* cultures after 2 hours incubation with 4×10^{-4}, 8×10^{-4}, 8×10^{-4} mg mL^{-1} CL (A) and 10^{-2}M DCMU (B).

Fig. 59 shows the changes in chlorophyll content, chlorophyll a/b ratio, and carotenoid content in the first three days of experiment 1, when the cell density of the experimental group decreased significantly after the introduction of clothianidin. Chlorophyll content and chlorophyll a/b ratio, both groups showed a downward trend in the first two days, and were

positively correlated with clothianidin concentration. The carotenoid content showed an increasing trend, and the change trend was positively correlated with the clothianidin concentration. Changes in all three values level off on the third day.

The fluorescence parameters Fv/Fm of the experimental group and the control group were measured using a multifunctional plant efficiency analyzer. Fv/Fm is the ratio of variable fluorescence to maximum fluorescence after dark adaptation and represents the maximum quantum yield of PSII (if all competent reaction centers are turned on). It can be used to detect stress in plants.

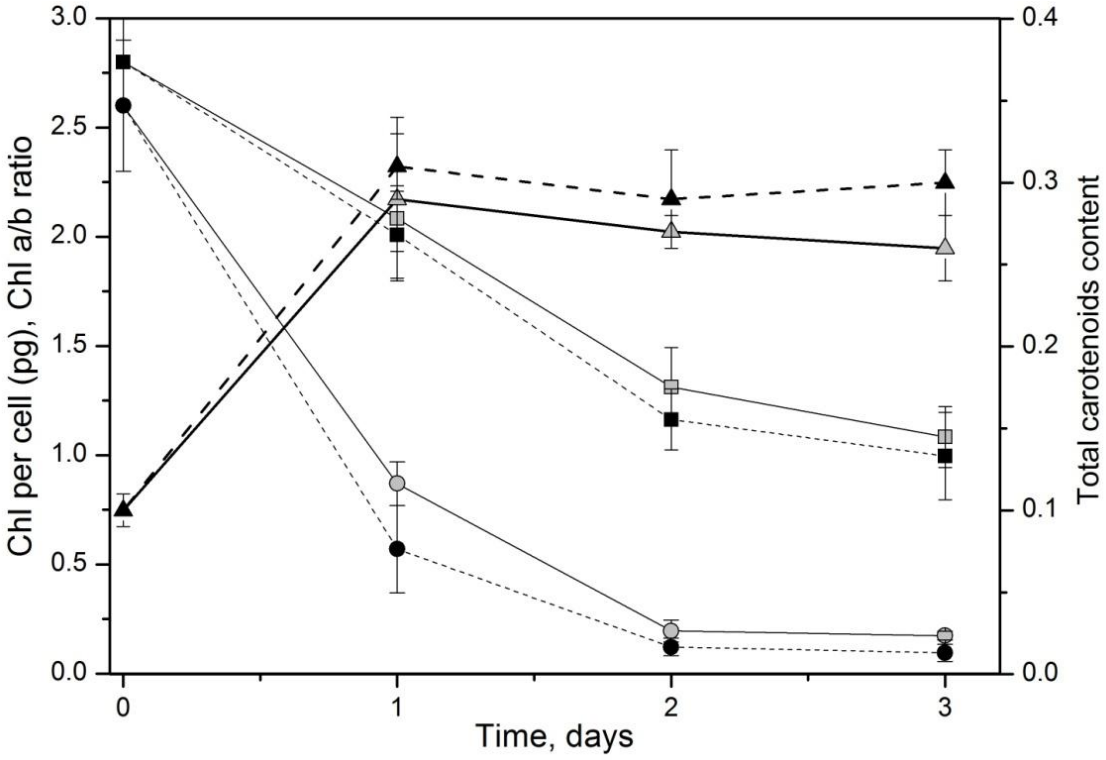

Fig. 59. Chl content (circles), total carotenoids per cell (triangles) and Chl a/b ratio (squares) in *C. reinhardtii* cultures during incubation with 0. 11 (grey color) and 0. 22 mg/L (black color) CL.

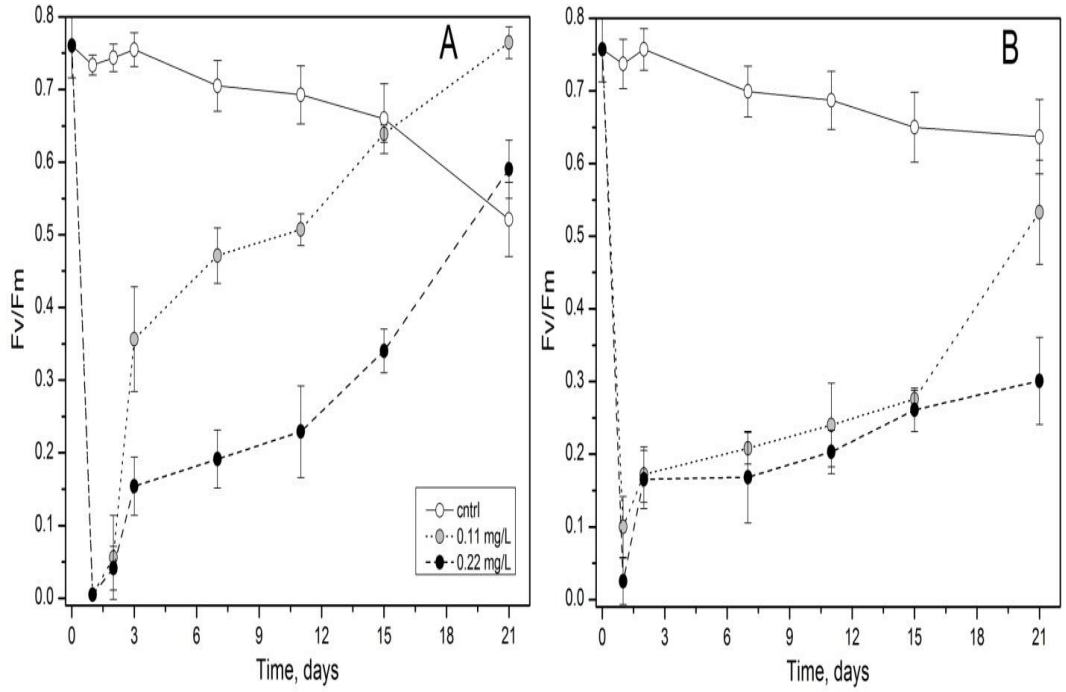

Fig. 60. The Fv/Fm ratio in *C. reinhardtii* cultures during incubation with 0 (control), 0.11 and 0.22 mg L^{-1} of CL measured on a fluorimeter FKMS-2 (A) and PEA (B). Initial cell concentration was ~2 × 10^6 cells mL^{-1}.

In this series of experiments, we used commercial equipment and original equipment created at the Department of Biophysics of Moscow State University in Moscow (fluorimeter FKMS-2 Fig. 61 (A) and PEA (B). Fig. 61 shows that the Fv/Fm value reached a minimum on the first day after binding to CL, followed by a significant upward trend over the next two days, after which the trend slowed down and slowly increased after ten days. This rebound trend was negatively correlated with CL concentration. This indicated that the available open reaction centers of photosystem 2 were actually closed on the day of binding to CL, and this situation was rapidly restored on the third day, followed by relief of plant stress.

The upward trend of this value after ten days was synchronized with the increase of cell density, and gradually approached the average value of the control group before growth inhibition occurred, which may indicate that the photosynthetic capacity of cells gradually recovered to a state unaffected by CL during this period.

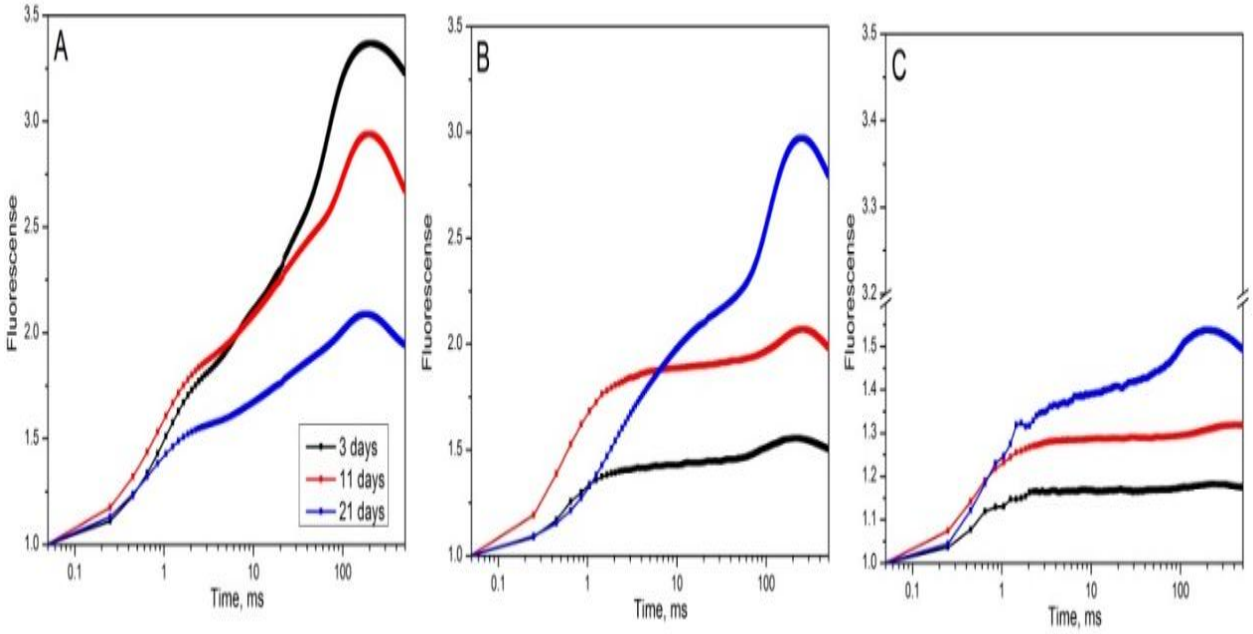

Fig. 61. OJIP transients recorded in C. reinhardtii cultures during 3, 11, 21 days of incubation with 0 (control, A), 0.11 mg/L (B) and 0.22 mg/L (C) clothianidin.

Light-induced fluorescence (OJIP) kinetics were studied in control cells and in the presence of 0.11 mg L^{-1} of CL and 0.22 mg L^{-1} of CL during 3, 11, 21 days. The OJ phase is due to light-induced Q_A reduction, associated with the shutdown of some PSII reaction centers. The JIP stage is mainly to reduce its reoxidation by reducing Q_B and quinone pool, thereby further accumulating reduced Q_A. The O and P energy levels correspond to the values of Fo and Fm: at the O energy level, the fluorescence quantum yield is smallest, because the chance of an incident photon triggering charge separation at one of the reaction centers is greatest. At the P level, the free plastoquinone pool reaches its peak decrease, and the fluorescence quantum yield also reaches its peak.

For the OJ stage (Fig. 61), the different experimental groups showed no significant difference within three days, but the experimental group with low concentration of CL showed a significant increase within 11 days, which was similar to the control group. For the JIP phase, both experimental groups showed an increase in the phase over time. In particular, on day 21, the P level in the low-concentration CL group was significantly higher than that in the control group. And during the three-day JIP phase, both experimental groups showed the exact opposite decline compared to the control group. This indicated that the concentration of 0.22 mg/L had a more significant effect on the level of Q_A reduction relative to the CL concentration of 0.11 mg/L.

Both concentrations of CL inhibit electron transfer from Q_A to the PQ pool for a short time. After prolonging the experiment time, the effect decreased obviously, and this decrease was negatively correlated with the concentration.

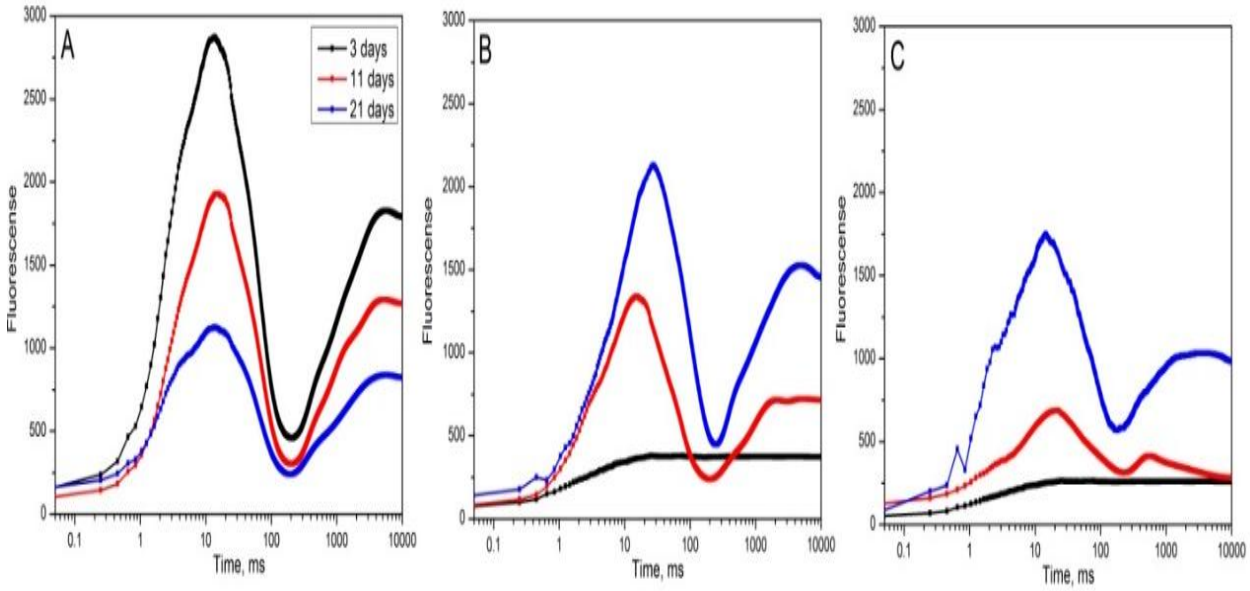

Fig. 62. DF induction kinetics recorded in C. reinhardtii cultures during 3, 11, 21 days of incubation with 0 (control, A), 0.11 (B) and 0.22 mg/L (C) CL.

The kinetics of delayed fluorescence (DF) depend on the activity of PSII centers and thylakoid membrane energy processes (fast phase), as well as a characterization of the ability to form a proton gradient (proton concentration outside the inner membrane is higher than inside the membrane), which is formed due to the electron transport chain (respiration) across the membrane (slow phase).

As can be seen inFig. 62, the experimental groups at both concentrations showed positive time-dependent increases in both the fast and slow phases. In a shorter period of time, the fluorescence intensity of both groups was lower than that of the control group. This demonstrates that CL in both experimental groups over 11 days had a significant effect on PSII center activity as well as the ability to form a proton gradient in the membrane.

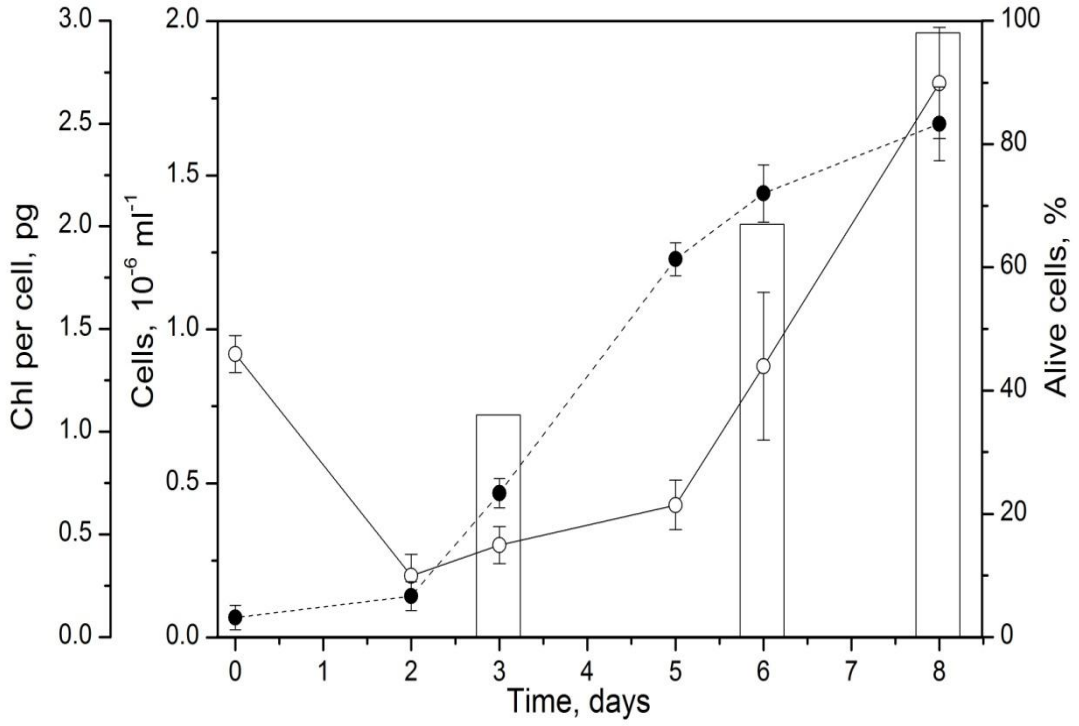

Fig. 63. Cells density (white circles), Chl content per cell (black circles) and percentage of alive cells in *C. reinhardtii* cultures during recovery of cells after 16 days incubation with 0.22 mg/L CL.

In the second part of the experiment, C. reinhardtii cultures were incubated with CL at a concentration of 0.22 mg/L for 16 days, and then the cells were extracted for 8 days of recovery culture. Fig. 63 shows the cell density, percent viable cells, and chlorophyll content over these eight days. The data showed that from the second day of recovery, the growth rate of cell density increased rapidly, and the percentage of surviving cells also increased to nearly 100% by the eighth day. Chlorophyll content also showed a very high growth rate during five days.

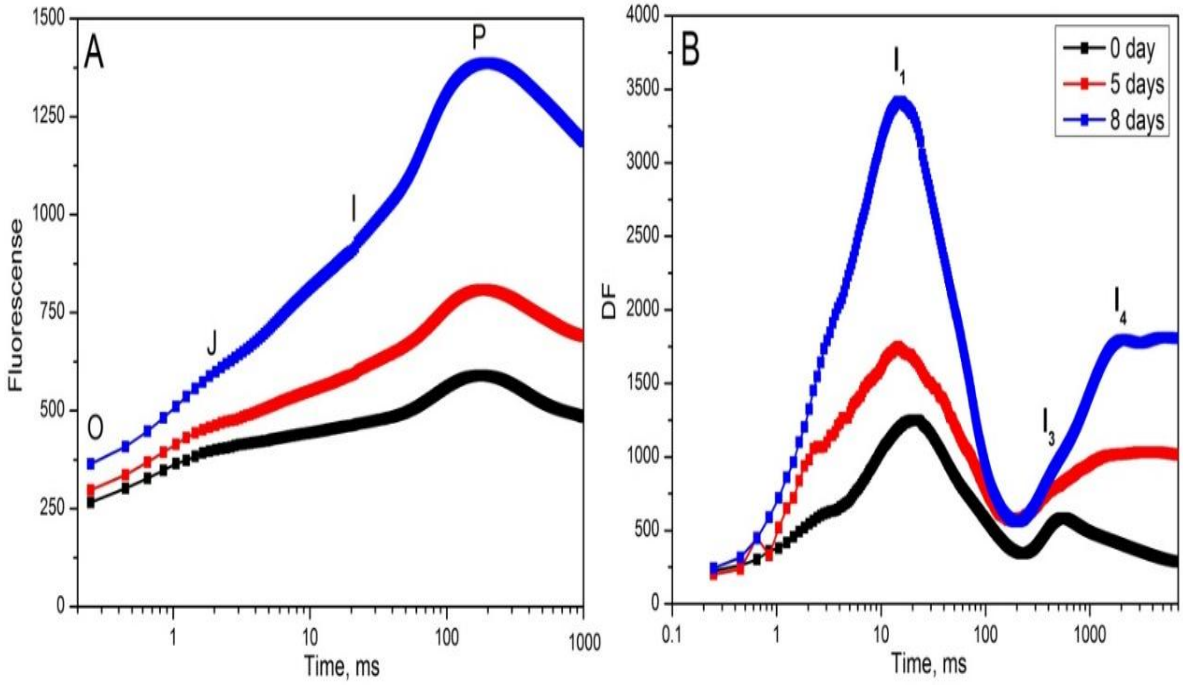

Fig. 64. OJIP transients recorded in *C. reinhardtii* cultures during recovery of cells after 16 days' incubation with 0.22 mg/L CL.

As can be seen fromFig. 64, the recovered cells exhibited different OJ, JI, and IP stages. OJ, JIP phase, and delayed fluorescence showed increases over time. This demonstrates that the effect of CL on the reduced level of Q_A and electron flow from Q_A to the PQ pool was significantly abolished as the recovery time increased to day eight. Delayed fluorescence spectra showed a relatively weak increase during the first five days of recovery and a significant increase on the eighth day. This indicated that after 8 days of recovery, the activity of the intracellular PSII center under the influence of CL had basically recovered, and an obvious peak appeared in I_1 (fast phase). The increase in I_3, I_4 (slow phase) also indicates the restoration of the ability to form a proton gradient in the cell membrane.

4.8 DFT calculations for study of Raman and IR spectra

In this series of experiments, a technology for mathematical characterization of Raman and IR spectra of carotenoids was developed to form a neural network model for assessing and predicting the results obtained. To determine the types of carotenoids, present in the study samples, a series of quantum mechanical calculations were performed for different levels of all-trans and cis isomers of carotene, β-cryptoxanthin, lycopene, lutein and zeaxanthin DFT with

different basis sets. Some functionals (B3LYP, BVP86, PBE1PBE) have been used for calculations of different basis sets (6-31+G**, DGDZVP, TZVP): optimized geometric parameters of equilibrium conformations have been obtained and frequency calculations have been obtained.

Some calculation results of carotene all-trans and (15-15') cis isomers obtained at the BVP86/TZVP level are shown in Fig. 65, where the theoretical spectra of the isomers were compared with the Raman spectra of carotene compared (Berezin & Nechaev, 2005; Saito & Tasumi, 1983).

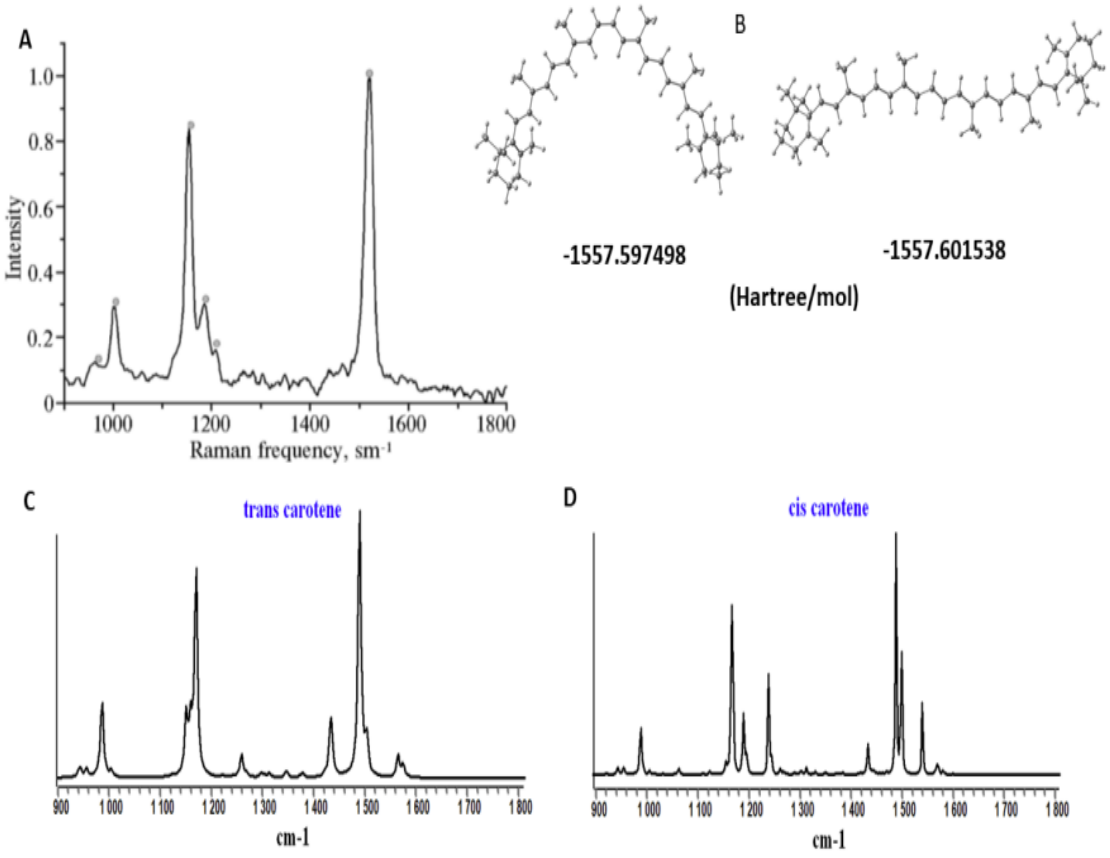

Fig. 65. A: Spectra observed from experiment. B: Energies of the all-trans and cis (15-15') isomers of carotene, optimized at the BVP86/TZVP level of the theoretical structure. C and D: Theoretical BVP86/TZVP RS of carotene trans and cis isomers in the 900-1800 cm^{-1} region.

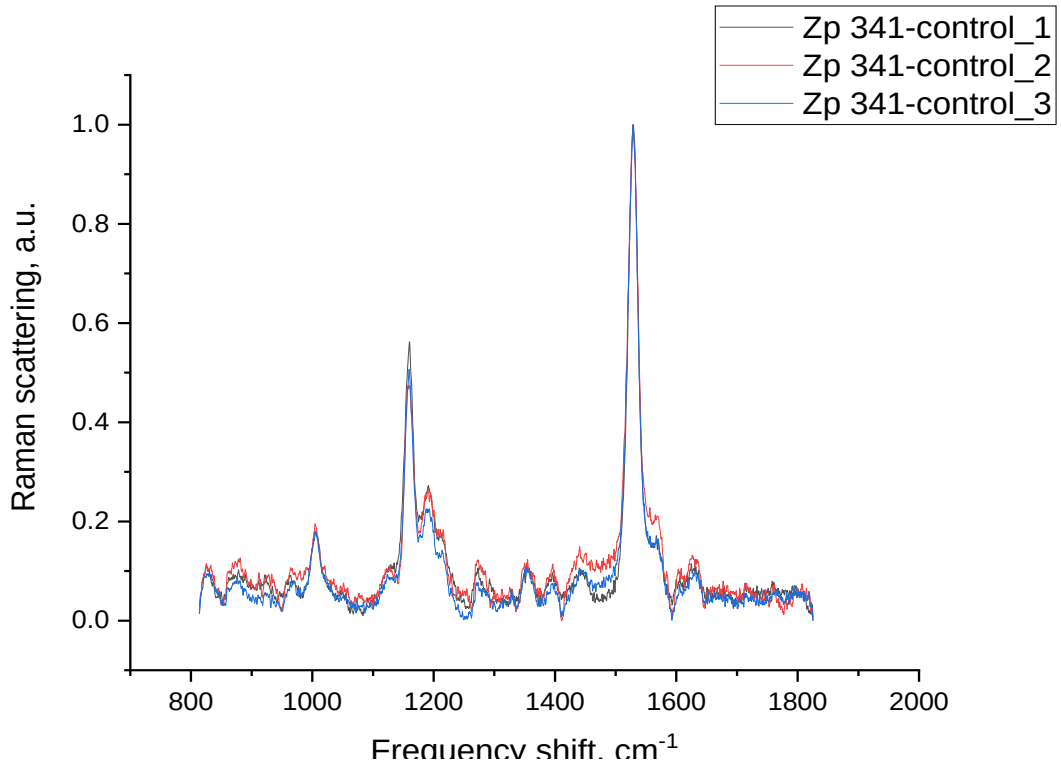

Fig. 66. Raman spectra of hybrid line zp 341 maize leaves

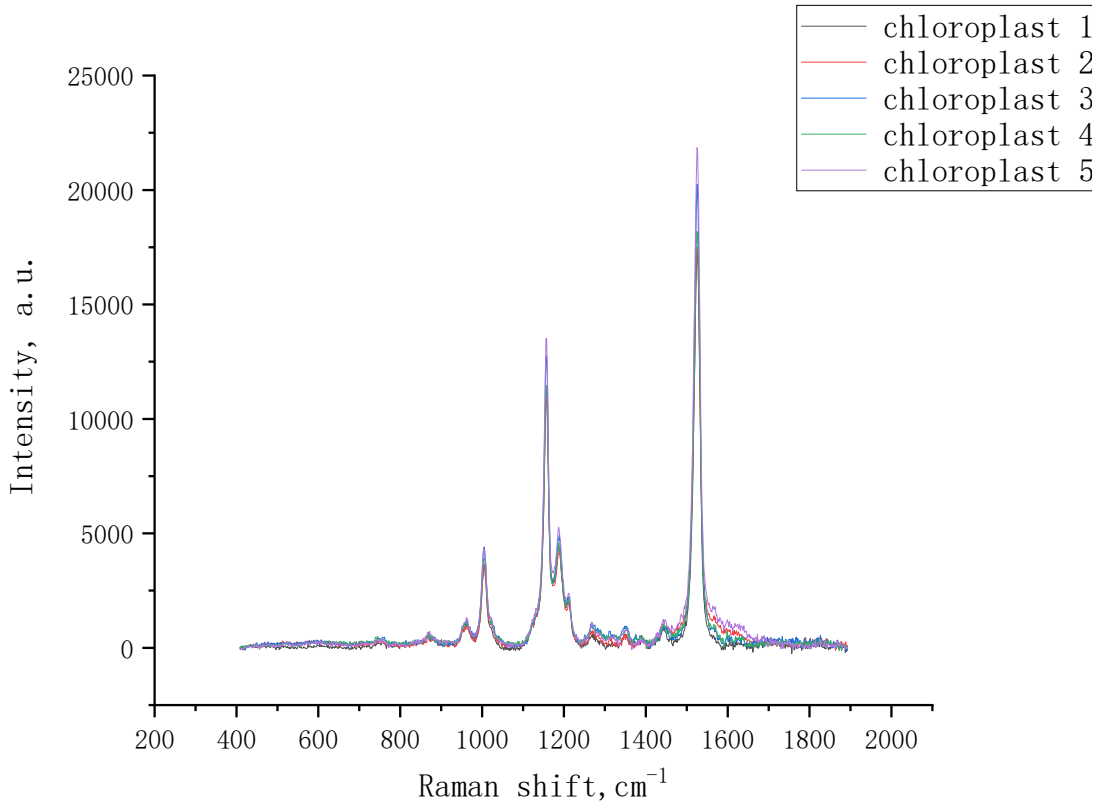

Fig. 67. Raman spectra of chloroplast

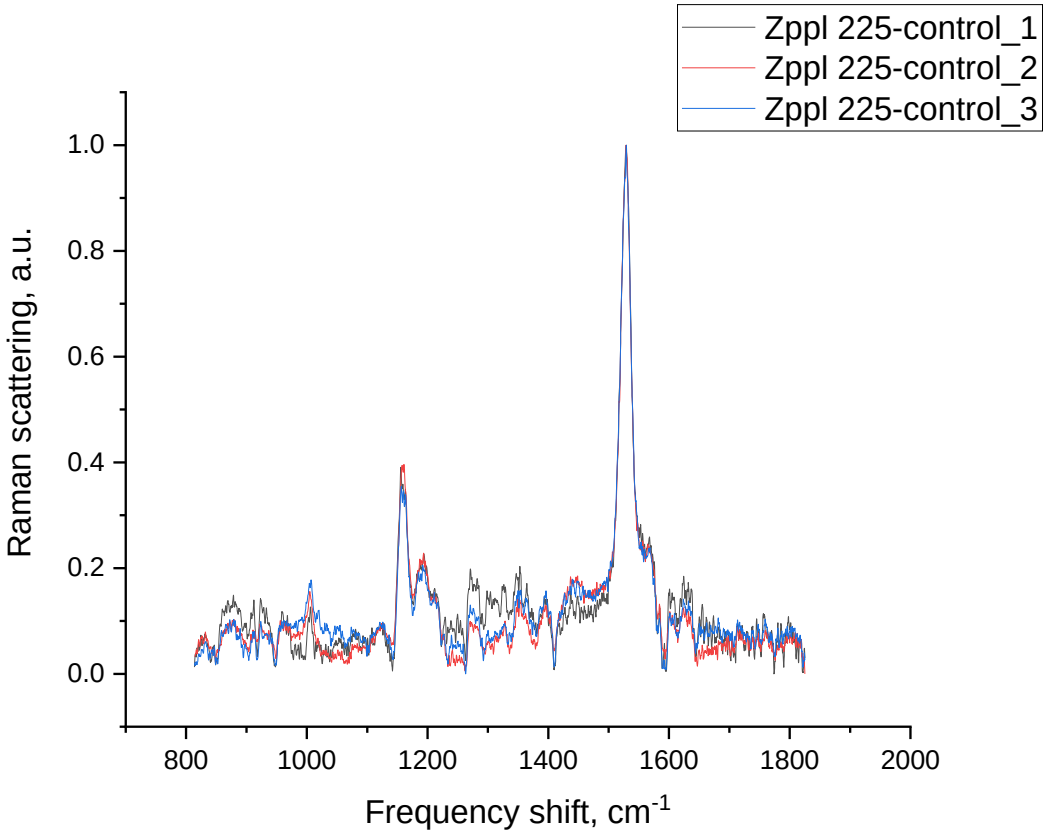

Fig. 68. Raman spectra of inbred line zppl 225 maize leaves.

Table 18. Raman peaks of BVP86/TZVP, zp 341, chloroplast, and zppl 225

Experimental Raman peaks, cm^{-1}			BVP86/TZVP, cm^{-1}		
Zp 341	chloroplast	Zppl 225	Carotene trans	assignment	Carotene cis
960	960	960	956	CH out-of-pl	987
1006	1003	1006	1032	CCH def	1062
1156	1156	1156	1159, 1162	C-C str	1167vs
1190	1186	1125	1170vs	C-C str	1195
1200	1210	-	1221,	C-C str	
-	-	-	1258.1270	CCH def, CH2def	1238,1244
					1487 (15-15)

1520	1524	1520	1503	C=C (15-15) cent str	1540

Comparison of BVP86/TZVP and Raman spectroscopy experimental data. The experimental Raman spectra (zppl 225, zp 341, and chloroplast) (Fig. 66 - Fig. 68)were compared with BVP86/TZVP results. In order to compare with detail, Raman peaks were analysed (Table 18). All experimental peaks are shown in BVP86/TZVP. Peaks 1258, 1270, 1248, 1244 and 1487 cm^{-1} representing CCHdef and CH2def are not shown in the experimental data. This means that BVP86/TZVP can provide researchers with more experimental ideas. It can also help researchers find details that may have been missed in experiments.

The analysis of the experimental and theoretical Raman spectra of trans and cis carotene allowed us to give more advantage to trans carotene, since the cis isomer has more energy in this region than trans carotene.

Using BVP86/TZVP can be a useful tool in biological research. Especially when it comes to Raman spectroscopy. It's more accurate and predictable. By using BVP86/TZVP, researchers can visualize which bonds are changing and which are missing.

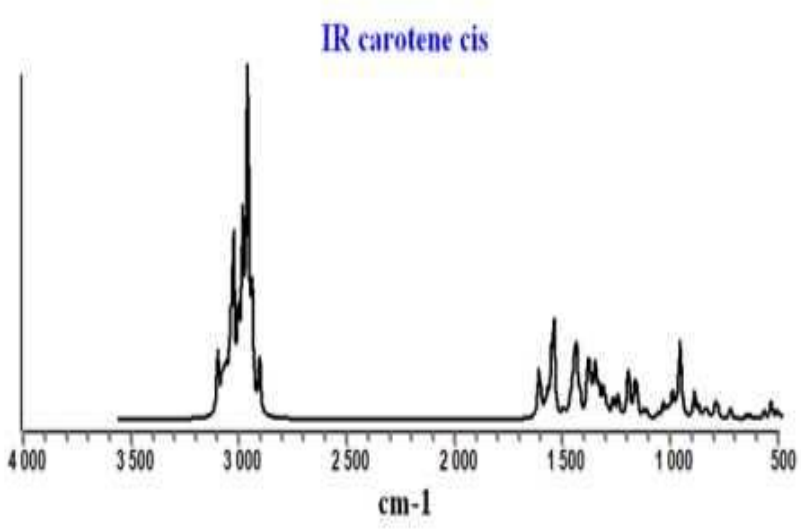

Fig. 69. Theoretical BVP86/TZVP IR spectra of cis-carotene.

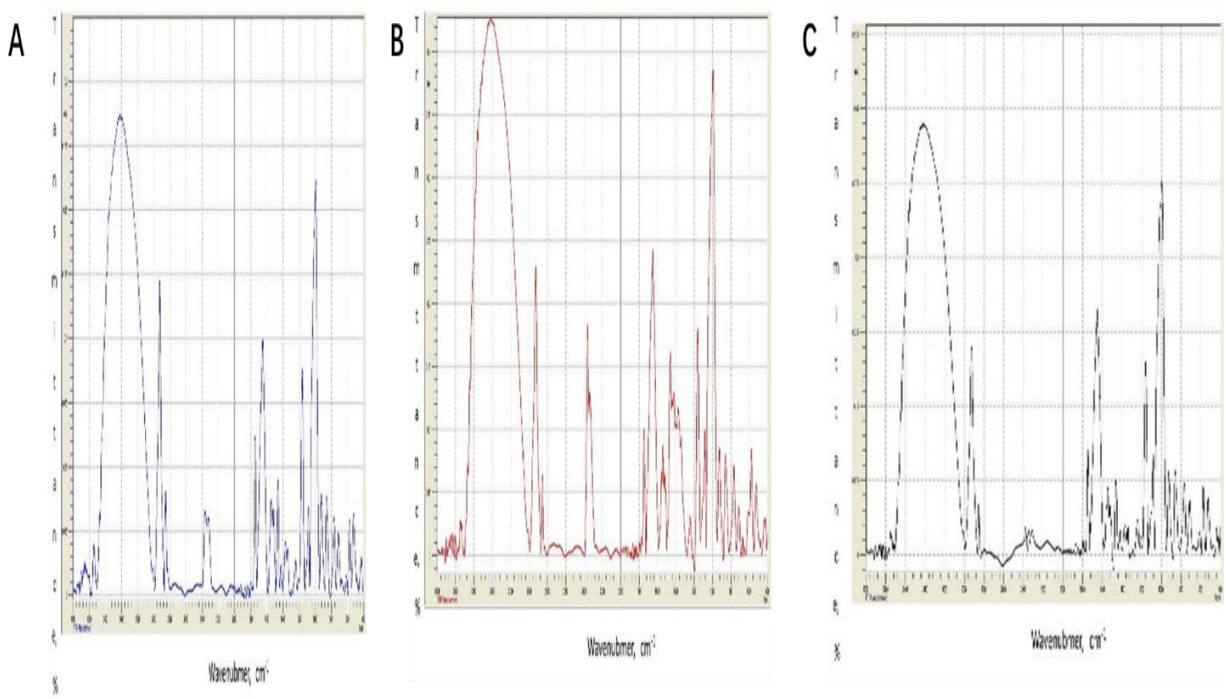

Fig. 70. IR spectrum obtained of different inbred line maize. A) zppl 186; B) zppl 225; C) zppl M1-3-3 Sdms

Table 19. IR peaks (cm^{-1}) of inbred line zppl 186, zppl 225, M1-3-3 Sdms, and BVP86/TZVP

zppl 186	zppl 225	M1-3-3 Sdms	assignment	BVP86/TZVP

3400	3400	3400	Alkanes	3116
2900	2925	2950	Alkynes	3092 3044
2850	2850	2850	Acyclic compounds	3030 2983
2375	2375	1650	Ethers	2976 2971
1775	1750	1750	Amines	2950 2932
1700	1675	-	Phenols	1626 1544
1550	1500	-	amines	1534 1523
1450	1475	1450	nitro compounds	1447 1436
1175	1175	1175	ketones	1402 1388
-	1100	1100	esthers	1354 1220
1000	1000	1000	sugars	1206 1162
900	925	950	proteins	1041 962
850	875	850	lipids	885 838
750	775	775	carboxylic acids	802 713
700	700	700		
640	-			
550	575			

Using the proposed approach, we showed that the infrared spectrum of the maize seed component molecules has symmetric and asymmetric stretching vibrations (band 2927-2852 cm^{-1}) and deformation characteristics of C – H groups. Vibration of the C-H group (1460 cm^{-1}). In addition, vibrations of the amide band bonds of protein amide I and amide II (1651 cm^{-1}, 1541 cm^{-1}) were found in the sample. The band in the infrared spectrum - 995 cm^{-1} may correspond to

the vibration of the Csp2-H bond of the alkene, and the less obvious bands - 860, 767, 711, 574 cm^{-1} - correspond to the stretching vibration of the alkene S – O, C-P, C-S keys.

The largest difference observed between samples of pure grain components is the vibration of Csp2-H bond of unsaturated hydrocarbons (995 cm^{-1}), and the intensity of this band is the smallest for species zpp l186 (Fig. 70). It was found that, in the samples studied, the 1082 cm^{-1} band of the infrared spectrum (deformation vibrations of the O – H bonds of the secondary alcohol molecules) was less pronounced than the vibration of the same group in the tertiary alcohols (1161 cm^{-1}).

In the course of the study, a strong band of deformed vibrational features of the saturated hydrocarbon CH bond (1460 cm^{-1}) and an asymmetric vibrational feature of the weak expression of the CH bond (2852 cm^{-1}) were found in the seed samples. Comparison with the symmetrical stretching vibration of the same bond (2926 cm^{-1}) and the stretching vibration of the C=O bond of amide 2 (1541 cm^{-1}), including the deformation vibration of the NH- bond and the stretching vibration of the CN bond. In amide 1 of the seed protein, IR bands (band 1747 cm^{-1}) of the carboxylic acid C=O bond stretching vibrations of aldehydes and ketones were found, most evident in the seeds of varieties ML3-3 SdmS and zppl 225.

IR peaks were analysed (see in Table 19) to compare BVP86/TZVP and IR spectra of inbred line maize (Fig. 69 and Fig. 70). It shows that even for the highest intensities the peaks are significantly shifted. There are some peaks shown in the experiment but not in BVP86/TZVP. This might due to the shifting of the peaks. BVP86/TZVP does show more detail than experiments. Compared with the experimental data, the peaks appear almost at the same position.

Using the proposed approach, we showed that combine DFT calculations with Raman and IR spectroscopy, it is possible to analyse complex object. The advantage of SERS is it offers a new solution to find peaks which has low intensity. It might be more efficiency for researcher if they can predict the wavenumber of spectrum.

5. Discussion

5.1 Study of the effect of pesticides on the state of plant material

In this study, the effect of pesticide on the leaf of maize plant were studied. The purpose of this series of experiments was to determine the effect of the pesticide on the condition of the pigments in the leaf. The pesticide is applied directly to the entire leaf, and then we check for changes in pigment fluorescence after the seedlings are buried in soil. Experimental investigation of the effect of thiamethoxam spray on the leaves of zppl 225 and zp 341 revealed that thiamethoxam was sprayed on the leaves when the 3rd leaf appeared (day 4). There is no significant difference between zp 341 hybrid corn line and zppl 225 inbred corn line in leaf pigment composition, but there were significant changes in the different genotypes following thiamethoxam application.

There was no change of thiamethoxam -treated hybrid line zp 341 in the pigment composition. In contrast, thiamethoxam decreased content of chlorophyll in leaves of inbred line zppl 225 to 0.61 mg/g (17% reduction in chlorophyll a and 24% reduction in chlorophyll b; $p < 0.05$).

Thiamethoxam treated sample caused changes in the OJIP of both maize type (Fig. 9, A, D). Normalization of the induction curves derive the relative fluorescence variable (V_t) function. The increase in ΔV_t of zp 341 and zppl 225 in O-J phase indicated the accumulation of reduced Q_A. The reduced Q_A due to the increased proportion of Q_B non-reducing centres of PSII, unable to conduct electron transport along the electron transport chain.(Lazár, 2006). The increase in ΔVt of thiamethoxam-treated zppl 225 at the O-J and J-I stages indicated the accumulation of reduced Q_A and plastoquinone molecules, which were unable to carry out the electron transfer of the dark photosynthetic reaction (Kalaji, Jajoo, et al., 2014).

The JIP-test was used to reveal thiamethoxam action on the important photosynthetic parameters derived from the OJIP transient (Table 2). The F_V/F_M correlates with the thermal quantum yield of PSII primary photochemical reactions and is used as an indicator of photosynthetic efficiency. There was no statistically significant difference between control and thiamethoxam-treated leaves of both maize type leaf in F_V/F_M. The correlation between PI_{ABS}

and plant viability reflects the function of PSA under current stresses (Živčák et al., 2014). It shows significant change under thiamethoxam treatment, PI_{ABS} decreased by 29% and 24% in thiamethoxam treated zppl 225 and zp 341 leaves, respectively. The reduction of PI_{ABS} in thiamethoxam treated zppl 225 leaves was due to a significant reduction in electron transfer (ψ_{Eo}) on the PSII receptor side. In contrast, the reduction of PI_{ABS} in zp 341 leaves might be related to a slight decrease in PSII photochemistry (F_V/F_M) and increased ABS/RC.

Redox transformation of the molecular reaction centre of PSI (P700) under the TMX treatment was assessed by MR kinetic analysis (Fig. 10, A, C) (Schansker et al., 2003). The MR kinetic signal drop during the first 15-20 ms reflects P700 oxidation (fast phase) and reaches a minimum at 20 ms (MR_{min}). MR_{min} is a transient steady state in which the rates of P700 oxidation and reductions are equal. Subsequently, the MR signal (slow phase) increases to a maximum at 200 ms (MR_{max}) due to the electron-donating reduction rate of PSII being superior to the oxidation rate(Strasser et al., 2010c).

It was found, leaf redox P700 transformations of both maize types were altered by thiamethoxam (Fig. 9, A, C). zppl 225 leaves showed chlorophyll changes in both the fast and slow phases of MR and were associated with a decrease in amplitude at 20 ms (Fig. 10, A). Analysis of MR kinetics showed an increase in reduced PSI receptors and a decrease in oxidized PSI receptors in zppl 225 leaves under the influence of thiamethoxam. This might be due to a reduced receptor pool on the receptor side of PSI. In contrast, there is no change in MR kinetics for zp 341(Fig. 10, B).

It was found, the rate of the recombination reaction is affected by vesicle membrane energization, and DF is proportional to the rate of the recombination reaction in PSII. The fast phase of DF associated with membrane potential formation(Goltsev et al., 2009a). Fig. 10 B, D shows the induction curves of DF normalized to the minimum fluorescence D_2. The decrease of the I1 peak on the microsecond time scale may be due to a decrease in the Z+ reduction rate of oxygen-4MnCa and/or a decrease in the QA reoxidation rate of oxygen-4MnCa (disturbed electron transfer on the PSII receptor side of the oxidizing complex (OEC)), which is induced by the oxidizing complex (OEC) of oxygen-4MnCa. (Goltsev et al., 2009a). During thiamethoxam treatment, I_1 amplitudes were reduced by 23% and 21% in zppl 225 and zp 341 leaves compared to controls, respectively.

It was found, the ratio of I_{1006}/I_{960} bands in maize leaves increased after thiamethoxam application (Fig. 12). Under the influence of thiamethoxam, the I_{1520}/I_{1006} ratio of zppl 225 decreased by 26%. In the leaves of the zp 341 hybrid, thiamethoxam caused a 43% and 16% increase in the ratios of I_{1520}/I_{1006} and I_{1520}/I_{1160}, respectively, suggesting a conformational change in the carotenoids.

In experiment study of the effect of thiamethoxam inject to the soil of two maize genotypes, TMX was inject into soil at 4th day when seedling in the soil (TMX(a)) and inject into soil at 8th day (TMX(b)). In this experiment, the pigment content of two maize genotypes under TMX treatment was measured (Table 3). It was found, after 12 days, the pigment composition of different maize genotypes was slightly different. The total chlorophyll content is 0.52 mg/g in zppl 225 and 0.64 mg/g in zp 341. In the presence of TMX, the chlorophyll content in zp 341 decreased from 0.64 mg/g to 0.31 mg/g (b). The initial carotenoid contents in zppl 225 and zp 341 were 0.14 and 0.13 mg/g, respectively.

In this study, the OJIP transients were recorded for maize hybrid (zp341) and inbred line (zppl 225) under TMX treatment, which was added 4th day when seedling seeds (a) and 8th day when 3rd leaf of plant appear (b) (Fig. 12). The kinetics showed a typical pattern for plants grown under the standard conditions with the J, I, and P steps at 2, 30, and ~200 ms for control group of zp 341 and zpple 225, respectively. TMX-treated plant showed modifications of the OJIP transients on the 10th and 12th days of growing. In zppl 225, the shape of the OJIP transient remained unchanged during TMX treatment (a), whereas pesticide-treated zp 341 showed increased levels of Chl fluorescence at the O-J-I-P step at day 10 compared to the control (Fig. 13 a, b). The effect of TMX was shown to be enhanced in zppl 225 plants, as evidenced by a decrease in the JIP phase under TMX (a) at day 12 (Fig. 13 c) and an increase in the I-P step under TMX (b) compared to the control. The effect of TMX on zp 341 OJIP transients was the same as in 10- and 12-day-old leaves (Fig. 13 d).

The probability of electron transfer from Q_A to the PQ pool (ψ_{Eo}), depends on the functional state of the donor and/or acceptor side of PSII. In the control, the ψ_{Eo} of leaves of zppl 225 and zp 341 at day 10 were 0.59 and 0.70, respectively. Under TMX treatment, ψ_{Eo} decreased ($P < 0.05$) in zp 341 but remained unchanged in zppl 225. In the control plants, the

leaf ψ_{Eo} of zppl 225 and zp 341 were 0.56 and 0.63 at day 12, respectively. Its value was increased in leaves of zppl 225 under TMX (b) treatment ($P < 0.05$).

The quantum yield (φ_{Eo}) of electron transport is proportional to F_V/F_M and ψ_{Eo}. At TMX treatment, the φ_{Eo} value of zp 341 leaves decreased due to the significant decrease of ψ_{Eo} value, while the F_V/F_M remained unchanged at the 10th day. Under TMX treatment, the probability of electron transfers from the intersystem electron carrier to the reducing end electron acceptor on the PSI acceptor side (δ_{R0}) in zp 341 decreased ($P < 0.05$). It was found, the quantum yield of terminal PSI electron acceptor reduction (φ_{Ro}) was about 0.26 in zp 341 leaves and decreased in TMX-treated plants. In contrast, the δ_{R0}, φ_{Eo}, and φ_{Ro} values of zppl 225 remained unchanged after 10 days. However, the δ_{R0} and φ_{Ro} values of zppl 225 increased ($P > 0.05$) under TMX (a) and remained unchanged or slightly decreased ($P > 0.05$) after 12 days under TMX (b).

The parameters PI_{ABS} and PI_{total} differed in response to the two TMX treatment variants in leaves of maize genotypes. PI_{ABS} describes the photosynthetic index relative to absorption, combining three PSII characteristic parameters: the maximum quantum yield of PSII photochemistry (Fv/Fm), the density of active PSII reaction centres per antenna (RC/ABS), and the electron probability from Q_A Transfer to PQ pool (ψEo). It was found, the PI_{ABS} of zppl 225 under TMX was slightly increased compared to the control on day 10 ($P > 0.05$). In contrast, zp 341 under TMX, especially PI_{ABS} decreased during TMX(a) treatment ($P < 0.05$). In most cases, the PI_{ABS} values of leaves of both genotypes increased after 12 days, indicating amplification of plant performance under TMX treatment. The total index (PI_{total}) of zp 341 attributable to PSII, PSI functional activity and electron transport between them decreased on TMX ($P < 0.05$), while the value of this parameter did not change significantly in zppl 225 leaves after 10 days. On day 12, an increase in PI_{total} was observed in zppl 225 leaves under TMX treatment. However, in zp 341, PI_{total} increased under TMX (a), while the value of this parameter did not change significantly ($P > 0.05$) during TMX (b).

TMX slightly affected the DF induction curve at day 10 in the leaves of both maize genotypes. In contrast, we observed a significant change in the TMX induction profile at day 12. Thus, the kinetic patterns measured in the two maize genotypes showed a decrease in the amplitude of I_1, while I_2 and I_4 remained unchanged. Peak I_1 was shifted from 7 ms to about 10

ms in control and TMX-treated zp 341 plants (Fig. 15 d). In zppl 225 and zp 341, a decrease in the energy of thylakoid membranes under TMX resulted in a decrease in I_1 after 12 days.

It was found, at TMX (a), the amplitudes of the fast and slow phases in leaves of both genotypes were significantly decreased ($P < 0.05$), while in the case of TMX (b) treatment, the MR amplitude was significantly lower after 10 days compared with the control remained unchanged (Fig. 16 a, b). After 12 days, the MR amplitude of zp 341 decreased under TMX (b) (Fig. 16 d). However, the MR amplitude of zppl 225 was increased under TMX (b) treatment (Fig. 16 c).

It was found, in the presence of TMX, the absolute value of the intensity and the position of the bands in the Raman spectrum are the same as in the control. The presence of peaks at 1190 and 1200 cm–1 in the Raman spectrum indicated the characteristic 15-cis conformational state of carotenoids and was not altered by TMX treatment (data not shown). In Raman spectrum, 1160 and 1520 cm–1bands correspond to the –C–C– and –C=C– vibrations of the carotenoid molecule bond, and the change in the intensity ratio I_{1520}/I_{116} reflects changes in the contribution of –C=C– bonds vs. –C–C- bonds of the polyene chain (Vlasov et al., 2020).(Vlasov et al., 2020).(Vlasov et al., 2020).

In the experiment study of the effect of thiamethoxam of different concentrations, TMX was spray on the leaves when 3rd leaf appearance (day 8) (TMX(c)) and spray on the soil when seedling into the soil (day 4) (TMX(d)). Comparison of TMX(c) at 0.2 mg/mL and 0.02 mg/mL concentrations treatment, concentration has evidently impact on spray TMX(c) on the surface of third leaf (measurement on day 10) (Fig. 17). Thiamethoxam at 0.02mg/mL has been determined to cause significant and opposite changes in the molecular conformation of carotenoids.

Measurement performed on day 12, hybrid (zp 341) shows a similar intensity ratio RS (I_{1520}/I_{1160}). 0.2 mg/mL TMX(c) leads visible difference to Zppl 225 (Fig. 17). Comparing with 3rd leaf and 5th leaf measurement. 0.2 mg/mL TMX(c) causes intensity increase in both Zp 341 and Zppl 225. In this case, 0.02 mg/mL thiamethoxam did not cause a significant change in the molecular conformation of carotene.

OJIP transients were recorded in inbred line (zppl 225) and hybrid (zp 341) of maize under 0.2 mg/mL and 0.02 mg/mL TMX(c), which were added after 3rd leaf appearance (Fig. 18). In control maize plants of zppl 225 and zp 341, the kinetics displayed a pattern typical of plants

grown under normal conditions, with J, I, and P steps of 2, 30, and ~200 ms, respectively. After TMX(c) treatment shows transient changes in OJIP at 10 and 12 days of growth. The initial level O corresponds to the fluorescence intensity at "open" PSII RCs (Fo), when all acceptors in PSII are oxidized and able to accept an electron: photoinduced reduction of Q_A^- could cause increase in the O-J phase.

Compare with the TMX(c) treated group and control on 10^{th} day measurement, zp 341 treated by 0.2 mg/mL TMX(c) and 0.02 mg/mL decreased by 5% and 26%; zppl 225 treated by 0.2 mg/mL and 0.02 mg/m TMX are not significant (Table 4). Compare with the TMX(c) treated group and control on 12^{th} day measurement, zp 341 treated by 0.2 mg/mL TMX(c) and 0.02 mg/mL decreased by 22% and 7%; for zppl 225 difference is not significant (Table 5). The significant decrease of zp 341 due to the decrease of electron transport at acceptor side of PSII.

TMX(c) causes changes in the redox P700 transformations in leaves of both the hybrid line (zp 341) and inbred line (zppl 225) (Fig. 22). 0.02 mg/mL TMX(c) cause significant increase rate in fast phase and slow phased on zp 341. Presumably due to a decrease in the acceptor pool. For Zppl 225, difference between two concentrations is not as significant as Zp 341, but 0.02 mg/mL TMX(c) still cause more decreased than 0.2 mg/mL TMX(c) and control.

Fig. 20 shows that the induction curves of zp341 and zppl 225 DF which treated by TMX(c). I_1 amplitude decreased in zppl 225 which might due to the decrease in the Q_A re-oxidation rate (disturbance of electron transport on the acceptor side of PSII) and/ or a decrease in the Z^+ reduction from 4MnCa of oxygen-evolving complex (OEC). Low concentration of TMX(c) caused more effect on zppl 225. For zp 341, measurement performed on 10^{th} day, I_1 amplitude also decreased for both concentrations. But the measurement performed on 12^{th} day, high concentration increased I_1 amplitude and low concentration decreased I_1 amplitude.

Measurement performed on day 12, TMX(d) leads visible difference to zp341 and zppl 225 (Fig. 22). For further analyse, I_{1520}/I_{1160} ratio of the Raman spectrum has been calculated (Fig. 23). 0.2 mg/mL TMX(d) effects more on zp341 then 0.02 mg/mL TMX(d). On the other hand, 0.02 mg/mL TMX(d) shows more effect then 0.2 mg/mL TMX(d) on zppl 225.

Comparing with effect of TMX(c) and TMX(d), spray TMX on soil drives more influence than spray on the leaf when 3^{rd} leaf appearance. In this case, the conformation of the carotene molecule changed dramatically when zppl 225 maize was exposed to low concentrations of

thiamethoxam. Importantly, the action of the pesticide changed the conformation of the carotene molecule in the leaves.

Compare with the control and TMX(d) treated group on 10^{th} day measurement, zp 341 treated by 0.2 mg/mL TMX(d) and 0.02 mg/mL decreased by 29% and 15%; zppl 225 treated by 0.2 mg/mL and 0.02 mg/m TMX(d) increased by 11% and 14% (Table 7). Compare with the TMX(d) treated group and control on 12^{th} day measurement, zp 341 treated by 0.2 mg/mL TMX(d) and 0.02 mg/mL decreased by 11% and 42%; for zppl 225 difference is not significant (Table 8). The significant decrease of zp 341 due to a decrease in the acceptor pool of PSII (ψ_{E0}).

Compare with TMX(c) and TMX(d), spray TMX on the soil when seedling the seeds cause more influence than spray on leaves when 3^{rd} leaf appearance. TMX cause decrease of electron transport at acceptor side of PSII. hybrid line (zp 341) is more sensitive to TMX effect than inbred line (zppl 225).

It was found, MR kinetics measurements on 10^{th} day (Fig. 25 a,b), two concentrations of TMX(d) cause zp 341 both decreased rate in fast phased and slow phase. Presumably due to a decrease in the acceptor pool. In 12^{th} day measurements (Fig. 25 c,d), high concentration of TMX(d) cause rate increase of zp 341. But for zppl 225, different concentration didn't cause much difference.

Compare with results of TMX(c) and TMX(d), treatment of TMX time cause different influence by the concentration. Hybrid line (zp 341) is more sensitive than inbred line (Zppl 225).

Fig. 26 shows that the induction curves of zppl 225 and zp 341 DF which treated by TMX(d). I_1 amplitude increased in zppl 225 which might due to the increase in the Q_A re-oxidation rate (disturbance of electron transport on the acceptor side of PSII) and/ or increase in the Z^+ reduction from 4MnCa of oxygen-evolving complex (OEC). Low concentration of TMX(d) caused more effect on zppl 225. For zp 341, measurement performed on 10^{th} day, I_1 amplitude also decreased for both concentrations. But the measurement performed on 12^{th} day, both concentrations cause increased I_1 amplitude.

Compare with TMX(c) and TMX(d), zp 341 is more sensitive to the TMX treatment. Spray TMX on the soil when seeding the seeds cause more effect than spray on the leaves when 3^{rd} leaf appearance.

It was found that during exposure to a pesticide, changes in the pigment state (chlorophyll, carotenoids) change and depend on a series of plant growth parameters and their genotype. This results of a study carried out on the leaves of two different maize genotypes (zppl 225 and zp 341) after exposure to a pesticide (TMX, external leaf spraying, or when applied to the soil by root irrigation of the plant) and chloroplasts (CL).To characterize the activity of PSII, changes in the parameters of the JIP test were recorded: ψ_{Eo} - the probability of electron transfer from Q_A^- to the quinone pool; F_V/F_M - the maximum quantum yield of primary charge separation in PSII; ABS/RC is the energy flux absorbed by one active RC, which is influenced by the ratio of active/inactive RC; PI_{ABS} is the index of functional activity PSII related to absorbed energy, and for PSI the kinetics of modulated reflection/absorption of light with a wavelength of 820 nm, as well as Raman spectroscopy of carotenoids.

When TMX acts directly on the PI_{ABS} leaf, the chlorophyll content decreases significantly (especially for zppl 225), which probably indicates a decrease in chlorophyll synthesis, but an increase in carotenoid synthesis. Note that we have not revealed any differences in the values of the maximum quantum yield of PSII (F_V/F_M) in control and thiamethoxam-treated leaves under conditions of spraying or after the introduction of TMX by root irrigation in both types of corn. An analysis of the kinetics of DF associated with the redox state of P700, when spraying TMX leaves, indicates a decrease in the formation of oxidized and an increase in the reduced forms of PSI (P700) acceptors of only zppl 225 leaves. This is probably due to a decrease in the pool of acceptors, such as P700, on the acceptor side of the PSI, which does not occur in the RC of the leaves of the hybrid zp 341. The fact that after the action of TMX, the conformation of the carotenoid molecule in the leaf of zppl 225 and zp 341 are opposite probably indicates a different mechanism of plant resistance to TMX.

In connection with the tasks, we conducted a study of the effect of CL (TMX derivative) not only on the functioning of photosynthetic processes (Pinnola & Bassi, 2018), but also on the structure(Chuartzman et al., 2008), as well as the viscosity of the chloroplast membrane (Havaux et al., 1998). It was found that the electron flux decreases in chloroplasts treated with CL, which is accompanied by a decrease in O_2 release. This is probably due to a decrease in the number of centers capable of reoxidation of Q_A, as well as an increase in the proportion of centers with an unfilled Q_B binding site. Since electron transport in PSII depends on the localization of electron

transporters and their red/ox potential, we investigated several reasons for the possible change in electron transport under the action of CL on chloroplasts. It is known that TMX is a pesticide similar in structure to CL, and is able to bind to proteins due to hydrogen, electrostatic and hydrophobic bonds (X. Su et al., 2021). Probably, CL is also capable of binding to hydrophobic and/or polar amino acids at the Q_B site of the D_1 protein due to similar interactions (Battaglino et al., 2021), competing for the binding site with plastoquinone. This assumption is consistent with our results indicating the appearance of Q_B centers with properties similar to the effects of DCMU. Indeed, DCMU (occupies the Q_B binding site) It can block direct electron transfer from Q_A^- without changing F_V/F_M(Henrysson & Sundby, 1990).

It is important that, under the action of CL, the morphology of chloroplasts changes due to a violation of granular structures in the region of the thylakoid membrane, where PSII is mainly localized. These changes can cause conformational changes in the D_1 protein and, as a result, modification of the Q_B site. Thus, changes in the functioning of ETC probably mainly depend on the state of the Q_B site, since the electron flow rate from H_2O to MV and the activity of PSII changed similarly under the action of CL.

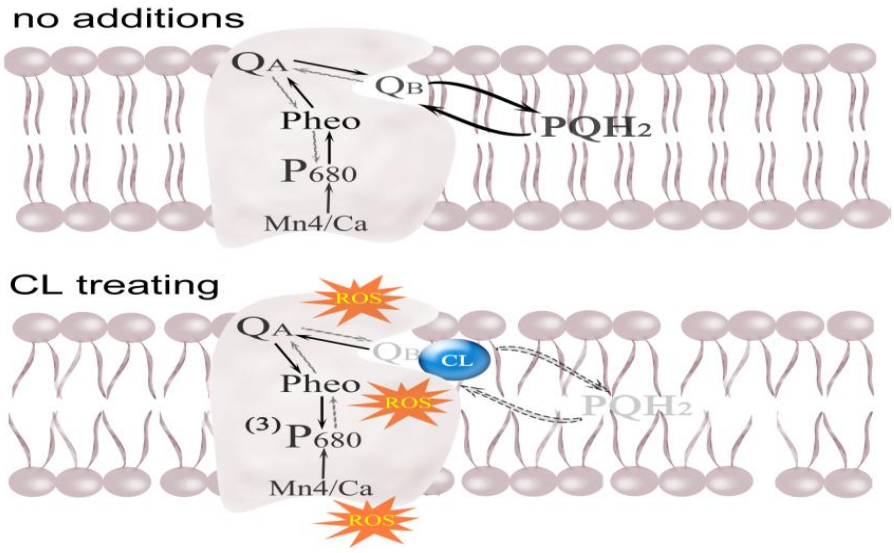

Fig. 71. Diagram of molecular action of CL on FSII

It is likely that disruptions in the electron transfer process between Q_A and Q_B initiate reverse electron transfer and charge recombination with the generation of a triplet state of chlorophyll (Rutherford et al., 2012). This process, as a rule, correlates with an increase in the

number of markers of oxidative stress (for example, malondialdehyde) (Mahapatra et al., 2019; Shahid et al., 2021), indicating the formation of reactive oxygen species (ROS)(Touzout et al., 2021). The data obtained using AFM and EPR, indicate both a change in the morphology of the chloroplast, as well as a violation of the integrity and viscosity of the thylakoid membrane, which can also lead to proton leakage through the membrane of chloroplasts. So, the effect of CL on chloroplasts changes electron transport due to either the Q_B site or the PSII site due to structural changes in the thylakoid membrane.

5.2 Study of the dependence of the state of pigments on the plant genotype.

As noted earlier, one of the objectives of our study was to compare changes in the molecular properties of pigments depending on the genotype. This approach makes it possible, firstly, to clarify the mechanism for studying pigments under the influence of pesticides, and secondly, to develop technologies for diagnosing the state of the plant and its selection. The objective of this work was to determine the effect of pesticide on photosynthetic pigments and the photochemical activity of the leaf photosynthetic apparatus of two maize genotypes using modern fluorescence and spectral methods.

We found that the inbred zppl 225 line had lower chlorophyll content, which could indicate that synthesis of these pigments was decreased under TMX influence, as well as the ratio of carotenoids to chlorophyll (a + b) which is usually associated with an increase in carotenoid content under conditions of stress. However, there was no change in pigment composition in leaves of zp 341.

Kinetic curves of PF describe the energy fluxes in different parts of the photosynthetic electron transport chain, and analysis by JIP test showed that the effect of thiamethoxam on the PSII photochemistry (F_V/F_M) of leaves of both studied genotypes was not significant ($p > 0.05$). We were able to detect changes on the PSII receptor side in leaves of the zppl 225 inbred line, whereby a decrease in electron transport probability (ψ_{Eo}) on the side of the PSII receptor led to a decrease in the function of PSII (PI_{ABS}).

Thus, spraying maize plants with the insecticide thiamethoxam resulted in reduced chlorophyll content in leaves of the zppl 225 inbred line. In zppl 225 and zp 341, thiamethoxam was determined to affect the functional activity of PSII, to decrease PI_{ABS} parameters, and to reduce the pigment-like membrane potential. It was found, thiamethoxam caused opposite changes in the conformation of carotenoid molecules, but not in their content.

In the experiment investigation of the identification of organic molecules between different hybrids of maize seeds, different genotype of maize seeds was studied. For ZP 684 the wavenumber 1017 cm^{-1} (for the common seed -100% - 88.52) is maximum in the pericarp and minimum in embryos. For ZP 677 The wavenumber 1016 cm^{-1} (control-100% -86.56) is maximum in pericarp and minimum in embryos. For ZP 633 the wavenumber 1016 cm^{-1} (control-100% -82.36) is maximum in endosperm and minimum in embryos. For ZP 735 the wavenumber 1017 cm^{-1} (control-100% -81.60) is maximum in endosperm and minimum in embryos. Probably, in this area (1017 -1054 cm^{-1}) due to aromatic CH-planar bending vibrations were detected in this area.

It was found, for ZP 684 the wavenumber 1648 cm^{-1} (control -100% -93.82) is maximum in the pericarp and minimum in embryos. For ZP 677 the wavenumber 1648 cm^{-1} (control -100% -95.38) is maximum in pericarp and minimum in embryos. For ZP 633 the wavenumber 1648 cm^{-1} (control -100% -92.53) is maximum in endosperm and minimum in embryos. For ZP 735 the wavenumber 1648 cm^{-1} (control -100% -92.99) is maximum endosperm and minimum in embryos. Probably connected with stretching vibrations of C = O in primary, secondary and tertiary amides, bending vibrations of N-H and C-N in secondary amides of protein molecules, peptides and free amino acids, also characterize OH groups of crystalline cellulose water

For ZP 684 the wavenumber 1744 cm^{-1} (control -100% -94.7). Is maximum in the endosperm and minimum in embryos. For ZP 677 the wavenumber 1744 cm^{-1} (control -100% -97.15) is maximum in endosperm and minimum in embryos. For ZP 633 the wavenumber 1745 cm^{-1} (control -100% -95.10) is maximum in endosperm and minimum in embryos. For ZP 735 the wavenumber 1744 cm^{-1} (control -100% -93.41) is maximum in endosperm and minimum in embryos. Probably connected with vibrations of the lipid hydroxyl group.

	Inbred	Hybrid				
	zppl225	zp 341	zp 684	zp 633	zp 735	zp 677
FAO maturity group	350-400	300	600	550-650	750-850	600
grain yield (t ha^{-1})	2.1	13	14	7.819	8.108	14
Pericarp, %	7.27	7.26	5.80	5.06	5.30	5.40
Germs, %	10.73	12.30	11.98	11.14	9.95	13.65
Endosperm, %	82.00	80.44	82.22	83.80	84.75	80.95
chlorophyll content (TMX treated)	0.74 mg/g to 0.61 mg/g	Not significant				
$PI_{ABS\ (TMX\text{-}treated)}$	Decrease 29%	Decrease 24%				
I_1 amplitudes (TMX-treated)	Decrease 23%	Decrease 21%				
$I_{1520}/I_{1006\ (TMX\text{-}treated)}$	Decrease 26%	Increase 43%				
Chl b content (TMX(b)-treated)	Not significant	Decrease from 0.64 to 0.31				
OJIP transients	unchanged	increase				
$\psi_{E0\ (TMX(b)\text{-}treated)}$	unchanged	decreased				
$PI_{ABS\ (TMX(a)\text{-}treated)}$	increased	decreased				
MR amplitude $_{(TMX(b)\text{-}treated)}$	increased	decreased				

PI_{ABS} (0.02 mg/mL TMX(c)-treated)	Not significant	Decreased 26%				
Redox P700 transformation (0.02 mg/mL TMX(c)-treated)	Not significant	Increase				
PI_{ABS} (0.2 mg/mL TMX(d)-treated)	Decreased 29%	Increased 11%				

Table 20 Summary table for the analysis of the effects of pesticides on pigments in the plant.

6. Conclusion

The results of a study of the photosynthetic apparatus of a plant carried out on the leaves of two different corn genotypes (zppl 225 and zp 341) after exposure to a pesticide (TMX, external spraying of the leaf or when it is introduced into the soil due to root watering of the plant and chloroplasts, CL).

1) It was found that the treatment of the plant with the pesticide thiamethoxam, both through leaf spraying and by root watering of the plant, changes the functional activity of photosystem II (PSII) (PI_{ABS}), but does not affect the maximum quantum yield of PSII (F_V/F_M) of the leaf in both the inbred line zppl 225 and and the hybrid zp 341.
2) When spraying a TMX leaf, a decrease in PI_{ABS} in the leaves of two corn genotypes is due to a decrease in the efficiency of electronic transport on the acceptor side of PSII (ψ_{Eo}).
3) When spraying TMX leaves of two corn genotypes (zppl 225 and zp 341), differences were revealed: a decrease in the chlorophyll content in the leaves of the inbred line zppl 225 compared with the hybrid line zp 341; in the leaves of zppl 225, a decrease in the electron flux from and to PSI was found, and opposite changes in the conformation of carotenoid molecules compared with zp 341.
4) It was found that in chloroplasts treated with CL (22 and 110 μg/L CL), in the presence of DCBQ, the number of PSII centers capable of carrying out the transfer reaction from Q_A to Q_B decreased by 23 and 26%, and the reaction rate decreased by 64 and 52%, respectively,

which correlates with the blocking of electron transfer between Q_A and DCBQ.

5) It was found that incubation with CL of functionally active PSII particles (particles capable and not capable of O_2 formation) with 0,11 mg/L of CL reduces the rate of O_2 release by 20%, which is consistent with the data obtained on PSII of whole chloroplasts. In preparations of both types of PSII particles, the recovery rate of the DCPIP electron acceptor in the presence of CL decreases.
6) Disruption of the electron transfer process between Q_A and Q_B increases the probability of a "triplet-triplet" electron transition from chlorophyll to an oxygen molecule, which is accompanied by an increase in the number of oxidative stress markers (malondialdehyde). It was found that after 3 minutes of illumination (100 μmol photons $m^{-2}c^{-1}$), the MDA content in chloroplasts treated with 0,11 mg/L CL increased by 46% compared with the control.
7) Using the atomic force microscopy method, it was found that in the control, chloroplasts have a typical discoid shape, and the membrane relief is due to the presence of globular structures. The effect on chloroplasts of 0,11 mg/L CL significantly changes the morphology of the chloroplast: 57% had a discoid shape, and the relief of the membrane surface was absent, probably due to the destruction of part of the thylakoid membranes.
8) EPR spectroscopy revealed changes in the viscosity of chloroplast membranes under the action of 0,11 mg/L of CL: the parameter τ decreased by 12%, which indicates a decrease in the ordering of the distribution of the "tails" of fatty acids of phospholipids of the lipid bilayer of the chloroplast membrane.

Acknowledgment

In the past four years, prof. G. Maksimov has provided me with great help. When I felt confused and lacked self-confidence, you always pointed out the direction for me and made me firmly complete my studies. You have built a great scientific world for us. Throughout the process, you have always inspired me by giving me a new perspective on the world.

Colleagues in the School of Biology are always friendly and patient. They helped me a lot in my experiments. Especially PhDs A. Volgushuva, E. Parshina and D. Todorenko.

In the last, I would like to express my deep gratitude to my parents and friends. In all the years of study, they have always by my side and provide me a lot of love. My mother and father offered me a safe place when I feel tied.

University study life is finished. I hope that myself in the future will keep the passion for science. I hope I can make a difference for the world, even a little bit.

List of references

Aboud, S. A., Altemimi, A. B., Al-HiIphy, A. R. S., Yi-Chen, L., & Cacciola, F. (2019). A comprehensive review on infrared heating applications in food processing. *Molecules*, *24*(22), 1–20. https://doi.org/10.3390/molecules24224125

Alcaíno, J., Baeza, M., & Cifuentes, V. (2016). Carotenoid distribution in nature. *Sub-Cellular Biochemistry*, *79*, 3–33. https://doi.org/10.1007/978-3-319-39126-7_1/FIGURES/4

Aliyeva, N. K., Aliyeva, D. R., Suleymanov, S. Y., Rzayev, F. H., Gasimov, E. K., & Huseynova, I. M. (2020). Biochemical properties and ultrastructure of mesophyll and bundle sheath thylakoids from maize (Zea mays) chloroplasts. *Functional Plant Biology : FPB*, *47*(11), 970–976. https://doi.org/10.1071/FP20004

Allakhverdiev, S. I. (2020). Optimising photosynthesis for environmental fitness. *Functional Plant Biology : FPB*, *47*(11), III–VII. https://doi.org/10.1071/FPV47N11_FO

Altangerel, N., Huang, P. C., Kolomiets, M. V., Scully, M. O., & Hemmer, P. R. (2021). Raman Spectroscopy as a Robust New Tool for Rapid and Accurate Evaluation of Drought Tolerance Levels in Both Genetically Diverse and Near-Isogenic Maize Lines. *Frontiers in Plant Science*, *12*, 621711. https://doi.org/10.3389/FPLS.2021.621711/BIBTEX

Anderson, J. C., Dubetz, C., & Palace, V. P. (2015). Neonicotinoids in the Canadian aquatic environment: A literature review on current use products with a focus on fate, exposure, and biological effects. *Science of The Total Environment*, *505*, 409–422. https://doi.org/10.1016/J.SCITOTENV.2014.09.090

Anderson, T. A., Salice, C. J., Erickson, R. A., McMurry, S. T., Cox, S. B., & Smith, L. M. (2013). Effects of landuse and precipitation on pesticides and water quality in playa lakes of the southern high plains. *Chemosphere*, *92*(1), 84–90. https://doi.org/10.1016/J.CHEMOSPHERE.2013.02.054

Antonsson, B. (1997). Phosphatidylinositol synthase from mammalian tissues. *Biochimica et Biophysica Acta (BBA) - Lipids and Lipid Metabolism*, *1348*(1–2), 179–186. https://doi.org/10.1016/S0005-2760(97)00105-7

Armstrong, G. A. (1997). GENETICS OF EUBACTERIAL CAROTENOID BIOSYNTHESIS: A Colorful Tale. *Annual Review of Microbiology*, *51*(1), 629–659. https://doi.org/10.1146/annurev.micro.51.1.629

Asselborn, V., Fernández, C., Zalocar, Y., & Parodi, E. R. (2015). Effects of chlorpyrifos on the growth and ultrastructure of green algae, Ankistrodesmus gracilis. *Ecotoxicology and Environmental Safety*, *120*, 334–341. https://doi.org/10.1016/J.ECOENV.2015.06.015

Baiz, C. R., Błasiak, B., Bredenbeck, J., Cho, M., Choi, J. H., Corcelli, S. A., Dijkstra, A. G., Feng, C. J., Garrett-Roe, S., Ge, N. H., Hanson-Heine, M. W. D., Hirst, J. D., Jansen, T. L. C., Kwac, K., Kubarych, K. J., Londergan, C. H., Maekawa, H., Reppert, M., Saito, S., … Zanni, M. T. (2020). Vibrational Spectroscopic Map, Vibrational Spectroscopy, and Intermolecular Interaction. *Chemical Reviews*, *120*(15), 7152–7218. https://doi.org/10.1021/ACS.CHEMREV.9B00813/SUPPL_FILE/CR9B00813_SI_001.PDF

Baseden, K. A., & Tye, J. W. (2014). Introduction to density functional theory: Calculations by hand on the helium atom. *Journal of Chemical Education*, *91*(12), 2116–2123. https://doi.org/10.1021/ED5004788/ASSET/IMAGES/MEDIUM/ED-2014-004788_0003.GIF

Battaglino, B., Grinzato, A., & Pagliano, C. (2021). Binding Properties of Photosynthetic Herbicides with the QB Site of the D1 Protein in Plant Photosystem II: A Combined Functional and Molecular Docking Study. *Plants 2021, Vol. 10, Page 1501*, *10*(8), 1501. https://doi.org/10.3390/PLANTS10081501

Bennett, D. I. G., Fleming, G. R., & Amarnath, K. (2018). Energy-dependent quenching adjusts the excitation diffusion length to regulate photosynthetic light harvesting. *Proceedings of the National Academy of Sciences of the United States of America*, *115*(41),

E9523–E9531. https://doi.org/10.1073/PNAS.1806597115/SUPPL_FILE/PNAS.1806597115.SAPP.PDF

Berezin, K. V., & Nechaev, V. V. (2005). Calculation of the IR spectrum and the molecular structure of β-carotene. *Journal of Applied Spectroscopy*, *72*(2), 164–171. https://doi.org/10.1007/S10812-005-0049-X/METRICS

Britton, G. (1995). Structure and properties of carotenoids in relation to function. *FASEB Journal : Official Publication of the Federation of American Societies for Experimental Biology*, *9*(15), 1551–1558.

Britton, G., Liaaen-Jensen, S., & Pfander, H. (Eds.). (2004). *Carotenoids*. https://doi.org/10.1007/978-3-0348-7836-4

Bulut, O., Akın, D., Sönmez, Ç., Öktem, A., Yücel, M., & Öktem, H. A. (2019). Phenolic compounds, carotenoids, and antioxidant capacities of a thermo-tolerant Scenedesmus sp. (Chlorophyta) extracted with different solvents. *Journal of Applied Phycology*, *31*(3), 1675–1683. https://doi.org/10.1007/S10811-018-1726-5

Casida, J. E., & Durkin, K. A. (2013). Neuroactive Insecticides: Targets, Selectivity, Resistance, and Secondary Effects. *Annual Review of Entomology*, *58*(1), 99–117. https://doi.org/10.1146/annurev-ento-120811-153645

Chen, W. L., Wagner, J., Heugel, N., Sugar, J., Lee, Y. W., Conant, L., Malloy, M., Heffernan, J., Quirk, B., Zinos, A., Beardsley, S. A., Prost, R., & Whelan, H. T. (2020). Functional Near-Infrared Spectroscopy and Its Clinical Application in the Field of Neuroscience: Advances and Future Directions. *Frontiers in Neuroscience*, *14*. https://doi.org/10.3389/FNINS.2020.00724

Choudhary, K., Garrity, K. F., Sharma, V., Biacchi, A. J., Hight Walker, A. R., & Tavazza, F. (2020). High-throughput density functional perturbation theory and machine learning predictions of infrared, piezoelectric, and dielectric responses. *Npj Computational Materials 2020 6:1*, *6*(1), 1–13. https://doi.org/10.1038/s41524-020-0337-2

Chuartzman, S. G., Nevo, R., Shimoni, E., Charuvi, D., Kiss, V., Ohad, I., Brumfeld, V., & Reicha, Z. (2008). Thylakoid Membrane Remodeling during State Transitions in Arabidopsis. *The Plant Cell*, *20*(4), 1029–1039. https://doi.org/10.1105/TPC.107.055830

Costas-Ferreira, C., & Faro, L. R. F. (2021). Neurotoxic Effects of Neonicotinoids on Mammals: What Is There beyond the Activation of Nicotinic Acetylcholine Receptors?—A Systematic Review. *International Journal of Molecular Sciences*, *22*(16), 8413. https://doi.org/10.3390/ijms22168413

Curtis, V. A., Brand, J. J., & Togasaki, R. K. (1975). Partial Reactions of Photosynthesis in Briefly Sonicated Chlamydomonas: I. Cell Breakage and Electron Transport Activities 1. *Plant Physiology*, *55*(2), 183. https://doi.org/10.1104/PP.55.2.183

Deng, Y. L., & Juang, Y. J. (2014). Black silicon SERS substrate: effect of surface morphology on SERS detection and application of single algal cell analysis. *Biosensors & Bioelectronics*, *53*, 37–42. https://doi.org/10.1016/J.BIOS.2013.09.032

di Tomo, P., Canali, R., Ciavardelli, D., di Silvestre, S., de Marco, A., Giardinelli, A., Pipino, C., di Pietro, N., Virgili, F., & Pandolfi, A. (2012). β-Carotene and lycopene affect endothelial response to TNF-α reducing nitro-oxidative stress and interaction with monocytes. *Molecular Nutrition & Food Research*, *56*(2), 217–227. https://doi.org/10.1002/mnfr.201100500

Douglas S. Auld, Ph. D., Peter A. Coassin, B. S., Nathan P. Coussens, Ph. D., Hensley, P., Klumpp-Thomas, C., Michael, S., G. Sitta Sittampalam, Ph. D., O. Joseph Trask, B. S., Bridget K. Wagner, Ph. D., Jeffrey R. Weidner, Ph. D., Mary Jo Wildey, Ph. D., & Jayme L. Dahlin, M. D. , Ph. D. (2020). Microplate Selection and Recommended Practices in High-throughput Screening and Quantitative Biology. *Assay Guidance Manual*. https://www.ncbi.nlm.nih.gov/books/NBK558077/

Erasmus, R. M., & Comins, J. D. (2019). Raman Scattering. *Handbook of Advanced Nondestructive Evaluation*, 541–594. https://doi.org/10.1007/978-3-319-26553-7_29

Evans, H., & Crofts, A. (1973). The relationship between delayed fluorescence and the H+ gradient in chloroplasts. *Biochimica et Biophysica Acta*, *292*, 130–139.

Fehr, W. R. (2015). Genetic contributions to yield gains of five major crop plants. *Genetic Contributions to Yield Gains of Five Major Crop Plants*, 1–101. https://doi.org/10.2135/CSSASPECPUB7

Finkeldey, R., & Gailing, O. (2013a). Chloroplasts. *Brenner's Encyclopedia of Genetics: Second Edition*, 525–527. https://doi.org/10.1016/B978-0-12-374984-0.00231-X

Finkeldey, R., & Gailing, O. (2013b). Chloroplasts. *Brenner's Encyclopedia of Genetics: Second Edition*, 525–527. https://doi.org/10.1016/B978-0-12-374984-0.00231-X

Finkelshtein, E. I., & Shamsiev, R. S. (n.d.). Estimation of conjugated C = C bonds effective number and conjugation energy of carotenoids. *Journal of Molecular Modeling*, *1*, 3. https://doi.org/10.1007/s00894-021-04896-w

Ford, K. A., & Casida, J. E. (2006). Unique and common metabolites of thiamethoxam, clothianidin, and dinotefuran in mice. *Chemical Research in Toxicology*, *19*(11), 1549–1556. https://doi.org/10.1021/TX0601859/ASSET/IMAGES/MEDIUM/TX0601859N00001.GIF

Ford, K. A., & Casida, J. E. (2008). Comparative Metabolism and Pharmacokinetics of Seven Neonicotinoid Insecticides in Spinach. *Journal of Agricultural and Food Chemistry*, *56*(21), 10168–10175. https://doi.org/10.1021/jf8020909

Fr, B., Pa Pa, C. N., & As, N. /. (1987). *ELECTRON SCATTERING AND NUCLEAR STRUCTURE*. www.annualreviews.org

Furutani, R., Ifuku, K., Suzuki, Y., Noguchi, K., Shimakawa, G., Wada, S., Makino, A., Sohtome, T., & Miyake, C. (2020). P700 oxidation suppresses the production of reactive oxygen species in photosystem I. *Advances in Botanical Research*, *96*, 151–176. https://doi.org/10.1016/BS.ABR.2020.08.001

García, J. J., Lõpez-Pingarrõn, L., Almeida-Souza, P., Tres, A., Escudero, P., García-Gil, F. A., Tan, D. X., Reiter, R. J., Ramírez, J. M., & Bernal-Pérez, M. (2014). Protective effects of melatonin in reducing oxidative stress and in preserving the fluidity of biological membranes: a review. *Journal of Pineal Research*, *56*(3), 225–237. https://doi.org/10.1111/JPI.12128

Giese, B., & McNaughton, D. (2001a). Surface-Enhanced Raman Spectroscopic and Density Functional Theory Study of Adenine Adsorption to Silver Surfaces. *Journal of Physical Chemistry B*, *106*(1), 101–112. https://doi.org/10.1021/JP010789F

Giese, B., & McNaughton, D. (2001b). Surface-Enhanced Raman Spectroscopic and Density Functional Theory Study of Adenine Adsorption to Silver Surfaces. *Journal of Physical Chemistry B*, *106*(1), 101–112. https://doi.org/10.1021/JP010789F

Giorio, G., Stigliani, A. L., & D'Ambrosio, C. (2007). Agronomic performance and transcriptional analysis of carotenoid biosynthesis in fruits of transgenic HighCaro and control tomato lines under field conditions. *Transgenic Research*, *16*(1), 15–28. https://doi.org/10.1007/s11248-006-9025-3

Goltsev, V., Zaharieva, I., Chernev, P., & Strasser, R. J. (2009a). Delayed fluorescence in photosynthesis. *Photosynthesis Research*, *101*(2–3), 217–232. https://doi.org/10.1007/S11120-009-9451-1

Goltsev, V., Zaharieva, I., Chernev, P., & Strasser, R. J. (2009b). Delayed fluorescence in photosynthesis. *Photosynthesis Research*, *101*(2–3), 217–232. https://doi.org/10.1007/S11120-009-9451-1/FIGURES/5

Goltsev, V., Zaharieva, I., Chernev, P., & Strasser, R. J. (2009c). Delayed fluorescence in photosynthesis. In *Photosynthesis Research* (Vol. 101, Issues 2–3, pp. 217–232). https://doi.org/10.1007/s11120-009-9451-1

Gomez, L., Bancel, D., Rubio, E., & Vercambre, G. (2007). The microplate reader: An efficient tool for the separate enzymatic analysis of sugars in plant tissues - Validation of a micro-method. *Journal of the Science of Food and Agriculture*, *87*(10), 1893–1905. https://doi.org/10.1002/JSFA.2924

Gorelik, V. S., Krylov, A. S., & Sverbil, V. P. (2014). Local Raman spectroscopy of DNA. *Bulletin of the Lebedev Physics Institute*, *41*(11), 310–315. https://doi.org/10.3103/s1068335614110025

Gosset, A., Oestreicher, V., Perullini, M., Bilmes, S. A., Jobbágy, M., Dulhoste, S., Bayard, R., & Durrieu, C. (2019). Optimization of sensors based on encapsulated algae for pesticide detection in water. *Analytical Methods*, *11*(48), 6193–6203. https://doi.org/10.1039/C9AY02145K

Graan, T., & Ort, D. R. (1986). Detection of oxygen-evolving Photosystem II centers inactive in plastoquinone reduction. *Biochimica et Biophysica Acta (BBA) - Bioenergetics*, *852*(2–3), 320–330. https://doi.org/10.1016/0005-2728(86)90238-0

Grudzinski, W., Janik, E., Bednarska, J., Welc, R., Zubik, M., Sowinski, K., Luchowski, R., & Gruszecki, W. I. (2016). Light-Driven Reconfiguration of a Xanthophyll Violaxanthin in the Photosynthetic Pigment-Protein Complex LHCII: A Resonance Raman

Study. *The Journal of Physical Chemistry. B*, *120*(19), 4373–4382. https://doi.org/10.1021/ACS.JPCB.6B01641

Gupta, R. (2020). The oxygen-evolving complex: a super catalyst for life on earth, in response to abiotic stresses. *Https://Doi.Org/10.1080/15592324.2020.1824721*, *15*(12). https://doi.org/10.1080/15592324.2020.1824721

Han, W., Tian, Y., & Shen, X. (2018). Human exposure to neonicotinoid insecticides and the evaluation of their potential toxicity: An overview. *Chemosphere*, *192*, 59–65. https://doi.org/10.1016/J.CHEMOSPHERE.2017.10.149

Han, X. X., Rodriguez, R. S., Haynes, C. L., Ozaki, Y., & Zhao, B. (2022). Surface-enhanced Raman spectroscopy. *Nature Reviews Methods Primers 2022 1:1*, *1*(1), 1–17. https://doi.org/10.1038/s43586-021-00083-6

Hanna, K., Krzoska, E., Shaaban, A. M., Muirhead, D., Abu-Eid, R., & Speirs, V. (2021). Raman spectroscopy: current applications in breast cancer diagnosis, challenges and future prospects. *British Journal of Cancer 2021 126:8*, *126*(8), 1125–1139. https://doi.org/10.1038/s41416-021-01659-5

Hanson, R. K., Spearrin, R. M., & Goldenstein, C. S. (2016). Rayleigh and Raman Spectra. *Spectroscopy and Optical Diagnostics for Gases*, 91–105. https://doi.org/10.1007/978-3-319-23252-2_6

Harris, E. H. (1989). *The Chlamydomonas Sourcebook : a Comprehensive Guide to Biology and Laboratory Use.* Elsevier Science. http://www.sciencedirect.com:5070/book/9780123268808/the-chlamydomonas-sourcebook

Hashimoto, H., Uragami, C., & Cogdell, R. J. (2016). Carotenoids and Photosynthesis. *Sub-Cellular Biochemistry*, *79*, 111–139. https://doi.org/10.1007/978-3-319-39126-7_4

Havaux, M., Tardy, F., & Lemoine, Y. (1998). Photosynthetic light-harvesting function of carotenoids in higher-plant leaves exposed to high light irradiances. *Planta*, *205*(2), 242–250. https://doi.org/10.1007/s004250050317

He, S., Xie, W., Zhang, P., Fang, S., Li, Z., Tang, P., Gao, X., Guo, J., Tlili, C., & Wang, D. (2018a). Preliminary identification of unicellular algal genus by using combined confocal resonance Raman spectroscopy with PCA and DPLS analysis. *Spectrochimica*

Acta Part A: Molecular and Biomolecular Spectroscopy, *190*, 417–422. https://doi.org/10.1016/J.SAA.2017.09.036

He, S., Xie, W., Zhang, P., Fang, S., Li, Z., Tang, P., Gao, X., Guo, J., Tlili, C., & Wang, D. (2018b). Preliminary identification of unicellular algal genus by using combined confocal resonance Raman spectroscopy with PCA and DPLS analysis. *Spectrochimica Acta. Part A, Molecular and Biomolecular Spectroscopy*, *190*, 417–422. https://doi.org/10.1016/J.SAA.2017.09.036

Hennessy, R. C., Stougaard, P., & Olsson, S. (2017). A Microplate Reader-Based System for Visualizing Transcriptional Activity During in vivo Microbial Interactions in Space and Time. *Scientific Reports 2017 7:1*, *7*(1), 1–6. https://doi.org/10.1038/s41598-017-00296-4

Henrysson, T., & Sundby, C. (1990a). Characterization of photosystem II in stroma thylakoid membranes. *Photosynthesis Research*, *25*(2), 107–117. https://doi.org/10.1007/BF00035459/METRICS

Henrysson, T., & Sundby, C. (1990b). Characterization of photosystem II in stroma thylakoid membranes. *Photosynthesis Research*, *25*(2), 107–117. https://doi.org/10.1007/BF00035459/METRICS

Hermsen, B., Stetzer, E., Thees, R., Heiermann, R., Schrattenholz, A., Ebbinghaus, U., Kretschmer, A., Methfessel, C., Reinhardt, S., & Maelicke, A. (1998). Neuronal Nicotinic Receptors in the Locust Locusta migratoria. *Journal of Biological Chemistry*, *273*(29), 18394–18404. https://doi.org/10.1074/jbc.273.29.18394

Hickey, L. T., N. Hafeez, A., Robinson, H., Jackson, S. A., Leal-Bertioli, S. C. M., Tester, M., Gao, C., Godwin, I. D., Hayes, B. J., & Wulff, B. B. H. (2019a). Breeding crops to feed 10 billion. *Nature Biotechnology*, *37*(7), 744–754. https://doi.org/10.1038/s41587-019-0152-9

Hickey, L. T., N. Hafeez, A., Robinson, H., Jackson, S. A., Leal-Bertioli, S. C. M., Tester, M., Gao, C., Godwin, I. D., Hayes, B. J., & Wulff, B. B. H. (2019b). Breeding crops to feed 10 billion. *Nature Biotechnology 2019 37:7*, *37*(7), 744–754. https://doi.org/10.1038/s41587-019-0152-9

Hladik, M. L., Main, A. R., & Goulson, D. (2018). Environmental Risks and Challenges Associated with Neonicotinoid Insecticides. *Environmental Science and Technology*, *52*(6), 3329–3335. https://doi.org/10.1021/ACS.EST.7B06388/ASSET/IMAGES/LARGE/ES-2017-063888_0002.JPEG

Hogg, R. C., Raggenbass, M., & Bertrand, D. (2003). Nicotinic acetylcholine receptors: from structure to brain function. *Reviews of Physiology, Biochemistry and Pharmacology*, *147*, 1–46. https://doi.org/10.1007/S10254-003-0005-1

Hokin, L. E. (2003). RECEPTORS AND PHOSPHOINOSITIDE-GENERATED SECOND MESSENGERS. *Https://Doi.Org/10.1146/Annurev.Bi.54.070185.001225*, *VOL. 54*, 205–235. https://doi.org/10.1146/ANNUREV.BI.54.070185.001225

House, M. A., Swanton, C. J., & Lukens, L. N. (2021). The neonicotinoid insecticide thiamethoxam enhances expression of stress-response genes in zea mays in an environmentally specific pattern. *Genome*, *64*(5), 567–579. https://doi.org/10.1139/gen-2020-0110

Huang, Y. Y., Beal, C. M., Cai, W. W., Ruoff, R. S., & Terentjev, E. M. (2010). Micro-Raman spectroscopy of algae: composition analysis and fluorescence background behavior. *Biotechnology and Bioengineering*, *105*(5), 889–898. https://doi.org/10.1002/BIT.22617

I. Yamamoto, & J.E. Casida. (1999). Nicotinoid Insecticides and the Nicotinic Acetylcholine Receptor. *Tokyo ; New York : Springer*. https://doi.org/10.1007/978-4-431-67933-2

Ihara, M., & Matsuda, K. (2018). Neonicotinoids: molecular mechanisms of action, insights into resistance and impact on pollinators. *Current Opinion in Insect Science*, *30*, 86–92. https://doi.org/10.1016/J.COIS.2018.09.009

Inoué, H., & Wada, T. (1987). Requirement of Manganese for Electron Donation of Hydrogen Peroxide in Photosystem II Reaction Center Complex. *Plant and Cell Physiology*, *28*(5), 767–773. https://doi.org/10.1093/OXFORDJOURNALS.PCP.A077357

Jan, S., Singh, R., Bhardwaj, R., Ahmad, P., & Kapoor, D. (2020). Plant growth regulators: a sustainable approach to combat pesticide toxicity. *3 Biotech*, *10*(11), 1–11. https://doi.org/10.1007/S13205-020-02454-4/TABLES/1

Jayasooriya, U. A., & Jenkins, R. D. (2002). Introduction to Raman Spectroscopy. *An Introduction to Laser Spectroscopy*, 77–104. https://doi.org/10.1007/978-1-4615-0727-7_3

Jeffrey, S. W., Sielicki, M., & Haxo, F. T. (1975). CHLOROPLAST PIGMENT PATTERNS IN DINOFLAGELLATES 1. *Journal of Phycology*, *11*(4), 374–384. https://doi.org/10.1111/J.1529-8817.1975.TB02799.X

Jena, S., Acharya, S., & Mohapatra, P. K. (2012). Variation in effects of four OP insecticides on photosynthetic pigment fluorescence of Chlorella vulgaris Beij. *Ecotoxicology and Environmental Safety*, *80*, 111–117. https://doi.org/10.1016/J.ECOENV.2012.02.016

Jones, C. K., Byun, N., & Bubser, M. (2011). Muscarinic and Nicotinic Acetylcholine Receptor Agonists and Allosteric Modulators for the Treatment of Schizophrenia. *Neuropsychopharmacology 2011 37:1*, *37*(1), 16–42. https://doi.org/10.1038/npp.2011.199

Jones, E., Michael, S., & Sittampalam, G. S. (2016). Basics of Assay Equipment and Instrumentation for High Throughput Screening. *Assay Guidance Manual*. https://www.ncbi.nlm.nih.gov/books/NBK92014/

Jones, R. R., Hooper, D. C., Zhang, L., Wolverson, D., & Valev, V. K. (2019). Raman Techniques: Fundamentals and Frontiers. *Nanoscale Research Letters 2019 14:1*, *14*(1), 1–34. https://doi.org/10.1186/S11671-019-3039-2

Junaedi, E., Lestari, K., & Muchtaridi, M. (2021). Infrared spectroscopy technique for quantification of compounds in plant-based medicine and supplement. *Journal of Advanced Pharmaceutical Technology & Research*, *12*(1), 1–7. https://doi.org/10.4103/JAPTR.JAPTR_96_20

Kaewlamun, W., Okouyi, M., Humblot, P., Techakumphu, M., & Ponter, A. A. (2011). Does supplementing dairy cows with β-carotene during the dry period affect postpartum ovarian activity, progesterone, and cervical and uterine involution? *Theriogenology*, *75*(6), 1029–1038. https://doi.org/10.1016/j.theriogenology.2010.11.010

Kalaji, H. M., Jajoo, A., Oukarroum, A., Brestic, M., Zivcak, M., Samborska, I. A., Cetner, M. D., Łukasik, I., Goltsev, V., Ladle, R. J., Dabrowski, P., & Ahmad, P. (2014). The Use of Chlorophyll Fluorescence Kinetics Analysis to Study the Performance of Photosynthetic Machinery in Plants. *Emerging Technologies and Management of Crop Stress Tolerance*, *2*, 347–384. https://doi.org/10.1016/B978-0-12-800875-1.00015-6

Kalaji, H. M., Oukarroum, A., Alexandrov, V., Kouzmanova, M., Brestic, M., Zivcak, M., Samborska, I. A., Cetner, M. D., Allakhverdiev, S. I., & Goltsev, V. (2014). Identification of nutrient deficiency in maize and tomato plants by in vivo chlorophyll a fluorescence measurements. *Plant Physiology and Biochemistry*, *81*, 16–25. https://doi.org/10.1016/J.PLAPHY.2014.03.029

Kalukula, Y., Stephens, A. D., Lammerding, J., & Gabriele, S. (2022). Mechanics and functional consequences of nuclear deformations. *Nature Reviews Molecular Cell Biology 2022 23:9*, *23*(9), 583–602. https://doi.org/10.1038/s41580-022-00480-z

Karger, S., Orlov, S. N., Luneva, O. G., Sidorenko, S. V, Ponomarchuk, O. O., Tverskoy, A. M., Cherkashin, A. A., Rodnenkov, O. V, Alekseeva, N. V, Deev, L. I., Maksimov, G. V, & Grygorczyk, R. (2016). Deoxygenation Affects Composition of Membrane-Bound Proteins in Human Erythrocytes. *Cell Physiol Biochem*, *39*, 81–88. https://doi.org/10.1159/000445607

Khachik, F., Carvalho, L., Bernstein, P. S., Muir, G. J., Zhao, D.-Y., & Katz, N. B. (2002). Chemistry, Distribution, and Metabolism of Tomato Carotenoids and Their Impact on Human Health. *Experimental Biology and Medicine*, *227*(10), 845–851. https://doi.org/10.1177/153537020222701002

Khan, N., Essemine, J., Hamdani, S., Qu, M., Lyu, M. J. A., Perveen, S., Stirbet, A., Govindjee, G., & Zhu, X. G. (2021). Natural variation in the fast phase of chlorophyll a fluorescence induction curve (OJIP) in a global rice minicore panel. *Photosynthesis Research*, *150*(1–3), 137–158. https://doi.org/10.1007/S11120-020-00794-Z

Kim, J., & DellaPenna, D. (2006). Defining the primary route for lutein synthesis in plants: the role of Arabidopsis carotenoid beta-ring hydroxylase CYP97A3. *Proceedings of the National Academy of Sciences of the United States of America*, *103*(9), 3474–3479. https://doi.org/10.1073/PNAS.0511207103

Kim, L., Rao, A. V., & Rao, L. G. (2003). Lycopene II—Effect on Osteoblasts: The Carotenoid Lycopene Stimulates Cell Proliferation and Alkaline Phosphatase Activity of SaOS-2 Cells. *Journal of Medicinal Food*, *6*(2), 79–86. https://doi.org/10.1089/109662003322233468

Kirchhoff, H. (2019). Chloroplast ultrastructure in plants. *New Phytologist*, *223*(2), 565–574. https://doi.org/10.1111/NPH.15730

Kochikov, I. V., Yagola, A. G., Kuramshina, G. M., Kovba, V. M., Pentin, Yu. A., Kochikov, I. V., Yagola, A. G., Kuramshina, G. M., Kovba, V. M., & Pentin, Yu. A. (1985). Calculation of force fields of chromium, molybdenum and tungsten hexafluorides and dioxodifluorides by means of the Tikchonov regularization method. *AcSpA*, *41*(1), 185–189. https://doi.org/10.1016/0584-8539(85)80095-7

Koster, H. J., Guillen-Perez, A., Gomez-Diaz, J. S., Navas-Moreno, M., Birkeland, A. C., & Carney, R. P. (2022). Fused Raman spectroscopic analysis of blood and saliva delivers high accuracy for head and neck cancer diagnostics. *Scientific Reports 2022 12:1*, *12*(1), 1–13. https://doi.org/10.1038/s41598-022-22197-x

Kou, Z., Hashemi, A., Puska, M. J., Krasheninnikov, A. V., & Komsa, H. P. (2020). Simulating Raman spectra by combining first-principles and empirical potential approaches with application to defective MoS2. *Npj Computational Materials 2020 6:1*, *6*(1), 1–7. https://doi.org/10.1038/s41524-020-0320-y

Kouzmanova, M., & Allakhverdiev, S. I. (2014). *Variable and Delayed Chlorophyll a Fluorescence-Basics and Application in Plant Sciences*. https://www.researchgate.net/publication/299847794

Krinsky, N. I. (1989). Antioxidant functions of carotenoids. *Free Radical Biology & Medicine*, *7*(6), 617–635. https://doi.org/10.1016/0891-5849(89)90143-3

Lane, H. M., Murray, S. C., Montesinos-López, O. A., Montesinos-López, A., Crossa, J., Rooney, D. K., Barrero-Farfan, I. D., De La Fuente, G. N., & Morgan, C. L. S. (2020). Phenomic selection and prediction of maize grain yield from near-infrared reflectance spectroscopy of kernels. *The Plant Phenome Journal*, *3*(1), e20002. https://doi.org/10.1002/PPJ2.20002

Lazár, D. (2006). The polyphasic chlorophyll a fluorescence rise measured under high intensity of exciting light. *Functional Plant Biology : FPB*, *33*(1), 9–30. https://doi.org/10.1071/FP05095

Legesse, F. B., Rüger, J., Meyer, T., Krafft, C., Schmitt, M., & Popp, J. (2018). Investigation of Microalgal Carotenoid Content Using Coherent Anti-Stokes Raman Scattering (CARS) Microscopy and Spontaneous Raman Spectroscopy. *Chemphyschem : A European Journal of Chemical Physics and Physical Chemistry*, *19*(9), 1048–1055. https://doi.org/10.1002/CPHC.201701298

Levey, A. I. (1996). Muscarinic acetylcholine receptor expression in memory circuits: Implications for treatment of Alzheimer disease. *Proceedings of the National Academy of Sciences of the United States of America*, *93*(24), 13541–13546. https://doi.org/10.1073/PNAS.93.24.13541/ASSET/0141DAA9-0DC8-4F79-A82F-8DE2634C4CF0/ASSETS/GRAPHIC/PQ2162486002.JPEG

Li, C., Swofford, C. A., & Sinskey, A. J. (2020). Modular engineering for microbial production of carotenoids. *Metabolic Engineering Communications*, *10*, e00118. https://doi.org/10.1016/J.MEC.2019.E00118

Li, Y.-S., & Church, J. S. (2014). Raman spectroscopy in the analysis of food and pharmaceutical nanomaterials. *Journal of Food and Drug Analysis*, *22*(1), 29–48. https://doi.org/10.1016/J.JFDA.2014.01.003

Lichtenthaler, H. K. (1987). Chlorophylls and carotenoids: Pigments of photosynthetic biomembranes. *Methods in Enzymology*, *148*(C), 350–382. https://doi.org/10.1016/0076-6879(87)48036-1

Lichtenthaler, H. K. (1999). THE 1-DEOXY-D-XYLULOSE-5-PHOSPHATE PATHWAY OF ISOPRENOID BIOSYNTHESIS IN PLANTS. *Annual Review of Plant Physiology and Plant Molecular Biology*, *50*(1), 47–65. https://doi.org/10.1146/annurev.arplant.50.1.47

Liu, Q., Wang, Z., Long, Y., Zhang, C., Fan, S., & Huang, W. (2022). Variety classification of coated maize seeds based on Raman hyperspectral imaging. *Spectrochimica Acta Part A: Molecular and Biomolecular Spectroscopy*, *270*, 120772. https://doi.org/10.1016/J.SAA.2021.120772

Louden, J. D. (1989). Raman Microscopy. In *Practical Raman Spectroscopy* (pp. 119–151). Springer Berlin Heidelberg. https://doi.org/10.1007/978-3-642-74040-4_6

Lovyagina, E. R., Davletshina, L. N., & Semin, B. K. (2022a). Peculiarities of Mn(II) Cation Oxidation in the Photosystem II without an Oxygen-Evolving Complex: Evolutionary Aspect. *Moscow University Biological Sciences Bulletin*, *77*(2), 92–97. https://doi.org/10.3103/S0096392522020055

Lovyagina, E. R., Davletshina, L. N., & Semin, B. K. (2022b). Peculiarities of Mn(II) Cation Oxidation in the Photosystem II without an Oxygen-Evolving Complex: Evolutionary Aspect. *Moscow University Biological Sciences Bulletin*, *77*(2), 92–97. https://doi.org/10.3103/S0096392522020055/METRICS

Macedo, W. R., Araújo, D. K., & Castro, P. R. de C. e. (2013). Unravelling the physiologic and metabolic action of thiamethoxam on rice plants. *Pesticide Biochemistry and Physiology*, *107*(2), 244–249. https://doi.org/10.1016/J.PESTBP.2013.08.001

Mahapatra, K., De, S., Banerjee, S., & Roy, S. (2019). Pesticide mediated oxidative stress induces genotoxicity and disrupts chromatin structure in fenugreek (Trigonella foenum - graecum L.) seedlings. *Journal of Hazardous Materials*, *369*, 362–374. https://doi.org/10.1016/J.JHAZMAT.2019.02.056

Maoka, T. (2020). Carotenoids as natural functional pigments. *Journal of Natural Medicines*, *74*(1), 1–16. https://doi.org/10.1007/S11418-019-01364-X/FIGURES/15

Marcek, J. M., Appell, L. H., Hoffman, C. C., Moredick, P. T., & Swanson, L. V. (1985). Effect of Supplemental β-Carotene on Incidence and Responsiveness of Ovarian Cysts to Hormone Treatment. *Journal of Dairy Science*, *68*(1), 71–77. https://doi.org/10.3168/jds.S0022-0302(85)80799-2

Matsuda, K., Shimomura, M., Ihara, M., Akamatsu, M., & Sattelle, D. B. (2005). Neonicotinoids Show Selective and Diverse Actions on Their Nicotinic Receptor Targets: Electrophysiology, Molecular Biology, and Receptor Modeling Studies. *Bioscience, Biotechnology, and Biochemistry*, *69*(8), 1442–1452. https://doi.org/10.1271/BBB.69.1442

Mavrogenis, M., Lepetit, B., Kroth, P. G., & Tsirtsis, G. (2023). Effects of dimethoate, an organophosphate insecticide, on photosynthesis of five selected phytoplankton species. *Global Nest Journal*, *25*(6), 23–34. https://doi.org/10.30955/gnj.004565

Melhus, H., Michaëlsson, K., Holmberg, L., Wolk, A., & Ljunghall, S. (1999). Smoking, Antioxidant Vitamins, and the Risk of Hip Fracture. *Journal of Bone and Mineral Research*, *14*(1), 129–135. https://doi.org/10.1359/jbmr.1999.14.1.129

Mohapatra, B. R., & Bapuji, M. (1997). Characterization of urethanase from Micrococcus species associated with the marine sponge (Spirasfrella species). *Letters in Applied Microbiology*, *25*(6), 393–396. https://doi.org/10.1111/J.1472-765X.1997.TB00003.X

Mohapatra, P. K., & Mohanty, R. C. (1992). Differential effect of dimethoate toxicity to Anabaena doliolum with change in nutrient status. *Bulletin of Environmental Contamination and Toxicology*, *48*(2), 223–229. https://doi.org/10.1007/BF00194375/METRICS

Mohapatra, P. K., Schubert, H., & Schiewer, U. (1997). Effect of Dimethoate on Photosynthesis and Pigment Fluorescence ofSynechocystissp. PCC 6803. *Ecotoxicology and Environmental Safety*, *36*(3), 231–237. https://doi.org/10.1006/EESA.1996.1503

Morioka, K., Osashima, M., Azuma, N., Qu, K., Hemmi, A., Shoji, A., Murakami, H., Teshima, N., Umemura, T., Uchiyama, K., & Nakajima, H. (2022). Development of a fluorescence microplate reader using an organic photodiode array with a large light receiving area. *Talanta*, *238*, 122994. https://doi.org/10.1016/J.TALANTA.2021.122994

Morrissey, C. A., Mineau, P., Devries, J. H., Sanchez-Bayo, F., Liess, M., Cavallaro, M. C., & Liber, K. (2015). Neonicotinoid contamination of global surface waters and associated risk to aquatic invertebrates: A review. *Environment International*, *74*, 291–303. https://doi.org/10.1016/J.ENVINT.2014.10.024

Mörtl, M., Takács, E., Klátyik, S., & Székács, A. (2020). Appearance of thiacloprid in the guttation liquid of coated maize seeds. *International Journal of Environmental Research and Public Health*, *17*(9). https://doi.org/10.3390/ijerph17093290

Mostafa, F. I. Y., & Helling, C. S. (2002). IMPACT OF FOUR PESTICIDES ON THE GROWTH AND METABOLIC ACTIVITIES OF TWO PHOTOSYNTHETIC ALGAE. *Journal of Environmental Science and Health. Part B - Pesticides, Food Contaminants, and Agricultural Wastes*, *37*(5), 417–444. https://doi.org/10.1081/PFC-120014873

Neuville, D. R., de Ligny, D., & Henderson, G. S. (2014). Advances in Raman Spectroscopy Applied to Earth and Material Sciences. *Reviews in Mineralogy and Geochemistry*, *78*(1), 509–541. https://doi.org/10.2138/RMG.2013.78.13

Nie, J., Sun, Y., Zhou, Y., Kumar, M., Usman, M., Li, J., Shao, J., Wang, L., & Tsang, D. C. W. (2020). Bioremediation of water containing pesticides by microalgae: Mechanisms, methods, and prospects for future research. *Science of The Total Environment*, *707*, 136080. https://doi.org/10.1016/J.SCITOTENV.2019.136080

Obermüller-Jevic, U. C., Francz, P. I., Frank, J., Flaccus, A., & Biesalski, H. K. (1999). Enhancement of the UVA induction of haem oxygenase-1 expression by β-carotene in human skin fibroblasts. *FEBS Letters*, *460*(2), 212–216. https://doi.org/10.1016/S0014-5793(99)01342-3

Olivo, M., & Dinish, U. S. (2015). Frontiers in biophotonics for translational medicine: In the celebration of year of light (2015). In *Frontiers in Biophotonics for Translational Medicine: In the Celebration of Year of Light (2015)*. https://doi.org/10.1007/978-981-287-627-0

Olson, J. A. (1996). Benefits and Liabilities of Vitamin A and Carotenoids. *The Journal of Nutrition*, *126*(suppl_4), 1208S-1212S. https://doi.org/10.1093/jn/126.suppl_4.1208S

Omenn, G. S., Goodman, G. E., Thornquist, M. D., Balmes, J., Cullen, M. R., Glass, A., Keogh, J. P., Meyskens, F. L., Valanis, B., Williams, J. H., Barnhart, S., & Hammar, S. (1996). Effects of a Combination of Beta Carotene and Vitamin A on Lung Cancer and Cardiovascular Disease. *New England Journal of Medicine*, *334*(18), 1150–1155. https://doi.org/10.1056/NEJM199605023341802

Papageorgiou, G. C., & Govindjee (Eds.). (2004). *Chlorophyll a Fluorescence*. *19*. https://doi.org/10.1007/978-1-4020-3218-9

PARK, C.-K., ISHIMI, Y., OHMURA, M., YAMAGUCHI, M., & IKEGAMI, S. (1997). Vitamin A and Carotenoids Stimulate Differentiation of Mouse Osteoblastic Cells. *Journal of Nutritional Science and Vitaminology*, *43*(3), 281–296. https://doi.org/10.3177/jnsv.43.281

Pinnola, A., & Bassi, R. (2018). Molecular mechanisms involved in plant photoprotection. *Biochemical Society Transactions*, *46*(2), 467–482. https://doi.org/10.1042/BST20170307

Prinsloo, L. C., Du Plooy, W., & Van Der Merwe, C. (2004). Raman spectroscopic study of the epicuticular wax layer of mature mango (Mangifera indica) fruit. *Journal of Raman Spectroscopy*, *35*(7), 561–567. https://doi.org/10.1002/JRS.1185

Prochazka, M. (2016). *Basics of Raman Scattering (RS) Spectroscopy*. 7–19. https://doi.org/10.1007/978-3-319-23992-7_2

Qin, J., Chao, K., & Kim, M. S. (2011). Investigation of Raman chemical imaging for detection of lycopene changes in tomatoes during postharvest ripening. *Journal of Food Engineering*, *107*(3–4), 277–288. https://doi.org/10.1016/J.JFOODENG.2011.07.021

Raczyńska, E. D., Duczmal, K., & Darowska, M. (2005). Experimental (FT-IR) and theoretical (DFT-IR) studies of keto–enol tautomerism in pyruvic acid. *Vibrational Spectroscopy*, *39*(1), 37–45. https://doi.org/10.1016/J.VIBSPEC.2004.10.006

Radenovic, C. N., Maksimov, G. V., Bajuk Bogdanovic, D., Hao, J., Radosavljevic, M. M., Delic, N. S., & Camdzija, Z. F. (2021). The infrared spectrum of the ultra quality maize hybrid preferable for human consumption: the identification of organic molecules and excited state of functional groups in spectral bands of the kernel, endosperm, pericarp and the germ. *Fiziologia Rastenij i Genetika*, *53*(4), 279–291. https://doi.org/10.15407/FRG2021.04.279

Radenović, Č. N., Maksimov, G. V., Kuramshina, G. M., Bogdanović, D. V. B., Mladenović, M. R., & Jovanović, P. Ž. (2023). The Analysis of Infrared Spectra and All Spectral Bands of Kernels, Endosperm, Pericarp and the Germ of Maize Hybrids: The Identification of Orbanic Molecules with the Excited State of Functional Groups and Valence Bonds. *Russian Agricultural Sciences*, *49*(1), 32–41. https://doi.org/10.3103/S1068367423010147

Radenovich, C., Maksimov, G. V., Tyutyaev, E. V., Shutova, V. V., Delich, N., Chamdzhiya, Z., Pavlov, Y., & Jovanovich, Z. (2016). Identification of characteristic organic molecules in kernels of maize (Zea mays L.) hybrid grain using infrared

spectroscopy. *Sel'skokhozyaistvennaya Biologiya*, *51*(5), 645–653. https://doi.org/10.15389/AGROBIOLOGY.2016.5.645ENG

Ralbovsky, N. M., & Lednev, I. K. (2020). Raman Spectroscopy and Advanced Statistics for Cancer Diagnostics. *Multimodal Optical Diagnostics of Cancer*, 273–323. https://doi.org/10.1007/978-3-030-44594-2_8/FIGURES/15

Ranilla, L. G. (2020). The application of metabolomics for the study of cereal corn (Zea mays L.). *Metabolites*, *10*(8), 1–24. https://doi.org/10.3390/metabo10080300

Rao, L. G., Krishnadev, N., Banasikowska, K., & Rao, A. V. (2003). Lycopene I—Effect on Osteoclasts: Lycopene Inhibits Basal and Parathyroid Hormone-Stimulated Osteoclast Formation and Mineral Resorption Mediated by Reactive Oxygen Species in Rat Bone Marrow Cultures. *Journal of Medicinal Food*, *6*(2), 69–78. https://doi.org/10.1089/109662003322233459

Rascio, N. (2013). Chloroplasts. *Encyclopedia of Biological Chemistry: Second Edition*, 506–510. https://doi.org/10.1016/B978-0-12-378630-2.00141-9

Rastogi, N. K. (2012a). Recent trends and developments in infrared heating in food processing. *Critical Reviews in Food Science and Nutrition*, *52*(9), 737–760. https://doi.org/10.1080/10408398.2010.508138

Rastogi, N. K. (2012b). Recent trends and developments in infrared heating in food processing. *Critical Reviews in Food Science and Nutrition*, *52*(9), 737–760. https://doi.org/10.1080/10408398.2010.508138

Rathna Priya, T. S., & Manickavasagan, A. (2021). Characterising corn grain using infrared imaging and spectroscopic techniques: a review. *Journal of Food Measurement and Characterization*, *15*(4), 3234–3249. https://doi.org/10.1007/S11694-021-00898-7/TABLES/5

Reski, R., & Abel, W. O. (1985). Induction of budding on chloronemata and caulonemata of the moss, Physcomitrella patens, using isopentenyladenine. *Planta*, *165*(3), 354–358. https://doi.org/10.1007/BF00392232/METRICS

Rodnenkov, O. V., Luneva, O. G., Ulyanova, N. A., Maksimov, G. V., Rubin, A. B., Orlov, S. N., & Chazov, E. I. (2005). Erythrocyte membrane fluidity and haemoglobin haemoporphyrin conformation: features revealed in patients with heart failure.

Pathophysiology : The Official Journal of the International Society for Pathophysiology, *11*(4), 209–213. https://doi.org/10.1016/J.PATHOPHYS.2004.12.001

Rodrigues Ribeiro, M., Lúcia Ferreira Simeone, M., dos Santos Trindade, R., Antônio dos Santos Dias, L., José Moreira Guimarães, L., Salete Tibola, C., & Cristina de Azevedo, T. (2023). Near infrared spectroscopy (NIR) and chemometrics methods to identification of haploids in maize. *Microchemical Journal*, *190*, 108604. https://doi.org/10.1016/J.MICROC.2023.108604

Rodríguez-Concepción, M. (2010). Supply of precursors for carotenoid biosynthesis in plants. *Archives of Biochemistry and Biophysics*, *504*(1), 118–122. https://doi.org/10.1016/J.ABB.2010.06.016

Rutherford, A. W., Osyczka, A., & Rappaport, F. (2012). Back-reactions, short-circuits, leaks and other energy wasteful reactions in biological electron transfer: Redox tuning to survive life in O2. *FEBS Letters*, *586*(5), 603–616. https://doi.org/10.1016/J.FEBSLET.2011.12.039

Rys, M., Juhász, C., Surówka, E., Janeczko, A., Saja, D., Tóbiás, I., Skoczowski, A., Barna, B., & Gullner, G. (2014). Comparison of a compatible and an incompatible pepper-tobamovirus interaction by biochemical and non-invasive techniques: chlorophyll a fluorescence, isothermal calorimetry and FT-Raman spectroscopy. *Plant Physiology and Biochemistry : PPB*, *83*, 267–278. https://doi.org/10.1016/J.PLAPHY.2014.08.013

Saito, S., & Tasumi, M. (1983). Normal-coordinate analysis of β-carotene isomers and assignments of the Raman and infrared bands. *Journal of Raman Spectroscopy*, *14*(5), 310–321. https://doi.org/10.1002/JRS.1250140504

Salvatori, E., Fusaro, L., Gottardini, E., Pollastrini, M., Goltsev, V., Strasser, R. J., & Bussotti, F. (2014). Plant stress analysis: Application of prompt, delayed chlorophyll fluorescence and 820 nm modulated reflectance. Insights from independent experiments. *Plant Physiology and Biochemistry*, *85*, 105–113. https://doi.org/10.1016/J.PLAPHY.2014.11.002

Samson-Robert, O., Labrie, G., Chagnon, M., & Fournier, V. (2014). Neonicotinoid-contaminated puddles of water represent a risk of intoxication for honey bees. *PloS One*, *9*(12). https://doi.org/10.1371/JOURNAL.PONE.0108443

Satoh, K., Oh-hashi, M., Kashino, Y., & Koike, H. (1995). Mechanism of Electron Flow through the QB Site in Photosystem II. 1. Kinetics of the Reduction of Electron Acceptors at the QB and Plastoquinone Sites in Photosystem II Particles from the Cyanobacterium Synechococcus vulcanus. *Plant and Cell Physiology*, *36*(4), 597–605. https://doi.org/10.1093/OXFORDJOURNALS.PCP.A078799

Schansker, G., Srivastava, A., Govindjee, & Strasser, R. J. (2003). Characterization of the 820-nm transmission signal paralleling the chlorophyll a fluorescence rise (OJIP) in pea leaves. *Functional Plant Biology*, *30*(7), 785–796. https://doi.org/10.1071/FP03032

Schansker, G., Tóth, S. Z., Holzwarth, A. R., & Garab, G. (2014). Chlorophyll a fluorescence: beyond the limits of the Q(A) model. *Photosynthesis Research*, *120*(1–2), 43–58. https://doi.org/10.1007/S11120-013-9806-5

Schneider, T. (2004). *Nonlinear Optics in Telecommunications*. https://doi.org/10.1007/978-3-662-08996-5

Schreier-Muccillo, S., Marsh, D., & Smith, I. C. P. (1976). Monitoring the permeability profile of lipid membranes with spin probes. *Archives of Biochemistry and Biophysics*, *172*(1), 1–11. https://doi.org/10.1016/0003-9861(76)90041-2

Seifert, J. (2014a). Neonicotinoids. *Encyclopedia of Toxicology: Third Edition*, 477–482. https://doi.org/10.1016/B978-0-12-386454-3.00168-8

Seifert, J. (2014b). Neonicotinoids. *Encyclopedia of Toxicology: Third Edition*, 477–482. https://doi.org/10.1016/B978-0-12-386454-3.00168-8

Semenova, A. A., Brazhe, N. A., Parshina, E. Y., Ivanov, V. K., Maksimov, G. V., & Goodilin, E. A. (2014). Aqueous diaminsilver hydroxide as a precursor of pure silver nanoparticles for SERS probing of living erythrocytes. *Plasmonics*, *9*(2), 227–235. https://doi.org/10.1007/S11468-013-9616-9/FIGURES/5

Shahid, M., Khan, M. S., Ahmed, B., Syed, A., & Bahkali, A. H. (2021). Physiological disruption, structural deformation and low grain yield induced by neonicotinoid insecticides in chickpea: A long term phytotoxicity investigation. *Chemosphere*, *262*, 128388. https://doi.org/10.1016/J.CHEMOSPHERE.2020.128388

Shakir, S. K., Irfan, S., Akhtar, B., Rehman, S. ur, Daud, M. K., Taimur, N., & Azizullah, A. (2018). Pesticide-induced oxidative stress and antioxidant responses in tomato

(Solanum lycopersicum) seedlings. *Ecotoxicology (London, England)*, *27*(7), 919–935. https://doi.org/10.1007/S10646-018-1916-6

Sharma, P., Sharma, A., Sodhi, M., Verma, P., Parvesh, K., Swami, S. K., Jast, A., Shandilya, U. K., & Mukesh, M. (2019). Characterizing binding sites of heat responsive microRNAs and their expression pattern in heat stressed PBMCs of native cattle, exotic cattle and riverine buffaloes. *Molecular Biology Reports*, *46*(6), 6513–6524. https://doi.org/10.1007/S11033-019-05097-8/FIGURES/4

Sharp, M. C. (2015). Biophotonics for Medical Applications. In *Biophotonics for Medical Applications*. Elsevier. http://www.sciencedirect.com:5070/book/9780857096623/biophotonics-for-medical-applications

Sim, E., Song, S., Vuckovic, S., & Burke, K. (2022). Improving Results by Improving Densities: Density-Corrected Density Functional Theory. *Journal of the American Chemical Society*, *144*(15), 6625–6639. https://doi.org/10.1021/JACS.1C11506/ASSET/IMAGES/MEDIUM/JA1C11506_0013.GIF

Stirbet, A., & Govindjee. (2012a). Chlorophyll a fluorescence induction: a personal perspective of the thermal phase, the J-I-P rise. *Photosynthesis Research*, *113*(1–3), 15–61. https://doi.org/10.1007/S11120-012-9754-5

Stirbet, A., & Govindjee. (2012b). Chlorophyll a fluorescence induction: a personal perspective of the thermal phase, the J–I–P rise. *Photosynthesis Research 2012 113:1*, *113*(1), 15–61. https://doi.org/10.1007/S11120-012-9754-5

Stirbet, A., & Govindjee. (2012c). Chlorophyll a fluorescence induction: a personal perspective of the thermal phase, the J–I–P rise. *Photosynthesis Research 2012 113:1*, *113*(1), 15–61. https://doi.org/10.1007/S11120-012-9754-5

Stocking, C. R., & Gifford, E. M. (1959). Incorporation of thymidine into chloroplasts of Spirogyra. *Biochemical and Biophysical Research Communications*, *1*(3), 159–164. https://doi.org/10.1016/0006-291X(59)90010-5

Strasser, R. J., Tsimilli-Michael, M., Qiang, S., & Goltsev, V. (2010a). Simultaneous in vivo recording of prompt and delayed fluorescence and 820-nm reflection changes during

drying and after rehydration of the resurrection plant Haberlea rhodopensis. *Biochimica et Biophysica Acta - Bioenergetics*, *1797*(6–7), 1313–1326. https://doi.org/10.1016/j.bbabio.2010.03.008

Strasser, R. J., Tsimilli-Michael, M., Qiang, S., & Goltsev, V. (2010b). Simultaneous in vivo recording of prompt and delayed fluorescence and 820-nm reflection changes during drying and after rehydration of the resurrection plant Haberlea rhodopensis. *Biochimica et Biophysica Acta (BBA) - Bioenergetics*, *1797*(6–7), 1313–1326. https://doi.org/10.1016/J.BBABIO.2010.03.008

Strasser, R. J., Tsimilli-Michael, M., Qiang, S., & Goltsev, V. (2010c). Simultaneous in vivo recording of prompt and delayed fluorescence and 820-nm reflection changes during drying and after rehydration of the resurrection plant Haberlea rhodopensis. *Biochimica et Biophysica Acta*, *1797*(6–7), 1313–1326. https://doi.org/10.1016/J.BBABIO.2010.03.008

Strasser, R. J., Tsimilli-Michael, M., Qiang, S., & Goltsev, V. (2010d). Simultaneous in vivo recording of prompt and delayed fluorescence and 820-nm reflection changes during drying and after rehydration of the resurrection plant Haberlea rhodopensis. *Biochimica et Biophysica Acta - Bioenergetics*, *1797*(6–7), 1313–1326. https://doi.org/10.1016/j.bbabio.2010.03.008

Strasser, R. J., Tsimilli-Michael, M., & Srivastava, A. (2004a). *Analysis of the Chlorophyll a Fluorescence Transient* (pp. 321–362). https://doi.org/10.1007/978-1-4020-3218-9_12

Strasser, R. J., Tsimilli-Michael, M., & Srivastava, A. (2004b). *Analysis of the Chlorophyll a Fluorescence Transient*. 321–362. https://doi.org/10.1007/978-1-4020-3218-9_12

Strasser, R. J., Tsimilli-Michael, M., & Srivastava, A. (2004c). *Analysis of the Chlorophyll a Fluorescence Transient*. 321–362. https://doi.org/10.1007/978-1-4020-3218-9_12

Strasser, R. J., Tsimilli-Michael, M., & Srivastava, A. (2004d). *Analysis of the Chlorophyll a Fluorescence Transient*. 321–362. https://doi.org/10.1007/978-1-4020-3218-9_12

Street, D. A., Comstock, G. W., Salkeld, R. M., Schüep, W., & Klag, M. J. (1994). Serum antioxidants and myocardial infarction. Are low levels of carotenoids and alpha-tocopherol risk factors for myocardial infarction? *Circulation*, *90*(3), 1154–1161. https://doi.org/10.1161/01.CIR.90.3.1154

Su, N. Q., & Xu, X. (2017). Development of New Density Functional Approximations. *Https://Doi.Org/10.1146/Annurev-Physchem-052516-044835*, *68*, 155–182. https://doi.org/10.1146/ANNUREV-PHYSCHEM-052516-044835

Su, X., Wang, L., Xu, Y., Dong, L., & Lu, H. (2021). Study on the binding mechanism of thiamethoxam with three model proteins:spectroscopic studies and theoretical simulations. *Ecotoxicology and Environmental Safety*, *207*. https://doi.org/10.1016/J.ECOENV.2020.111280

Sun, T., Rao, S., Zhou, X., & Li, L. (2022). Plant carotenoids: recent advances and future perspectives. *Molecular Horticulture 2022 2:1*, *2*(1), 1–21. https://doi.org/10.1186/S43897-022-00023-2

Sun, Z., Cunningham, F. X., & Gantt, E. (1998). Differential expression of two isopentenyl pyrophosphate isomerases and enhanced carotenoid accumulation in a unicellular chlorophyte. *Proceedings of the National Academy of Sciences of the United States of America*, *95*(19), 11482–11488. https://doi.org/10.1073/PNAS.95.19.11482/ASSET/56A35F27-188D-4DBE-8600-26E23B658910/ASSETS/GRAPHIC/PQ1882334007.JPEG

Takahashi, T. (2019). New trends and perspectives in the function of non-neuronal acetylcholine in crypt–villus organoids in mice. *Methods in Molecular Biology*, *1576*, 145–155. https://doi.org/10.1007/7651_2016_1/TABLES/2

Takaichi, S. (2011). Carotenoids in Algae: Distributions, Biosyntheses and Functions. *Marine Drugs 2011, Vol. 9, Pages 1101-1118*, *9*(6), 1101–1118. https://doi.org/10.3390/MD9061101

Tanumihardjo, S. A. (2013). Carotenoids: Health Effects. *Encyclopedia of Human Nutrition*, *1–4*, 292–297. https://doi.org/10.1016/B978-0-12-375083-9.00045-3

Terao, J. (1989). Antioxidant activity of beta-carotene-related carotenoids in solution. *Lipids*, *24*(7), 659–661. https://doi.org/10.1007/BF02535085

Todorenko, D. A., Hao, J., Slatinskaya, O. V., Allakhverdiev, E. S., Khabatova, V. V., Ivanov, A. D., Radenovic, C. N., Matorin, D. N., Alwasel, S., Maksimov, G. V., & Allakhverdiev, S. I. (2021). Effect of thiamethoxam on photosynthetic pigments and primary photosynthetic reactions in two maize genotypes (Zea mays). *Functional Plant Biology : FPB*, *48*(10), 994–1004. https://doi.org/10.1071/FP21134

Todorenko, D., Timofeev, N., Kovalenko, I., Kukarskikh, G., Matorin, D., & Antal, T. (2020). Chromium effects on photosynthetic electron transport in pea (Pisum sativum L.). *Planta*, *251*(1), 1–13. https://doi.org/10.1007/S00425-019-03304-1/FIGURES/6

Tomizawa, M., & Casida, J. E. (2003). Selective toxicity of neonicotinoids attributable to specificity of insect and mammalian nicotinic receptors. *Annual Review of Entomology*, *48*, 339–364. https://doi.org/10.1146/ANNUREV.ENTO.48.091801.112731

Toti, E., Oliver Chen, C. Y., Palmery, M., Valencia, D. V., & Peluso, I. (2018). Non-Provitamin A and Provitamin A Carotenoids as Immunomodulators: Recommended Dietary Allowance, Therapeutic Index, or Personalized Nutrition? *Oxidative Medicine and Cellular Longevity*, *2018*. https://doi.org/10.1155/2018/4637861

Touzout, N., Mehallah, H., Moralent, R., Moulay, M., & Nemmiche, S. (2021). Phytotoxic evaluation of neonicotinoid imidacloprid and cadmium alone and in combination on tomato (Solanum lycopersicum L.). *Ecotoxicology*, *30*(6), 1126–1137. https://doi.org/10.1007/s10646-021-02421-6

Tretyni, A., Bossen, M. E., & Kendrick, R. E. (1992). *Evidence for different types of acetylcholine receptors in plants* (pp. 306–311). https://doi.org/10.1007/978-94-011-2458-4_34

Vass, I., Kirilovsky, D., & Etienne, A. L. (1999). UV-B Radiation-Induced Donor- and Acceptor-Side Modifications of Photosystem II in the Cyanobacterium Synechocystis sp. PCC 6803†. *Biochemistry*, *38*(39), 12786–12794. https://doi.org/10.1021/BI991094W

Vlasov, A. V., Maliar, N. L., Bazhenov, S. V., Nikelshparg, E. I., Brazhe, N. A., Vlasova, A. D., Osipov, S. D., Sudarev, V. V., Ryzhykau, Y. L., Bogorodskiy, A. O., Zinovev, E. V., Rogachev, A. V., Manukhov, I. V., Borshchevskiy, V. I., Kuklin, A. I., Pokorný, J., Sosnovtseva, O., Maksimov, G. V., & Gordeliy, V. I. (2020). Raman

Scattering: From Structural Biology to Medical Applications. *Crystals 2020, Vol. 10, Page 38*, *10*(1), 38. https://doi.org/10.3390/CRYST10010038

Volgusheva, A. A., Petrova, E. V., Kukarskikh, G. P., Dubini, A., & Antal, T. K. (2022). Influence of Fermentation Reactions on Continuous Hydrogen Photoproduction by Microalga Chlamydomonas reinhardtii under Sulfur Deficiency. *Moscow University Biological Sciences Bulletin*, *77*(1), 25–31. https://doi.org/10.3103/S0096392522010060/FIGURES/2

Wang, L., Gaziano, J. M., Norkus, E. P., Buring, J. E., & Sesso, H. D. (n.d.). *Associations of plasma carotenoids with risk factors and biomarkers related to cardiovascular disease in middle-aged and older women*.

Yagi, K., Yamada, K., Kobayashi, C., & Sugita, Y. (2019). Anharmonic Vibrational Analysis of Biomolecules and Solvated Molecules Using Hybrid QM/MM Computations. *Journal of Chemical Theory and Computation*, *15*(3), 1924–1938. https://doi.org/10.1021/ACS.JCTC.8B01193/ASSET/IMAGES/LARGE/CT-2018-01193V_0006.JPEG

Yamamoto, I., Tomizawa, M., Saito, T., Miyamoto, T., Walcott, E. C., & Sumikawa, K. (1998). Structural factors contributing to insecticidal and selective actions of neonicotinoids. *Archives of Insect Biochemistry and Physiology*, *37*(1), 24–32. https://doi.org/10.1002/(SICI)1520-6327(1998)37:1<24::AID-ARCH4>3.0.CO;2-V

YAMAMOTO, I., YABUTA, G., TOMIZAWA, M., SAITO, T., MIYAMOTO, T., & KAGABU, S. (1995). Molecular Mechanism for Selective Toxicity of Nicotinoids and Neonicotinoids. *Journal of Pesticide Science*, *20*(1), 33–40. https://doi.org/10.1584/jpestics.20.33

Yu, H., Peng, Y., Yang, Y., & Li, Z. Y. (2019). Plasmon-enhanced light–matter interactions and applications. *Npj Computational Materials 2019 5:1*, *5*(1), 1–14. https://doi.org/10.1038/s41524-019-0184-1

Zavyalova, E., Ambartsumyan, O., Zhdanov, G., Gribanyov, D., Gushchin, V., Tkachuk, A., Rudakova, E., Nikiforova, M., Kuznetsova, N., Popova, L., Verdiev, B., Alatyrev, A., Burtseva, E., Ignatieva, A., Iliukhina, A., Dolzhikova, I., Arutyunyan, A., Gambaryan, A., & Kukushkin, V. (2021). SERS-Based Aptasensor for Rapid Quantitative

Detection of SARS-CoV-2. *Nanomaterials (Basel, Switzerland)*, *11*(6). https://doi.org/10.3390/NANO11061394

Zhang, Y., Liu, Z., Sun, J., Xue, C., & Mao, X. (2018). Biotechnological production of zeaxanthin by microorganisms. *Trends in Food Science & Technology*, *71*, 225–234. https://doi.org/10.1016/J.TIFS.2017.11.006

Zhang, Y., Sun, X., Bajwa, S. G., Sivarajan, S., Nowatzki, J., & Khan, M. (2018). Plant Disease Monitoring With Vibrational Spectroscopy. *Comprehensive Analytical Chemistry*, *80*, 227–251. https://doi.org/10.1016/BS.COAC.2018.03.006

Živčák, M., Olšovská, K., Slamka, P., Galambošová, J., Rataj, V., Shao, H. B., & Brestič, M. (2014). Application of chlorophyll fluorescence performance indices to assess the wheat photosynthetic functions influenced by nitrogen deficiency. *Plant, Soil and Environment*, *60*(5), 210–215. https://doi.org/10.17221/73/2014-PSE

Александровна, Б. Н., & Александрович, Ч. А. (n.d.). *Исследование конформации гемопорфирина гемоглобина с использованием спектроскопии комбинационного рассеяния*.